VOLUME 75 NOVEMBER 25, 1971 NUMBER 24

JPCHAx

THE JOURNAL OF PHYSICAL CHEMISTRY

PUBLISHED BIWEEKLY BY THE AMERICAN CHEMICAL SOCIETY

THE JOURNAL OF

PHYSICAL CHEMISTRY

AMERICAN CHEMICAL SOCIETY, *1155 Sixteenth St., N.W., Washington, D. C. 20036*
FREDERICK T. WALL, *Executive Director*

Books and Journals Division
JOHN K CRUM, *Director (Acting)*
JOSEPH H. KUNEY, *Head, Business Operations Department*
RUTH REYNARD, *Assistant to the Director*

 Published biweekly by the American Chemical Society at 20th and Northampton Sts., Easton, Pa. 18042. Second-class postage paid at Washington, D. C., and at additional mailing offices.

All manuscripts should be sent to *The Journal of Physical Chemistry,* Department of Chemistry, University of Minnesota, Minneapolis, Minn. 55455.

Additions and Corrections are published once yearly in the final issue. See Volume 74, Number 26 for the proper form.

Extensive or unusual alterations in an article after it has been set in type are made at the author's expense, and it is understood that by requesting such alterations the author agrees to defray the cost thereof.

The American Chemical Society and the Editor of *The Journal of Physical Chemistry* assume no responsibility for the statements and opinions advanced by contributors.

Correspondence regarding accepted copy, proofs, and reprints should be directed to Editorial Production Office, American Chemical Society, 20th and Northampton Sts., Easton, Pa. 18042. Manager: CHARLES R. BERTSCH. Assistant Editor: EDWARD A. BORGER. Editorial Assistant: WILLIAM T. BOYD.

Advertising Office: Century Communications Corporation, 142 East Avenue, Norwalk, Conn. 06851.

Business and Subscription Information

Remittances and orders for subscriptions and for single copies, notices of changes of address and new professional connections, and claims for missing numbers should be sent to the Subscription Service Department, American Chemical Society, 1155 Sixteenth St., N.W., Washington, D. C. 20036. Allow 4 weeks for changes of address. Please include an old address label with the notification.

Claims for missing numbers will not be allowed (1) if received more than sixty days from date of issue, (2) if loss was due to failure of notice of change of address to be received before the date specified in the preceding paragraph, or (3) if the reason for the claim is "missing from files."

Subscription rates (1971): members of the American Chemical Society, $20.00 for 1 year; to nonmembers, $40.00 for 1 year. Those interested in becoming members should write to the Admissions Department, American Chemical Society, 1155 Sixteenth St., N.W., Washington, D. C. 20036. Postage to Canada and countries in the Pan-American Union, $4.00; all other countries, $5.00. Single copies for current year: $2.00. Rates for back issues from Volume 56 to date are available from the Special Issues Sales Department, 1155 Sixteenth St., N.W., Washington, D. C. 20036.

This publication and the other ACS periodical publications are now available on microfilm. For information write to: MICROFILM, Special Issues Sales Department, 1155 Sixteenth St., N.W., Washington, D. C. 20036.

Notice to Authors last printed in the issue of June 10, 1971

THE JOURNAL OF

PHYSICAL CHEMISTRY

Volume 75, Number 24 November 25, 1971

NOTES

COMMUNICATIONS TO THE EDITOR

AUTHOR INDEX

In papers with more than one author the name of the author to whom inquiries about the paper should be addressed is marked with an asterisk in the by-line.

THE JOURNAL OF
PHYSICAL CHEMISTRY

VOLUME 75, NUMBER 24 NOVEMBER 25, 1971

Structure of Fluorine-Supported Flames. I. Method of Investigation. The Dichlorodifluoromethane–Fluorine Flame

by K. H. Homann[1] and D. I. MacLean*

Department of Chemistry, Boston College, Chestnut Hill, Massachusetts 02167 *(Received March 4, 1971)*

Publication costs assisted by the Office of Naval Research

The stoichiometric dichlorodifluoromethane–fluorine combustion reaction has been studied in a low-pressure flame at 77 mm. Concentration profiles across the reaction zone of the flame have been measured by a molecular beam sampling technique on a time-of-flight mass spectrometer. The reaction mechanism proposed is

$$F + CCl_2F_2 \longrightarrow CClF_3 + Cl \quad (1)$$

$$Cl + F_2 \longrightarrow ClF + F \quad (2)$$

$$F + CClF_3 \longrightarrow CF_4 + Cl \quad (3)$$

$$Cl + ClF \rightleftarrows Cl_2 + F \quad (4)$$

Values for the ratios $k_1/k_3 \approx 7$ and $k_2/k_1 \approx 50$ are reported for temperatures of approximately 1600 and 1500°K, respectively.

Introduction

Since Moissan's work[2] it is well known that a large number of substances, for example, substances containing carbon and hydrogen, burn violently when reacting with pure fluorine, owing to the large exothermicity of the reactions involved. The flame temperatures obtained belong to the highest that can be reached in combustion processes.

Some methods for preparative fluorination are based on the gas phase reaction of the substances with fluorine. However, in these procedures great efforts are taken to run the reactions under very mild conditions and to avoid any cracking or polymerization due to high temperature in the reactors. This is done by cooling and diluting the reactants in a suitable way, for which Bigelow and coworkers[3] have developed some sophisticated devices.

In recent years the high temperature combustion with fluorine has attracted increasing interest mainly due to the search for powerful oxidizers for rocket propellants. In addition, combustion with fluorine seems to be a promising source for chemical lasers.[4]

On the other hand, it has become possible by modern techniques to follow directly elementary reactions of fluorine atoms which are considered to be the most important active species in the combustion with fluorine.[5] Some of these combustions, in particular those of the halogenated hydrocarbons,[6] seem to be governed by comparatively simple reaction mechanisms. Thus, with the knowledge of some separately

(1) Affiliation: Institut für Physikalische Chemie der Universität, Göttingen, Germany.

(2) H. Moissan, *C. R. Acad. Sci.*, **102**, 1543 (1886); see also "Le Fluor et ses Composés," Steinheil, Paris, 1900.

(3) E. A. Tyczkowski and L. A. Bigelow, *J. Amer. Chem. Soc.*, **75**, 3523 (1953).

(4) See, *e.g.*, *Appl. Opt.*, Supplement 2: Chemical Lasers (1965).

(5) K. H. Homann, W. C. Solomon, J. Warnatz, H. Gg. Wagner, and C. Zetsch, *Ber. Bunsenges. Phys. Chem.*, **74**, 585 (1970).

(6) K. H. Homann and D. I. MacLean, *Combust. Flame*, **14**, 409 (1970).

measured rate constants of fluorine and other halogen atoms, together with the profiles of the reacting species measured in flames, there is a good chance for a better understanding of the fluorine flame chemistry and the kinetics of the reactions involved.

Compared to the combustion processes with oxygen very little is known about those supported by fluorine. An exception is the hydrogen–fluorine reaction which has been studied more thoroughly.[7]

The first study of the reaction of fluorine with a perhalogenated organic compound, CCl_4, was reported by Ruff in 1931.[8] Later Bigelow[3] and also Miller[9] studied the mild fluorination of various organic halogen compounds but mainly with the purpose of preparing new fluorine-containing species. Fletcher and coworkers studied flame and detonation velocities of halocarbon–fluorine systems.[10]

A spectroscopic investigation of flames of organic halogen compounds with fluorine was carried out by Durie.[11] He noticed a characteristic difference in the spectra of these flames depending on whether the fuel contained hydrogen or not. When burning chloroform in a certain mixture ratio with fluorine, a strong yellow luminosity due to carbon formation was observed. The same was true for mixtures of carbon tetrachloride and hydrogen. But CCl_4 alone did not show any sign of carbon luminosity independently of the mixture ratio in the flame. This indicates a significant difference in the reaction mechanisms of these two flames.[6] Therefore, the combustion of hydrogen-free halogen compounds and those with hydrogen in the fuel molecule or in the burning mixture will be studied separately.

Experimental Method

The principle of the method is to obtain a flat, quasi-premixed flame with a sufficiently extended reaction zone so that samples can be taken through a molecular beam sampling system and analyzed directly by mass spectrometry. This method of analysis had proved to be successful for the study of the structure of various flames burning with oxygen.[12]

1. The Burner. Since most of the organic halides and other substances that are to be used as fuels ignite spontaneously with fluorine, the reactants could not be premixed. Therefore, a so-called multidiffusion burner was used to stabilize the flames. On this burner fuel and oxidizer are mixed shortly before they enter the reaction zone of the flame. The burner used for this purpose is shown in Figure 1. It is made of copper. Fluorine flows from the upper chamber to the burner mouth through a pattern of *ca.* 150 holes of 0.04-in. diameter each in the upper plate; the fuel flows from the lower chamber through a bunch of capillaries extending through the fluorine chamber and ending regularly between the holes for the fluorine outlet. The fuel chamber is fed through the shaft of the burner while

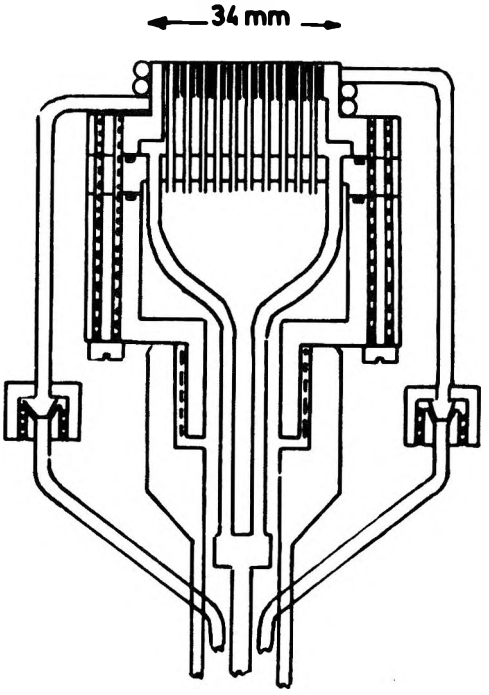

Figure 1. Copper, watercooled, multidiffusion burner designed for low-pressure, fluorine–fuel flames.

fluorine is supplied by means of a separate tube within the shaft. Tubes for cooling water also come up through the shaft of the burner and are soldered around the burner mouth which has a diameter of 34 mm.

Since there are limits for the area density of the outlet holes for fluorine and fuel a quasi-premixed, flat flame will result only if the flame burns under conditions where the mixing above the burner is sufficiently faster than the chemical reactions. How much the pressure has to be reduced depends on the rate of interdiffusion and the burning velocity of the fuel–fluorine pair in question. A reduction in pressure is also necessary to spread out the reaction zone in the direction of flow in order to get a satisfactory spatial resolution for sampling. The burner is surrounded by a housing which is pumped by a Stokes Model 212 Microvac rotary pump. A special charcoal trap, the flow resistance of which could be varied for different throughputs and varying fluorine concentrations in the burned gas, was installed in the pumping line to protect the pumps from fluorine. Between the charcoal trap and

(7) J. B. Levy and B. K. W. Copeland, *J. Phys. Chem.*, **67**, 2156 (1963); **72**, 3168 (1968); G. A. Kapralova, L. Ju. Rusin, E. M. Trofimova, A. M. Chaikin, and A. E. Shilov, *Kinet. Katal.*, **4**, 653 (1963); G. A. Kapralova and A. M. Chaikin, *Combust. Flame*, **13**, 557 (1969).

(8) O. Ruff and R. Keim, *Z. Anorg. Allg. Chem.*, **201**, 245 (1931).

(9) W. T. Miller, *J. Amer. Chem. Soc.*, **62**, 341 (1940).

(10) E. A. Fletscher and D. J. Parks, *Combust. Flame*, **13**, 487 (1969).

(11) R. A. Durie, *Proc. Roy. Soc., Ser. A*, **211**, 110 (1952).

(12) K. H. Homann, M. Mochizuki, and H. Gg. Wagner, *Z. Phys. Chem. (Frankfurt am Main)*, **37**, 299 (1963).

the burner housing were two cold traps made of copper in which condensables such as HF, ClF, etc., could be frozen out at liquid nitrogen temperature and carefully disposed of after each experiment.

2. The Molecular Beam Sampling System. The sampling system (Figure 2) has been constructed in a way very similar to those described earlier.[13] To shorten the length of the pumping line to the ion source chamber the burner and the direction of the sampling beam has been inverted so that the gas flow in the flame is directed downwards. Quartz as a material for the sampling nozzle was tried but soon abandoned because it reacted with the flame gases. A recrystallized aluminum oxide probe was used instead. This was also slightly attacked by the flame gases, but the probes could be used for several hours with flames burning at pressures of a few centimeters. Depending on the burning pressure the orifice diameter was chosen between about 0.2 and 0.8 mm. All diffusion pumps were equipped with liquid nitrogen cooled baffles to protect the pumps and to increase the pumping speed since a great part of the flame products was condensable. The mass spectrometer was a Bendix 3012 time-of-flight model and was operated at an electron energy of 22 eV.

3. The Gas Metering System. All noncorrosive gases were metered by means of capillary flow meters at atmospheric pressure. Fluorine was taken from a tank at a pressure of about 1.5 atm and measured by a floating ball type flowmeter (Matheson) at atmospheric pressure. This was controlled by means of a mercury bubbler connected to the flowmeter by a line filled with dry nitrogen and a valve which was opened only occasionally. Two fine-regulating stainless steel needle valves on both ends of the flowmeter served to set the desired flow rate. Since dichlorodifluoromethane (CCl_2F_2) generally does not ignite spontaneously with F_2 at pressures around 100 mm, a little hydrogen had to be mixed to the fuel to light the flame. After ignition the hydrogen was shut off.

The purity of the CCl_2F_2 (Matheson) was 99% and mass spectrometric analysis showed the absence of hydrogen-containing compounds. The fluorine (Allied Chemical) was more than 98.5% pure, the principal contaminant being HF. No oxygen was found when analyzed in the mass spectrometer.

Results

1. Appearance of the CCl_2F_2–F_2 Flame. The flame emits a grayish white light the intensity of which is relatively weak compared to the total emission of hydrocarbon–fluorine flames.[14] Preliminary spectroscopic observations show that this light appears to come mainly from a continuum between about 4500 and 5500 Å. For an equimolar mixture of CCl_2F_2 and F_2 and a mean linear flow velocity from the burner mouth of about 12.5 cm/sec at a burning pressure of

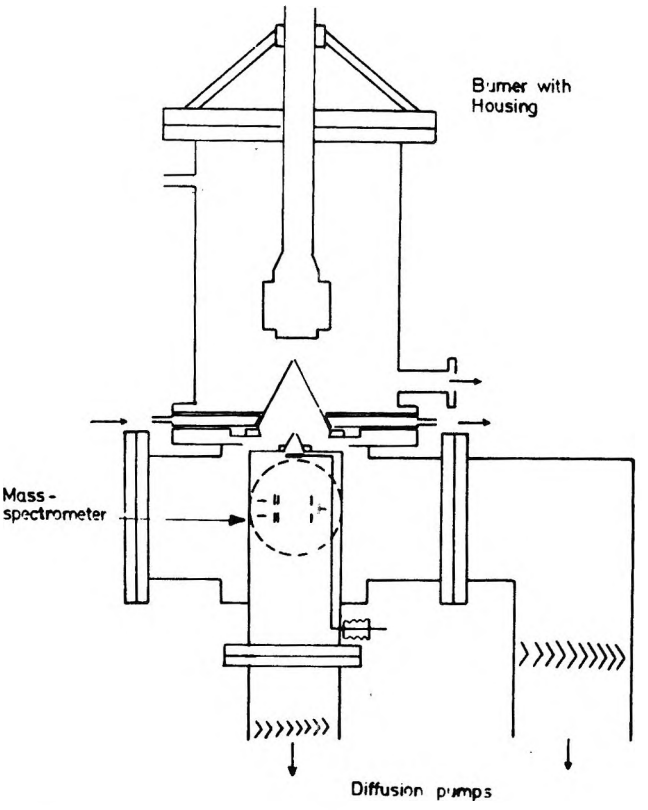

Figure 2. Burner arrangement and molecular beam sampling system for mass spectrometric analysis of low pressure flames.

80 mm (normalized to room temperature) the thickness of the luminous zone is about 16 mm. The luminosity can be made to extend far more into the burned gas if the flow of CCl_2F_2 is increased. Addition of a little hydrogen weakens this grayish white emission; carbon luminosity appears when the hydrogen flow is increased.

2. Concentration Profiles. Figure 3 gives the concentration profiles in stoichiometric CCl_2F_2–F_2 flame at a burning pressure of 77 mm. The flow rates measured at a pressure of 1 atm were 6.0 cc/sec each for CCl_2F_2 and F_2. Six stable compounds are involved in the flame reaction. Starting from the reactants CCl_2F_2 and F_2, ClF and ClF_3 are formed as intermediates which react further to the final products Cl_2 and CF_4. A profile of chlorine atom concentration could be determined only qualitatively because of the lack of the exact mass spectrometric calibration factor. The profile drawn is based on an estimate of the ionization probability of chlorine atoms taking into account its size and ionization potential. HCl was identified in the mass spectral pattern, but it appears to have originated in the ion source and not the flame.[15]

The flame can be divided into two overlapping reaction zones which are, however, not visually distin-

(13) K. H. Homann, G. Krome, and H. Gg. Wagner, *Ber. Bunsenges. Phys. Chem.*, 72, 998 (1968).

(14) G. Skirrow and H. G. Wolfhard, *Proc. Roy. Soc., Ser. A*, 232, 78 (1955).

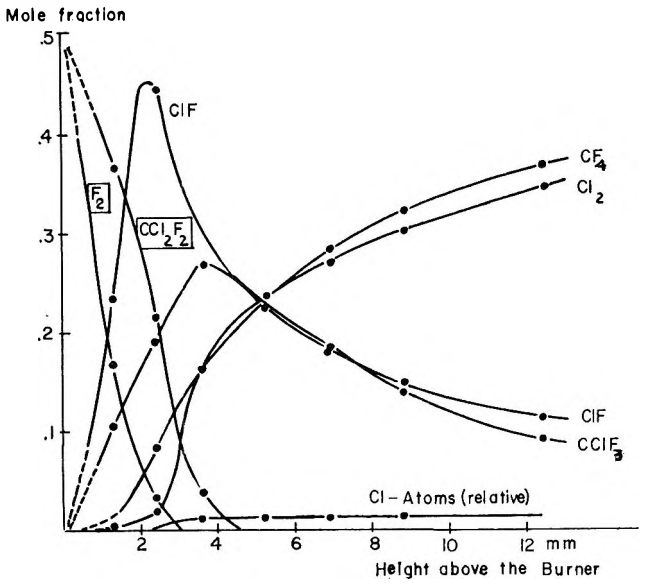

Figure 3. Concentration profiles for a stoichiometric CCl_2F_2–F_2 flame burning at a pressure of 77 mm. Flow rates measured at 1 atm pressure were 6.0 cc/sec each for fuel and oxidizer.

guishable. In the first zone extending to about 2.5–3 mm above the burner F_2 is the oxidizing agent. The ClF formed during the phase of the reaction almost reaches the input concentration level of F_2. The second flame zone begins with an increase in the concentration of Cl_2 which is barely formed in the first phase of the reaction. In the second flame zone no more F_2 is present and the ClF now acts as an oxidant. The fact that the ClF concentration decreases much more slowly than that of F_2 although the temperatures in the second flame zone are higher than in the first, shows that the net reaction $ClF + CF_3Cl \rightarrow CF_4 + Cl_2$ is much slower than the net reaction $F_2 + CCl_2F_2 \rightarrow CF_3Cl + ClF$. The former finally becomes so slow that no further change in concentration can be measured under these conditions although the thermodynamic equilibrium is on the side of CF_4 and Cl_2. The profile of chlorine atoms rises at the end of the fluorine reaction zone and shows comparatively little change afterwards. The concentration of fluorine atoms was below the limits of detectability for this species which was about 0.005 mole fractions. These reaction profiles confirm the previous finding that no product with more than one carbon atom per molecule is formed.[6]

Discussion

Chlorine and fluorine atoms have been identified as active particles and probably chain carriers. Fluorine atoms reached the limit of detectability only in the F_2 reaction zone of the flame. Concentrations of both atoms are connected to those of ClF and Cl_2 through the reaction

$$Cl + ClF \rightleftarrows F + Cl_2 \qquad (4)$$

It has recently been shown by Warnatz and coworkers[16] that this reaction is extremely rapid in the backward direction. The Arrhenius expression for the rate constant is given as

$$k_{-4} = 5.5 \times 10^{14} \exp(-1400/RT) \text{ cm}^3 \text{ mol}^{-1} \text{ sec}^{-1}$$

The equilibrium constant of reaction 4 and its temperature dependence is known[17] so that the rate constant of the reaction can be calculated

$$k_4 \approx 4.7 \times 10^{14} \exp(-3400/RT) \text{ cm}^3 \text{ mol}^{-1} \text{ sec}^{-1}$$

Thus, both reactions are fast enough to justify the assumption of chemical equilibrium of reaction 4 throughout the whole flame. That is, with the knowledge of the equilibrium constant K_4 and the measured concentrations of ClF and Cl_2 the ratio of the fluorine atom to chlorine atom concentration can be evaluated at every site in the flame

$$\frac{[F]}{[Cl]} = K_1 \frac{[ClF]}{[Cl_2]}$$

K_4 is dependent on the temperature, but this dependence is rather weak since the value of K_4 changes from 600 to 1600°K only by a factor of 3, namely from 0.16 to 0.48 and by a factor of 2 between 800 and 1600°K.

Owing to experimental difficulties a temperature profile has not yet been measured in this flame. Direct measurements by means of a thermocouple failed because of the lack of a suitable coating material in an environment containing F_2, ClF, and F atoms. A thin coating of sapphire on a Pt—Pt-Rh thermocouple would be the most promising, but it was not possible to obtain a suitably thin-walled tube. Van Tiggelan and coworkers have thrown some doubt on the applicability of the sodium line reversal method to fluorine supported flames.[18] A reexamination of this method in the special case of halocarbon–fluorine flames is underway, but it would be preferable to have an independent method by which the results of the

(15) It was first thought that the HCl was due to an impurity containing hydrogen in the Freon-12. However, in that case HF and not HCl should be formed in the flame. Moreover, careful mass spectral analysis of the Freon-12 revealed no significant contamination. Most probably the HCl results from the reaction of Cl atoms from the beam with water on the wall of the mass spectrometer. The Cl-atom profile through the flame is similar to that of HCl. The same effect has been observed in recent experiments in Göttingen.

(16) J. Warnatz, H. G. Wagner, and C. Zetsch, *Ber. Bunsenges. Phys. Chem.*, **75**, 119 (1971).

(17) Thermochemical Data from JANAF Thermochemical Tables and Addenda, Dow Chemical Co., Midland, Mich., 1965–1969. $CClF_3$: J. W. Coomber and E. Whittle, *Trans. Faraday Soc.*, **63**, 2656 (1967); CF_4: J. R. Lacher and H. A. Skinner, *J. Chem. Soc. A*, 1034 (1968).

(18) P. J. Slootmaekers and A. VanTiggelan, *Bull. Soc. Chim. Belg.*, **67**, 135 (1958). In an attempt to apply the Na-line reversal technique to temperature measurements of H_2–F_2 flames in our laboratory no emission was observed from the Na doublet. This may be explained by the displacement of the dissociation equilibrium of the salt ($NaF \rightleftarrows Na + F$) due to the large concentration of F atoms in the flame.

line reversal method could be checked. For this reason only an estimate of the temperature profile can be presented here.

The adiabatic flame temperature for a burning mixture $CCl_2F_2 + F_2$ at 77 Torr is about 2040°K for an equilibrium composition of mainly $CF_4 + 1.72Cl + 0.14Cl_2$. This temperature is not reached in the flame since the reaction does not go to completion, and an appreciable amount of heat is lost to the cooled burner and to the surroundings. Very probably the temperature does not increase above 1700°K. With the assumption of 20% heat loss to the burner, which is a reasonable figure for the type of burner used, one calculates a rise in temperature to about 1500°K at the height of maximum ClF concentration. The temperature will rise a little further in the ClF reaction zone but will soon level off due to heat losses to the surroundings of the flame. The temperature in this zone of the flame should be somewhere between 1500 and 1700°K. The temperature profile from the burner mouth to 1500°K at the height of the ClF maximum is taken as linear. Since the temperature profile thus obtained is used only to obtain a value for the equilibrium constant K_4 which, as we have seen, is not strongly dependent on temperature in this range, this rough estimate appears justified.

The value of the [F]/[Cl] ratio through the flame can then be calculated and is presented in the following table.

Height above the burner, mm	1.3	2.4	3.6	5.2	6.9	8.8	12.4
[F]/[Cl] ratio	15	10	0.9	0.5	0.3	0.2	0.15

In the F_2 reaction zone the F-atom concentration is much higher than that of the Cl atom due to a rapid increase in the ClF concentration. Close to the point of disappearance of F_2 the concentration of Cl atoms equals that of F atoms. After this point there is a steady decrease in the absolute F-atom concentration as can be judged from the almost constant Cl-atom concentration (Figure 3). This is in line with the decrease in reaction rate in the ClF reaction zone as seen from the profiles. The reaction does not go to completion although the equilibrium is far on the side of CF_4 and Cl_2.

In contrast to hydrocarbon–oxygen and hydrocarbon–fluorine flames[19] products with more than one carbon atom per molecule are not formed in flames of perhalogenated methanes with fluorine. This is also true for fuel-rich mixtures of this type. In the pyrolysis of CCl_2F_2 and related compounds at higher temperatures, however, such products are found. This shows that carbon-containing radicals such as $CClF_2\cdot$, $CF_2\cdot\cdot$, or $CCl_2F\cdot$ do not reach a concentration large enough to make them important intermediates in the reaction mechanism of this flame. This can be understood in view of the fact that reactions such as

$$F + CClF_3 \longrightarrow CF_3 + ClF$$

are endothermic by about 25 kcal/mol.[17] The possibility of disregarding reactions with carbon-containing radicals simplifies the reaction mechanism considerably. Thus only those reactions need be considered in which chlorine atoms are directly displaced by fluorine atoms.

The simplest reaction mechanism which explains all experimental results would then be

	ΔH°_{298} (kcal/mol)[17]	
$F + CCl_2F_2 \longrightarrow CClF_3 + Cl$	−44	(1)
$Cl + F_2 \longrightarrow ClF + F$	−22	(2)
$F + CClF_3 \longrightarrow CF_4 + Cl$	−43	(3)
$ClF + Cl \rightleftarrows Cl_2 + F$	+2	(4)

What reaction products would result if radicals played a role in this flame can easily be demonstrated if hydrogen is added to the burning mixture. Hydrogen atoms which are then formed give rise to radicals *via* abstraction reactions of the type

$$CClF_3 + H \longrightarrow HCl + CF_3 \qquad (5)$$

which in turn lead to a variety of higher fluorinated hydrocarbons such as C_2F_4, C_3F_6, C_4F_8, etc.[6]

Evidence for substitution reactions such as reactions 1 and 3 also comes from the work of Wai and Rowland who studied reactions of nuclear recoil chlorine-38 and chlorine-39 atoms.[20] The atoms undergo substitution reactions with normal Cl atoms in organic halides with almost complete retention of the optical configuration at the asymmetric C atom to which the Cl is bound. Similarly "concerted" substitution reactions with hot F atoms have been observed by McKnight, *et al.*[21]

As could be expected from the shock tube data on the rate of the unimolecular decomposition of fluorine[22] the reaction

$$F_2 \longrightarrow 2F \qquad (6)$$

does not play a great role for the disappearance of F_2 in this flame. This can be judged from the very low concentration of Cl atoms in the F_2 reaction zone of the flame. During the steep decrease of the F_2 concentration the combustion is mainly governed by the reactions 1 and 2. If reaction 6 had to be included a

(19) K. H. Homann and D. I. MacLean, *Ber. Bunsenges. Phys. Chem.*, **75**, 945 (1971).

(20) C. M. Wai and F. S. Rowland, *J. Phys. Chem.*, **71**, 2752 (1967).

(21) C. F. McKnight, N. J. Parks, and J. W. Root, *ibid.*, **74**, 217 (1970).

(22) R. W. Diesen, *J. Chem. Phys.*, **44**, 3662 (1966); *J. Phys. Chem.*, **72**, 108 (1968).

steady-state treatment for the F atoms would lead to a rate for the Cl-atom formation

$$\frac{d[Cl]}{dt} \approx 2k_6[F_2]$$

about equal to the F-atom production from the assumed unimolecular decomposition of F_2. The experiment shows that the increase in Cl-atom concentration in the first part of the flame is far from being comparable to the decrease of F_2. For the problem of flame ignition and propagation in this system, however, reaction 6 can be important.

Reaction 2 has not yet been measured directly. It is probably comparable in rate to the back reaction of 4. In the second reaction zone of the flame beginning where the F_2 is consumed ClF acts as the oxidizer. This zone is mainly governed by reactions 3 and 4. In its beginning reaction 1 still plays a role. The steep increase in Cl_2 concentration is due to the equilibration of (4). As soon as the F_2 concentration is sufficiently down, Cl_2 is formed by (4) almost as rapidly as the ClF in the F_2 reaction zone of the flame. The slowing down of the Cl_2 production at about 4 mm above the burner is connected to the disappearance of CCl_2F_2 at this height. Reaction 3 must be slower than reaction 1, and this means that the formation of Cl atoms is correspondingly slower and as a consequence the Cl_2 formation, too. The continuing decrease of the F-atom concentration then leads to a further deceleration of the conversion of $CClF_3$ and ClF into CF_4 and Cl_2.

A value for the ratio k_1/k_3 at the site of the $CClF_3$ maximum, that is, at a temperature of about 1600°K, is given by

$$\frac{k_1}{k_3} = \frac{[CClF_3]_{max}}{[CCl_2F_2]} \approx 7$$

Absolute rate constants are not known for these two reactions.

A rough estimate of the ratio k_2/k_1 can be given for the 2.4-mm height above the burner, *i.e.*, for a temperature of about 1500°K, from the slopes of the F_2 and the CCl_2F_2 profiles together with the [F]/[Cl] ratio at this point

$$\frac{k_2}{k_1} \approx \frac{d[F_2]}{d[CCl_2F_2]} \cdot \frac{[CCl_2F_2][F]}{[F_2][Cl]} \approx 50$$

It shows at least that reactions 1 and 3 are much slower than reactions 2 and 4, which is probably due to an appreciable activation energy of the former. This is in line with recent measurements of the rate of reaction of F atoms with CCl_4 at room temperature[23] which is found to be much lower ($k = 4 \times 10^{10}$ cm^3 mol^{-1} sec^{-1}) than the rate of the reverse reaction of (4).

Acknowledgment. This research was supported in part by the Air Force Office of Scientific Research under Grant No. 68-1523 and by the Office of Naval Research under THEMIS Contract N00014-69-A-0453. One of the authors (K. H. Homann) expresses his gratitude to the National Science Foundation for a Senior Foreign Scientist Fellowship.

(23) C. Zetsch, Dissertation, University of Göttingen, 1971.

Energy Partitioning on Photolysis of Di-*tert*-butyl Peroxide

by F. H. Dorer* and S. N. Johnson

Chemistry Department, California State College, Fullerton, California 92631 *(Received June 14, 1971)*

Publication costs borne completely by The Journal of Physical Chemistry

The pressure dependence of the unimolecular rate constant for the decomposition of vibrationally excited *tert*-butoxy radicals produced on photolysis of di-*tert*-butyl peroxide and isopropyl-*tert*-butyl peroxide by 313-, 256-, and 249-nm radiation has been measured. Comparison of the experimental results to rate constants calculated for *tert*-butoxy radical decomposition using RRKM theory indicate that energy partitioning on photolysis of the peroxides is nonrandom. The *tert*-butoxy radicals have a fairly narrow internal energy distribution function which is independent of the choice of peroxide reactant, and it changes relatively little on significantly increasing the excitation energy of the peroxide. The energy partitioning and quantum yield measurements do indicate that on absorption of a photon the peroxides directly dissociate to products by a single process.

Introduction

By observing the kinetic behavior of the vibrationally excited products produced in the primary process, it has been possible to extend the investigation of energy partitioning in photochemical reactions to molecules sufficiently complex[1] that they cannot be studied by the elegant spectroscopic techniques used for smaller molecules.[2] To date the photodissociation reactions that have been studied in some quantitative detail by this kinetic technique have been generally of the type in which the chromophore is not actually the site of chemical bond breaking. Particularly for cyclobutanone[1a,b] and 1-pyrazoline photolysis,[1e-h] it is plausible that at least some of the initially localized electronic excitation energy must become vibrational energy before fragmentation can occur,[3] and the product energy distribution may reflect the mechanistic details of the fragmentation reaction.[1e-g] By contrast, the photolysis of the alkyl peroxides represent a type of reaction in which fragmentation occurs at the bond which has initially been excited by absorption of the photon, and it is likely that absorption leads to direct dissociation to products by simple O–O bond rupture.[4] The photolysis of di-*tert*-butyl peroxide offers the added advantage over many systems in that, since there is only one kind of fragment produced in the primary step, it is possible to measure all of the energy that appears as vibrational energy of the reaction products.

McMillan and coworkers have investigated the extent of fragmentation of the alkoxy radicals produced on photolysis in the gas phase of several alkyl peroxides.[1i,5] However, for several reasons that are mentioned in the Discussion, their data are only of qualitative significance. We, therefore, have carried out this study characterizing the internal energy content of the *tert*-butoxy radicals produced on photolysis of di-*tert*-butyl peroxide and isopropyl-*tert*-butyl peroxide. The results of the energy partitioning experiments prompted us to also measure the absolute quantum yield for decomposition of di-*tert*-butyl peroxide near its long wavelength absorption limit.

Experimental Section

The di-*tert*-butyl peroxide was from a commercial sample that had been purified by distillation at reduced pressure and subsequently dried over anhydrous magnesium sulfate. The isopropyl-*tert*-butyl peroxide was prepared from *tert*-butyl hydroperoxide and isopropyl bromide by the method of Dickey and Bell.[5a] The distilled product was further purified by glpc. Instrument grade isobutane was used as a diluent. The small amount of hydrocarbon impurities in the diluent did not interfere with the product analysis.

The products were analyzed by glpc. A 20% diethylene glycol succinate on Chromosorb P column (DEGS) was used for the analysis of acetone, *tert*-butyl alcohol, isopropyl alcohol, the reactant peroxide, and isobutane. Methane and CO were separated on a Linde 13X molecular sieve column. For a number of

(1) (a) R. F. Klemm, D. N. Morrison, P. Gilderson, and A. T. Blades, *Can. J. Chem.*, **43**, 1934 (1965); (b) R. J. Campbell and E. W. Schlag, *J. Amer. Chem. Soc.*, **89**, 5103 (1967); (c) B. C. Roquette, *J. Phys. Chem.*, **70**, 1334 (1966); (d) H. M. Frey and I. D. R. Stevens, *J. Chem. Soc.*, 4700 (1964); (e) T. F. Thomas, C. I. Sutin, and C. Steel, *J. Amer. Chem. Soc.*, **89**, 5107 (1967); (f) F. H. Dorer, *J. Phys. Chem.*, **73**, 3109 (1969); *ibid.*, **74**, 1142 (1970); (g) F. H. Dorer, E. Brown, J. Do, and R. Rees, *ibid.*, **75**, 1640 (1971); (h) P. Cadman, H. M. Meunier, and A. F. Trotman-Dickenson, *J. Amer. Chem. Soc.*, **91**, 7640 (1969); (i) D. Durant and G. R. McMillan, *J. Phys. Chem.*, **70**, 2709 (1966).

(2) (a) N. Basco and R. G. W. Norrish, *Discuss. Faraday Soc.*, **33**, 99 (1962); (b) R. C. Mitchell and J. P. Simons, *ibid.*, **44**, 208 (1967); (c) T. Carrington, *J. Chem. Phys.*, **41**, 2012 (1964); (d) K. E. Holdy, L. C. Klotz, and K. R. Wilson, *ibid.*, **52**, 4588 (1970); (e) M. J. Berry and G. C. Pimentel, *ibid.*, **51**, 2274 (1969).

(3) S. A. Rice, I. McLaughlin, and J. Jortner, *ibid.*, **49**, 2756 (1968).

(4) D. H. Volman, "Advances in Photochemistry," Vol. I, W. A. Noyes, Jr., G. S. Hammond, and J. N. Pitts, Jr., Ed., Interscience, New York, N. Y., 1963, p 69.

(5) (a) G. R. McMillan, *J. Amer. Chem. Soc.*, **84**, 2514 (1962); (b) *ibid.*, **82**, 2422 (1960).

experiments at 256 nm we also determined the relative amounts of ethane, neopentane, and isobutylene on a 30% hexamethyl phosphoramide on Chromosorb P column kept at 0° followed by the DEGS column at 60°. The 256-nm experiments were analyzed on a Loenco Model 15B chromatograph, and the 249- and 313-nm experiments were analyzed on a Hewlett-Packard Model 5750 instrument. The retention times and relative thermal conductivity cell sensitivities for all of the products were determined by calibration mixtures made up from authentic samples. Analysis of the 256-nm runs was achieved by admitting a known fraction of the entire run mixture (after photolysis) into the vacuum inlet loop of the glpc. For the other two wavelengths the noncondensables at liquid nitrogen temperature were first separated by use of a Toepler pump; then the acetone, peroxide, and *tert*-butyl alcohol were separated from the isobutane and other products by fractional distillation at −115°. The carbon monoxide and methane were then frozen into the glpc inlet loop packed with Linde 5A molecular sieve kept at liquid nitrogen temperature.

All gas handling was carried out on a conventional high vacuum apparatus. Two cylindrical photolysis cells were used; one was 50-mm o.d. with a total volume of 302 cm^3, and the other was 25-mm o.d. with a total volume of 51 cm^3.

The light source for the 256-nm runs was an Hanovia 550-W mercury lamp enclosed in a water-cooled housing. A three-compartment quartz solution filter served to isolate the 254-nm region of the lamp output.[6] Superposition of the lamp output, solution filter transmission curve, and absorption spectra of the peroxide[7] gave the average wavelength absorbed by the reactant to be 256 nm. The 249- and 313-nm radiation source was an Osram HBO 200-W super pressure mercury lamp followed by a Bausch and Lomb high intensity monochromator (Model No. 5). The output of this combination was calibrated by the use of a Hilger-Engis 1000 grating monochromator. All photolysis experiments were carried out at room temperature.

The quantum yield measurements at 313 nm were made by using conventional potassium ferrioxalate actinometry[8] to determine the incident light intensity. By use of an appropriate system of lenses the incident radiation was collimated through the photolysis cell and then focused on a IP-28 photomultiplier tube. The relative light intensity was continuously recorded throughout each quantum yield experiment.

Results

The primary photodissociation process that occurs on photolysis of di-*tert*-butyl peroxide is[9]

$$(CH_3)_3COOC(CH_3)_3 + h\nu \longrightarrow 2(CH_3)_3CO\cdot^* \quad (a)$$

The *tert*-butoxy radicals formed in (a) have sufficient internal energy to undergo further fragmentation unless they are collisionally stabilized by the bath molecules

$$(CH_3)_3CO\cdot^* \xrightarrow{k_a} CH_3\cdot + (CH_3)_2C{=}O \quad (b)$$

$$\xrightarrow{\omega} (CH_3)_3CO\cdot \quad (c)$$

When the photolysis is carried out with a large excess of isobutane (isobutane/peroxide > 20:1) the collisionally stabilized *tert*-butoxy radicals are effectively scavened by abstracting a hydrogen atom from isobutane to form *tert*-butyl alcohol. McMillan[5b] has shown that under these conditions free-radical reactions with the peroxide reactant are negligible. Therefore, the unimolecular rate constant for decomposition of the vibrationally excited *tert*-butoxy radicals formed in (a) can be calculated from

$$k_a = \omega(\text{acetone}/\textit{tert}\text{-butyl alcohol}) \quad (1)$$

where ω is the collisional deactivation rate. The small amount of the acetone that is photolyzed is included in eq 1 by measurement of the relative amount of CO in the products. That eq 1 is appropriate, when applied to the photolysis of dilute mixtures of peroxide in isobutane, was further substantiated by the independence of the calculated values of k_a on mixture ratio (20:1 to 75:1), and the per cent of the peroxide converted into products.

The collisional deactivation rate, ω, was calculated using Lennard-Jones collision cross sections;[10,11] the Lennard-Jones potential constant parameters were estimated for *tert*-butoxy radicals. The assumption of unit collision efficiency of deactivation of *tert*-butoxy by isobutane seems particularly valid since only ~10 kcal mol^{-1} need be removed from the radicals to take them out of the reaction channel.[12] The deactivation rate calculated for the *tert*-butoxy radicals having a Boltzmann distribution of velocities at 25° is

$$\omega/p = 2.17 \times 10^7 \text{ collisions}/(\text{sec Torr}) \quad (2)$$

The experimental k_a values are illustrated in Figures 1 and 2 for photolysis of di-*tert*-butyl peroxide and isopropyl-*tert*-butyl peroxide at effective wavelengths of 249, 256, and 313 nm. These wavelengths represent the superposition of the energy distribution from the light sources and filter combinations or monochromator and the absorption spectrum of the peroxide.[7] The

(6) J. G. Calvert and J. N. Pitts, Jr., "Photochemistry," Wiley, New York, N. Y., 1966, p 729.

(7) Reference 6, p 443.

(8) Reference 6, p 783.

(9) Reference 6, p 447.

(10) J. O. Hirschfelder, C. F. Curtiss, and R. B. Bird, "Molecular Theory of Gases and Liquids," Wiley, New York, N. Y., 1954.

(11) G. H. Kohlmaier and B. S. Rabinovitch, *J. Chem. Phys.*, **38**, 1962 (1963).

(12) (a) G. H. Kohlmaier and B. S. Rabinovitch, *ibid.*, **38**, 1709 (1963); (b) J. W. Simons, B. S. Rabinovitch, and D. W. Setser, *ibid.*, **41**, 800 (1964).

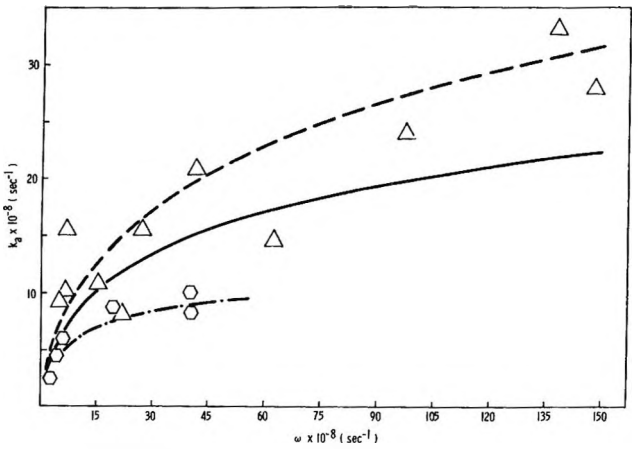

Figure 1. The experimental and calculated values of k_a as a function of ω: △ are experimental points for photolysis of di-*tert*-butyl peroxide by 313-nm radiation; ○ are experimental points for photolysis of isopropyl-*tert*-butyl peroxide by 313-nm radiation. The broken line is a calculated curve with E_{mp} = 19.5 kcal mol^{-1} and σ = 3.5 kcal mol^{-1}; the solid line is a calculated curve with E_{mp} = 19 kcal mol^{-1} and σ = 3 kcal mol^{-1}; —·— is a calculated curve with E_{mp} = 18.5 kcal mol^{-1} and σ = 2 kcal mol^{-1}.

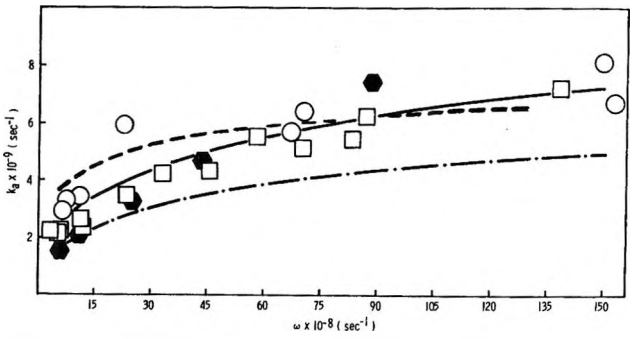

Figure 2. The experimental and calculated values of k_a as a function of ω: ○ are experimental points for 249-nm photolysis of di-*tert*-butyl peroxide; □ are experimental points for 255-nm photolysis of di-*tert*-butyl peroxide; ○ are experimental points for 255-nm photolysis of isopropyl-*tert*-butyl peroxide. The solid line is a calculated curve with E_{mp} = 22 kcal mol^{-1} and σ = 3 kcal mol^{-1}; the broken line is a calculated curve with E_{mp} = 22 kcal mol^{-1} and σ = 2 kcal mol^{-1}; —·— is a calculated curve with E_{mp} = 21 kcal mol^{-1} and σ = 3 kcal mol^{-1}.

band pass of the incident radiation at these three wavelengths was 10, 18, and 11 nm, respectively.

The relationship between the experimentally observed unimolecular rate constants and the microscopic unimolecular rate constants for decomposition of a *tert*-butoxy radical with internal energy content E, k_E, is

$$k_a = \omega \frac{\sum_{E_T} \frac{k_E}{k_E + \omega} f(E)}{\sum_{E_T} \frac{\omega}{k_E + \omega} f(E)} \quad (3)$$

where f(E) is the internal energy distribution function of the radicals formed in (a). The rate constants, k_E, were calculated using the RRKM rate expression.[13] The details of all of the rate and energy distribution calculations, including the necessary molecular vibrational frequency assignments and the thermochemistry, are given in the Appendix. We assumed f(E) to be a Gaussian;[1e-g] therefore, there are only two adjustable parameters for fitting the calculated curves to the experimental data E_{mp}, the most probable energy of the formed *tert*-butoxy radicals, and σ, the dispersion of f(E). The calculated curves that best fit the experimental data are also illustrated in Figures 1 and 2. These curves were calculated assuming the *tert*-butoxy radicals have a thermal velocity distribution at 25°.

In Table I we give the results of the quantum yield measurements for decomposition of di-*tert*-butyl peroxide by 313-nm radiation using a value of 0.85 l. mol^{-1} cm^{-1} for ϵ, the extinction coefficient.[7] Our measurement of ϵ, using the Cary 15 instrument and a 10-cm path length cell, is 1.2 l. mol^{-1} cm^{-1} which leads to a quantum yield for decomposition of 0.81 ± 0.07. The data of Table I indicate that within the uncertainty of the value of ϵ the quantum yield is unity at 313 nm, and it is pressure independent to ~1 atm. The quantum yield at 254 nm is also unity.[14]

Table I: Quantum Yield Measurements for Decomposition of Di-*tert*-butyl Peroxide by 313-nm Radiation[a]

Total pressure, Torr	Peroxide pressure, Torr	$I_0 \times 10^{-17}$,[b] photons/min	Photolysis time, min	Per cent reaction[c]	ϕ_0[d]
24	1.4	6.1	57	2.1	0.95
31	2.0	5.8	66	2.6	1.1
192	2.2	5.9	60	2.8	1.2
635	1.4	6.0	57	2.2	1.0
685	3.3	5.9	89	3.9	1.2

[a] Quantum yields measured at room temperature in a 10-cm path length cell of 51 cm^3 total volume. The diluent gas is isobutane. [b] Total incident photon intensity. [c] Measured by the relative amount of acetone and *tert*-butyl alcohol produced. [d] Assuming the extinction coefficient at 313 nm is 0.85 l. mol^{-1} cm^{-1} (ref 7).

Discussion

The extent of fragmentation of the alkoxy radicals formed on photolysis of various alkyl peroxides has been semiquantitatively studied using the nitric oxide radical trapping technique.[5a] Our results for the photolysis by 256-nm radiation of di-*tert*-butyl peroxide indicate a much greater degree (a factor of ~2 to 3) of fragmentation of the excited *tert*-butoxy radicals formed in (a) than observed by the nitric oxide trapping technique. The implication, particularly in view of its probable rel-

(13) R. A. Marcus, *J. Chem. Phys.*, **43**, 2658 (1965); *ibid.*, **20**, 359 (1952).

(14) L. M. Dorfman and Z. W. Salsburg, *J. Amer. Chem. Soc.*, **73**, 255 (1951).

ative inefficiency in vibrationally deactivating excited species,[12] is that nitric oxide also scavenges an appreciable fraction of the vibrationally excited *tert*-butoxy radicals. Therefore, quantitative comparison of the results of this earlier work to the present study is perhaps not appropriate.

One model for energy partitioning is that all of the energy in excess of that required to rupture O–O bond, E^+, is randomly distributed to the degrees of freedom of the reaction products. For such a model one would calculate the internal energy content of the vibrational degrees of freedom of the *tert*-butoxy fragments from[1g,15]

$$f(E) = \frac{N(E) \sum_{E^+}^{E^+-E} P_R(E^+ - E)}{\sum_{E^+} P^+(E_v)} \quad (4)$$

where $N(E)$ is the density of states for the internal degrees of freedom of the peroxide activated complex that will become internal degrees of freedom of the *tert*-butoxy fragment, and the sum term in the numerator is the sum of states for those internal degrees of freedom that will become the translational and rotational degrees of freedom of the fragments, and the internal degrees of freedom of the complementary fragment. The normalization term in the denominator is the sum of states for all of the internal degrees of freedom of the peroxide complex having excess energy E^+. By use of both the appropriate approximation[16] and an exact sum computer program[17] to evaluate (4), we find that a statistical model for energy partitioning would result in *tert*-butoxy radicals having internal energy contents of 35 and 25 kcal mol^{-1} for photolysis at 254 nm (E^+ = 83 kcal mol^{-1} including the thermal energy of the reactant) and 313 nm (E^+ = 61 kcal mol^{-1}). The results illustrated in Figures 1 and 2 indicate that the internal energy content of the *tert*-butoxy radicals is considerably less, particularly for photolysis at 249 and 256 nm, than predicted by statistical theory. Moreover, the widths (2σ) of the Gaussians that best fit the experimental data are substantially narrower than the widths of the statistical distribution functions calculated from (3). For photolysis at 254 nm a statistical $f(E)$ would have a width of ~17 kcal mol^{-1}; the width would be 11 kcal mol^{-1} on photolysis by 313-nm radiation. For both wavelengths the Gaussians that best fit the data have widths of only 6–7 kcal mol^{-1}, and part of this energy spread is due to the bandwidth of the absorbed radiation and the thermal energy of the reactant.

If the methyl groups did effectively participate in any electronic-vibrational intramolecular energy relaxation process that might occur prior to actual fragmentation of the peroxide, eq 3 allows one to predict that the *tert*-butoxy radicals produced on photolysis of isopropyl-*tert*-butyl peroxide would contain about 3.6 kcal mol^{-1} greater internal energy than the *tert*-butoxy radicals formed on photolysis of di-*tert*-butyl peroxide at the same wavelength. Our RRKM calculations would then indicate that k_a for the *tert*-butoxy fragments derived from 313-nm photolysis of the asymmetric peroxide would be four times greater than the value for radicals produced by 313-nm photolysis of di-*tert*-butyl peroxide. The data in Figures 1 and 2 illustrate that considerably altering the vibrational complexity of the molecule at positions removed from the reaction center does not affect energy partitioning.

At this point it is appropriate to summarize the pertinent experimental observations. Although the uncertainty associated with the choice of the kinetic parameters for *tert*-butoxy radical decomposition makes the actual magnitude of their internal energy content less well known, the observation that the radicals formed in (a) are relatively monoenergetic, and that their internal energy content is insensitive to the vibrational complexity of the reactant, illustrates that intramolecular energy relaxation on photodissociation of the peroxides studied here is nonrandom.

On rupturing of the O–O bond both ends of the molecule receive about the same amount of vibrational energy. Increasing the excess energy available for partitioning from 61 to 84 kcal mol^{-1} only increases the total vibrational energy of the fragments by about 6 kcal mol^{-1}.

These experimental observations combined with the fact that the absorption spectrum of di-*tert*-butyl peroxide is continuous and structureless from about 350 nm,[7] and the quantum yield for decomposition is unity at 313 nm and independent of pressure, indicate that, like hydrogen peroxide photolysis,[4] absorption results in direct dissociation by only one process.

A limiting model that might describe energy partitioning for direct dissociation would be an impulsive model.[2d,18] If it is assumed that all of the excess energy is initially partitioned to translation of the oxygen atoms, and then the oxygen atoms essentially collide in a "half-collision"[2d] with the *tert*-butyl groups, the conservation of linear momentum would require that 22% of the total excess energy be partitioned to relative translation of the *tert*-butoxy fragments. Correction of the thermal collision frequency, ω, corresponding to the fragments having translational velocities of 6 to 8 kcal mol^{-1} [19] raises the E_{mp} values deduced from the experimental results by ~2 kcal mol^{-1}. If the excited state retained the ground-state geometry, the C–O–O bond angle 105°;[20] consequently, only about 7% of the

(15) Y. N. Lin and B. S. Rabinovitch, *J. Phys. Chem.*, **74**, 1769 (1970).

(16) G. Z. Whitten and B. S. Rabinovitch, *J. Chem. Phys.*, **38**, 2466 (1963).

(17) Kindly supplied by Professor Rabinovitch.

(18) G. Karl, P. Kruus, and J. C. Polanyi, *J. Chem. Phys.*, **46**, 224 (1967).

(19) S. W. Benson, "The Foundations of Chemical Kinetics," McGraw-Hill, New York, N. Y., 1960, p 152.

remaining energy would appear as vibration of the CO bond; about 93% would appear as rotational excitation of the fragments. It would seem unlikely that of the energy partitioned to overall rotation, 70 to 90% of it, depending on wavelength of photolysis, would in turn be partitioned to a bending vibrational mode of the *tert*-butoxy fragment.

Since the initial excitation of the peroxide is supposed to be a $\pi^* \rightarrow \sigma^*$ type,[7] implying some bound nature in the excited state, conceivably there could be a curve crossing to a repulsive surface at a larger C–O–O bond angle which leads to dissociation. An impulsive model would be consistent with the experimental results if this crossing were in the region of a C–O–O bond angle of 150° for 313-nm photolysis and about 10° less for 249-nm photolysis.

There has been some success at correlating product energy distributions in some photochemical reactions with structure changes that must occur on forming products.[1e-g,2b] A model for these peroxides might be that all of the vibrational excitation of the *tert*-butoxy fragment is initially localized in the CO bond due to a change in its bond length on going from the electronically excited di-*tert*-butyl peroxide to a ground electronic state *tert*-butoxy fragment. If the *tert*-butoxy fragment is approximated to be essentially a diatomic molecule with a dissociation energy of 91 kcal mol^{-1} [21] and a vibrational frequency of 1400 cm^{-1}, use of a Morse potential function would indicate that the C–O bond length must change by ~0.07 Å on going from the reactant to products in order to cause the *tert*-butoxy radicals to receive about 17 kcal mol^{-1} of internal energy.

Comparison of the structure of hydrogen peroxide[22] with the structure of an OH radical indicates that, at most, a change of ~0.02 Å is more likely. It appears that for this system bond length changes cannot account for the product energy distribution.

Acknowledgments. This work has been supported by the National Science Foundation (NSF Grants GP-9489 and GP-28266). The valuable assistance of Mr. James Do with the computer calculations is gratefully acknowledged.

Appendix

The vibrational frequency assignments for the *tert*-butoxy radical and its activated complex are given in Table II. The ratio of the products of the principal moments of inertia was taken to be 2.1,[23] and the reaction path degeneracy to form acetone and a methyl radical is three. This model gave a calculated[24] thermal frequency factor of $10^{14.96}$ at 400°K; a value which is in good agreement with the value of Quee and Thynne.[25] However, the corresponding activation energy measurement, 22.8 kcal mol^{-1},[25] gave E_{mp} values that were greater than the total amount of energy available to the reaction products on photolysis by 313-nm radiation. Therefore, we used the more generally accepted value of 16.5 kcal mol^{-1} [23,26] for these calculations. The density of states for the radical was calculated using the approximation of Whitten and Rabinovitch;[16] an exact sum computer program was used for calculating the sum of states.[17] The complex assignment was grouped into a seven frequency model of the appropriate degeneracies for the sum calculation.

Table II: Vibrational Frequency Assignment for the *tert*-Butoxy Radical and Activated Complex

Molecule	Complex
2958 (6)	2964 (9)
2920 (2)	1392 (12)
2907 (1)	905 (4)
1477 (1)	589 (2)
1450 (5)	458 (3)
1400 (1)	229 (2)
1394 (1)	151 (3)
1370 (2)	
1184 (1)	
1172 (2)	
966 (3)	
918 (2)	
795 (1)	
463 (2)	
433 (1)	
367 (2)	
220 (2)	
200 (1)	

The vibrational frequency assignment for the di-*tert*-butyl peroxide activated complex that is needed to evaluate eq 4 was made up of two *tert*-butyl fragments plus those vibrational degrees of freedom of the complex that become translational and rotational degrees of freedom of the fragments. These latter modes were the double degenerate C–O–O deformation (94 cm^{-1}), the doubly degenerate C–O torsion (38 cm^{-1}), the O–O torsion (56 cm^{-1}), and the O–O stretching mode. This complex gave a calculated thermal frequency factor that agreed within 0.2 log units of the experimental value.[27] The critical energy for O–O bond rupture was 36.4 kcal mol^{-1}.[27]

(20) W. Lobuenz, J. R. Rittenhouse, and J. G. Miller, *J. Amer. Chem. Soc.*, **80**, 3505 (1958).

(21) Reference 6, p 820.

(22) V. Kaldor and I. Shavitt, *J. Chem. Phys.*, **44**, 1823 (1966).

(23) D. M. Golden, R. K. Solly, and S. W. Benson, *J. Phys. Chem.*, **75**, 1333 (1971).

(24) S. Glasstone, K. J. Laidler, and H. Eyring, "The Theory of Rate Processes," McGraw-Hill, New York, N. Y., 1941, p 191.

(25) M. Y. Quee and J. C. J. Thynne, *Trans. Faraday Soc.*, **63**, 2970 (1967).

(26) L. Batt and F. R. Cruickshank, *J. Phys. Chem.*, **71**, 1836 (1967).

(27) L. Batt and S. W. Benson, *J. Chem. Phys.*, **36**, 895 (1962).

Vacuum-Ultraviolet Photolysis of the C_4H_6 Isomers. III. Cyclobutene

by A. DeLeon and R. D. Doepker*

Department of Chemistry, University of Miami, Coral Gables, Florida 33124 *(Received June 25, 1971)*

Publication costs assisted by The National Science Foundation

The photolysis of cyclobutene was investigated, using xenon (147.0 nm), krypton (123.6 nm), and argon (106.7–104.8 nm) resonance radiation. The major products observed were acetylene, ethylene, vinyl acetylene, 1,3-butadiene, and hydrogen. Data are presented that suggest a $(C_4H_6)^{\ddagger}$ diradical as the precursor for vinyl acetylene and a major fraction of the acetylene and ethylene.

$$c\text{-}(C_4H_6) + h\nu \longrightarrow (C_4H_6)^{\ddagger}$$

$$(C_4H_6)^{\ddagger} \longrightarrow C_2H_2 + C_2H_4$$

$$(C_4H_6)^{\ddagger} \longrightarrow 2H + C_4H_4$$

$$(C_4H_6)^{\ddagger} \longrightarrow H_2 + C_2H_2 + C_2H_2$$

The formation of 1,3-butadiene and minor amounts of ethylene were attributed to the reaction sequence

$$H + c\text{-}(C_4H_6) \longrightarrow 1,3\text{-}C_4H_6 + H$$

$$H + c\text{-}(C_4H_6) \longrightarrow C_2H_4 + C_2H_3$$

Although ionization was established during both the krypton and argon photolysis and used as the basis of quantum yield determination at these wavelengths, no products could be identified as originating exclusively from an ion–molecule path.

Introduction

Even though there has been a sharp increase of interest in vacuum-ultraviolet photochemistry during the past few years, a rapid scan of the recent reviews[1-6] of the area still reveals a considerable lack of knowledge of the photochemistry of unsaturated hydrocarbon systems. With this in mind, an investigation of the vacuum-ultraviolet photolysis of cyclobutene is reported here as a continuation of studies to determine the modes of decomposition of electronically excited C_4H_6 molecules.[7,8]

A previous study of the gas-phase photolysis of cyclobutene was conducted by Haller and Srinivasan[9] as part of an investigation of the photolysis of 1,3-butadiene-*1,1,4,4-d*$_4$. The yields of ethylene and acetylene were reported as a function of cyclobutene pressure for the mercury-sensitized photolysis of cyclobutene.

Of particular interest in the photolysis of cyclobutene is a comparison of its modes of decomposition with those of 1,3-butadiene[7] and with its saturated counterpart, cyclobutane.[10]

Experimental Section

Materials. Cyclobutene was prepared from the pyrolysis of trimethyl cyclobutylammonium hydroxide.[11] Cyclobutane carboxylic acid (Aldrich Chemcial Co.) was converted to the trimethylcyclobutylammonium hydroxide through the cyclobutylamine hydrochloride[12] and the trimethylcyclobutylammonium iodide.[13] The resulting cyclobutene was purified by gas chromatography, using a 15-ft, 30% squalane column. The purified material contained 0.006% 1,3-butadiene. No other impurities were observed. D_2S, ND_3, and D_2 were obtained from Merck Sharp and Dohme, Montreal, Canada, and were used without further purification. Purification of other materials used has been described in previous studies.[7,8]

Irradiation. The irradiation procedure has been described previously,[7,8] except for one modification. The cold finger of both the xenon and krypton lamps was replaced by a ballast volume of about 250 cm^3. On the interior of this ballast volume was deposited a thin film of titanium. The construction of these, as well as the

(1) J. R. McNesby and H. Okabe, *Advan. Photochem.*, **3**, 157 (1964).

(2) J. R. McNesby, *Actions Chim. Biol. Radiat.*, **9**, 36 (1966).

(3) P. Ausloos and S. G. Lias in "The Chemistry of Ionization and Excitation," G. R. A. Johnson and G. Scholes, Ed., 1967, p 77.

(4) P. Ausloos and S. G. Lias, *Radiat. Res. Rev.*, **1**, 75 (1968).

(5) P. Ausloos and S. G. Lias, *Ber. Bunsenges. Phys. Chem.*, **72**, 187 (1968).

(6) L. W. Sieck in "Fundamental Processes in Radiation Chemistry," P. Ausloos, Ed., Interscience, New York, N. Y., 1968, p 119.

(7) R. D. Doepker, *J. Phys. Chem.*, **72**, 4037 (1968).

(8) R. D. Doepker and K. L. Hill, *ibid.*, **73**, 1313 (1969).

(9) I. Haller and R. Srinivasan, *J. Amer. Chem. Soc.*, **88**, 3694 (1966).

(10) R. D. Doepker and P. Ausloos, *J. Chem. Phys.*, **43**, 3814 (1965).

(11) J. D. Roberts and C. W. Sauer, *J. Amer. Chem. Soc.*, **71**, 3925 (1949).

(12) G. B. Heisig, *ibid.*, **63**, 1698 (1941).

(13) M. Schlatter, *ibid.*, **63**, 1733 (1941).

argon Titanium Getter lamps, has been described recently by Ausloos and Lias.[4]

Quantum yield determinations in the photoionization region were carried out using a 290-cm³ cell equipped with a pair of 4.5-cm diameter nickel electrodes, positioned 4 to 5 cm apart. This cell was similar to the photolysis vessel described by Ausloos and Lias,[4] except that this contained only one chamber. A Fluke Model 415A high-voltage power supply and a Victoreen Model 1002 picoammeter were used in conjunction with the photoionization cell.

The ultraviolet photolysis reported in this study was carried out in a 500-cm³ Vycor reaction vessel, utilizing a Hanovia utility quartz medium-pressure lamp. All experiments were conducted at room temperature, to about 0.5% conversion. A series of mercury-photosensitized experiments were carried out in a 1-l. Vycor reaction vessel using a Gelman-Camag low-pressure (253.7 nm) Universal uv lamp. Photolysis times were 2 min in duration, equivalent to about 1% conversion.

Analysis. After irradiation, an aliquot of the sample was introduced into a dual flame gas chromatograph. Separation was achieved on a 25-ft, 30% squalane column, or a 35-ft, 15% dimethylsulfolane–8-ft, 30% squalane combination column. The latter column was used primarily to check the purity of the reported vinyl acetylene and 1,3-butadiene products.

Noncendensable products were distilled at −210°, collected, and analyzed with a CEC-21-103 C mass spectrometer. Products of special interest were separated by means of vapor chromatography, trapped with liquid nitrogen, and also analyzed with the CEC-21-103 C mass spectrometer.

Results

Using photoionization techniques the quantum yield for ionization (ionization efficiency) was determined for cyclobutene assuming a value of 0.77 for nitric oxide[4] and 0.16 for cyclopentene[14] at 10 eV, and a value of 0.37 for cyclopentene[14] at 11.6–11.8 eV. The efficiencies for cyclobutene were 0.26 and 0.60, respectively. Table I reports the quantum yields of the major products as determined in these experiments.

The product yields in Tables II–V have been given relative to the yield of acetylene. No actinometry was carried out at 147.0 nm or in the 220.0–260.0-nm region. "Relative quantum yields" obtained at 147.0 nm verified the results obtained in Table I, that the quantum yield of acetylene was independent of cyclobutene pressure from 0.5 to 30 Torr. Further experiments at 147.0 and 123.6 nm demonstrated that the quantum yield of acetylene was independent of additive with the exception of H_2S or where abnormally high concentration of additives were used. Determination of "relative quantum yields," when hydrogen sulfide is present, is extremely uncertain due to sulfur deposition on the lamp windows.

Table I: Products Formed in the Photolysis of Cyclobutene[a] at 123.6 and 106.7–104.8 nm

c-C_4H_6 P, Torr	Quantum yields CH_4	C_2H_2	C_2H_4	C_3H_6	C_4H_4	1,3-C_4H_6
			123.6 nm			
0.5	Nd[b]	0.40	0.42	0.01	0.13	0.49
1.2	Nd	0.39	0.42	0.01	0.13	0.44
5.0	Nd	0.41	0.42	0.01	0.14	0.37
			106.7–104.8 nm			
0.7	0.02	0.65	0.69	0.03	0.21	0.66
1.4	0.02	0.65	0.68	0.03	0.21	0.54
3.2	0.02	0.65	0.70	0.03	0.20	0.37

[a] All experiments carried out in the presence of 5% O_2 as a radical scavenger. [b] Not determined.

Table II: Photolysis 147.0 nm of Cyclobutene in the Presence and Absence of Additives

c-C_4H_6 P, Torr	Additive P, Torr	Relative yields, C_2H_2 = 100 H_2	CH_4	C_2H_4	C_4H_4	1,3-C_4H_6
1.0	None	Nd[a]	22	115	37	92
5.0	None	Nd	16	99	43	30
0.1	NO–0.01	Nd	Nd	102	35	171
0.5	NO–0.05	Nd	Nd	101	38	116
1.0	NO–0.1	Nd	Nd	94	36	65
5.0	NO–0.5	15	Nd	84	39	31
10.0	NO–1.0	12	Nd	85	40	23
1.0	H_2S–0.2	Nd	69	132	30	68
5.0	H_2S–1.0	Nd	27	114	28	68
0.05	MA[b]–0.45	Nd	t[c]	201	29	320
0.14	MA–0.45	Nd	t	178	32	222

[a] Not determined. [b] Methylamine. [c] Trace.

Table III: Photolysis (123.6 nm) of Cyclobutene in the Presence and Absence of Additives

c-C_4H_6 P, Torr	Additive P, Torr	Relative yields, C_2H_2 = 100 H_2	CH_4	C_2H_4	C_4H_4	1,3-C_4H_6
5.0	None	47	t[a]	118	39	128
0.1	NO–0.01	Nd[b]	Nd	125	36	379
0.5	NO–0.05	Nd	Nd	106	43	149
1.0	NO–0.1	60	Nd	85	45	95
5.0	NO–0.5	52	Nd	80	36	67
10.0	NO–1.0	48	Nd	98	33	65
30.0	NO–3.0	Nd	Nd	81	41	60
5.0	H_2S–6.0	Nd	198	172	36	86
30.0	H_2S–6.0	Nd	36	139	44	147
0.045	MA[c]–0.45	Nd	t	225	27	575
0.14	MA–0.45	Nd	t	165	27	320

[a] Trace. [b] Not determined. [c] Methylamine.

(14) R. Lesclaux, S. Searles, L. W. Sieck, and P. Ausloos, to be published.

Table IV: Photolysis (106.7–104.8 nm) of Cyclobutene in the Presence of Additives

c-C_4H_6 P, Torr	Additive P, Torr	Relative yields, C_2H_2 = 100					
		H_2	C_2H_4	C_2H_6	C_3H_6	C_4H_4	1,3-C_4H_6
1.0	NO–0.1	106	91	0	t[a]	23	115
5.0	NO–0.5	84	83	0	17	26	17
20.0	NO–2.0	Nd[b]	83	0	13	36	3
5.0	H_2S–1.0	Nd	154	12	28	28	180

[a] Trace. [b] Not determined.

Table V: Photolysis (220.0–260.0 nm) of Cyclobutene, at 28°

C_4H_6 P, Torr	Additive P, Torr	Relative yields, C_2H_2 = 100					
		CH_4	C_2H_4	C_2H_6	C_3H_6	C_3H_4[a]	1,3-C_4H_6
1.0	None	t[b]	250	125	t	0	438
1.0	NO–0.1	Nd[c]	167	0	27	22	413
5.0	NO–0.5	Nd	152	0	30	36	752
1.0	O_2–0.1	Nd	303	0	42	0	300
1.0	H_2S–0.2	835	588	t	76	0	641

[a] Methylacetylene. [b] Trace. [c] Not determined.

Table II reports the 147.0-nm photolysis of cyclobutene–additive mixtures. In addition to these data, the following observations were made.

1. When a radical scavenger was present, relative products yields were insensitive to irradiation time, with the exception of 1,3-butadiene. The ratio 1,3-C_4H_6/C_2H_2 for a 1-Torr cyclobutene–NO sample decreased by nearly a factor of 2 as the conversion increased from 0.02 to 1.2%, based on the yield of acetylene.

2. When the surface/volume ratio was decreased by a factor of 2, the ratio 1,3-C_4H_6/C_2H_2 increased by nearly 1.5 for a 0.5-Torr cyclobutene–NO mixture.

3. The addition of carbon dioxide or neon to a 0.5-Torr cyclobutene–NO system reduced the relative yields of both 1,3-butadiene and ethylene to the same degree as an equal increase of cyclobutene pressure.

The results obtained for the 123.6-nm photolysis of cyclobutene and cyclobutene–additive mixtures are given in Table III. The effects observed in the 147.0-nm region were verified at 123.6 nm. In addition, it was established that an increase in nitric oxide concentration from 5 to 25% of the cyclobutene had no effect on relative yields for a 0.5-Torr sample, while a slight reduction in ethylene and 1,3-butadiene was observed when the pressure was 5.0 Torr.

Table IV contains the results of the argon (106.7–104.8 nm) photolysis. Ion currents were measured in this region as well as in the krypton region, which were the basis of the quantum yields reported in Table I.

Since the direct ultraviolet photolysis of cyclobutene has not been previously reported, a preliminary investigation was carried out as a part of this study. Some of these data are reported in Table V.

In order to differentiate between a bimolecular reaction channel and a unimolecular one, common practice in radiation chemistry would call for the photolysis of a 1:1 mixture of cyclobutene-h_6–cyclobutene-d_6. Unfortunately, it was not possible to obtain cyclobutene-d_6. Therefore, in an attempt to elucidate the formation of hydrogen, ethylene, and 1,3-butadiene, a series of experiments was designed to substitute for the unavailability of cyclobutene-d_6. The mercury-photosensitized dissociation of deuterium in the presence of cyclobutene (Table VI) led to the formation of ethylene and 1,3-butadiene as the only major products. Small amounts of acetylene, propylene, and butenes were present even when additional radical scavenger was added to the mixture.

Table VI: Mercury-Photosensitized Dissociation of Deuterium in the Presence of Cyclobutene

Pressure of reactant,[a] mTorr				Major products			
				Ethylenes		1,3-Butadienes	
c-C_4H_6	O_2	NO	C_2H_4	C_2H_3D	$C_2H_2D_2$	C_4H_6	C_4H_5D
200	0	0	39	48	13	10	90
200	80	0	40	48	12	12	88
200	0	80	42	50	8	10	90

[a] Deuterium pressure 12 Torr.

In other experiments D_2S was used in place of H_2S as a diagnostic test for free radicals[15] (Table VII), while ammonia-d_3 was photolyzed in the presence of cyclobutene

Table VII: Photolysis of Cyclobutene (123.6 nm) in the Presence of D_2S

c-C_4H_6 P, Torr	Additive P, Torr	Ethylenes		Hydrogens		
		C_2H_4	C_2H_3D	H_2	HD	D_2
1.0	0.12[a]	68	32	77	23	Trace
1.0	0.25[b]	73	27	54	37	9

[a] Relative yields: C_2H_2 = 100, C_2H_4 = 164, H_2 + HD = 25. [b] Relative yields: C_2H_2 = 100, C_2H_4 = 160, H_2 + HD = 24.

Table VIII: Photolysis of ND_3 (123.6 nm) in the Presence of Cyclobutene

ND_3 P, Torr	c-C_4H_6 P, Torr	1,3-Butadienes		Hydrogens		
		C_4H_6	C_4H_5D	H_2	HD	D_2
1.2	0.13	67	33	55	23	22
1.5	0.10[a]	56	44	45	22	33

[a] Ethylene contained approximately 5% C_2H_3D.

(15) P. Ausloos and S. G. Lias, *J. Chem. Phys.*, **44**, 521 (1966).

(Table VIII) as a test for the importance of hydrogen atom in the vacuum-ultraviolet photolysis of cyclobutene.

Discussion

It has been well established that molecular hydrogen elimination occurs with a low probability in the vacuum-ultraviolet photolysis of cyclobutane.[10] If a parallelism exists between cyclobutane and cyclobutene, it would be logical to expect this process to be of minor importance for cyclobutene. The low hydrogen yield at 147.0 nm (Table II), as well as the relatively small vinyl acetylene yields (Tables II–IV), are indicative of the validity of this comparison. This low probability for molecular hydrogen elimination has also been found for cyclopropane[16,17] and methylcyclopropane.[18] Cyclopentane,[19] in contrast, has as a major mode of fragmentation the molecular detachment of a hydrogen molecule. The higher hydrogen yield found at 123.6 nm (Table III) or at 106.7–104.8 nm (Table IV) when compared to the value obtained at 147.0 nm (Table II) is inconsistent with a molecular hydrogen detachment process, since it is the normal tendency for the molecular hydrogen elimination process to be favored at the longer wavelength. Furthermore, molecular detachment from an excited parent molecule would be expected to be pressure independent over the range of pressures used in these experiments. Results given in Tables II–IV clearly demonstrate a decreasing hydrogen yield with increasing pressure.

A second major comparison of cyclobutene to cyclobutane may be expected in the formation of an intermediate diradical structure. It has been pointed out that the major primary process in the vacuum-ultraviolet photolysis of small ring hydrocarbons results in ring opening through initial C–C cleavage[6,15,16]

$$c\text{-}(C_nH_{2n}) + h\nu \longrightarrow (C_nH_{2n})^{\ddagger} \quad (1)$$

where $n = 3$ or 4 and $(C_nH_{2n})^{\ddagger}$ denotes a diradical with possible internal energy content. Unfortunately, direct evidence for this intermediate is slight. Major arguments in its favor are found in the solid phase studies or in rearrangements that most surely do occur *via* a diradical precursor. Although here direct evidence for radical intermediate is also lacking, its presence is assumed

$$c\text{-}(C_4H_6) + h\nu \longrightarrow (C_4H_6)^{\ddagger} \quad (1a)$$

where $(C_4H_6)^{\ddagger}$ denotes a diradical species containing excess internal energy. Although there are two possible diradicals, separation of the species is but speculation.

Vinyl Acetylene Formation. It is noted in Tables I–IV that vinyl acetylene is independent of cyclobutene pressure and unaffected by the presence or absence of additives. The formation of vinyl acetylene in the vacuum-ultraviolet photolysis of 1,3-butadiene[7] and 1,2-butadiene[8] occurs through the elimination of two hydrogen atoms, either stepwise or simultaneously. This process applied to cyclobutene is depicted by the following reaction sequence

$$(C_4H_6)^{\ddagger} \longrightarrow H + (C_4H_5)^* \quad (2)$$

$$(C_4H_5)^* \longrightarrow H + C_4H_4 \quad (3)$$

where $(C_4H_6)^{\ddagger}$ is a diradical species and $(C_4H_5)^*$ is a radical with excess internal energy. In order to be consistent with the data in Tables I–IV, the lifetime of the $(C_4H_5)^*$ must be less than the collision interval at the pressure range used in this study. This mode of formation is also consistent with the observation that vinyl acetylene is not observed in the 220.0–260.0-nm photolysis of cyclobutene (Table V). The photon energies in this range are insufficient for this process.

$$c\text{-}(C_4H_6) + h\nu \longrightarrow 2H + C_4H_4 \quad (\Delta H = 142 \text{ kcal/mol}) \quad (4)$$

Although the diradical formation is consistent with the majority of the experimental observations to be discussed in this work, the loss of an H atom followed by ring opening also must occur, especially at shorter wavelength.

$$c\text{-}(C_4H_6) + h\nu \longrightarrow H + c\text{-}(C_4H_5)^* \quad (1b)$$

$$c\text{-}(C_4H_5)^* \longrightarrow (C_4H_5)^* \quad (2a)$$

The results of this reaction sequence may not be distinguishable from those of reactions 1a and 2. For this reason this mechanism will be considered, in the discussions, as equivalent to the diradical concept.

1,3-Butadiene Formation. Cooper and Walters[20] studied the thermal isomerization of cyclobutene at 150°. This isomerization was unimolecular with a calculated activation energy of 32.5 kcal/mol. The mechanism by which 1,3-butadiene was formed was described in terms of the breaking of the 3–4 carbon bond. Later, Elliot and Frey[21] corroborated this work, finding an activation energy of 32.3 kcal/mol while invoking a 1–4 biradical as an intermediate. Such an isomerization process in the vacuum-ultraviolet photolysis of cyclobutene is inconsistent with the data presented.

As is seen in Tables I–IV, the yield of 1,3-butadiene decreases with increasing cyclobutene pressure. The excited diradical species possesses in the neighborhood of 180-kcal/mol excess energy (in the case of the xenon photolysis) which would be carried over to the isomer-

(16) C. L. Currie, H. Okabe, and M. R. McNesby, *J. Phys. Chem.*, **67**, 1494 (1963).

(17) A. A. Scala and P. Ausloos, *J. Chem. Phys.*, **49**, 2282 (1968).

(18) R. D. Doepker, *J. Phys. Chem.*, **73**, 3219 (1969).

(19) R. D. Doepker, S. G. Lias, and P. Ausloos, *J. Chem. Phys.*, **46**, 4340 (1967).

(20) W. Cooper and W. D. Walters, *J. Amer. Chem. Soc.*, **80**, 4220 (1958).

(21) C. S. Elliot and H. W. Frey, *Trans. Faraday Soc.*, **62**, 895 (1966).

ized product. The resulting 1,3-butadiene molecule would indeed fragment,[7] unless it could be deactivated through some collision process. This would predict an increase in the 1,3-butadiene with increasing additive pressure, which is contrary to observation.

It has been noted that the formation of vinyl acetylene is accompanied by the elimination of two hydrogen atoms. The addition of a hydrogen atom to cyclobutene is exothermic and will result in the fragmentation of the resulting molecule, unless collisionally deactivated.

$$c\text{-}(C_4H_6) + H \longrightarrow (C_4H_7)^* \quad (5)$$

$$(C_4H_7)^* \longrightarrow 1,3\text{-}C_4H_6 + H \quad (6)$$

$$(C_4H_7)^* + M \longrightarrow (C_4H_7) \quad (7)$$

The formation of 1,3-butadiene through this mechanism is consistent with the observed pressure dependency. Furthermore, the yield of 1,3-butadiene would be expected to decrease with an increase in the surface to volume ratio of the reaction vessel. This also was observed (see Results).

When a deuterium–cyclobutene–mercury (D_2/c-C_4H_6 = 60) mixture was photolyzed with 253.7 nm (Table VI), ethylene and 1,3-butadiene were the major products. Mass spectral analysis of the 1,3-butadiene product produced nearly 90% C_4H_5D with the D atom located most likely in a terminal position. The predominance of the C_4H_5D molecule in the mixture indicates that addition of a deuterium atom to cyclobutene results first in a C_4H_6D molecule which then emits a hydrogen atom forming 1,3-butadiene.

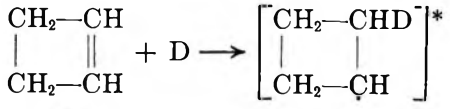

(5a)

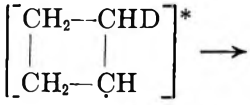

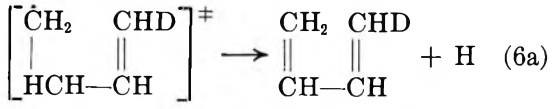

(6a)

Thus the splitting of the 1–4 bond in the above mechanism would lead exclusively to C_4H_5D, while the splitting of the 3–4 bond should result in a ratio of C_4H_5D to C_4H_6 of nearly 1, neglecting any strong isotope effect. The 10% light butadiene observed could arise from this process but may well be explained through direct Hg-sensitization of cyclobutene since nearly 10% of the excited mercury molecules would be expected to be quenched by cyclobutene.

In the 147.0-nm photolysis of methylamine, Magenheimer, Varnerin, and Timmons[22] showed that 80% of the primary process is involved in the elimination of a hydrogen atom. When methylamine was photolyzed in the presence of 10% cyclobutene, 1,3-butadiene and ethylene were the major products (Tables II and III). Presumably, this is due to the addition of a hydrogen atom from the methylamine to the cyclobutene and its subsequent fragmentation.

The experiments with ND_3 (Table VIII) are somewhat ambiguous but do demonstrate the importance of a hydrogen atom mechanism to the formation of 1,3-butadiene. If the H_2/D_2 ratio could be used as an approximation of the relative photolysis of cyclobutene to ammonia-d_3, then a major portion of the C_4H_6 found in these experiments could arise through H atoms produced from the photolysis of cyclobutene. The remaining 1,3-butadiene, mainly C_4H_5D, would result through the 1–4 carbon split of the C_4H_6D molecule as postulated for the Hg-sensitized study. This certainly would be expected unless the hydrogen atom generated in the vacuum-ultraviolet photolysis would contain considerable excess energy.

Ethylene–Acetylene Formation. The formation of ethylene and acetylene presents a very interesting problem. In the vacuum-ultraviolet photolysis of cyclobutane[10] and methylcyclopropane[18] the formation of ethylene and acetylene was explained through the following mechanism

$$c\text{-}C_4H_8 + h\nu \longrightarrow (C_4H_8)^{\ddagger} \quad (8)$$

$$(C_4H_8)^{\ddagger} \longrightarrow C_2H_4 + (C_2H_4)^* \quad (9)$$

$$(C_2H_4)^* \longrightarrow H_2 + C_2H_2 \quad (10)$$

$$(C_2H_4)^* + M \longrightarrow C_2H_4 \quad (11)$$

where $(C_4H_8)^{\ddagger}$ represents a diradical species with large internal energy content and $(C_2H_4)^*$ also a molecule with excess internal energy. The pressure dependency on the C_2H_2/C_2H_4 ratio agreed with this mechanism. It was estimated that 172 kcal/mol has to be partitioned between the two ethylene molecules[10] formed in reaction 9. This value is based on the reasonable assumption that the dissociative lifetime of the $(C_4H_8)^{\ddagger}$ is shorter than the collision interval of about 10^{-7} to 10^{-9} sec. A similar argument presented for cyclobutene would produce 166 kcal/mol to be partitioned between the ethylene and acetylene fragment. If a major portion of this energy would reside with the ethylene fragment, then reactions 10 and 11 should produce a pressure dependency that is *not* observed in this study.

It becomes apparent in Table I that the quantum yield of acetylene is independent of cyclobutene pressure. This fact would preclude a mechanism parallel to that of cyclobutane. It is interesting to note that in the case of the C_4H_6 compounds thus far reported,[7,8] as well as studies underway in our laboratory on other C_4H_6 isomers, all of these isomers show the absence of a pressure effect on the formation of acetylene and ethylene that would be predicted by the cyclobutane mech-

(22) J. Magenheimer, R. E. Varnerin, and R. B. Timmons, *J. Phys. Chem.*, 73, 3904 (1969).

anism. It appears that only a fraction of the ethylene formed in dissociation of the excited (cyclobutene) diradical has sufficient energy to eliminate a hydrogen molecule. The lifetime of this species must be shorter than the collision interval at the pressures used in this study.

$$(C_4H_6)^{\ddagger} \longrightarrow C_2H_2 + C_2H_4 \quad (12)$$

$$\longrightarrow C_2H_2 + C_2H_2 + H_2 \quad (13)$$

In comparing hydrogen and acetylene yields at all three wavelengths it can be concluded that the ratio of reaction 12 to reaction 13 increases with increasing photon energy. This would indeed be as expected.

A secondary source of acetylene may be attributed to a process similar to that for the formation of vinyl acetylene

$$(C_4H_5)^* \longrightarrow C_2H_2 + C_2H_3 \quad (14)$$

Ethylene may also be produced by a process similar to vinyl acetylene

$$(C_4H_5)^* \longrightarrow C_2H + C_2H_4 \quad (15)$$

Since the ethynyl radical is not scavenged by nitric oxide[23] but may abstract a hydrogen atom from an olefin,[24] additional acetylene may also arise from this reaction.

A number of complicating features in the formation of ethylene must be considered. The experiments with mercury photosensitization (Table VI) clearly display that ethylene may be formed through a hydrogen atom mechanism.

$$c\text{-}C_4H_6 + H \longrightarrow (C_4H_7)^* \quad (16)$$

$$(C_4H_7)^* \longrightarrow C_2H_3 + C_2H_4 \quad (17)$$

If the fact is taken into account that there is incomplete scavenging of vinyl radicals even in the presence of O_2 and NO in those experiments, it becomes apparent that the $(C_4H_6D)^*$ formed in reaction 16 leads to nearly equal amounts of C_2H_3D and C_2H_4 *via* reaction 17. This would seem to indicate that the $(C_4H_6D)^*$ molecule has an equal *a priori* probability to split perpendicular or parallel to the original double bond.

$$\begin{bmatrix} CH_2\text{—}CHD \\ | \quad\quad | \\ CH_2\text{—}\dot{C}H \end{bmatrix}^* \longrightarrow \begin{matrix} CH_2{=}CHD \\ + \\ CH_2{=}\dot{C}H \end{matrix} \quad (17a)$$

$$\begin{bmatrix} CH_2\text{—}CHD \\ | \quad\quad | \\ CH_2\text{—}\dot{C}H \end{bmatrix}^* \longrightarrow \begin{matrix} CH_2 & CHD \\ \| & + \; \| \\ CH_2 & \dot{C}H \end{matrix} \quad (17b)$$

If then the formation of ethylene by a hydrogen atom mechanism is superimposed on the reaction sequence 12–13, the observed pressure dependency of the C_2H_2/D_2H_4 may be explained. Although the major portion of the ethylene is expected to arise from the dissociation of the diradical, reaction 12, an additional source related to the hydrogen atom must be included. The experiments containing methylamine (Tables II and III) indicate increased ethylene production parallel with the formation of 1,3-butadiene.

Radical Formation. The use of hydrogen sulfide as a diagnostic test for the presence of free radicals has been successfully used in the earlier studies of the C_4H_6 isomers.[7,8] The presence of vinyl radicals is established through an increase in ethylene when H_2S is added to the system.

Methane formation in the presence of H_2S reflects the formation of a methyl or methylene radical. Small amounts of methyl radicals point to rearrangements that must occur within the diradical intermediate. The radicals, on the other hand, would be expected from diradicals formed through the scission of the 3–4 carbon–carbon bond in the excited cyclobutene, followed by the fragmentation of the diradical into two vinyl radicals. This has been shown to be an important process in the photolysis of 1,3-butadiene.[7]

Due to the unavailability of $c\text{-}C_4D_6$, it was necessary to photolyze $c\text{-}C_4H_6$ in the presence of D_2S. This system has many drawbacks related to the competitive kinetics involved.[15] The results in Table VII clearly demonstrate the presence of vinyl radical, seen as C_2H_3D, but these experiments cannot be used as a quantitative measure of the radical.

Small amounts of ethynyl radical may also be inferred through the relative increase in the C_2H_2/C_4H_4 ratio, when H_2S is present. The origin of this radical would be expected from reaction 15.

Effect of Photon Energy. Unfortunately, it is extremely difficult to assess the relative importance of different dissociative processes from purely end-product analysis and the limited isotopic techniques that were employed. It can be seen in Tables II and III that an increase of photon energy from 8.4 to 10.0 eV has very little effect on relative product yields, with the exception of hydrogen. This increase in hydrogen coupled with small increases in vinyl acetylene and 1,3-butadiene would reflect increased hydrogen atom detachment and its subsequent reaction and an energy dependence associated with reaction 13. Increasing the photon energy to 11.6–11.8 eV appears to have considerable effect on the quantum yield of acetylene. This may well be evidence for an increased importance of processes 13–15.

The 220.0–260.0-nm photolysis is indeed complex. 1,3-Butadiene is formed both through a hydrogen atom reaction as well as through direct isomerization followed by pressure stabilization. Furthermore, rearrangements within supposedly the parent molecule is reflected by the unexpectedly large methane yield when H_2S was

(23) A. G. Sherwood and H. E. Gunning, *J. Phys. Chem.*, **69**, 1732 (1965).

(24) A. M. Tarr, O. P. Strausz, and H. E. Gunning, *Trans. Faraday Soc.*, **62**, 1221 (1966).

added to the system. Since this table reports only a preliminary analysis of the 220.0–260.0-nm photolysis of cyclobutene, further discussion would be unwarranted.

Ion–Molecule Reactions. The ionization energy of cyclobutene is 9.16 eV. Although ion currents were measured using a photolysis cell of the type described by Ausloos and Lias[4] for both the argon and krypton resonance radiation, no products could be identified as originating exclusively from an ion–molecule path. Attempts to include additives such as trimethylamine (I.P. = 7.82) failed to demonstrate any charge transfer process resulting in isomerization of the cyclobutene. Studies in this area of photoionization of cyclobutene are presently under investigation in the laboratories of Ausloos.[25]

Acknowledgment. The authors wish to thank Dr. P. Ausloos for a preprint of his paper on cyclopentene and Dr. L. J. Stief for some timely conversation and a preprint of his work with propyne. Furthermore, the authors wish to acknowledge the National Science Foundation which supported this investigation under Grant No. NSF-GP-11265 and NSF-GP-20878.

(25) P. Ausloos and L. W. Sieck, private communication.

Quenching of Excited States of Fluorobenzene in the Gas Phase

by Kh. Al-Ani and David Phillips*

Department of Chemistry, The University, Southampton, SO9 5NH, U.K. *(Received June 28, 1971)*

Publication costs borne completely by The Journal of Physical Chemistry

The quenching of the first excited singlet and triplet states of monofluorobenzene vapor by O_2, various olefins, and pentan-2-one is reported, and quenching parameters are tabulated. A comparison of the two methods available for measurement of the triplet-state quantum yield indicates that the triplet-state yield of fluorobenzene excited in the 0–0 transition is of the order of 0.82 ± 0.05. This coupled with a fluorescence quantum yield of 0.22 ± 0.04 shows that no other nonradiative decay process occurs from this level.

Introduction

The photochemistry of the fluorobenzenes has attracted much interest of late, and the subject has been reviewed recently.[1] Of the fluorine-substituted aromatics studied thus far, monofluorobenzene has received the most attention. The first study[2] concluded that the quantum yield of fluorescence excited at 253.7 nm extrapolated to zero pressure was 0.235, a result which has been largely substantiated recently.[3] However, the original estimate of the triplet-state yield[1] based on the sensitization of biacetyl phosphorescence under various conditions was shown to be in error in a later study.[4] Moreover, the strong dependence of the quantum yield of fluorescence as a function of pressure of aromatic reported originally[1] was later shown to be due largely to artifacts connected with the geometry of the viewing system.[4] Similar effects have been shown to occur in other substituted benzenes.[5] The difficulty in interpretation of data obtained using wide band-pass exciting radiation has been clearly pointed out,[4] and to some extent this has been overcome in a recent study using excitation sources of narrower bandwidth.[3] In the latest work it was concluded that although resonance fluorescence from fluorobenzene was strongly quenched by the addition of chemically inert gases such as CH_4, C_2H_6, *cis*-but-2-ene, the total fluorescence yield excited by wavelengths longer than 255 nm was invariant with pressure and with wavelength of excitation. It can be concluded therefore that under these conditions the initially excited fluorobenzene behaves as if it were a vibrationally equilibrated molecule.

Triplet-state yields have been measured also by the method of sensitization of the cis–trans isomerization of but-2-ene.[6,7] It was originally observed that above a

(1) D. Phillips, Chemical Society Specialist Periodical Report 8, *Photochemistry*, 2, 168 (1971).

(2) I. Unger, *J. Phys. Chem.*, 69, 4284 (1965).

(3) K. Nakamura, *J. Chem. Phys.*, 53, 998 (1970).

(4) M. E. MacBeath, G. P. Semeluk, and I. Unger, *J. Phys. Chem.*, 73, 995 (1969).

(5) D. Gray, Kh. Al-Ani, and D. Phillips, *J. Chem. Soc., A*, 905 (1971).

(6) D. Phillips, *J. Phys. Chem.*, 71, 1839 (1967).

(7) R. B. Cundall, A. S. Davies, and K. Dunnicliff, "The Triplet State," A. B. Zahlan, Ed., Cambridge University Press, Cambridge, 1967, p 183.

pressure of 100 Torr of olefin the yield of sensitized cis–trans isomerization was invariant with pressure and of wavelength above 248 nm.[6] The quantum yield of triplet-state formation was estimated to be 0.86, somewhat higher than that obtained in a similar study.[7]

Notwithstanding the relatively large amount of data already published in the literature on the basic photophysical processes occurring upon excitation of fluorobenzene in the gas phase, it was felt worthwhile to reinvestigate briefly on the same apparatus the quantum yield of triplet-state formation by the two available techniques and also to investigate the quenching of the excited singlet and triplet states of the molecule by various added gases. Chloroform and carbon monoxide have been shown to have no effect upon the singlet state of fluorobenzene,[8] but appear to assist in the vibrational relaxation of "hot" triplet biacetyl formed by energy transfer from the triplet state of fluorobenzene.[8] Xenon, as might be expected, enhances the S_1–T_1 intersystem crossing in fluorobenzene,[9] but apparently does not affect the triplet state of biacetyl, contrary to an earlier report.[10] Further consideration of this and other work alluded to above will be found in the Discussion section of this report.

Experimental Section

The techniques and vacuum, optical, and analytical systems used in this study have been adequately described in earlier reports.[11,12]

Materials. Fluorobenzene was obtained from Koch-Light Laboratories Ltd. Glpc analysis on a 20% Carbowax 20M column indicated that it was 99.5% pure. It was used without further purification. Benzene was chromatoquality obtained from Matheson Coleman and Bell, Inc., and contained no detectable impurities. Biacetyl was obtained from British Drug Houses Ltd. It contained no impurities and was stored in a blackened bulb at room temperature. *cis*-But-2-ene was obtained from Cambrian Chemicals Ltd. as a research grade chemical. It contained 0.07% of *trans*-but-2-ene as an impurity. *trans*-But-2-ene was obtained from Phillips Petroleum Co. as a research grade chemical and contained 0.05% *cis*-but-2-ene as an impurity. Sulfur hexafluoride was from the Matheson Chemical Co. and contained 0.2% impurity. Oxygen was prepared on the line by heating Analar grade potassium permanganate crystals under vacuum. Buta-1,3-diene was obtained from British Drug Houses Ltd. as a research grade chemical. Analysis showed it to contain approximately 0.3% but-2-enes as impurity, plus approximately 0.2% of another unidentified impurity. Perfluorobut-2-ene was obtained from Air Products Ltd. and was 98% pure. 1,1-Difluoroethylene was obtained from Air Products Ltd. and was 99% pure. Ethylene was obtained from Air Products Ltd. and was found to be 99.8% pure. Octafluorocyclobutane was 99.9% pure, and was obtained from Air Products Ltd.

Results and Discussion

Fluorescence Yield. We have not attempted any new estimation of the absolute quantum yield of total fluorescence of fluorobenzene since two recent studies[3,4] are in essential agreement in placing the value at 0.22, independent of pressure over a limited range and of exciting wavelength above 255 nm. It should be pointed out that one study indicated a maximum in the fluorescence yield at excitation wavelength 259 nm,[4] but this was not revealed in the later more careful observations.[3] The earlier work also indicated that at high pressures of aromatic, the quantum yields of fluorescence were smaller, indicating a slight self-quenching.[4] Since the difficulties in interpretation of this kind of data are well known,[4,5] it was decided to carry out an independent check on whether or not self-quenching was of importance. As has been indicated in a prior report,[5] any quenching of the singlet state of an aromatic would result in parallel quenching of the triplet state or any processes arising from it. Thus with certain assumptions, the variation of the quantum yield of sensitized cis–trans isomerization of but-2-ene with pressure of aromatic may be taken as a measure of the extent of self-quenching of the singlet state. Figure 1 shows that over the admittedly limited pressure range studied, no variation in yield of sensitized cis–trans isomerization occurs, confirming that in this molecule little or no self-quenching is important at least at 265-nm exciting wavelength. We have thus accepted the fluorescence quantum yield of fluorobenzene in the pressure range 1–5 Torr as being 0.22 for 265-nm excitation, and the values at other wavelengths have been calculated relative to this value. Thus at 253.7 and 248 nm the values ob-

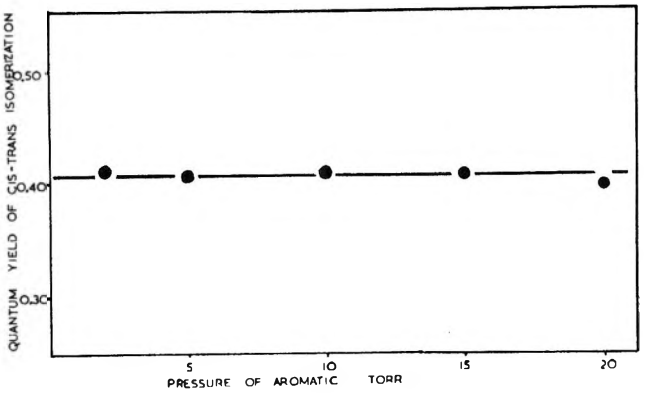

Figure 1. Quantum yield of sensitized cis–trans isomerization of but-2-ene as a function of fluorobenzene pressure; but-2-ene pressure 80 Torr, exciting wavelength 265.3 nm.

(8) M. E. MacBeath and I. Unger, *Can. J. Chem.*, **48**, 1607 (1970).
(9) M. E. MacBeath and I. Unger, *ibid.*, **49**, 594 (1971).
(10) A. Cook, G. P. Semeluk, and I. Unger, *ibid.*, **47**, 4527 (1969).
(11) Kh. Al-Ani and D. Phillips, *J. Phys. Chem.*, **74**, 4046 (1970).
(12) Kh. Al-Ani and D. Phillips, submitted for publication in *J. Phys. Chem.*

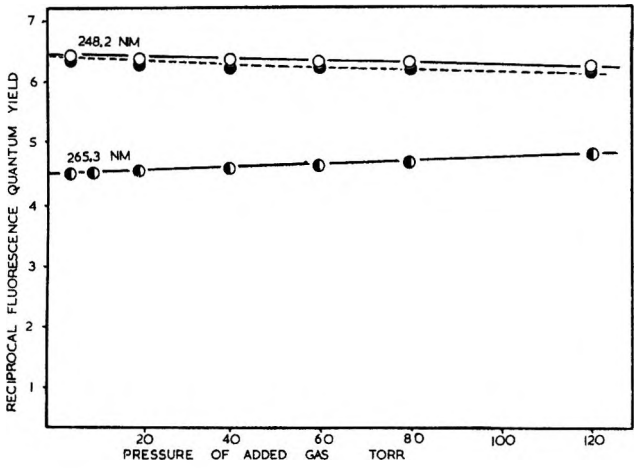

Figure 2. Reciprocal fluorescence quantum yield as function of added gas pressure, fluorobenzene pressure 4 Torr: open circles, but-2-enes, perfluorocyclobutane, perfluorobut-2-ene, and SF_6 at 248.2 nm; filled circles, ethylene at 248.2 nm; half-filled circles, but-2-enes, ethylene, and perfluorobut-2-ene at 265.3 nm.

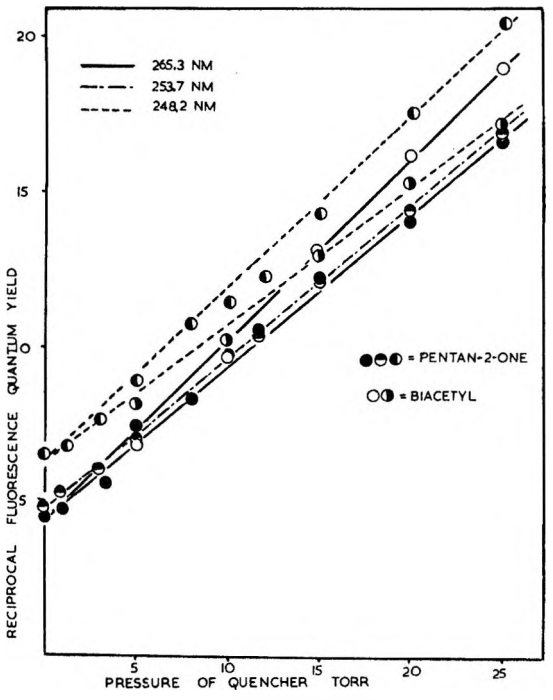

Figure 3. Reciprocal quantum yield of fluorescence of fluorobenzene at various exciting wavelengths as a function of added pentan-2-one and biacetyl pressure. Results with biacetyl at 253.7 nm have been omitted for clarity fluorobenzene pressure 4 Torr.

tained here are 0.205 and 0.133, respectively, which are very similar to those obtained recently.[3]

Quenching of Excited Singlet State of Fluorobenzene. Biacetyl has previously been shown to quench the excited singlet state of fluorobenzene at all exciting wavelengths,[2,4] but the effect of other quenching gases has been little studied. We report here the effect of some

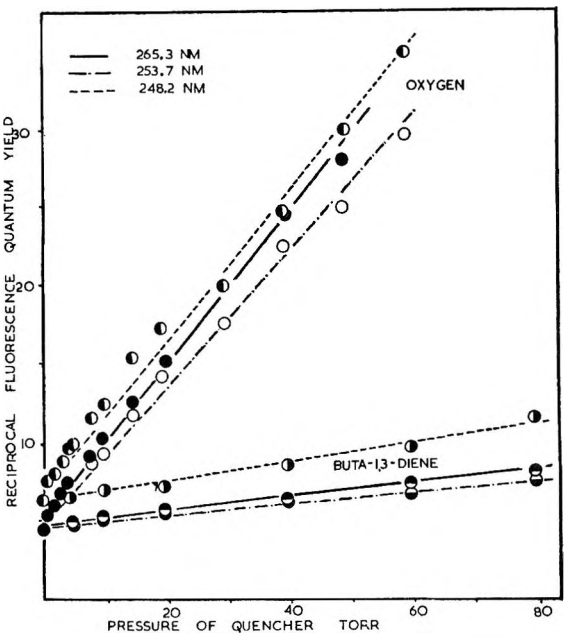

Figure 4. Reciprocal fluorescence quantum yield of fluorobenzene fluorescence as a function of added molecular oxygen and buta-1,3-diene pressure at various wavelengths of excitation; fluorobenzene pressure 4 Torr.

chemically inert and some π-bonded molecules upon the excited singlet state of fluorobenzene.

With 265-nm exciting wavelength, addition of up to 160 Torr of c-C_4F_8 and SF_6 caused no variation in the fluorescence yield of fluorobenzene. Similar results were obtained at 254 nm with these compounds, and in addition, no quenching was observed by but-2-ene, ethylene, perfluorobut-2-ene, and 1,1,difluoroethylene. At 265 nm, slight quenching of the fluorescence by the olefins was observed, as shown in Figure 2.

At 248 nm, addition of but-2-ene, perfluorobut-2-ene, and ethylene showed similar behavior to that of SF_6 and c-C_4F_8 in that as light enhancement of fluorescence was observed (Figure 2).

Buta-1,3-diene, oxygen, biacetyl, and pentan-2-one were all found to quench the fluorescence of fluorobenzene excited at all wavelengths. The data are summarized in Figures 3 and 4.

Mechanism. It has been pointed out that since the quantum yield of fluorescence of fluorobenzene is invariant with wavelength of excitation about 255 nm, one can treat the excited state so formed as if it were in thermal equilibrium with the surroundings.[3] Thus for simplicity, a very simple scheme will suffice to describe the behavior of fluorobenzene at 254 and 265 nm.

$$A + h\nu \longrightarrow {}^1A_0 \quad (1)$$

$${}^1A_0 \longrightarrow A + h\nu_f \quad (2)$$

$${}^1A_0 \longrightarrow {}^3A_n \quad (3)$$

$${}^1A_0 \longrightarrow A, X, \text{etc.} \quad (4)$$

$${}^1A_0 + Q \longrightarrow \text{product, energy transfer} \quad (5)$$

where X is an isomer and Q is a quenching molecule. A classical Stern–Volmer relationship then obtains for quenching, *i.e.*

$$\Phi_F^{-1} = 1 + \frac{(k_3 + k_4)}{k_2} + \frac{k_5}{k_2}[Q] \qquad (6)$$

In order to evaluate rate constants k_5 from plots of ϕ_F^{-1} against [Q], it is necessary to have a value of k_2, the rate constant for the radiative process. Since there is conflict in the literature concerning this value, some discussion of the point is required.

First, the rate constant k_2 is given by the inverse of the natural or mean radiative lifetime (τ_0) of the excited state. Conventionally this has been obtained by integration of the area under absorption curves, and such a treatment using the data of Ballester, *et al.*,[13] results in a value for τ_0 of 110 nsec,[2] which is in agreement with that obtained independently of 100 nsec.[3] However, since the relationship that $\tau = \tau_0\Phi_F$ holds, where ϕ_F is the fluorescence yield and τ is the fluorescence decay time, measurement of τ and ϕ_F can yield a value of τ_0. At 265 nm, $\phi_F = 0.22$. Berlmann has measured τ in solution as 8 nsec,[14] and a gas phase value of 8.4 nsec for 254-nm excitation has recently been obtained.[15] Acceptance of the latter value yields a result for τ_0 of 38 nsec, in reasonable agreement with that obtained in solution of 33.8 nsec, but very much different from that obtained by integration of the area under absorption curves. Since the procedure by which τ_0 is obtained from an integration of the area under absorption curves is only approximate, whereas measured decay times and fluorescence quantum yields give an unequivocal value for τ_0, the latter value has been used here. Rate constant data reported in Table I are therefore based on a value of τ_0 of 38 nsec, giving $k_2 = 2.62 \times 10^7$ sec^{-1}. It should be noted that this value is of a similar order to that used in Table V of ref 4, although that value was incorrectly taken as the reciprocal of a derived value of τ rather than τ_0. Because of this error, rate constant data in ref 4 must be recalculated.

For comparison in Table I, relative rate constants and cross sections for the quenching of benzene fluorescence by the same added molecules is included.[16] It can be seen that quenching by molecules to which electronic energy may be transferred is a very efficient process (O_2, biacetyl, pentan-2-one), whereas chemical quenching by olefins is much less effective. The use of the value of τ_0 of 38 nsec yields rate constants which are rather larger than the corresponding values for benzene and as can be seen, give extremely high cross sections. Adoption of a value of $k_2 = 10^7$ sec^{-1} reduces these values by a factor of approximately 3, giving cross sections of the order expected for gas kinetic collisions. The result would suggest that either (a) the measured decay times are too short, (b) fluorescence yields are too small, or (c) the cross sections are really very large. Further work is necessary to resolve this difficulty, although it is unlikely that (b) is a contributory factor.

Table I: Rate Parameters for the Quenching of Excited Singlet Fluorobenzene Vapor at 25°

Added gas	Wavelength, nm	Quenching rate constant, k_5, ml molecule^{-1} sec^{-1} × 10^{10}	Quenching cross section × 10^{16} cm^2
O_2	265.3	3.7 ± 0.2	22.8 ± 1
O_2	253.7	2.9 ± 0.2	17.7 ± 1
Biacetyl	265.3	6.2 ± 0.3	53 ± 2
Biacetyl	253.7	4.65 ± 0.3	43.5 ± 2
Biacetyl	248.2	4.55 ± 0.3	41 ± 2
Pentan-2-one	265.3	4.0 ± 0.2	34 ± 2
Pentan-2-one	253.7	3.95 ± 0.2	33.6 ± 2
Buta-1,3-diene	265.3	0.38 ± 0.04	3.2 ± 0.3
Buta-1,3-diene	253.7	0.29 ± 0.03	2.15 ± 0.2
cis-But-2-ene	265.3	0.011 ± 0.002	0.085 ± 0.002
Octafluoro-but-2-ene	265.3	0.029 ± 0.003	0.30 ± 0.03
1,1-Difluoro-ethylene	265.3	0.003 ± 0.0006	0.026 ± 0.005
Ethylene	265.3	0.009 ± 0.002	0.051 ± 0.01
Comparable Values for Benzene at 253.7 Å[a]			
O_2		1.66	
Biacetyl		1.98	
Pentan-2-one		2.35	
Buta-1,3-diene		0.055	

[a] Data from ref 16 based upon a value for the fluorescence decay time of benzene of 80 nsec. Errors in rate constants and cross sections based on least-squares analysis.

At 248-nm excitation, an excited state is produced for which the quantum yield of emission is less than that at longer wavelengths. Consequently, vibrational relaxation will cause an enhancement of the fluorescence yield as observed with inert added gases here and in earlier work.[4] In the presence of a quencher, competition between quenching and relaxation will be expected. However, with the strong quenchers used here the former will predominate, and thus a simple mechanism will still suffice. Quenching parameters in Table I for all wavelengths are based on the value of k_2 given earlier.

Triplet State

Sensitized Phosphorescence of Biacetyl. Values of the quantum yield of sensitized phosphorescence from biacetyl as a function of biacetyl pressure at different exciting wavelengths are shown in Figure 5. These results at 265.3 nm are some 20% higher than those obtained in the spectrofluorometric study at 264 nm.[4] We can offer little explanation of the discrepancy except

(13) M. Ballester, J. Palau, and J. Riera, *J. Quant. Spectrosc. Radiat. Transfer*, 4, 819 (1964).

(14) I. Berlman, "Handbook of Fluorescence Spectra of Aromatic Molecules," Academic Press, New York, N. Y., 1965.

(15) E. K. C. Lee and G. Breuer, private communication.

(16) E. K. C. Lee, M. W. Schmidt, R. G. Shortridge, Jr., and G. A. Haninger, Jr., *J. Phys. Chem.*, 73, 1805 (1969).

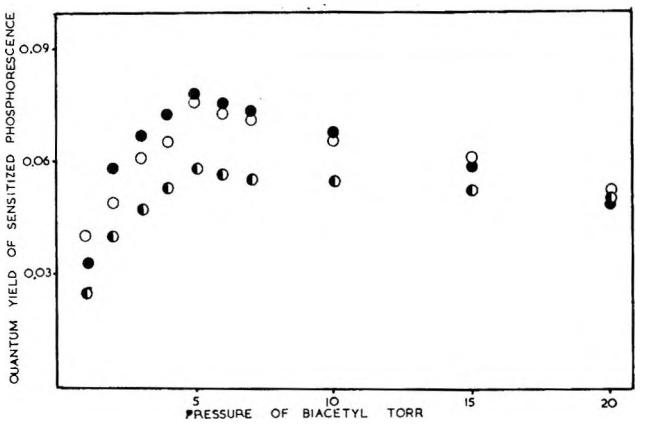

Figure 5. Quantum yield of sensitized phosphorescence from biacetyl as a function of added biacetyl pressure, fluorobenzene pressure 4 Torr: filled circles, 265.3-nm; open circles, 253.7-nm; and half-circles, 248.2-nm excitation.

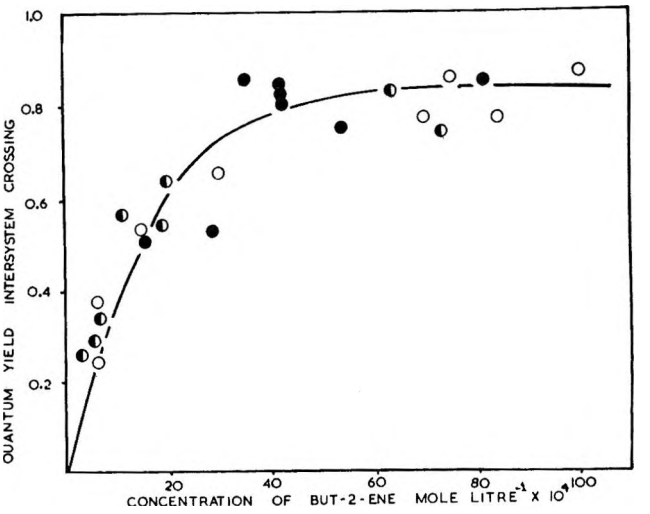

Figure 6. Quantum yield of apparent triplet-state formation for fluorobenzene as a function of added but-2-ene: filled circles, this work, 265.3 nm; open circles, data from Figure 1 of ref 7 corrected for new benzene calibration figure, 253.7-nm excitation, fluorobenzene concentration 6×10^{-5} *M*; half circles, as for open except fluorobenzene concentration = 1.1×10^{-4} *M*.

to point out that in the present study the results have been corrected for the effect of viewing geometry which in our system is severe,[5] and that the results quoted in ref 4 are strongly wavelength dependent, and thus the agreement between the studies carried out in very different systems with different exciting wavelengths is perhaps reasonable. However, in order to calculate triplet-state yields from the yield of sensitized phosphorescence observed, it is necessary to take into account the quenching of the singlet state of fluorobenzene by biacetyl. The values obtained in this study for this singlet quenching quoted in Table I are significantly in excess of those quoted in ref 4, and thus triplet-state yields derived here are also larger than those quoted earlier.[4] The discrepancy between the two studies has caused some concern, but two independent studies on different systems have given results within 10% of our quoted result, and corrections have been applied to account for the absorption of biacetyl during these experiments.[17] We are thus satisfied that the results obtained here are correct, and their use gives values for the quantum yield of intersystem crossing to the triplet state at 2.65.3, 253.7, and 248.2 nm of 0.82 ± 0.05, 0.76 ± 0.05, and 0.57 ± 0.05, respectively.

Sensitization of cis–trans Isomerization of But-2-ene. The technique and reaction mechanism have been fully described many times[6,7] and will not be enlarged upon here. As has been pointed out,[18] in order to interpret quantum yields of cis–trans isomerization in terms of intersystem crossing rates in the aromatic donor molecules, it is necessary to know the "branching ratio," *i.e.*, the relative rates of decay of excited triplet but-2-ene to the cis and trans ground states for the particular donor. Results in Table II show that for fluorobenzene, as for benzene, the ratio is within experimental error of unity, unlike the situation for some aromatic donors.[18] Values of the quantum yield of $S_1 \rightarrow T_1$ intersystem crossing based upon a value for the benzene yield of 0.72 are shown in Figure 6. Also shown in Figure 6 are values obtained by other workers[7] which have been adjusted to the benzene calibration of 0.72 from the value used in ref 7 of 0.63. It can be seen that although there is some scatter of experimental points, the two sets of data are in essential agreement, and yield a value for Φ_{ISC} at long wavelengths of 0.82 ± 0.4, in good agreement with the value obtained by the biacetyl method in the present system. Results in Figure 6 can also be compared with those shown in Figure 1 of ref 6. Agreement is good, although fortuitous, since results in ref 6 were based on a benzene calibration in which the triplet-state yield for benzene was taken as 0.63, and the branching ratio for benzene as 1.37. Thus results in

Table II: Branching Ratio for Fluorobenzene-Sensitized Isomerization of But-2-ene at 25°, 253.7 nm

Aromatic donor	Donor pressure, Torr	But-2-ene pressure, Torr cis	But-2-ene pressure, Torr trans	Time of photolysis, hr	Intensity absorbed, arbitrary units	% isomerization	Branching ratio
Benzene	6	10	...	5	0.1	0.46	1.02
Benzene	6	...	10	5	0.1	0.45	
Fluorobenzene	5	80	...	21	0.32	0.77	1.01
Fluorobenzene	5	...	80	25	0.33	0.88	

(17) H. Ishikawa and W. A. Noyes, Jr., *J. Amer. Chem. Soc.*, **84**, 1502 (1962).

(18) D. Gray, Kh. Al-Ani, and D. Phillips, *J. Chem. Soc., A*, 2949 (1971).

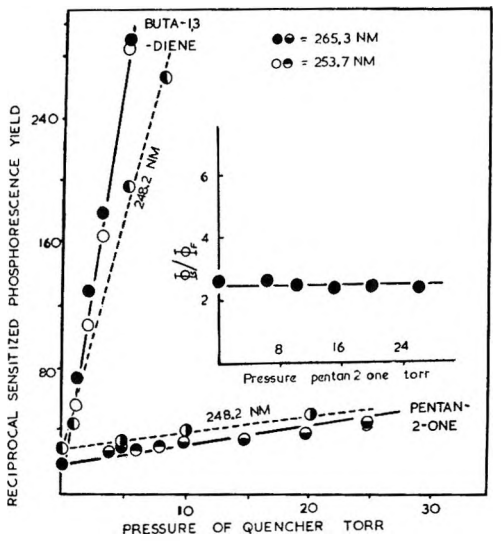

Figure 7. Competitive quenching of excited triplet state of fluorobenzene by biacetyl and buta-1,3-diene and biacetyl and pentan-2-one; fluorobenzene pressure 4 Torr.

Figure 1 of ref 6 must be multiplied by (0.72/0.63)(0.50/0.57) to be compared with those obtained here. This factor is almost exactly unity, meaning that results in Figure 1 of ref 6 are fortuitously correct.

Although results obtained by both the but-2-ene and biacetyl methods are in agreement at the longest wavelength, this is not the case for shorter wavelength excitation. This is not surprising in view of the large pressure of olefin in the former method which undoubtedly contributes to vibrational relaxation, and although vibrational relaxation produces a state with the same quantum yield of fluorescence as that initially produced, it does not necessarily follow that the quantum yield of intersystem crossing will be the same, since other nonradiative processes may occur from the unrelaxed state.

Quenching of Excited Triplet State of Fluorobenzene. The effect of adding oxygen and pentan-2-one to mixtures of fluorobenzene and biacetyl is shown in Figure 7. Since the singlet state of fluorobenzene is also quenched by these molecules, account must be taken of this. Kinetic analysis shows that plots of Φ_F/Φ_S (where Φ_F is the fluorescence yield in the presence of a quencher and Φ_S is the quantum yield of sensitized phosphorescence of the biacetyl) should yield a straight line whose slope gives a measure of the quenching rate constant for the added molecule relative to that of biacetyl.[19] Such plots for pentan-2-one show that this molecule does not apparently quench the triplet state of fluorobenzene. This result may be due to the excited triplet fluorobenzene of pentan-2-one followed by energy transfer from the excited ketone to biacetyl, resulting in no net quenching of the sensitized phosphorescence. A similar plot with buta-1,3-diene is unnecessary since the singlet state is essentially unaffected by the pressures of olefin used in the triplet quenching experiments.

Quenching parameters for buta-1,3-diene are shown in Table III compared with those for benzene.[20] It can be seen that for fluorobenzene as for benzene buta-1,3-diene is a much more efficient triplet quencher than biacetyl.

Table III: Competitive Quenching of Benzene[a] and Fluorobenzene Triplet States with Biacetyl and Buta-1,3-diene

Donor	Pressure of biacetyl, Torr	Pressure of buta-1,3-diene for half-quenching, Torr	k_B/k_Q[b]
Benzene[a]	0.31	0.058	0.183
Fluorobenzene	5	0.5	0.10

[a] Reference 20. [b] k_B is the rate constant for quenching of the excited triplet state of the aromatic donor by biacetyl, k_Q that by buta-1,3-diene. Since k_B is not known absolutely for the fluorobenzene donor, only relative rate constants can be quoted.

Acknowledgments. Thanks are due to Dr. D. Gray for help with setting up the experimental system and to Mr. M. G. Rockley for checking some of the results. Financial support from NATO Scientific Affairs Division, European Office, and from The British Council for payment of fees to Kh. Al-Ani during the tenure of a research studentship are gratefully acknowledged.

(19) G. Das Gupta and D. Phillips, submitted for publication in *J. Phys. Chem.*

(20) G. A. Haninger, Jr., and E. K. C. Lee, *ibid.*, **73**, 1815 (1969).

Pathways of Radiative and Radiationless Transitions in Europium(III) Solutions: Role of Solvents and Anions

by Yehuda Haas and Gabriel Stein*

Department of Physical Chemistry, Hebrew University, Jerusalem, Israel *(Received December 24, 1970)*

Publication costs assisted by Hebrew University

Absorption and emission spectra of europium perchlorate and europium nitrate have been measured in protonated and deuterated solvents (water, dimethyl sulfoxide, methanol, and acetonitrile). The line shape of these spectra is shown to depend strongly on the solvent and anion. Ion pairing takes place, depending on the combination of solvent and anion. Quantum yields and lifetimes of fluorescence from the $^5D_0$ level are reported. An isotopic enhancement factor of 40 is found in water, while in other solvents it is much smaller. The rate constants for radiative and radiationless processes are calculated. The radiationless constants range from about 10^4 sec^{-1} for light water to about 10 for deuterated dimethyl sulfoxide in which the fluorescent quantum yield on direct excitation to $^5D_0$ approaches unity. The suitability of this system for use as a liquid laser is indicated. It is shown that the anions also quench $^5D_0$ fluorescence. Radiationless rate constants for CNS^- and NO_3^- anions are calculated to be about 10^3 sec^{-1}. Fluorescence from the $^5D_1$ level is weak in all solvents. Its quantum yield is about 10^{-4} to 10^{-5}. The isotopic effect for this fluorescence is only 3. The probability for decay from the $^5D_1$ level directly to ground state is about the same for all systems, ~0.5, suggesting a common mechanism for this process.

Introduction

The study of the luminescent properties of the rare earths in solution has advanced considerably in recent years, especially as they form possible systems for liquid lasers.[1] In addition to the immediate practical value of such work our understanding of radiative and radiationless transitions might effectively benefit from this research. Thus it has been shown that the highest isotopic effect on fluorescent yields and lifetimes occurs in members of the rare earth series.[2-4] Very extensive work has been done on transfer of energy, in solution, between a rare earth ion and other solutes, following the pioneering work of Weissman,[5] which led eventually to the chelate laser. To be able to formulate a quantitative theory of these processes one has to know quantum yields, radiative and nonradiative rate constants, bimolecular quenching rates, and other relevant quantitative parameters. Such data are very scarce in literature especially as concerns unchelated rare earth ions. Yet it is in these that the role of the solvent medium in radiationless transitions of the rare earth ion might be expected to manifest itself more clearly. In our work on radiationless transitions we found it desirable to compare quantitatively such parameters for several polar solvents. In this work we report the results for solutions of europium salts in water, methanol, acetonitrile, and dimethyl sulfoxide, all both protonated and deuterated.

The intensities of radiative transitions in the rare earths, including Eu(III) in aqueous solution, have been extensively investigated recently.[6] Quantum yields for transitions from the $^5D_0$ level have been reported only for solutions of Eu(III) nitrate in CH_3OH and CH_3OD.[7] The only other experimental result relevant to our study of which we are aware is the quantum yield in crystals of $Eu_2(SO_4)_3 \cdot 8H_2O$, reported by Rinck to be 1.25%.[8] Lifetime data are more abundant and are given for the nitrate in methanol[7] and for several salts in H_2O and D_2O.[2,3]

Experimental Section

Materials. Aqueous solutions of Eu(III) were prepared from the oxide (99.9%, Fluka) by dissolving in the appropriate acid. We used the spectroscopic grade solvents acentonitrile (Fluka), dimethyl sulfoxide (DMSO) (Matheson), and methanol (Mallinckrodt) without further purification. CD_3CN (98.1% isotopic purity) and $(CD_3)_2SO$ (99% isotopic purity) were obtained from Miles Yeda, Rehovot, and D_2O (99.7%) from Fluka.

Apparatus. Fluorescence spectra were taken on a Turner "Spectro" Model 210 spectro fluorimeter (allowing the recording of corrected emission and excitation spectra) and absorption spectra on a Cary 14 spec-

(1) A. Heller, *Phys. Today*, **20**, 34 (1967).

(2) J. L. Kropp and M. W. Windsor, *J. Chem. Phys.*, **42**, 1599 (1965).

(3) P. K. Gallagher, *ibid.*, **43**, 1742 (1965).

(4) A. Heller, *J. Amer. Chem. Soc.*, **88**, 2058 (1966).

(5) S. I. Weissman, *J. Chem. Phys.*, **10**, 214 (1942).

(6) W. T. Carnall, P. R. Fields, and K. Rajnak, *ibid.*, **49**, 4450 (1968).

(7) W. R. Dawson and J. L. Kropp, *J. Opt. Soc. Amer.*, **55**, 828 (1965).

(8) B. Rinck, *Z. Naturforsch.*, **39**, 406 (1948).

trophotometer. All measurements were made at room temperature.

Liefetime measurements were made with a flash photolysis apparatus, modified to allow for emission studies.

Sample Preparation. The anhydrous salts were prepared from the aqueous solutions by evaporating almost to dryness and then heating under vacuum (10^{-4} Torr) at 200° for 48 hr. At first the solvent was distilled into the flask attached to the vacuum system, but experience has shown that it is possible to dissolve the anhydrous salt after disconnecting the vessel and quickly adding the solvent. The amount of water introduced by this method was less than 0.1% in most cases. Where more H_2O than this was present, the fact will be mentioned in the text.

The temperature and duration of heating proved crucial. Higher temperatures caused partial decomposition leading to the formation of the oxide, and lower temperatures or shorter times caused insufficient dehydrating. Analysis for water was made, when necessary, by nmr spectroscopy.

The concentration of Eu(III) was 0.5–1 *M* for measurements at 526- and 592-nm excitation and 0.02–0.05 *M* for 394-nm excitation.

Quantum Yield Measurements. Only fluorescence from the $^5D_0$ level will be considered in detail in this paper. The only other emitting level in solution is $^5D_1$. Its fluorescence is very weak compared to the $^5D_0$ emission. We report in this paper an estimate of the quantum yield from $^5D_1$.

We have recently reported our results on the role of the $^5D_1$ level in the depopulation of the $^5D_0$ level.[9] In the present paper we report the absolute yield of fluorescence from $^5D_0$. The $^5D_0$ emission consists of seven bands at about 580, 592, 618, 650, 700, 750, and 810 nm, due to transitions to the seven levels of the ground ^7F manifold. The three lines shown in Figure 1 usually account for over 95% of the intensity. These are the $^5D_0 \rightarrow {}^7F_1$, $^5D_0 \rightarrow {}^7F_2$, and $^5D_0 \rightarrow {}^7F_4$ lines, at 592, 618, and 700 nm, respectively. The combined intensity of these lines was taken to be proportional to the fluorescence intensity.

The fluorescence was excited by monochromatic light, thus exciting selected levels. These were the resonant level $^5D_0$, and the higher levels $^5D_1$ and $^5L_6$. Dawson and Kropp[7] analyzed the necessary conditions for quantum yield measurements of this kind. The main difficulty is the fact that the absorption spectrum consists of discrete, narrow bands. This forces one to adjust the excitation conditions so that only one discrete band is excited, and that the amount of light absorbed by it be accurately known This, in turn, requires precise knowledge of the shape of this band, as the absorbance varies considerably over the wavelength range transmitted by the excitation slit. Dawson and Kropp determined the quantum yield of $Eu(NO_3)_3 \cdot 6H_2O$ in CH_3OH by an absolute method. We used this material as a primary

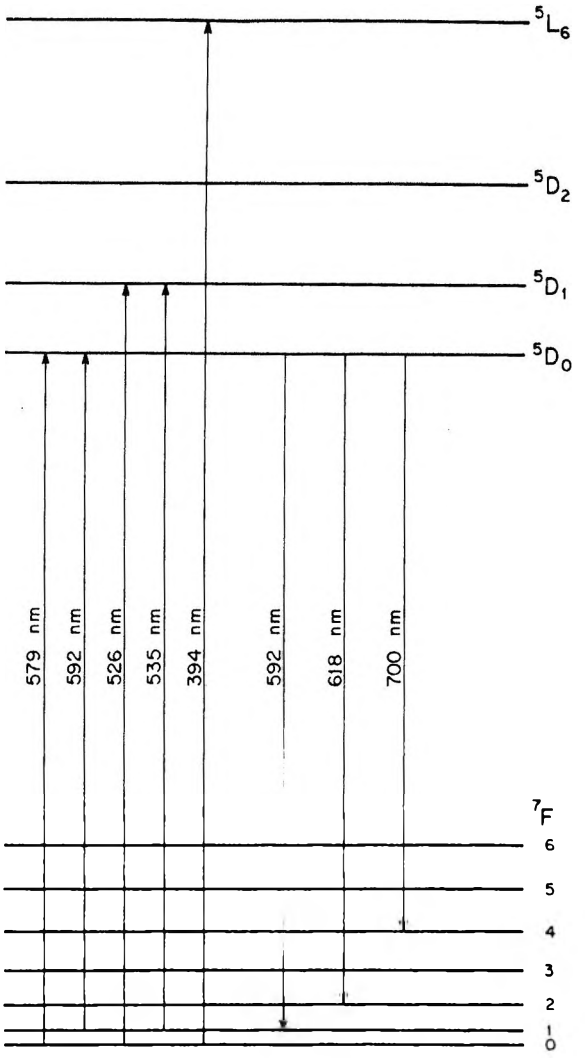

Figure 1. Partial energy level diagram of Eu^{3+} in solution. Only levels relevant to this work are shown.

standard. As it is sensitive to atmospheric moisture, we used aqueous solutions of $Eu(ClO_4)_3$ as a secondary standard. The procedure was the following: the absorption spectrum of the bands at 395, 526, or 592 nm (leading to the $^5L_6$, $^5D_1$, and $^5D_0$ levels, respectively) was taken, and the area under the curve was determined. The emission spectra of the unknown and the standard solutions were taken with the same instrumental set-up, with individual adjustment of the excitation wavelength. This adjustment was necessary because of minor changes in absorption line shapes and maxima and never exceeded 1–2 mμ. The slit width was always kept small enough so that excitation to other levels was excluded. Let s denote standard solution, u unknown solution, *A* the area under the absorption curve in the excitation band, *B* the combined area under the three main emission bands of the $^5D_0$ level, and *Q* the quantum yield. The unknown quantum yield was calculated from the equation

(9) Y. Haas and G. Stein, *Chem. Phys. Lett.*, 8, 366 (1971).

$$Q_u = \frac{Q_s B_u A_s}{B_s A_u} \quad (1)$$

Equation 1 does not take into account any effect of changes in refractive index on the fluorescence intensity. In the experimental arrangement of the apparatus such effects are largely canceled out.

Results

Absorption Spectra. As shown in ref 6, the energy separation between the levels of the f^6 configuration in Eu^{3+} are not very sensitive to the host. It is shown there that the energies in aqueous solution and in $LaCl_3$ host are very similar. This is due to the fact that crystal field splittings are small compared to electrostatic and spin-orbit interactions within the ion. This point is exemplified also in our results on the absorption spectra of $Eu(ClO_4)_3$ and $Eu(NO_3)_3$ in water, methanol, acetonitrile, and dimethyl sulfoxide (perchlorate only) shown in Table I, where we give the molar extinction coefficients (ϵ) calculated for the maxima of the lines. ϵ for the 592-nm line varies in the range of 0.01–0.02, and for the 526-nm line in the range 0.085–0.14. The 579-nm line is absent in the perchlorate solutions in water, methanol, and DMSO and appears very weakly in acetonitrile. It is much more enhanced in the nitrate solutions, especially again in acetonitrile. The most drastic changes occur in the 535-nm line where ϵ increases from 7×10^{-3} in the perchlorate–water system to 0.1 in the nitrate–acetonitrile system. We note that the strongly affected transitions are of the $\Delta J = 0$ type, whereas those with $\Delta J = 1$ are far less affected. Both these latter lines have been found to be due to magnetic dipole transitions.[10,11] Those strongly affected we consider to be electric dipole transitions. In view of the known tendency of the rare earth ions to form complexes with nitrate ions,[12] it is reasonable to suppose that the formation of these complexes causes a decrease in the symmetry of the ion, thus allowing forbidden transitions by admixture of higher configurations into the f^6 ground configuration. This point is further dealt with in the discussion of the emission spectra. The intensity of the $\Delta J = 0$ lines can give a qualitative measure of the tendency to form complexes. With nitrate as the anion, complexing power decreases in the order acetonitrile > methanol > water. This is in accord with the known properties of these substances as solvents of ionic compounds. It is customary to assume that perchlorate does not form complexes with cations. The appearance of the absorption line at 579 nm is a first indication that in acetonitrile, the solvent most weakly bound to Eu(III), some form of association is formed between ClO_4^- and Eu^{3+}.

Table I: Molar Extinction Coefficients (ϵ) of Various Solutions of Eu^{3+}

Salt	Solvent	Wavelength of absorption line, nm: 526	535	579	592
$Eu(ClO_4)_3$	Water	0.10	0.007	...	0.014
$Eu(ClO_4)_3$	Methanol	0.13	0.013	...	0.013
$Eu(ClO_4)_3$	Acetonitrile	0.14	0.04	0.007	0.02
$Eu(ClO_4)_3$	DMSO	0.10	0.018	...	0.012
$Eu(NO_3)_3$	Water	0.13	0.04	0.02	0.022
$Eu(NO_3)_3$	Methanol	0.085	0.08	0.017	0.017
$Eu(NO_3)_3$	Acetonitrile	0.08	0.1	0.041	0.010

Emission Spectra. The emission spectra of the solutions discussed in the foregoing section are given in Figure 2. Only the main lines of the $^5D_0$ level are shown. It is again seen that whereas the position of the lines is not affected by the solvent, the relative intensities are. It should be noted that since the main purpose of the work was to determine the quantum yield and not the structure, the spectra were usually taken with low resolution. A few examples are given for high resolution work mainly for the sake of comparison. The 618-nm band in the perchlorate–DMSO solution is shown to consist at least of four superimposed lines (of theoretical five). The removal of the degeneracy of the five $^7F_2$ sublevels results in most solvents only in an unstructured broadening of the band. In DMSO the mixing of the m_j states of $^7F_2$ is not efficient, and the spectrum resembles that in the glassy state.[13] In no other solvent did we find similar fine structure.

The line shape of the emission spectrum gives also some insight into the nature of the solvated species. As Gallagher[14] has shown, the 618-nm band is the most sensitive to environmental changes, due to the fact that it is mainly an electric dipole transition, while the 592 nm is essentially a magnetic dipole transition. We see that the 618-nm band is the most prominent in the nitrate solutions, and in perchlorate in acetonitrile, where we have good reasons to suppose that complexation with the anion distorts strongly the symmetry about the ion, thus allowing electric dipole transitions. This point is further amplified by considering the influence of several anions on the line shape in aqueous solutions (Figure 3). It is seen that high concentration of anions enhance the 618-nm band relative to the 592-nm band in the following order: $CNS^- > NO_3^- > Cl^- > ClO_4^-$. The thiocyanate ion is known to form a stable complex with Eu^{3+} in water.[15] The data allow us to conclude that indeed an association is formed between the Eu^{3+} ion and the nitrate—especially at high concentrations, even in wa-

(10) S. P. Sinha, "Europium," Springer-Verlag, Berlin, 1967, p 111.

(11) D. G. Miller, E. V. Sayre, and S. Freed, *J. Chem. Phys.*, **29**, 454 (1958).

(12) I. Abrahamer and Y. Marcus, *J. Inorg. Nucl. Chem.*, **30**, 1563 (1968).

(13) C. R. Kurkjian, P. K. Gallagher, W. R. Sinclair, and E. A. Sigety, *Chem. Phys. Glasses*, **4**, 239 (1965).

(14) P. K. Gallagher, *J. Chem. Phys.*, **41**, 3061 (1964).

(15) J. C. Barnes, *J. Chem. Soc.*, 3880 (1964).

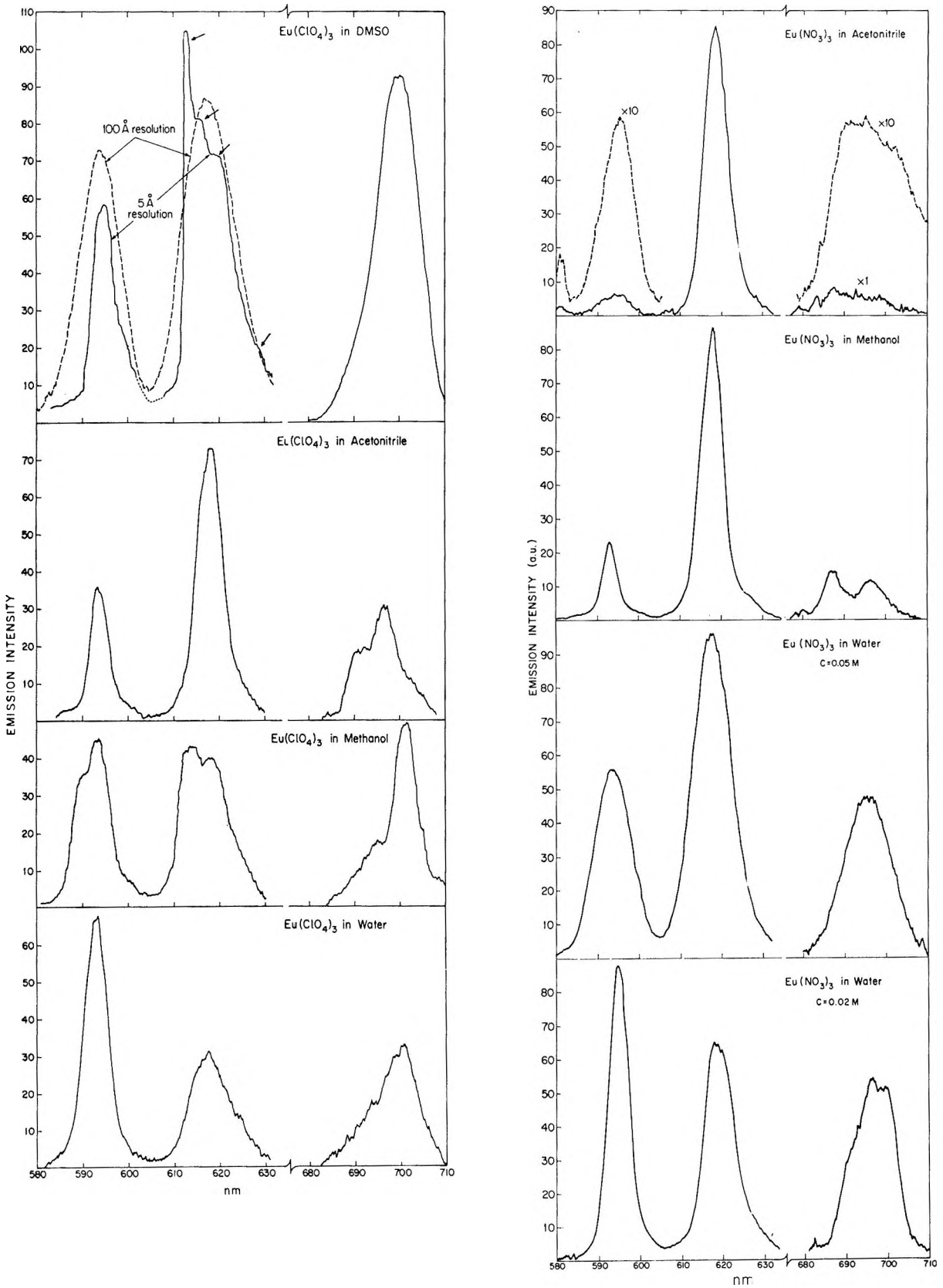

Figure 2. Emission spectra of the $^5D_0$ level of Eu^{3+} in various solvents; a, $Eu(ClO_4)_3$; b, $Eu(NO_3)_3$. Emission intensity in arbitrary units. For quantitative discussion of ratios see text.

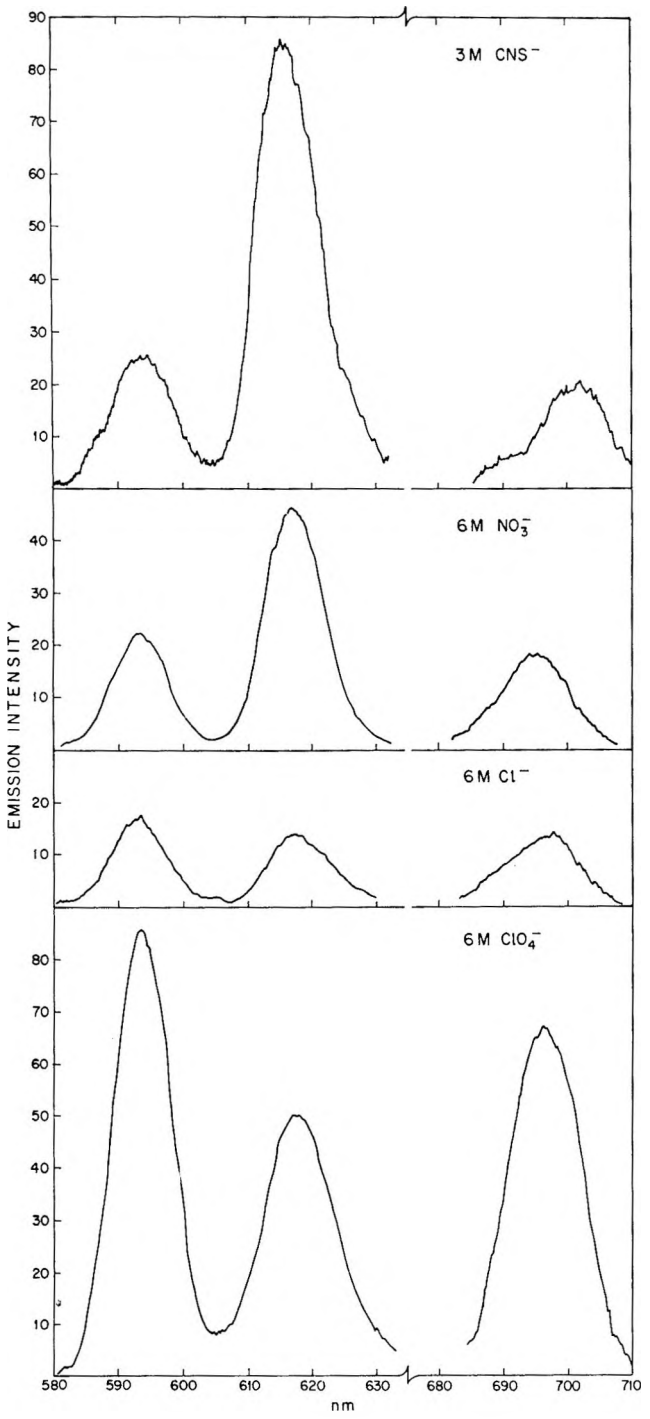

Figure 3. Effect of addition of different anions on the fluorescence spectrum of $EuClO_4$ in D_2O. Emission intensity in arbitrary units. For quantitative comparison see text.

ter, and with perchlorate in acetonitrile. We note that changes in concentration do not affect the line shape of $Eu(NO_3)_3$ in acetonitrile, including also the relative intensity of the $^5D_0 \rightarrow {}^7F_0$ band in emission—which appears only in these solutions. These observations are taken as proof that in acetonitrile the formation constant of the complex with nitrate is high, and essentially all the Eu^{3+} ions are complexed even in dilute solution.

Quantum Yields of Fluorescence. Having established qualitatively the interaction of the Eu^{3+} ion with the solvent and the anion, we turn to the quantitative determination of the quantum efficiency of fluorescence from the $^5D_0$ level. Direct excitation to this level is possible, and so the degree of nonradiative dissipation of energy from this state can be determined. We also excited to two higher levels ($^5D_1$ and $^5L_6$), thus enabling determination of losses of excitation energy on the route to the emitting state. The results are given in Table II.

The very low absorption in the 500–600-nm range dictated use of concentrated solutions (0.5–1.0 *M*) for determining the quantum yield upon excitation to the $^5D_0$ and $^5D_1$ levels. Much more dilute solutions were used when exciting to the $^5L_6$ level. In view of the ion-pair formation described in the previous section, we might expect differences in concentration to interfere with quantum yield measurements, at least with nitrate solutions. We refer to this problem in the next section, dealing with the influence of anion concentration on quantum yields.

Discussing pathways from higher levels to the $^5D_0$ state we shall compare only the results obtained with the same concentration, *i.e.*, those pertaining to excitation to $^5D_0$ and $^5D_1$, and not to $^5L_6$. As an example of possible consequences of this concentration effect, we note the differences in enhancement of fluorescence upon deuteration. In aqueous perchlorate solution we find a ratio of $D/H = 35$–38 upon excitation to all three levels. In aqueous nitrate solutions, and in methanolic perchlorate solutions, the ratio is higher with $^5L_6$ excitation (dilute solutions) than with either $^5D_0$ or $^5D_1$ excitation (concentrated solutions). We have not fully established the cause for this difference. It is likely to be due to anion concentration quenching which is more efficient in the weak quencher than in the good one (see Table III further on). However, possibly the presence of some light water in the concentrated solutions may also have affected the results.

Table II highlights the following.

(a) The role of the O–H bond in quenching is displayed; H_2O and CH_3OH are the best quenchers. Methanol and acetonitrile have similar dielectric constants and dipole moments and still differ strongly as far as quenching is concerned.

(b) The quantum yield is strongly dependent on the anion. Thus in good quenchers the quantum yield is higher in nitrate solutions than in perchlorate solutions, indicating the existence of an insulating sheath formed by nitrate ions. In bad quenchers, such as D_2O and CH_3CN, the emission efficiency is about equal, and maybe somewhat *higher* in the perchlorate solution, indicating that the interaction of the perchlorate ion with the Eu^{3+} ion is weak. The NO_3^-–Eu^{3+} interaction is of comparable strength to the solvent–Eu^{3+} interaction, resulting in incomplete, asymmetric NO_3^- complexing.

Table II: Per Cent Quantum Yields of the $^5D_0$ Emission of Eu(III) upon Excitation to Selected Levels

Excited level	$Eu(ClO_4)_3$[a] Water H	Water D	Methanol H	Methanol D	Acetonitrile H	Acetonitrile D	DMSO H	DMSO D
$^5D_0$	1.9 ± 0.1	78 ± 2	5.6 ± 0.1	(13.5)[b]	58 ± 4	72 ± 4	50 ± 2	95 ± 3
$^5D_1$	1.1 ± 0.1	42 ± 2	2.1 ± 0.1	(5.5)	26 ± 2	38 ± 2	29 ± 2	72 ± 3
$^5L_6$	0.57 ± 0.05	20 ± 1	0.7 ± 0.05	4.7 ± 0.2	11 ± 2	...	18 ± 1	...
$p(^5D_1 \rightarrow {}^5D_0)$	0.57	0.54	0.38	0.41	0.45	0.52	0.58	0.76

Excited level	$Eu(NO_3)_3$ Water H	Water D	Acetonitrile H	Methanol H	Methanol D[c]
$^5D_0$	4.0 ± 0.2	(48)	58 ± 2	31 ± 2	78
$^5D_1$	1.85 ± 0.1	(22)	34 ± 2	13 ± 1	44
$^5L_6$	0.73 ± 0.05	16.3 ± 1.0	16.7 ± 1.0	5.5 ± 0.5	25
$p(^5D_1 \rightarrow {}^5D_0)$	0.46	0.46	0.59	0.42	0.56

[a] $Eu(ClO_4)_3$ in D_2O: values in presence of <0.5% H_2O. [b] Values in parentheses: lower limits; H_2O content: 0.5 to 2%. [c] Data from ref 7.

The difference between H_2O and CH_3OH is bigger with nitrate solutions than with perchlorate and seems to become even smaller in the latter as solutions are diluted, weakening cation–anion interaction.

(c) The ratio of the quantum efficiency of fluorescence from the $^5D_0$ level upon excitation to $^5D_1$, to that obtained with direct excitation to $^5D_0$ gives the probability of an ion in the $^5D_1$ level to decay to the $^5D_0$ level. This probability, designated $p(^5D_1 \rightarrow {}^5D_0)$ is given in the last line in Table II. The efficiency of nonradiative transitions from the $^5D_1$ level directly to ground state is $1 - p(^5D_1 \rightarrow {}^5D_0)$ and is seen from the data to be remarkably constant. The probability of energy dissipation is 0.4–0.6 except for perchlorate in $(CD_3)_2SO$. The case of perdeuterated dimethyl sulfoxide is exceptional, as the quantum yield upon direct excitation to $^5D_0$ level is very close to 100%. In this case the excited states of the ion are well shielded from interaction with perturbing molecules or anions. It is clear that the absolute quantum efficiency of emission from the $^5D_0$ level has no correlation with the fate of an ion in a $^5D_1$ level. In all cases an ion in the $^5D_1$ level has about equal probability to lose its energy by decaying directly to the ground multiplet or by decaying to the nearby $^5D_0$ state. The direct radiative coupling of $^5D_1$ to ground state has been found by us to be small in all cases (see next paragraph).

(d) We have not determined quantitatively the quantum yield of emission from the $^5D_1$ level. This yield is very low, so that the signal to noise ratio is small. The emission from the $^5D_1$ level is composed of seven lines corresponding to transitions to the ^7F states (*cf.* the discussion of the $^5D_0$ emission in the Introduction). Only three of these lines appear at wavelengths lower than the lowest $^5D_0$ emission. The others are not observable because of the far stronger overlapping $^5D_0$ fluorescence. We can thus only compare quantum yields in similar solvents (such as H_2O and D_2O) where the line shape does not change significantly. Estimates of absolute quantum yields can be made by assuming that the combined emission of the four hidden lines is about the same as that of the three observable ones. These are the $^5D_1 \rightarrow {}^7F_0$, $^7F_1$, $^7F_2$ at 526, 535, and 555 nm, respectively. In all the solvents used the most intense is the 555-nm line. The relative enhancement of fluorescence upon deuteration of water was determined by measuring the increase of intensity of this peak. It is for $Eu(ClO_4)_3$ in 0.1 *M* solution 2–3. This should be compared to the value of 40 obtained for the $^5D_0$ emission. The absolute quantum yield of the $^5D_1$ emission did not vary much in the range of solvents used by us. In all it is estimated to be 10^{-4} to 10^{-5}.

Effect of Anions of the Quantum Yields. To establish the role of the anion in radiationless processes, we performed two series of measurements. First we studied the influence of increasing nitrate ion (added as NH_4NO_3) concentration on the quantum yields in H_2O and D_2O. The effect in heavy water was much more pronounced and easier to follow than in light water. We therefore limited the second series—the study of the influence of various anions—to D_2O as a solvent.

The first series is summarized in Table III. Excitation was to the $^5L_6$ level, and $Q(^5L_6)$ denotes efficiency of fluorescence from the $^5D_0$ level upon excitation to the $^5L_6$ level. The table shows that the nitrate ion is indeed

Table III: Influence of Nitrate Ion Concentration on Per Cent Quantum Yield of $^5D_0$ Fluorescence in Light and Heavy Water on Excitation to $^5L_6$. $[Eu(NO_3)_3]$ = 0.025 in D_2O, 0.03 in H_2O

Nitrate concentration, *M*	$Q(^5L_6)$ in H_2O	$Q(^5L_6)$ in D_2O	Enhancement factor
0.1	0.7	16.3	23.2
1	0.8	11.5	14.4
3	0.95	7.2	7.6

a less effective quencher than H_2O but a better one than D_2O. The last column in Table III shows that the enhancement factor upon deuteration is dependent on the nitrate concentration. This result is in line with the results of Table II where it was shown that the isotopic enhancement in concentrated solution of $Eu(NO_3)_3$ was only 12, compared to 23 in dilute solutions.

The results of the second series are given in Table IV. The solutions used were 0.02 *M* in Eu^{3+} and contained about 2% H_2O. The anions were added as anhydrous ammonium salts, which were further dehydrated before use. It is possible that very small quantities of light water did get into the solution, accounting for the decrease in the perchlorate solution. Another problem is the changes in absorption spectrum, *i.e.*, the appearance of a broad band in the near-uv causing differences in absorption near 394 nm, the $^7F_0 \rightarrow {}^5L_6$ band. This broad band has been assigned in the case of CNS^- [15] to charge-transfer transitions. Halide anions have been shown to form a CT complex in ethanol,[16] so that it is probably a similar band in water. The nitrate ion absorbs strongly in the 300-nm range, so that even if there is a CT band one cannot observe it. A measure of the reproducibility of the method may be found by comparing the results with 3 *M* nitrate in Tables III and IV. With these reservations in mind we can deduce from Table IV the following order of quenching power: $CNS^- > Cl^- > NO_3^- > ClO_4^-$. This is also the expected order of their formation constants for CT complexes. The CNS^- system was investigated further by excitation to the $^5D_1$ level, in order to avoid overlapping of charge transfer with f–f absorption bands. In this case Eu^{3+} concentration was 0.1 *M* and CNS^- was 1 *M*. The yield dropped from 19% in the absence to 7.5% in the presence of CNS^-. According to Barnes' [15] data, in this case about 80% of the Eu^{3+} ions are in the form of $[Eu\text{–}CNS]^{2+}$ complex.

Lifetimes of the $^5D_0$ State in Different Solvents. Table V shows the results in dilute and concentrated solutions. In cases previously investigated[2-4] our results agree well with published values.

Lifetimes longer than 50 μsec could be measured with our instrument, and estimates could be made down to 10 μsec. The lifetimes were determined from the oscillograms that represented in all cases an exponential decay. In a few cases the oscillogram was composed of two parts: an initial increase in light intensity and then a decay. Both were exponential. The results quoted in Table V are for the decreasing part of the picture. The increase was too short to be measured accurately. It was found in solutions of $Eu(ClO_4)_3$ in acetonitrile, where it is estimated to be 30 μsec, and in dimethyl sulfoxide, where it is about 15 μsec. The increase represents the growing in of the $^5D_0$ population from the higher level. Heber[17] found in hydrated crystals of Eu(III) similar growing in curves which corresponded to the decay of $^5D_1$. The effect of anions was determined for thiocyanate, where the lifetime was reduced from 2850 μsec for a perchlorate solution in D_2O to 800 μsec in the presence of added 1 *M* NH_4CNS, and for the nitrate, where the lifetime was reduced from 2950 μsec for dilute nitrate solution in D_2O to 950 μsec with 3 *M* NH_4NO_3 added.

Table IV: Quantum Yields of Solutions of $Eu(ClO_4)_3$ in D_2O as a Function of Anion Concentration; 0.06 *M* Perchlorate Always Present

Added anion concentration, *M*	Cl^-	NO_3^-	CNS^-	ClO_4^-
0	16.0	16.0	16.0	16.0
1	9.2	12.2	3.2	...
3	4.5	7.5	0.9	...
6	2.3	4.8	...	11.7

Table V: Lifetimes of Eu^{3+} Ion in Different Solutions (μsec)[a]

Salt solvent	$Eu(ClO_4)_3$ a	$Eu(ClO_4)_3$ b	$Eu(NO_3)_3$ a	$Eu(NO_3)_3$ b
H_2O	104 ± 5	104 ± 5	116 ± 5	127 ± 5
D_2O[b]	4100	4100	2800	3200
CH_3CN	775 ± 30	1220 ± 50	680 ± 50	770 ± 50
CD_3CN	1400 ± 100	2000 ± 200	...	...
$(CH_3)_2SO$	1500 ± 50	1440 ± 50	...	...
$(CD_3)_2SO$	2850 ± 100	...	...	...
CH_3OH	230 ± 30	...	370 ± 10	365 ± 10

[a] a, concentration range 0.01–0.05 *M*; b, concentration range 0.5–1.0 *M*. [b] Obtained by extrapolating experimental values to zero H_2O concentration.

Discussion

The main part of the Discussion will be devoted to evaluation of rate constants for radiative and nonradiative processes in the various systems studied. As an introduction to this quantitative discussion, it is useful at this stage to summarize some of the results so far cited and have an overall look on the present state of our knowledge of the problem.

Of all the systems dealt with in this work, the most extensive work was done on H_2O–D_2O as solvents. Our results compare well with those of previous works.[2,3] We note that these studies were made on the chlorides or the nitrates. Since they dealt only with dilute solutions, the appearance of ion pairs and complexes did not interfere with their results. Also, they reported results with 394-nm excitation only. Our work shows that the enhancement factor does not depend on the wavelength used for excitation, as long as the Eu^{3+} ion is free from ion pairing. Our work shows that the decay from higher

(16) C. K. Jorgenson, *Mol. Phys.*, 5, 271 (1963).
(17) J. Heber, *Phys. Kondens. Materie.*, 6, 381 (1967).

levels to the emitting level is relatively fast and only slightly affected by solvent deuteration, compared to the decay of the $^5D_0$ level.

This point is further amplified by considering the difference in the isotopic effect on $^5D_0$ and $^5D_1$ emission. Although the latter could not be accurately established, it is evident that the $^5D_1$ level is affected to a far lesser degree than the $^5D_0$. This can hardly be explained by the difference in the energy gap between the emitting level and the ground manifold. We discuss this point further in a forthcoming paper.[18]

Rate Constants for Radiative and Radiationless Transitions. The information obtained from lifetime and quantum yield measurements enables us to calculate the natural lifetime of the Eu^{3+} ion in different systems, and also some of the rates of radiationless transitions. The observed lifetime τ is related to the natural lifetime τ_0 by $\tau = \tau_0 Q$, where Q is the quantum yield upon direct excitation to the emitting level. The quantum yield may be expressed also as

$$Q = \frac{k_f}{k_f + \Sigma k_i} \tag{2}$$

where k_f is the radiative rate constant, defined as τ_0^{-1} and k_i is the rate constant for the ith quenching process. If another solute which serves as a quencher is present it is more customary to write the quantum yield as

$$Q = \frac{k_f}{k_f + \sum_i k_i + \sum_x k_x[X]} \tag{3}$$

where [X] is the concentration of the quencher and k_x a bimolecular rate constant.

We can calculate τ_0 and thus k_f only for the concentrated solutions. As stated above, the differences between dilute and concentrated solutions are caused mainly by different degrees of association between the Eu^{3+} cation and the anions. In water and DMSO solutions of Eu(III) perchlorate neither lifetime nor the line shape are dependent on concentration. We may conclude that in these solutions there is no ion pairing and the fluorescing species is the solvated Eu^{3+} ion. In methanol and acetonitrile solutions (and with nitrate as the ion also in aqueous solutions) it is evident that there is strong ion pairing. In this case the emitting level can no longer be associated with the solvated ion, but rather with the solvated ion pair or complex. The data of Tables I and V enable us to arrange the solvents used in a series according to their solvating power, which is a measure of polarity; thus $H_2O(D_2O) \sim$ DMSO > MeOH > MeCN. In the case of acetonitrile it is seen that in the presence of a strong complexing agent as NO_3^- ions, even in dilute solutions (0.034 M) the dominant species is the complex.

Using the relation shown in eq 4

$$Q = \frac{k_f}{k_f + k_s + k_a[A]} \tag{4}$$

where k_s is the rate constant due to interaction with the solvent and k_a is the rate constant due to interaction with anion A

$$k_s + k_a[A] = \frac{k_f(1 - Q)}{Q} \tag{5}$$

and hence we calculate $k_s + k_a[A]$. The results are given in Table VI.

Some generalizations can be made from the limited range of data in Table VI, mainly as guides to further study and criticism.

Table VI: Rate Constants for Radiative (k_f) and Radiationless ($k_s + k_a[A]$) Depopulation of the $^5D_0$ Level

Solvent	k_f, sec^{-1}	Q, %	$k_s + k_a$ [A], sec^{-1}
	$EuClO_4$		
H_2O	183	1.9	9800
D_2O	191	78	51
CH_3CN	475	58	344
CD_3CN	475	72	185
CH_3OH	~220[a]	6.5	3150
$(CH_3)_2SO$	333	50	333
$(CD_3)_2SO$	333	95	17
	$EuNO_3$		
H_2O	325	4	7800
D_2O	325	48[b]	325
CH_3CN	935	58	690
CH_3OH	860	31	2000
CH_3OD[c]	350	78	145

[a] Approximate value. [b] Lower limit. [c] From ref 7. The value of k_f should in principle be the same as for CH_3OH. We could not obtain CH_3OD sufficiently free of H_2O to check the values of ref 7.

First, the quenching rate constants are more sensitive to the nature of the solvent when perchlorate is the anion than with nitrate. They span a range of almost three orders of magnitude. This is probably due to the fact that the perchlorate anion is itself only negligibly involved in quenching mechanism. Thus the values of ($k_s + k_a[A]$) appearing in the last column of Table VI represent to a good approximation k_s, the quenching constant associated with the solvent. We divide the solvents according to this property into three groups: hydroxylic solvents, with k_s exceeding 1000 sec^{-1} ($k_s \gg k_f$), other protonated solvents with k_s in the range 100–1000 sec^{-1} ($k_s \approx k_f$), and deuterated solvents with k_s below 100 sec^{-1} ($k_s \ll k_f$). CD_3CN is an obvious exception. The discrepancy may be caused by the C≡N bond, whose vibrational energy is high (~3000 cm^{-1}),

(18) Y. Haas and G. Stein, to be published.

Table VII: Radiative and Quenching Rates for the System Eu^{3+}–CNS^-

Experiment	Observed lifetime τ, μsec	$k = 1/\tau$, sec^{-1}	k(EuCNS) from eq 9, sec^{-1}	Q (estimated)	$k_f = kQ$, sec^{-1}	k_f(EuCNS) from eq 9, sec^{-1}	k_a(CNS) = k(EuCNS) − k_f(EuCNS), sec^{-1}
1	530	1900	2340	0.2	950	1100	1330
2	860	1500	1350	0.2	430	460	810

or by the formation of an ion pair with the perchlorate. In the last group, radiationless processes are almost eliminated, and the observed lifetimes approach the radiative lifetimes. Such systems are favorable for obtaining laser oscillations. The $(CD_3)_2SO$ system looks most promising in this respect.

Anion Effects. The Eu(III) ion is surrounded by a number of solvent molecules in the first solvation layer. In a following paper[19] we shall show for H_2O in acetonitrile as the solvent that every additional molecule of H_2O entering the first solvation layer contributess equally to quenching. From our present results we attempt to calculate the order of magnitude of quenching due to a single anion, CNS^- or NO_3^- entering the first solvation layer. Similar results concerning acetate ion have been obtained by Kropp and Windsor.[20]

First let us consider the case of an equilibrium between two forms of the same electronic state, both emitting, *e.g.*, Eu^{3+} and $[Eu\text{–}A]^{2+}$. The equations for the observed decay time in this case are derived as follows. The equilibrium between the two forms is determined by an equilibrium constant K, so that the equation

$$B = KA \tag{6}$$

holds, B and A being the concentrations of two forms of the same state. The two species are characterized by different decay rates k_A and k_B, and their combined concentration is determined by the equation

$$\frac{d(A + B)}{dt} = k_A A + k_B B \tag{7}$$

which can also be written

$$\frac{dA}{dt} = \frac{k_A + k_B K}{1 + K} \cdot A \tag{8}$$

Provided equilibrium is established in times shorter than the lifetime of the excited states, an exponential decay will be observed, with a new rate constant

$$k = \frac{k_A + k_B K}{1 + K} \tag{9}$$

when K is very small, the rate will be essentially k_A, while for large K it will be k_B. A similar equation holds for the radiative natural rate constant, which is the reciprocal of natural lifetime. K used in the above equations should be the value pertaining to the excited states involved in the equilibrium in question.

For the system $(EuCNS)^{2+}$, Barnes[15] quotes an equilibrium constant of 5 in the ground state. We shall use this value for the $^5D_0$ excited state as an approximation. Using eq 9 and the similar one for the radiative rate constant, we get for two experiments with thiocyanate added to $Eu(ClO_4)_3$ in D_2O the results in Table VII. Q is the quantum yield which could be only estimated since the area under the absorption curve was too small to be accurately determined. It is also noted that since the heavy water used was not completely free from light water, and in view of the other approximations, the results can be taken only as indicating an order of magnitude. The meaning of the rate constant should be understood as follows. The $^5D_0$ level loses its energy to the surroundings at a rate of about 1000 sec^{-1} when associated with one thiocyanate ion. This value is independent of the solvent. Thus the quenching is considerable in D_2O and negligible in H_2O.

For the nitrate ion we have no data for the formation constant of the complex $(EuNO_3)^{2+}$. From our work we assume that it is less than that of the $(EuCNS^-)^{2+}$ complex. Calculations based on the data presented in the text yield the values given in Table VIII for different formation constants. These approximate calculations thus yield the order of magnitude of anion quenching for the two cases. The results seem reasonable, since they account for the relative efficiencies of the anions in light and heavy water solutions.

Table VIII: Radiative and Quenching Rates for the System Eu^{3+}–NO_3^-

Formation constant	k(EuNO$_3$), sec^{-1}	k_f(EuNO$_3$), sec^{-1}	k_a(NO$_3$), sec^{-1}
2	1300	310	990
4	1125	290	835
10	1020	275	745

Kropp and Windsor[20] obtained for acetate ion a radiative constant k_f of about 180 sec^{-1} for acetate concentrations above 1 M. No results were quoted for

(19) Y. Haas and G. Stein, *J. Phys. Chem.*, 75, 3677 (1971).
(20) J. L. Kropp and M. W. Windsor, *ibid.*, 71, 477 (1967).

$k_a(Ac^-)$. They point out that acetate ion is a better quencher than D_2O but less effective than H_2O. In the absence of a value for the association constant, the quenching constant $k_a(Ac^-)$ could not be calculated. Our considerations on the role of anions are in line with those of Kropp and Windsor.

Pathways of Radiative and Radiationless Transitions in Europium(III) Solutions: the Role of High Energy Vibrations

by Yehuda Haas and Gabriel Stein*

Department of Physical Chemistry, Hebrew University, Jerusalem, Israel *(Received December 24, 1970)*

Publication costs assisted by Hebrew University

The fluorescence of the $^5D_0$ level of $Eu(ClO_4)_3$ in mixtures of water and acetonitrile has been investigated. The quenching of this fluorescence by water is shown to be proportional to the number of water molecules entering the first solvation layer. The quenching reaches its value in pure water when there are nine water molecules per one Eu^{3+} ion. This suggests that each molecule acts independently. The rate constant for quenching by one water molecule is 1100 sec^{-1}. The role of high OH vibration in this specific effect is discussed.

In our preceding paper[1] we reported the fluorescent behavior of the $^5D_0$ level of Eu^{3+} in solution in different environments. This level behaves in a number of solvents essentially as in the solid state, so that its lifetime is relatively long ($\sim 10^{-3}$ sec). Excitation directly to this level in solution leads to a higher quantum yield than excitation to higher levels, *e.g.*, $^5D_1$ (see also ref 2).

The $^5D_0$ level is shielded from interactions leading to rapid loss of electronic energy and therefore long-lived. Less efficient quenching mechanisms may thus effectively operate on it. These are not general to the liquid state as such, but specific in the sense that they can be assigned to a definite molecule or ion interacting with the europic ion. One such mechanism with a rate constant of about 1000 sec^{-1} is due to interaction with an ion such as nitrate or thiocyanate, possibly by a charge-transfer mechanism.[1] Another is selective interaction with the high energy O–H vibration.[1-5] The rate constant for this process for the fully hydrated Eu(III) ion has been found by us[1] to be 9800 sec^{-1}.

The large isotopic effect has been the subject of several experimental as well as theoretical[6-8] studies in the solid and liquid states. It has been attributed to the large difference in vibrational energy between the O–H and the O–D bonds. Energy transfer is less likely to occur with D_2O, as in order to have adequate energy matching this molecule has to be excited to an even higher vibrational state than H_2O. This process is by far less probable and cannot compete with other deactivation processes.

To have a better physical description of the situation we isolated the Eu–H_2O system in an inert medium. Usually work has been done with H_2O–D_2O mixtures, where rapid exchange between these similar molecules takes place in the solvation layer of Eu^{3+}. In such a system it is difficult to specify the water molecule that interacts with the ion. A system in which the Eu^{3+} ion is dissolved in a relatively inert (from the point of view of quenching) solvent and contains in its first solvation shell a controlled number of water molecules is $Eu(ClO_4)_3$ in acetonitrile. Preliminary fluorescence studies, as well as nmr experiments,[9] convinced us that the Eu–H_2O association constant is much higher than the Eu–CH_3CN association constant, and so it is possible to have species such as monohydrated, dihydrated, etc., Eu^{3+} ions when the water concentration is low enough. Furthermore, acetonitrile is sufficiently polar to dissolve $Eu(ClO_4)_3$ to high concentrations, and the quan-

(1) Y. Haas and G. Stein, *J. Phys. Chem.*, **75**, 3668 (1971).

(2) W. R. Dawson and J. L. Kropp, *J. Opt. Soc. Amer.*, **55**, 822 (1965).

(3) J. L. Kropp and M. W. Windsor, *J. Chem. Phys.*, **42**, 1599 (1965).

(4) P. K. Gallagher, *ibid.*, **43**, 1742 (1965).

(5) A. Heller, *J. Amer. Chem. Soc.*, **88**, 2058 (1966).

(6) J. Heber, *Phys. Kondens. Materie*, **6**, 381 (1967).

(7) D. N. Terpilovskii, *Opt. Spektrosk.*, **24**, 596 (1968); *Opt. Spectrosc.*, **24**, 313 (1968).

(8) R. E. Ballard, *Spectrochim. Acta, Part A*, **24**, 65 (1968).

(9) Y. Haas and G. Navon, to be published.

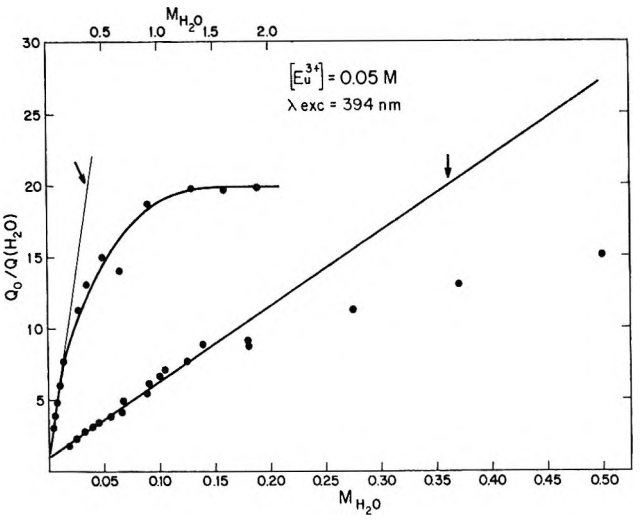

Figure 1. Quenching of Eu^{3+} fluorescence from $^5D_0$ by H_2O in CH_3CN solution, excitation wavelength 394 nm to $^5L_6$. Upper curve shows the complete concentration range of H_2O used (not all points shown). Lower curve gives the details of the low concentration part of the upper curve.

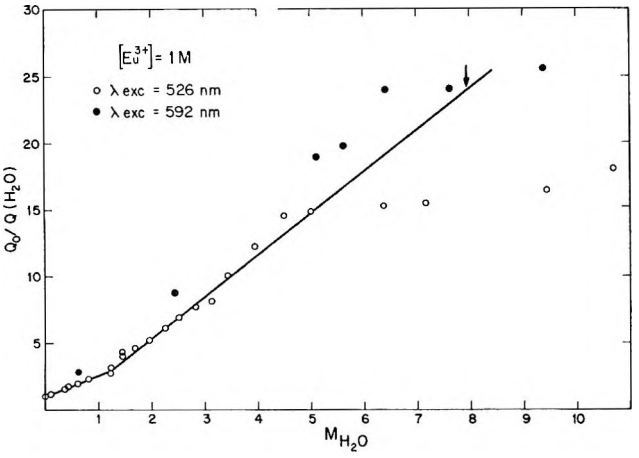

Figure 2. Quenching of Eu^{3+} fluorescence from $^5D_0$ by H_2O in CH_3CN solution, excitation wavelengths 526 ($^5D_1$) and 592 nm ($^5D_0$). The arrow points to the limiting value of $Q_0/Q(H_2O = 100\%) = 24$, on excitation to $^5D_1$. The corresponding value for excitation directly to $^5D_0$ is 30.

tum yield of $^5D_0$ emission in it is much higher than that of aqueous solutions.[1]

Experimental Section

Solutions were prepared as previously described.[1] Water was added to the dry ($H_2O < 0.1\%$) acetonitrile solutions by a microsyringe. Its concentration was thus known and further checked by nmr spectroscopy. Quantum yield and lifetime measurements were performed as described in ref 1.

Results

Quantum Yields in Acetonitrile as a Function of Water Concentration. In Figure 1 we give the influence of water concentration on the quantum yield of the $^5D_0$ emission from acetonitrile solutions, upon excitation to the $^5L_6$ level. (For the term scheme see Figure 1 of ref 1.) Figure 2 shows the effect of water on the quantum yield for excitation to the $^5D_1$ level (526 nm) and directly to the $^5D_0$ level (592 nm). The concentration of $Eu(ClO_4)_3$ is 1 *M* for the latter figure, and 0.05 *M* for Figure 1. Figure 3 gives the lifetime of concentrated solutions as a function of water concentration. Quantum yields are given as $Q_0/Q(H_2O)$, lifetimes as $\tau_0/\tau(H_2O)$ where $Q_0(\tau_0)$ denotes quantum yield (or lifetime) for water-free acetonitrile solutions ($\tau_0 \simeq 1250$ sec) and $Q(H_2O)$ ($\tau(H_2O)$), the quantum yield (lifetime) in the presence of the given concentration of water.

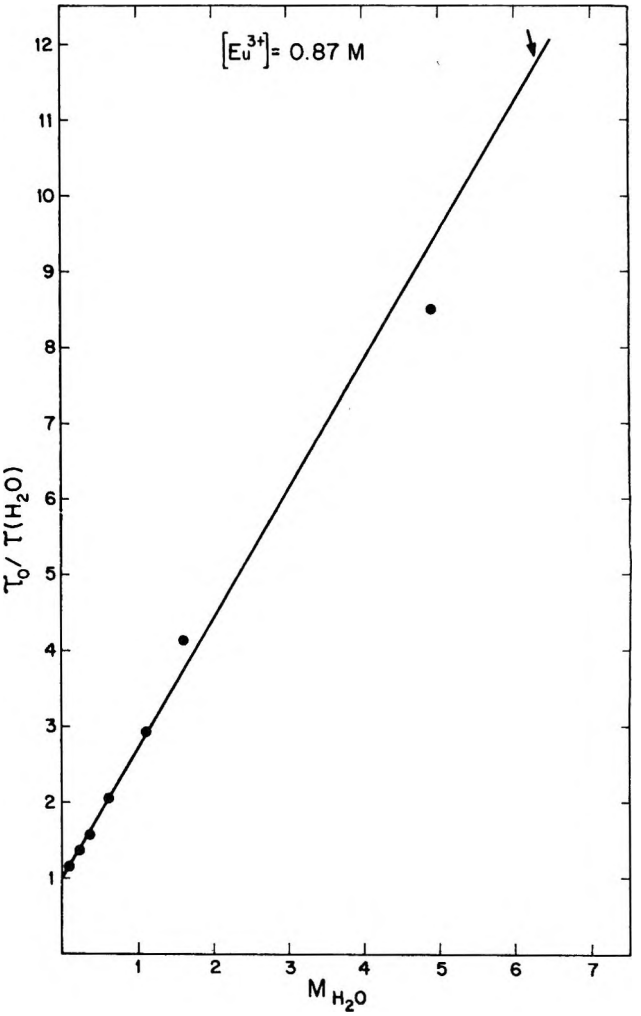

Figure 3. Lifetime of $^5D_0$ emission in acetonitrile solution of $Eu(ClO_4)_3$ as a function of water concentration.

As discussed later on, the straight lines drawn through the experimental points in Figures 1–3 have no simple physical meaning. An approximate equation for the theoretical line is given in the Discussion. Straight lines *are* obtained, at least for a considerable span of water concentrations. The arrows in the figures indicate the point the ordinate of which corresponds to the ratio of Q's (and τ's) of pure acetonitrile to pure water. The abscissas at the arrows give approximately

the same water concentration when divided by the Eu^{3+} concentration: (The value for 592-nm excitation could not be obtained, for lack of sufficient experimental data.) The water concentration at this point turns out to be seven to eight times the Eu^{3+} concentration. This value is near the accepted coordination number of trivalent europium in solution and led us to assume a stepwise quenching mechanism, as discussed below.

Effect of Perchlorate Concentration. The spectrum of $Eu(ClO_4)_3$ in acetonitrile both in absorption and emission strongly resembles that of $Eu(NO_3)_3$ in water. Since in the latter, association between the cation and the anion is known to take place,we found it desirable to find out whether the perchlorate anion forms an ion pair with the europic ion in acetonitrile and whether it influences the quantum yield.

The solutions used were 0.2 *M* in Eu^{3+}, and water concentration was in one series 0.5 *M*, in the other 2 *M*. In the latter where $[H_2O]/[Eu^{3+}] = 10$ the quantum yield without perchlorate added was near the quantum yield in water.

Three concentrations of ClO_4^- ion were used. Saturation was reached at about 3 *M* in the "dry" solution, and at 5 *M* in the water-rich solution. Admittedly, the results may be influenced by factors such as viscosity changes, impurities, etc., at such high concentrations. The results, given in Table I, are consistent

Table I: Quantum Yield of the $^5D_0$ Level of Eu^{3+} in Acetonitrile Solutions as a Function of Water and Perchlorate Anion Concentration; Excitation at 526 nm (to $^5D_1$)

M_{H_2O}	$M_{ClO_4^-}$	Q, %
0.5	0.6	15.5
0.5	1.7	10.8
0.5	2.7	6.8
2	0.6	1.5
2	2.7	1.7
2	5.0	2.0

with the assumption of some interaction between perchlorate and Eu^{3+}. The line shape of emission in the "dry" solution did not change much, except for slight reduction in intensity of the 618-nm band in the most concentrated perchlorate solution. The quantum yield decreases monotonously as the anion concentration is increased. When the water concentration is 2 *M*, the quantum yield increases with perchlorate concentration, and the line shape concurrently changes, as the 618-nm band becomes steadily stronger relative to the 592-nm band. These results are similar to those obtained with nitrate in H_2O–D_2O mixtures.[1] The evidence is not conclusive. The results nevertheless may be taken as indicating ion pairing between Eu^{3+} and ClO_4^-, at least in the $^5D_0$ excited state of the former.

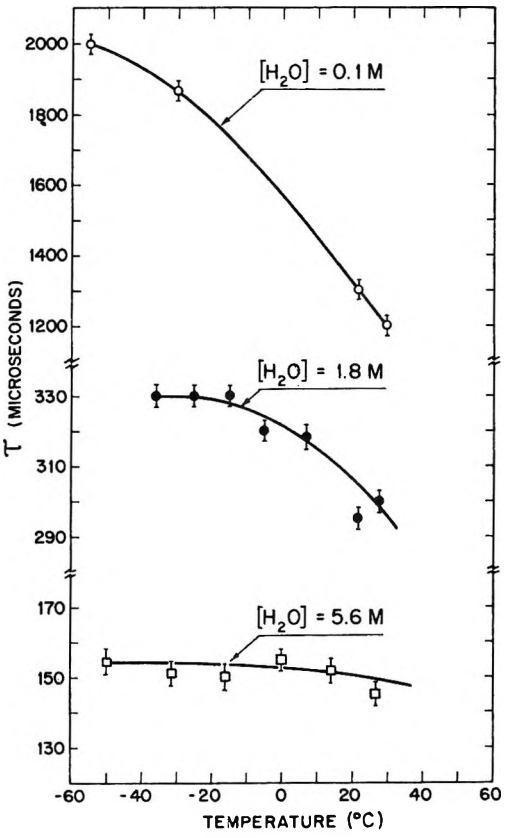

Figure 4. Temperature dependence of lifetime of $^5D_0$ emission in acetonitrile solutions. Water concentration expressed as $[H_2O]/[Eu^{3+}]$. $Eu(ClO_4)_3$ concentration is 0.87 *M*.

The rate constant of quenching by a perchlorate ion turns out to be of the same order of magnitude as for the nitrate,[1] *i.e.*, $\sim$1000 sec^{-1}.

Temperature Effects. The lifetime of the $^5D_0$ fluorescence is nearly constant in aqueous solution over the range -5 to $+30°$. In acetonitrile solution the lifetime increases from about 1220 μsec at 30° to about 2000 μsec at $-50°$ just above the freezing point. In intermediate concentrations of water the lifetime at room temperature attains intermediate values. We expected to find a decrease in lifetime upon cooling, as we assumed that the equilibrium

$$Eu(H_2O)_x(CH_3CN)_{n-x} + H_2O \rightleftharpoons Eu(H_2O)_{x+1}(CH_3CN)_{n-x-1} + CH_3CN$$

pertaining to the excited state of Eu^{3+}, will be shifted to the right. The results for three concentrations of water are given in Figure 4. The middle curve is for H_2O/Eu ratio of 1.8 (solution I) and the lower curve is for the ratio of 5.6 (solution II). The lifetime drops in the middle curve to about 300 μsec at room temperature, indicating strong hydration, and increases upon cooling. With the more fully hydrated species in the second experiment the lifetime was almost constant over the same temperature range. Solution I reached a constant lifetime at about $-20°$, compared to an increase

in water-free solution down to the freezing point. Using the formula

$$k(T) = \left(\frac{1}{\tau} - \frac{1}{\tau_m}\right) = A \exp(-\Delta E/RT)$$

where τ_m is the lifetime in the absence of temperature-dependent quenching processes, we obtain an energy of activation of about 2500 cm^{-1} for solution I. This value may point to quenching *via* the $^5D_1$ level, 1700 cm^{-1} above $^5D_0$, as suggested in ref 10b. We found that in deuterated acetonitrile thermal population of $^5D_1$ level is indeed obtained upon populating by light absorption selectively only the $^5D_0$ level.[11]

Discussion

As noted in the previous paper[1] and further discussed above, there are good reasons to believe that in concentrated Eu^{3+} solutions in pure acetonitrile some ion pair Eu^{3+}–ClO_4^- is formed. This ion pair does not exist to any significant extent in water. Thus, addition of water to a solution of europium perchlorate in acetonitrile leads to dissociation of this ion pair. It is possible that the bend observed in Figure 2 at about 1 *M* water is caused by this effect. Note that no such bend is found in Figure 1, dealing with dilute solutions. In our discussion we shall ignore the ion pairing.

The change in the solvation shell of the ion upon altering solvent composition changes at least two parameters of interest to us. These are the natural lifetime and the quenching rate. The quantum yield in a solution containing *m* moles of water can be written as

$$Q = \frac{k_f^m}{k_f^m + k_x^m + k_H \cdot [H_2O]} \quad (1)$$

where k_f is the radiative rate constant, specific for the given composition, k_x is a first-order rate constant taking care of all other quenching processes, and k_H is a bimolecular rate constant for the reaction

$$(Eu^{3+})_{el}^* + H_2O \xrightarrow{k_H} Eu^{3+} + (H_2O)_{vibr}^* \quad (2)$$

Since k_f and k_x are unknown functions of *m*, there is no theoretical ground to expect a straight line in Figure 3, and similarly in Figures 1 and 2.

If we assume that k_x does not change much upon addition of water (a plausible assumption, since it seems that unless there are specific quenching mechanisms, the quenching rates are similar for different liquids[1]), we can rewrite formula 1 as

$$\frac{k_f^m}{Q} - k_f^m = k_x^m + k_H \cdot [H_2O] \quad (3)$$

Q and k_f can be determined experimentally for each composition, and thus the left side of eq 3 can be plotted against water concentration. The intercept of the straight line observed should yield k_x and the slope k_H.

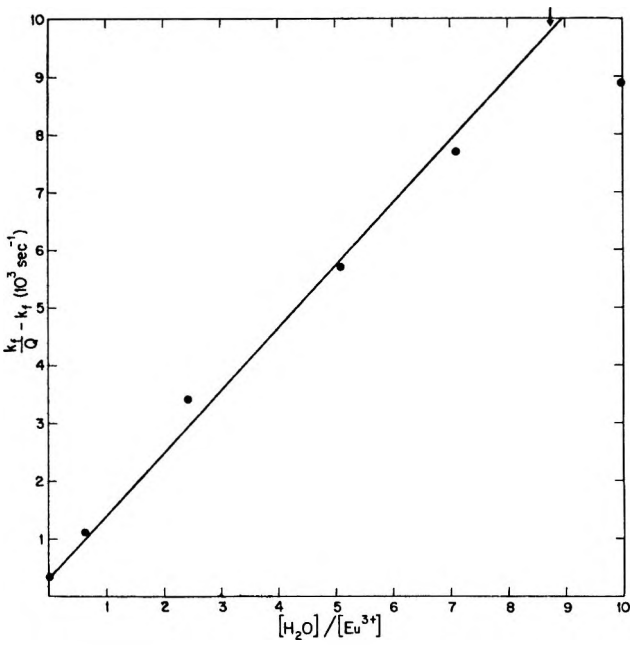

Figure 5. Quenching of $^5D_0$ fluorescence as a function of H_2O/Eu ratio.

The least-squares plot based on the first five points is given in Figure 5. k_x is seen to be 315 sec^{-1} and k_H 1100 sec^{-1}. In our work on solvent effects[1] we found that the total quenching rate constant in aqueous solution is 9800 sec^{-1}. Combining these results we obtain formally that nine molecules only participate in the quenching process in aqueous solution. This may be taken as an effective coordination number for the $^5D_0$ excited state of the europic ion in solution, as has been established[12] in several hydrated salts.

This result, with due reservations owing to the approximations made, may be taken as an indication that in acetonitrile–water mixtures each water molecule bound in the solvation layer of Eu^{3+} acts independently in the quenching process. Of course the equilibrium constant for binding need not be identical for all nine.[9]

The straight lines obtained in Figures 1–3 can be explained by considering eq 4.

$$\frac{\tau^\circ}{\tau^m} = \frac{k_f^m + k_x^m}{k_f^\circ + k_x^\circ} + \frac{k_H \cdot [H_2O]}{k_f^\circ + k_x^\circ} \quad (4)$$

It is evident that if k_f^m and k_x^m are weakly dependent on *m*, the second term will dominate. This is clearly the situation in our case. For the quantum yields, the proper equation is

$$\frac{Q^\circ}{Q^m} = \frac{p^\circ \cdot k_f^\circ (k_f^m + k_x^m + k_H \cdot [H_2O])}{p^m \cdot k_f^m (k_f^\circ + k_x^\circ)} \quad (5)$$

(10) (a) W. R. Dawson, J. L. Kropp, and M. Windsor, *J. Chem. Phys.*, **45**, 2410 (1966); (b) J. L. Kropp and W. R. Dawson, *ibid.*, **45**, 2419 (1966).

(11) Y. Haas and G. Stein, *Chem. Phys. Lett.*, **8**, 366 (1971).

(12) L. Helmholtz, *J. Amer. Chem. Soc.*, **61**, 1544 (1939).

where p is the probability for population of the emitting $^5D_0$ level from the level excited by monochromatic light. $p(^5D_1 \rightarrow {}^5D_0)$ is 0.45 for acetonitrile and 0.57 for pure water solution;[1] therefore it is a slowly varying function of water concentration.

We can thus use eq 5 as a starting point for analyzing Figures 1 and 2. In the low water concentration region, the $k_H \cdot [H_2O]$ term dominates, and straight lines are obtained. In the case of excitation to $^5D_1$ (Figure 2) there appear two straight lines. With concentrations up to about 1 M of H_2O the slope is about half that with concentrations in the range 1–6 M. This is due to the existence of an ion pair between the europic ion and the perchlorate ion. The solvation layer surrounds both species, and statistically it is less probable that energy be transferred from the Eu^{3+} ion to the water molecule. Increasing water concentration leads to dissociation of the ion pair and to enhancement of quenching efficiency.

In the more dilute solutions, excited to the $^5L_6$ level, this behavior was not found. The concentration of ClO_4^- is apparently too low to form a stable ion pair, so that quenching is efficient even with minute amounts of water. We note that departure from the straight line is obtained with relatively lower concentrations of water in the more dilute solutions. Furthermore, as Table II shows, the line shape of the emission spectrum is different from that of pure aqueous solution even when a H_2O/Eu^{3+} ratio of near 40 has been reached. Yet the quenching is complete at this ratio. The early departure from the straight line in quenching is accounted for by the competition between H_2O and CH_3CN molecules for a place in the first solvation layer.

Table II: The Relative Intensities of the 618- and 592-nm Lines in $Eu(ClO_4)_3$ Solutions in Acetonitrile as a Function of Water Concentration Eu^{3+} = 0.05 M

H_2O concn, M	Relative intensity 618/592
0	2.6
0.025	2.15
0.055	1.9
0.075	1.65
0.150	1.6
0.350	1.3
0.640	1.2
1.300	1.0
1.900	1.0
Aqueous solution	0.8

In conclusion, it is evident from our results that each water molecule acts as an independent quencher. The maximum number of water molecules that can be simultaneously in contact with the Eu^{3+} ion is nine, so that in aqueous solution the quenching rate constant (probability) is nine times that of an individual water molecule. The quenching does not necessarily take place through a long-lived static association between the ion and the water molecule, but through a dynamic equilibrium between solvent molecules in the bulk and in the solvation layer.

Vapor-Phase Charge-Transfer Complexes. VI. Diethyl Ether–Iodine

by Just Grundnes, Milton Tamres,* and S. N. Bhat

Chemistry Department, University of Michigan, Ann Arbor, Michigan 48104 *(Received June 23, 1971)*

Publication costs assisted by the National Science Foundation

The spectral and thermodynamic properties of the diethyl ether–iodine complex in the vapor phase have been reinvestigated. Analysis of the charge-transfer spectral data shows there is considerable uncertainty in separating the equilibrium constant (K_c) and the extinction coefficient (ϵ_{max}) from the $K_c\epsilon_{max}$ product. The change in internal energy on complexation (ΔE), obtained from the temperature dependence of $K_c\epsilon_{max}$, is -4.5 ± 0.2 kcal mol^{-1}. This value is larger than previously reported. It is shown also that a blue-shifted iodine band is present, although the characterization of this band is not established.

Introduction

Several spectrophotometric studies have been made of the diethyl ether–iodine complex in solution.[1-5] However, only one such study of this complex has been made in the vapor phase,[6] with rather different spectral and thermodynamic results.

It is reported that the charge-transfer (CT) band of diethyl ether–iodine is blue-shifted and the equilibrium constant is increased in going from solution to the vapor phase.[6] Such changes seem to be typical for complexes that are weak to only moderately strong[7] but not for the strongest complexes.[8] There are, however, other aspects of the reported vapor-phase results that warrant further consideration. First, the shape of the vapor CT band is far more skewed, with a steep slope on the high-energy side, compared to the same band in solution or compared to the vapor CT band for diethyl sulfide–iodine.[9,10] Second, the conditions for separating the equilibrium constant (K_c) and the extinction coefficient (ϵ) from the $K_c\epsilon$ product are at about the limit of the criteria that have been recommended.[11,12] The results are rendered more uncertain by the fact that the total absorbances are rather low (<0.08), so that minor corrections become relatively important in the $K_c\epsilon$ separation.[12] Third, the reported heat of complexation in the vapor phase is appreciably smaller than that in solution. Such a result would not have been anticipated for this complex based on a model by Christian, *et al.*,[8b,13] of solvent loss on complexation and the relative solvation energies of the complex, the donor and the acceptor. Finally, in view of the fact that a blue-shifted iodine band recently has been observed for the diethyl sulfide–iodine complex,[14] the question is raised whether this band exists in the case of diethyl ether–iodine. Previously it had been reported that no blue-shifted band existed[6] or, at best, such a band would have to be quite broad.[15]

Diethyl ether–iodine is one of the "classical" CT complexes, and it was felt important to reinvestigate this system to clarify the above points.

Experimental Section

The experimental procedure for handling and mixing the reagents and controlling the temperature has been presented.[16,17] The more convenient break-seal tube described previously[16] was blown to size to hold the desired volume of ether.

Concentrations were determined from the weights of the reagents and the volumes of the cells. Individual weighings were precise to ± 0.1 mg and the volumes to ± 2 ml. The break-seal tube was weighed empty and weighed again after adding the reagent. Then the bulb with sample was cooled to liquid nitrogen temperature, evacuated, and sealed. The weight of iodine ranged from 11.9 to 21.4 mg corresponding

(1) H. A. Benesi and J. H. Hildebrand, *J. Amer. Chem. Soc.*, **71**, 2703 (1949).

(2) (a) J. S. Ham, *J. Chem. Phys.*, **20**, 1170 (1952); (b) J. S. Ham, *J. Amer. Chem. Soc.*, **76**, 3875 (1954).

(3) (a) M. Brandon, M. Tamres, and S. Searles, *ibid.*, **82**, 2129 (1960); (b) M. Tamres and M. Brandon, *ibid.*, **82**, 2134 (1960).

(4) (a) P. A. D. de Maine and P. Carapellucci, *J. Mol. Spectrosc.*, **7**, 83 (1961).

(5) G. Kortüm and G. Friedheim, *Z. Naturforsch.*, **20**, 29 (1947).

(6) F. T. Lang and R. L. Strong, *J. Amer. Chem. Soc.*, **87**, 2345 (1965).

(7) See, for example, R. S. Mulliken, The Robert A. Welch Foundation Conferences on Chemical Research. XI. Radiation and the Structure of Matter, Houston, Texas, Dec 4–6, 1967.

(8) (a) S. D. Christian and J. Grundnes, *Nature (London)*, **214**, 1111 (1967); (b) J. Grundnes and S. D. Christian, *J. Amer. Chem. Soc.*, **90**, 2239 (1968); (c) *Acta Chem. Scand.*, **23**, 3583 (1969).

(9) J. M. Goodenow and M. Tamres, *J. Chem. Phys.*, **43**, 3393 (1965).

(10) M. Tamres and S. N. Bhat, *J. Amer. Chem. Soc.*, in press.

(11) W. B. Person, *ibid.*, **87**, 167 (1965).

(12) R. A. LaBudde and M. Tamres, *J. Phys. Chem.*, **74**, 4009 (1970).

(13) S. D. Christian, J. R. Johnson, H. E. Affsprung, and P. J. Kilpatrick, *ibid.*, **70**, 3376 (1966).

(14) M. Tamres and S. N. Bhat, *ibid.*, **75**, 1057 (1971).

(15) C. N. R. Rao, G. C. Chaturvedi, and S. N. Bhat, *J. Mol. Spectrosc.*, **33**, 554 (1970).

(16) M. Tamres and J. Grundnes, *J. Amer. Chem. Soc.*, **93**, 801 (1971).

(17) M. Kroll, *ibid.*, **90**, 1097 (1968).

Table I: Concentration and Spectral Data for Diethyl Ether–Iodine in the Vapor Phase in a 100.0-Cm Cell at the Wavelength 234 mμ

Run	$10^5[I_2]$, M	10^2[ether], M	Corrected absorbance[a] 59.8°	67.0°	80.0°	89.8°	97.8°	ϵ_{I_2}(λ 480 mμ),[b] M^{-1} cm^{-1}
1	4.49	1.277	0.351	0.299	0.232	0.195	0.175	350
2	4.58	1.389	0.378	0.326	0.256	0.216	0.188	348
3	4.42	1.476	0.396	0.335	0.265	0.220	0.193	350
4	4.85	2.004	0.599	0.510	0.404	0.339	0.298	348
5	4.24	2.836	0.736	0.626	0.491	0.414	0.364	348
6	3.11	3.821	0.698	0.612	0.490	...	...	352
7	2.78[c]	5.523	0.906	0.780	0.610	0.514	0.451	364
8	2.71[c]	5.625	0.904	0.773	0.611	0.513	0.439	358

[a] Error limit ~0.005 unit. [b] Calculated from the absorbance of the mixture at 100° in the visible region and the concentration of iodine determined by weight. Iodine vapor alone or in the presence of hydrocarbons shows little temperature dependence in the region of 480 mμ,[15] and ϵ_{I_2} at 480 mμ has been determined as 350 ± 2 M^{-1} cm^{-1}. [c] If the concentrations were to be calculated from the absorbances, assuming no effect of the ether on the iodine absorbance, then the concentration in runs 7 and 8 would be increased to 2.89×10^{-5} and 2.7×10^{-5} M, respectively, based upon ϵ_{I_2} equal to 350 M^{-1} cm^{-1}. This corresponds to a change of 4.1 and 2.4%, respectively.

to a concentration from 2.71×10^{-5} to 4.85×10^{-5} M. An approximate check of the concentration was made at the end of a run by taking the system to 100° and recording the absorbance at 480 mμ,[16] as will be mentioned in the Discussion. This check by the two determinations, weight and spectral, indicated an error in iodine concentration of the order of 1%, although it may have been as high as 2% in a few runs. The much larger weights of ether, 1.628–7.212 g, make the errors in ether concentration negligible. The concentration range was 1.28×10^{-2} to 5.62×10^{-2} M; the highest concentration corresponds to a pressure of 1.71 atm at 97.8°.

Because of the donor volatility, the ether break-seal tube was opened first. Then the iodine was introduced into the main body of the cell either by gently heating the opened iodine break-seal tube or by condensing the ether in with the iodine and washing it out into the cell. The cells used had a path length of 100.0 cm as determined with a Wild cathetometer. Their volumes ranged from 1720 to 1740 ml; the small variation was due to differing lengths and bulb sizes of the break-seal tubes.

In a few experiments, a slow irreversible reaction occurred as evidenced by an increase in absorbance at 260 mμ and a decrease at 480 mμ, as had been observed by Lang and Strong[6] above 90°. For the data reported in this paper, the diethyl ether–iodine system was stable for the duration of the run (~8–10 hr). Temperature dependence was studied going down from 97 to 60° and back up again. Reproducibility was excellent, of the order of 0.005 absorbancy unit.

The source and purification of iodine has been described.[3a] Mallinckrodt diethyl ether from a freshly opened container was used without purification. In several runs, freshly distilled ether was used with no noticeable difference in results.

All calculations were programmed for the IBM 360-67 computer.

Results

The experimental data for eight ether–iodine mixtures are presented in Table I. Special care was taken to correct for the small contribution of ether and of iodine to the total absorbance by studying their spectra separately from different samples over the temperature range of interest.

Figure 1 shows the spectrum of the diethyl ether–iodine CT band in the vapor phase, with a maximum at 234 mμ, as found by Lang and Strong.[6] The absorbance scale here is about 10 times that of Lang and Strong, which corresponds to the factor difference in cell paths in the two studies. The temperature dependence of the absorbance is shown in Figure 2.

The study of the blue-shifted iodine band is shown in Figure 3. There is a small but distinct enhancement in the iodine absorbance at wavelengths shorter than 480 mμ. Further, this enhancement shows a small decrease with an increase in temperature, which is opposite to the effect due to normal temperature broadening but is in accord with the effect due to dissociation of a complex. A similar but much more pronounced effect has been reported recently for the stronger diethyl sulfide–iodine complex.[14]

Discussion

The CT band of diethyl ether–iodine, shown in Figure 1, is more symmetrical than that reported by Lang and Strong.[6] The reason for this difference apparently is in the reported spectrum of free iodine in the ultraviolet region. The higher absorbance in the figure of Lang and Strong results in a larger free iodine correction on the short-wavelength side of the total absorbance curve of the mixture. The half-width at

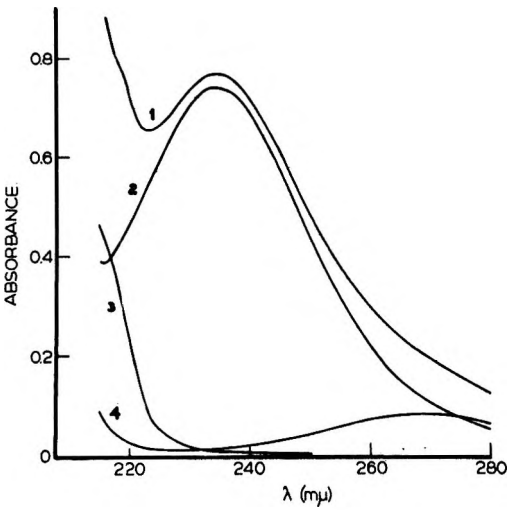

Figure 1. Diethyl ether–iodine spectrum in the vapor phase at 59.8° in a 100.0-cm cell: (4) iodine, 4.24×10^{-5} M; (3) diethyl ether, 2.836×10^{-2} M; (1) mixture of 3 + 4; (2) complex.

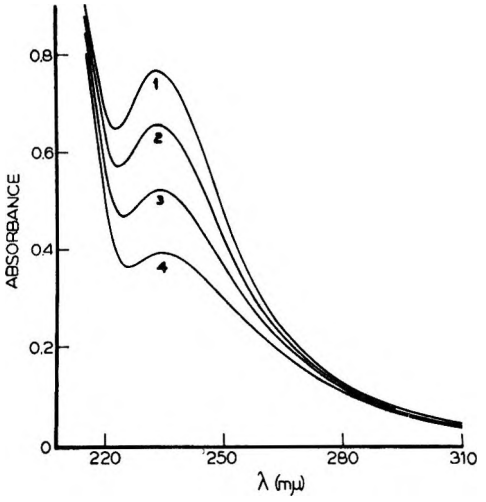

Figure 2. Temperature dependence of the diethyl ether–iodine absorption in the vapor phase; iodine, 4.24×10^{-5} M; diethyl ether, 2.836×10^{-2} M; cell, 100.0 cm: (1) 59.8°, (2) 67.0°, (3) 80.0°, (4) 97.8°.

half-maximum of the CT band, taken as $\bar{\nu}_{max} - \bar{\nu}_{1/2}$ (long-wavelength side), has an average value of ~3150 cm^{-1} over the temperature range 59.8–97.8°. This is perhaps only a little larger than that for the iodine complex with mesitylene[18] or with diethyl sulfide.[9,17,19]

The data in Table I were analyzed in the usual fashion to determine the constants K_c and ϵ using the quadratic equation

$$\frac{D_0A_0}{OD'} = \frac{1}{\epsilon'}\left[\frac{1}{K_c} + (D_0 + A_0) + \frac{OD'}{\epsilon'}\right] \quad (1)$$

where D_0 and A_0 are the initial concentrations of donor and acceptor, respectively, OD′ is the corrected optical density,[12] and ϵ' is the corrected extinction coefficient ($= \epsilon_{CT} - \epsilon_D - \epsilon_A$).[12] Actually, two sets of values are given; those in parentheses correspond to slightly different iodine concentrations for runs 7 and 8 as will be mentioned.

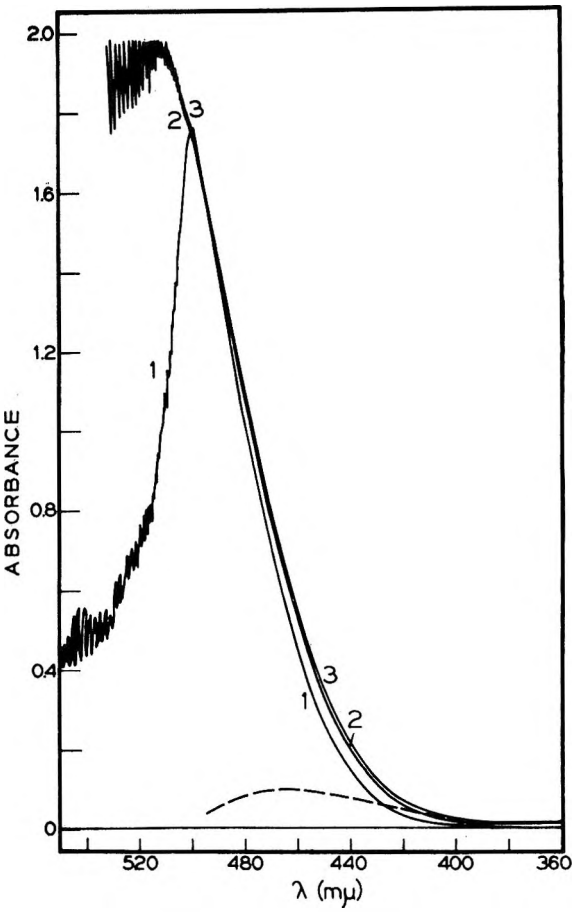

Figure 3. Diethyl ether–iodine absorption in the vapor phase in the visible region; 75.0-cm cell; iodine, 3.97×10^{-5} M; diethyl ether, 4.914×10^{-2} M; (1) iodine alone at 45°, (2) iodine + ether at 80°, (3) iodine + ether at 60°.

It has been discussed[11,12] that meaningful separation of K_c and ϵ depends upon the relative magnitudes of the terms $1/K_c$ and $(D_0 + A_0)$. (The last term within the brackets in eq 1 corresponds to the concentration of the complex, which is small in this case and need not be considered.) Because of the limitations in pressure within the cell (*e.g.*, a concentration of 10^{-1} M at 100° corresponds to a pressure of ~3 atm) the concentration in the present study did not exceed $\sim 5.6 \times 10^{-2}$ M.[20] If K_c is of the order of ~1–2 M^{-1}, then the ratio of $1/K_c$ to $(D_0 + A_0)$ is just about at the condition where separation of the $K_c\epsilon$ product into the individual values of K_c and ϵ is difficult to achieve within the desired confidence level. The

(18) W. K. Duerksen and M. Tamres, *J. Amer. Chem. Soc.*, 90, 1379 (1968).

(19) The value in ref 17 is for the full width at half-maximum, *i.e.*, $\bar{\nu}_{1/2}$(short-wavelength side) − $\bar{\nu}_{1/2}$(long-wavelength side).

(20) In one study at a concentration of $\sim 7 \times 10^{-2}$ M in D_0, which corresponds to ~2 atm pressure at 80°, a quartz window in the particular cell used was blown out.

Table II: Analysis of K_c and ϵ_{max} for the Diethyl Ether–Iodine Complex[a,b]

Temp, °C	$K_c\epsilon_{max}$, M^{-2} cm^{-1}	ϵ_{max}, M^{-1} cm^{-1}	K_c, M^{-1}	r[c]	$K_{c_{av}}$[d] M^{-1}
59.8	6140 ± 180	8,720 ± 10,460	0.705 ± 0.864	0.639	0.741
	(6230 ± 209)	(4,160 ± 2,690)	(1.50 ± 1.02)	(0.838)	(1.94)
67.0	5230 ± 96	11,150 ± 12,650	0.469 ± 0.539	0.660	0.630
	(5300 ± 156)	(4,230 ± 2,880)	(1.25 ± 0.884)	(0.827)	(1.65)
80.0	4100 ± 107	11,320 ± 23,530	0.363 ± 0.762	0.434	0.495
	(4160 ± 169)	(3,630 ± 3,730)	(1.15 ± 1.22)	(0.697)	(1.30)
89.8	3440 ± 89	9,470 ± 20,070	0.363 ± 0.777	0.478	0.415
	(3490 ± 126)	(2,890 ± 2,570)	(1.21 ± 1.11)	(0.792)	(1.08)
97.8	3050 ± 110	3,770 ± 4,980	0.810 ± 1.09	0.657	0.368
	(3100 ± 127)	(1,850 ± 1,340)	(1.68 ± 1.27)	(0.846)	(0.964)

[a] Upper values based on data in Table I; lower values (in parentheses) obtained by increasing the iodine concentration in runs 7 and 8 by 4.1 and 2.4%, respectively. [b] Error limits for 95% confidence level. [c] Correlation constant. [d] $K_{c_{av}} = K_c\epsilon_{max}/\epsilon_{av}$.

$K_c\epsilon$ product itself is quite good, however. These aspects are reflected in the error limits associated with the values reported in Table II.

The relative contribution of $(D_0 + A_0)$ to $1/K_c$ can be readily noted from the data in Table I by making a plot of the linear form of eq 1. The change in the y coordinate (D_0A_0/OD) is not more than 5% over the entire range of the x coordinate $(D_0 + A_0)$. Contributing factors to this change are the errors in absorbance (estimated to be 0.005 unit) and in the iodine concentration (estimated to be 1% and perhaps 2% in some cases). The error limits for the latter are based on the following consideration. A check on the iodine concentration was made after each analysis of the CT region by taking the visible spectrum at 100°. The value at 480 mμ of ϵ_{I_2} 350 ± 2 M^{-1} cm^{-1} had been established previously.[16] Analysis of a slow-scan spectrum of the mixture in Figure 3 showed that, for the concentrations used, the absorbance of iodine at 480 mμ in the presence of diethyl ether is enhanced <8% at 60° and <4.5% at 80°, and it is estimated to be <2.5% at 100°. Therefore, the concentration of iodine, determined from the weight of iodine and the volume of the cell, divided into the optical density at 100° should give an ϵ quite close to 350 M^{-1} cm^{-1} and not more than ~2% higher. The last column in Table I shows that this is the case. In runs 7 and 8, at the highest ether concentrations, ϵ_{I_2} came out a little higher, by 4.1 and 2.4%, respectively. It is felt, therefore, that the largest error in the iodine concentration is not more than ~2%.

The fact that $\Delta y/y$ is small for the full range of x makes the K_c and ϵ separation sensitive to small variations in the data. This is reflected in the large error limits at the 95% confidence level and in the low correlation constant. To emphasize how sensitive the results can be, a second calculation for K_c and ϵ_{max} was made by increasing the iodine concentrations in runs 7 and 8 by 4.1 and 2.4%, respectively (so that the calculated ϵ_{I_2} is 350 M^{-1} cm^{-1}). The results are given in parentheses in Table II. There is very little change in the $K_c\epsilon_{max}$ product. However, the separate K_c and ϵ_{max} values are altered severalfold. Thus for conditions such as those pertaining to the present system, these values cannot be considered to give anything better than the order of magnitude. Similarly, the agreement for K_c between the CT study of Lang and Strong[6] ($K_c(25°) = 6.4 \pm 1.2\ M^{-1}$) and the nonspectral studies of Grundnes, Christian, and Cheam[21] ($K_c(35°) = 4.4 \pm 0.3\ M^{-1}$) and of Brüll and Ellerbrock[22] ($K_c(35°) \simeq 5.5\ M^{-1}$) should be construed only as being qualitative.

The values for $K_c\epsilon_{max}$ obtained in the temperature range studied are a little lower than those of Lang and Strong,[6] although extrapolation in each case to 25° happens to give coinciding results. This is due to different values for the change in internal energies (ΔE) in the two studies.

Because of the uncertainty and scatter in separating K_c and ϵ_{max}, calculation of ΔE was based on evaluating the slope from a plot of log $K_c\epsilon_{max}$ *vs.* $1/T$. The value of $\Delta E = -4.5 \pm 0.2$ kcal mol^{-1} is larger than that reported in the previous CT study (-3.2 ± 0.1 kcal mol^{-1})[6,23] or that obtained in an early study of the saturation concentration of iodine in ether vapor (-2.7 ± 0.3 kcal mol^{-1}).[22] This procedure of using the $K_c\epsilon_{max}$ product assumes that ϵ_{max} is independent of temperature, which is in error. It would be expected that ϵ_{max} decreases with increasing temperature as a result of band broadening. Therefore, the value of -4.5 kcal mol^{-1} for ΔE represents an upper limit. An improved value for ΔE would be obtained if calculation could be made using the $K_c\epsilon$ products at a wavelength where ϵ does not

(21) J. Grundnes, S. D. Christian, and V. Cheam, *Acta Chem. Scand.*, **24**, 1836 (1970).

(22) W. Brüll and W. Ellerbrock, *Z. Anorg. Allg. Chem.*, **216**, 353 (1934).

(23) F. T. Lang, Ph.D. Dissertation, Renssalaer Polytechnic Institute, Troy, N. Y., 1964.

vary with temperature. In the present case, the absorbance curve dependence on temperature could not be reduced to the corresponding ϵ curve. However, analysis of the half-width at half-maximum of the CT band at each temperature indicates about a 10% change over the 40° temperature range. If this is assumed to produce a corresponding change in ϵ_{max}[8b] (although it probably is an overcompensation), the value for ΔE would become ~ -3.8 kcal mol^{-1}. Analysis of the temperature dependence of $K_c\epsilon$ at longer wavelengths (λ 240, 245, 250 and 255 mμ) gave generally decreasing values of ΔE ($= -4.6$, -4.1, -3.9, and $-3.5 \pm$ (0.2–0.3) kcal mol^{-1}, respectively) as expected from band broadening.

Another procedure to determine ΔE, particularly for relatively weak complexes, is to plot directly log OD *vs.* $1/T$ for a single concentration of the mixture.[24-26] The result obtained in this way for each set of data at the five temperatures in Table II was the same (within ± 0.1 kcal mol^{-1}) as that from the $K_c\epsilon_{max}$ analysis.

A model has been developed by Christian, *et al.*,[8,13] for the effect of solvation on ΔE. This model assumes a proportionality, α, between the solvation energy of the complex and the sum of the solvation energies of the donor and the acceptor in going from the vapor phase to solution. The factor α varies with the strength of the complex. For a strong, polar CT complex, $\alpha > 1$, and $\Delta E(\text{soln}) > \Delta E(\text{vap})$, as in the case of trimethylamine–sulfur dioxide[8] where the vapor value is -9.1 kcal mol^{-1} and that in *n*-heptane solution is -11.0 kcal mol^{-1}. For a weak complex, $\alpha < 1$ and $\Delta E(\text{soln}) < \Delta E(\text{vap})$. This is the case apparently for benzene–iodine, although the data are rather scattered. The values reported (in kcal mol^{-1}) in the vapor phase[6,18] are -1.8 and -2.0, while those in solution are -1.6 in *n*-heptane,[27] -1.7 in cyclohexane[27] and methylcyclohexane,[27] -1.3 in *n*-hexane,[28,29] and -1.3 to -1.4 in carbon tetrachloride.[27,30-32] For diethyl ether–iodine, ΔE in *n*-heptane[3-5] is ~ -4.2 to -4.4 kcal mol^{-1}. Since this is a relatively weak complex, the previously reported vapor-phase values of Lang and Strong[6] and of Brüll and Ellerbrock[22] would seem low. The present results are more in accord with the Christian, *et al.*, model.[8,13]

It is apparent in Figure 3 that, in the presence of diethyl ether, the iodine absorbance shows a small increase in the continuum region of the visible spectrum. Although the effect is much smaller than that reported recently for diethyl sulfide–iodine,[14] it is sufficient nevertheless to establish the existence of a blue-shifted iodine band. As in the sulfide case, no maximum is observed in the absorbance curves for the mixtures, but again the difference of the iodine absorption in the presence and absence of donor passes through a maximum. This is shown as the dashed curve in Figure 3, which was obtained as the difference between

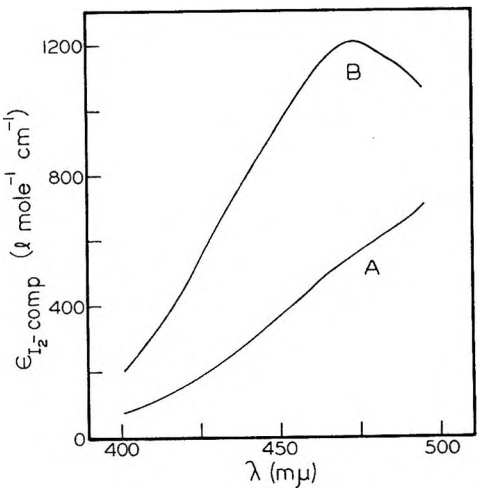

Figure 4. Attempted resolution of the blue-shifted iodine band for diethyl ether–iodine at 60°: (A) $K = 2.4\ M^{-1}$; (B) $K = 0.74\ M^{-1}$.

curve 3 (at 60°) and curve 1 (after correction for temperature broadening from 45 to 60°). The maximum at ~460–470 mμ is not as far into the uv as that observed with the diethyl sulfide donor (~445–450 mμ),[14] as would be expected from the relative strengths of these donors toward iodine.

Separation of the total absorbance into free and complexed iodine components requires knowledge of K_c and of ϵ_{I_2}. Data for the latter were obtained previously.[14] Combining the recently reported result of $K_c = 4.4 \pm 0.3\ M^{-1}$ at 35.0° obtained by a nonspectral method[21] with the ΔE of the present study gives a calculated value of $K_c = 2.4 \pm 0.2\ M^{-1}$ at 60°. Based on this value, separation of curve 3 in Figure 3 gives curve A in Figure 4. Using the smaller value of $K_c \simeq 0.74$ (Table II, which is admittedly less reliable) gives curve B in Figure 4. But this attempt to characterize the blue-shifted band for diethyl ether–iodine is very uncertain because the diethyl ether produces a relatively small change in the iodine spectrum, and the errors inherent in obtaining small differences may well obscure characterization of the blue-shifted band in relation to the value of K_c.

It should be emphasized, however, that combining

(24) R. S. Drago, R. L. Carlson, N. J. Rose, and D. A. Wenz, *J. Amer. Chem. Soc.*, 83, 3572 (1961).

(25) M. Tamres in "Molecular Complexes," R. Foster, Ed., Logos Press Ltd., London, in press.

(26) E. A. Ogryzlo and B. C. Sanctuary, *J. Phys. Chem.*, 69, 4423 (1965).

(27) B. B. Bhowmik, *Spectrochim. Acta, Part A*, 27, 321 (1971).

(28) J. S. Ham, *J. Amer. Chem. Soc.*, 76, 3875 (1954).

(29) J. A. A. Ketelaar, *J. Phys. Radium*, 15, 197 (1954).

(30) T. M. Cromwell and R. L. Scott, *J. Amer. Chem. Soc.*, 72, 3825 (1950).

(31) R. M. Keefer and L. J. Andrews, *ibid.*, 77, 2164 (1955).

(32) P. A. D. de Maine, M. M. de Maine, and C. Froese, *J. Mol. Spectrosc.*, 8, 373 (1962).

the nonspectral value of K_c[21] with the $K_c\epsilon_{max}$ product from this study gives $\epsilon_{max} \simeq 2500 \pm 200$ M^{-1} cm^{-1}. This is appreciably lower than the value in *n*-heptane solution,[3b] in agreement with the suggestion of Rice[33] that more random orientations of the complex exist in the vapor phase which would diminish ϵ.

Acknowledgment. This research was supported by the National Science Foundation in part through Grant GP-9216 and in part through Grant GP-10367 to this department for the purchase of the Cary 14 spectrophotometer used in this study.

(33) O. K. Rice, *Int. J. Quantum Chem., Symp.*, **No. 2**, 219 (1968).

Pure and Mixed Second Virial Coefficients of Line-Core Molecules. I. Theory[1a]

by B. W. Gainey*[1b] and C. P. Hicks

Department of Physical Chemistry, The University, Bristol, England *(Received May 27, 1970)*

Publication costs borne completely by The Journal of Physical Chemistry

General equations are derived for the second virial coefficient for spherical molecules, spherocylindrical molecules, and mixtures of spherical and spherocylindrical molecules, using line cores. The derivation is equivalent to, but simpler than, that of Kihara. The equations are made explicit in terms of the Sutherland–Kihara (∞:6) potential.

Mayer and Mayer[2] have established that the second virial coefficient is to be attributed to two-body interactions, the third virial coefficient to three-body interactions, and so on. The general equation for the second virial coefficient of two molecules interacting with a potential energy function $u(\vec{r})$ is

$$B = -\frac{\bar{N}}{2}\iiint (e^{-u(\vec{r})/kT} - 1)\mathrm{d}\vec{r} \qquad (1)$$

where the vector $\vec{r}$ includes all the coordinates necessary to describe the relative positions and orientations of both molecules.

The interaction between a body whose force field is centrosymmetrical and any other body may be described by equipotential surfaces located relative to an axis or axes of the second body. To deal with the case of two asymmetrical bodies, two procedures are possible, according to which simplifying assumptions are made. A central axis may be specified for each molecule, as, *e.g.*, a permanent dipole; then the two-body interaction potential may be regarded as being determined only by the distance between centers and the angle between the two central axes. This is the principle of Stockmayer's method.[3] Alternatively, following Kihara,[4] the interaction potential may be regarded as being determined solely by the shortest distance between two axial lines which extend equal distances on either side from the centers of the two bodies. These axial lines are called line cores and may or may not be the same length in the two bodies. In the case of a point-core body interacting with a line core, $u(\vec{r})$ may be represented by a series of equipotential surfaces, which are in fact spherocylinders centered on the line core of that body. A similar, but more complicated result holds for the interaction of two line-core bodies.

Theoretical Considerations

Kihara based his second virial coefficient calculations on various topological theorems applicable for any shape of (convex) core. The general expression tends to obscure the actual situations to which it refers and the origin of its form. The method of derivation of the equipotential surface used here gives an insight into the results of Kihara. We hold the cores at constant separation, and move one into all orientations about the other, thereby calculating the expression for the equipotential surface.

The Sphere–Sphere Interaction. Equation 1 for two spheres interacting with a potential $u(r)$ reduces to[2,5]

(1) Part II: (a) B. W. Gainey and C. P. Hicks, *J. Phys. Chem.*, **75**, 3691 (1971); (b) correspondence should be addressed to Koninklijke/Shell-Laboratorium, Amsterdam, Badhuisweg 3, Amsterdam-N, Holland.

(2) J. E. Mayer and M. J. Mayer, "Statistical Mechanics," Wiley, New York, N. Y., 1940, p 12; see also D. H. Everett, *Educ. Chem.*, **4**, 21 (1967).

(3) W. H. Stockmayer, *J. Chem. Phys.*, **9**, 398 (1941).

(4) T. Kihara, *J. Phys. Soc. Jap.*, **6**, 289 (1951); *ibid.*, **8**, 686 (1953); *Rev. Mod. Phys.*, **27**, 412 (1955); *Advan. Chem. Phys.*, **5**, 147 (1961).

$$B = -2\pi\tilde{N}\int_0^\infty (e^{-u(r)/kT} - 1)r^2 dr \qquad (2)$$

where r is the separation of the point cores (*i.e.*, centers of the spheres).

The Sphere–Spherocylinder Interaction. The spherocylinder (a cylinder capped on each end by a hemisphere of equal radius) is fixed so that its line core lies along the z axis of a three-dimensional coordinate system with the midpoint of its core at the origin. If the center of the sphere is moved so that it is at all times a constant distance, r, from the line core, it will trace out the surface of a spherocylinder for every value of r. The surface area of this equipotential spherocylinder is

$$A(r) = 4\pi r^2 + 2\pi r l_1 \qquad (3)$$

where l_1 is the length of the line core. The second virial coefficient for this case is then

$$B = -\frac{\tilde{N}}{2}\int_0^\infty (e^{-u(r)/kT} - 1)A(r)dr \qquad (4)$$

If $l_1 = 0$ in eq 3, eq 4 reduces immediately to eq 2—the sphere–sphere case. Thus the sphere–spherocylinder case is expressible as the sum of two terms corresponding to the two terms in eq 3. These two contributions will be designated B^{AA} (sphere–sphere) and B^{AB} (sphere–cylinder). B^{AA} corresponds to the distance of closest approach being through one of the two hemispherical ends; B^{AB} corresponds to it being through the cylindrical surface. In the integration for the B^{AB} contribution of eq 1 it is clear that certain constraints must be imposed on the integration volume. Obviously the point center of the sphere must be confined to the cylindrical volume swept by the curved surface of the cylinder as it is moved out to infinity. This restriction is expressed in the integration limits.

The spherocylindrical molecule is placed with its axis along the z axis of a three-dimensional coordinate system with the midpoint of its line core as the origin, so that the integration limits for the cylinder are from $-l_{1/2}$ to $+l_{1/2}$ in the z direction, but to infinity in the x and y directions. Therefore,

$$B^{AB} = -4\tilde{N}\operatorname*{Lt}_{a\to\infty}\int_0^{l_{1/2}}\int_0^a\int_0^{\sqrt{a^2-y^2}} \times (e^{-u(r)/kT} - 1)dxdydz$$

Changing to polar cylindrical coordinates[6]

$$B^{AB} = -4\tilde{N}\int_0^{l_{1/2}}\int_0^{\pi/2}\int_0^\infty (e^{-u(r)/kT} - 1)rdrd\theta dz$$

which becomes, on carrying out the first two integrations

$$B^{AB} = -\pi\tilde{N}l_1\int_0^\infty (e^{-u(r)/kT} - 1)rdr \qquad (5)$$

The Spherocylinder–Spherocylinder Interaction. The interaction of a spherocylindrical molecule with another spherocylindrical molecule may, by similar arguments to those of the previous section, be split into a sphere–sphere interaction, two sphere–cylinder interactions, and a cylinder–cylinder interaction. We have already derived expressions for all of these but the last, which we denote as B^{BB}. Thus for a spherocylinder–spherocylinder interaction we have

$$B = B^{(AA+AB+BA+BB)} = B^{AA} + B^{AB} + B^{BA} + B^{BB} \qquad (6)$$

To evaluate the cylinder–cylinder interaction, we fix one of our cylinders as before, with its line core along the z axis, and the midpoint of this core at the origin, of an x, y, z coordinate frame. Now the second cylinder is moved around the first, complying with the important restriction that the cylinder ends must play no part in the interaction (their contribution being assessed in the calculations with superscript A).

This means that for the orientation to be included here, the line of closest approach must be the common perpendicular of the cores, and that the feet of this perpendicular must lie on the unprojected cores. This condition is expressed in the integration limits

$$B^{BB} = -\frac{\tilde{N}}{2}\int_0^\infty sds\cdot 2\int_0^{l_2/2}\frac{db}{l_2}\cdot 2\int_0^{l_1/2}da \times \int_{\cos\phi_1=0}^{\frac{l_2/2-b}{a}} d\phi_1\int_{\cot\theta_1=0}^{\frac{a\sin\phi_1}{r}} d\theta_1\int_0^{2\pi} d\phi_2(e^{-u(r)/kT} - 1) \qquad (7)$$

where the relevant lengths and angles are as shown in Figure 1. s is the length of the perpendicular from the center of molecule 1 onto the line core of molecule 2. r is the length of the common perpendicular of the two line cores and is therefore the shortest distance between them. Changing variables from s to r using

$$sds = \frac{rdr}{\sin^2\theta_1}$$

which may easily be verified from Figure 1 gives

$$B^{BB} = -4\pi\tilde{N}\int_0^\infty rdr\int_0^{l_2/2}\frac{db}{l_2}\int_0^{l_1/2}da \times \int_{\cos\phi_1=0}^{\frac{l_2/2-b}{a}} d\phi_1\int_{\cot\theta_1=0}^{\frac{a\sin\phi_1}{r}}\frac{d\theta_1}{\sin^2\theta_1}(e^{-u(r)/kT} - 1) \qquad (8)$$

Evaluation of this integral yields

$$B^{BB} = -\tilde{N}\frac{\pi}{4}l_1l_2\int_0^\infty (e^{-u(r)/kT} - 1)dr \qquad (9)$$

Equations 2, 5, and 9 agree with those Kihara[4] calcu-

(5) See, for example, J. O. Hirschfelder, C. F. Curtiss, and R. B. Bird, "Molecular Theory of Gases and Liquids," Wiley, New York, N. Y., 1954.

(6) H. Margeneau and G. M. Murphy, "The Mathematics of Physics and Chemistry," Van Nostrand, Princeton, N. J., 2nd ed, p 177.

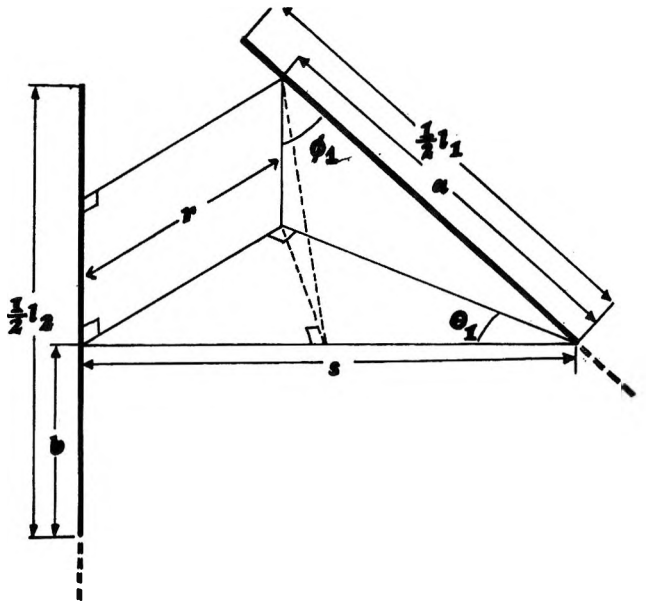

Figure 1. The interaction of two line cores.

lated by the topological method, which does not involve the necessity of choosing integration limits in the calculation of the average potential surfaces.

Explicit Potential Function. As an example we use the (∞:6) potential which we shall call[5] the Sutherland–Kihara potential. It is defined by

$$u(r) = \infty \text{ when } r \leqslant \rho_{12}$$

$$u(r) = -\epsilon_0\left(\frac{\rho_{12}}{r}\right)^6 \text{ when } r > \rho_{12}$$

i. Sphere–Sphere. The previously derived eq 2 may be separated into two parts having integration limits of 0 to ρ_{12} and ρ_{12} to ∞, and then the appropriate substitution is made for $u(r)$. Hence eq 2 becomes

$$B^{AA} = -2\pi\tilde{N}\int_0^{\rho_{12}}(e^{-u(r)/kT} - 1)r^2dr - 2\pi\tilde{N}\times \int_{\rho_{12}}^{\infty}(e^{-u(r)/kT} - 1)r^2dr$$

The first integral is easily solved, and the second is evaluated by use of the exponential expansion, when we may say

$$-2\pi\tilde{N}\int_{\rho_{12}}^{\infty}(e^{A/r^6} - 1)r^2dr = -2\pi\tilde{N}\left[\sum_{n=1}^{\infty}\left\{\left(\frac{A}{r^6}\right)^n\frac{-1}{(6n-3)n!}\right\}\right]_{\rho_{12}}^{\infty}$$

where

$$A = \frac{\epsilon_0}{kT}(\rho_{12})^6$$

The final second virial coefficient formula is therefore

$$B^{AA} = \frac{\tilde{N}}{2}V_{sphere}\{1 - 3\sum\alpha_n(x)\} \qquad (10)$$

where

$$V_{sphere} = {}^4/_3\pi\rho_{12}^3$$

$$\sum\alpha_n(x) = \sum_{n=1}^{\infty}\frac{x^n}{(6n-3)n!}$$

$$x = \frac{\epsilon_0}{kT}$$

ii. Sphere–Cylinder. The B_{AB} contribution may be integrated in a fashion identical with that used to obtain eq 10, thus

$$B^{AB} = \frac{\tilde{N}}{2}V_{cyl_1}\{1 - 2\sum\beta_n(x)\} \qquad (11)$$

where

$$V_{cyl_1} = \pi\rho_{12}^2l_1$$

$$\sum\beta_n(x) = \sum_{n=1}^{\infty}\frac{x^n}{(6n-2)n!}$$

and x is as previously defined.

iii. Cylinder–Cylinder. Integration of eq 9 using the same general method gives

$$B^{BB} = \frac{\tilde{N}}{2}V_{ex}\{1 - \sum\gamma_n(x)\} \qquad (12)$$

where

$$V_{ex} = \frac{\pi}{2}\rho_{12}l_1l_2$$

$$\sum\gamma_n(x) = \sum_{n=1}^{\infty}\frac{x^n}{(6n-1)n!}$$

Summing the various contributions to the spherocylinder–spherocylinder interaction, *cf.* eq 6

$$B^{(AA+AB+BA+BB)} = \frac{\tilde{N}}{2}[V_{sph} + V_{cyl_{1+2}} + V_{ex} - 3V_{sph}\sum\alpha_n(x) - 2V_{cyl_{1+2}}\sum\beta_n(x) - V_{ex}\sum\gamma_n(x)] \qquad (13)$$

where

$$V_{cyl_{1+2}} = V_{cyl_1} + V_{cyl_2}$$

It is now possible to use these equations to evaluate mixed and pure second virial coefficients for spherical spherocylindrical molecules.[1a] A tabulation of the α, β, and γ summations is given in the Appendix.

Discussion

Firstly we show that with an ∞:6 potential instead of the 12:6 potential used by Kihara,[4] his general second virial coefficient formulas reduce to eq 13 above, in the case of interacting prolate spherocylinders.

Kihara has derived general second virial coefficient formulas for the interactions of rigid convex molecules using a core model and a potential which expressed the

interactions as a function of the shortest distance between cores. The core was assumed to be impenetrable and surrounded by a potential field that was described by a 12:6 potential. The general second virial coefficient formula derived for like molecules is

$$\frac{B}{\bar{N}} = \frac{2\pi}{3}\rho^3 F_3(x) + M_0\rho^2 F_2(x) + \left(S_0 + \frac{M_0^2}{4\pi}\rho\right)F_1(x) + \left(V_0 + \frac{M_0 S_0}{4\pi}\right) \quad (14)$$

where

$$x = \frac{\epsilon_0}{kT}$$

and where the $F_t(x)$ are functions defined by the general formula

$$F_t(x) = -\frac{t}{12}\sum_{s=0}^{\infty}\frac{1}{s!}\Gamma\left[\frac{6s-t}{12}\right]2^s(x)^{(6s+t)/12} \quad (15)$$

where $\Gamma[(6s + t)/12]$ is a γ function.[7]

V_0, S_0, and M_0 may be calculated directly from a knowledge of the core shape and size and are defined as V_0 = volume of the core, S_0 = surface area of the core, M_0 = mean curvature integrated over the whole surface of the core. For unlike cores Kihara showed that for two molecules i and j

$$\frac{B_{ij}}{\bar{N}} = \frac{2\pi}{3}\rho_{ij}^3 F_3 + \frac{M_{0i} + M_{0j}}{2}\rho_{ij}^2 F_2 + \left[\frac{S_{0i} + S_{0j}}{2} + \frac{M_{0i}M_{0j}}{4\pi}\right]\rho_{ij}F_1 + \left[\frac{V_{0i} + V_{0j}}{2} + \frac{M_{0i}S_{0j} + M_{0j}S_{0i}}{8\pi}\right] \quad (16)$$

with definitions as just given. The $F_t(x)$ functions have been tabulated by previous workers as well as V_0, M_0, and S_0 values for a variety of core shapes.[8] For the point and line cores used in this work, both V_0 and S_0 are zero. For the point core M_0 is also zero, reducing the Kihara formula to that of Lennard-Jones as has been previously mentioned.[9] For a line core, M_0 has a value of πl.

A transformation is made from the full Kihara B_{12} equation to an equation which uses the Sutherland–Kihara potential (eq 13) by the following substitutions

$$\{1 - 3\sum\alpha_n(x)\} \text{ for } F_3$$

$$\{1 - 2\sum\beta_n(x)\} \text{ for } F_2$$

$$\{1 - \sum\gamma_n(x)\} \text{ for } F_1$$

which gives

$$\frac{B_{ij}}{\bar{N}} = \frac{2}{3}\pi\rho_{ij}^3\{1 - 3\sum\alpha_n(x)\} + \frac{M_{0i} + M_{0j}}{2}\rho_{ij}^2\{1 - 2\sum\beta_n(x)\} + \left[\frac{S_{0i} + S_{0j}}{2} + \frac{M_{0i}M_{0j}}{4\pi}\right]\rho_{ij}\{1 - \sum\gamma_n(x)\} + \left[\frac{V_{0i} + V_{0j}}{2} + \frac{M_{0i}S_{0j} + M_{0j}S_{0i}}{8\pi}\right] \quad (17)$$

Equation 17 reduces to eq 13 in the specific case of spherocylinder–spherocylinder interaction as then only

Table I[a]

x	$\Sigma\alpha_n(x)$	$\Sigma\beta_n(x)$	$\Sigma\gamma_n(x)$
1.0	0.4023	0.3127	0.2574
1.1	0.4522	0.3527	0.2912
1.2	0.5042	0.3948	0.3270
1.3	0.5587	0.4391	0.3648
1.4	0.6157	0.4858	0.4049
1.5	0.6755	0.5351	0.4473
1.6	0.7382	0.5870	0.4922
1.7	0.8040	0.6420	0.5399
1.8	0.8733	0.7000	0.5906
1.9	0.9461	0.7615	0.6445
2.0	1.0229	0.8266	0.7018
2.1	1.1039	0.8956	0.7627
2.2	1.1893	0.9689	0.8277
2.3	1.2796	1.0467	0.8970
2.4	1.3752	1.1294	0.9709
2.5	1.4763	1.2174	1.0498
2.6	1.5835	1.3111	1.1341
2.7	1.6972	1.4110	1.2243
2.8	1.8179	1.5175	1.3208
2.9	1.9461	1.6311	1.4241
3.0	2.0826	1.7526	1.5347
3.1	2.2278	1.8824	1.6534
3.2	2.3826	2.0212	1.7807
3.3	2.5477	2.1699	1.9173
3.4	2.7239	2.3291	2.0641
3.5	2.9121	2.4998	2.2218
3.6	3.1133	2.6829	2.3914
3.7	3.3285	2.8794	2.5739
3.8	3.5590	3.0905	2.7704
3.9	3.8060	3.3174	2.9820
4.0	4.0708	3.5614	3.2100

[a] For the range of values presented here the convergence of the series is comparatively rapid, though about 14 terms were required by the time $x = 4$ was reached. The functions as calculated are accurate to the sixth significant figure, to which they were calculated and rounded off by the computer. This computer output in units of $x = 0.01$ from $x = 0$ to $x = 4.00$ is available from the authors on request. The figures presented here are a condensed version of the more accurate values rounded to four significant figures and are of sufficient accuracy for most calculations.

(7) Reference 6, p 93; ref 5, p 189.

(8) Reference 5, p 1179.

(9) T. Kihara, *Rev. Mod. Phys.*, **25**, 831 (1953).

M_0 is nonzero, with a value πl. Thus, by using the values of V_0, S_0, and M_0 tabulated by Kihara it is possible to calculate equations equivalent to (17) for any core with a convex shape. The calculation of the parameters, the use of these equations to calculate both pure and mixed second virial coefficients, and a comparison with experimental data from the literature are given in an accompanying paper.[1a] The insertion of a full Kihara 12:6 potential into the derived equations is in progress, as is the problem of dealing with side-chain and disk-shaped molecules. It is also possible that an extension of this method will prove superior to previous attempts to treat molecules with permanent dipoles. A similar technique could well prove profitable for evaluating third virial coefficients.

Acknowledgments. Both authors gratefully acknowledge financial support from the Science Research Council, England. We record that Professor D. H. Everett suggested the project, and thank Dr. C. L. Young and Mr. A. J. B. Cruickshank for many helpful discussions.

Appendix

A table of values is presented (Table I) for $\Sigma\alpha_n(x)$, $\Sigma\beta_n(x)$, and $\Sigma\gamma_n(x)$ for a range of x in steps of 0.1. The computer evaluation of each sum was terminated when successive terms fell below 10^{-6}.

Pure and Mixed Second Virial Coefficients of Line-Core Molecules.

II. Comparison with Experiment[1a]

by B. W. Gainey*[1b] and C. P. Hicks

Department of Physical Chemistry, The University, Bristol, England *(Received May 27, 1970)*

Publication costs borne completely by The Journal of Physical Chemistry

Part I proposes equations from which second virial coefficients for like (11) or unlike (12) interactions may be determined provided that certain parameters of the effective molecular interaction potential and of the molecular model are known. This paper describes a method of obtaining these parameters. The principle of corresponding states is used to calculate two parameters which relate molecular potential parameters to the macroscopic properties by fitting to second virial coefficient data for pure substances. The near equivalence of these equations to an empirical one proposed by McGlashan and Potter is demonstrated, and experimental mixed second virial coefficients (B_{12}) are compared with values calculated by several alternative procedures. In most cases the new equations predict these data more precisely than previous equations, even when used with the naive Sutherland–Kihara potential.

Introduction

In part I[1a] we showed that equations can be formulated to express the second virial coefficient for like or unlike molecules of various shapes in terms of molecular size and energy parameters. The required molecular parameters may be evaluated by making use of the principle of corresponding states.[2,3] This way of looking at the problem assumes implicitly that even though the exact nature of the intermolecular potential is uncertain, it is possible to compare the macroscopic properties calculated therefrom for all substances. It has been shown that the principle is strictly valid only for molecules with a central, two-parameter potential, but a more general expression can often be made since the deviations of many substances from strict adherence to the principle are slight. It may be extended to molecules of different shapes by the use of extra parameters, when it is better regarded as a family of principles, rather than as one unique all embracing rule.[3] Pitzer[4] has proposed

(1) Part I: B. W. Gainey and C. P. Hicks, *J. Phys. Chem.*, **75**, 3687 (1971). (b) Correspondence should be addressed to Koninklijke/Shell-Laboratorium, Amsterdam, Badhuisweg 3, Amsterdam-N, Holland.

(2) E. A. Guggenheim, *Rev. Pure Appl. Chem.*, **3**, 1 (1953); see also, I. Prigogine, "The Molecular Theory of Solutions," North-Holland Publishing Co., Amsterdam, 1957; J. S. Rowlinson, "Liquids and Liquid Mixtures," Butterworths, London, 1959; E. A. Guggenheim, "Mixtures," OUP, London, 1959.

(3) J. O. Hirschfelder, C. F. Curtiss, and R. B. Bird, "Molecular Theory of Gases and Liquids," Wiley, New York, N. Y., 1954.

(4) K. S. Pitzer and R. F. Curl, Jr., *J. Amer. Chem. Soc.*, **79**, 2369 (1957).

such a parameter, the so-called acentric factor; McGlashan and Potter,[5] on the other hand, fitted the virial coefficient data for n-alkanes to an equation of the same form as that proposed by Guggenheim and McGlashan[6] for the noble gases, but included an extra term in reduced temperature. The coefficient of this term is a function of the number of carbon atoms, n; this equation is

$$\frac{B}{V^c} = 0.430 - 0.886\left(\frac{T^c}{T}\right) - 0.694\left(\frac{T^c}{T}\right)^2 - 0.0375(n-1)\left(\frac{T^c}{T}\right)^{4.5} \quad (1)$$

Using the principle of corresponding states, we assume that the critical temperature, T^c, of a molecular species is related to the maximum depth of the interaction energy well by the parameter ϕ defined by

$$\phi T^c = \frac{\epsilon_0}{k} \quad (2a)$$

where ϵ_0 is the maximum depth of the energy well in the interaction. Similarly the critical volume V^c is assumed to be related to the molecular excluded volume, so that for spherical molecules with point cores[1a]

$$\frac{V^c}{\tilde{N}} = \kappa(^4/_3\pi\rho^3) \quad (2b)$$

where $\tilde{N}$ is Avogadro's number, and ρ is the separation of the molecular cores at the energy minimum.

Evaluation of the Corresponding States Parameters

We have estimated the values of ϕ and κ for spherical molecules with point cores by comparing virial coefficient data for the noble gases (except helium) over a wide temperature range with the equations derived in part I. The procedure is as follows. The second virial coefficient equation derived in part I for the interactions of molecules with point cores, whose interaction follows the Sutherland–Kihara potential, is combined with eq 2a and 2b to give

$$B = \frac{V^c}{2\kappa}\left[1 - 3\sum\alpha_n\left(\phi\frac{T^c}{T}\right)\right] \quad (3)$$

Expanding the summation term and neglecting terms of order higher than the fourth in ϕ (an approximation good to 3% for $\phi T^c/T$ in the range 1 to 2.5) gives

$$\frac{B}{V^c} = \frac{1}{2\kappa}\left[1 - \phi\left(\frac{T^c}{T}\right) - \frac{\phi^2}{6}\left(\frac{T^c}{T}\right)^2 - \frac{\phi^3}{30}\left(\frac{T^c}{T}\right)^3 - \frac{\phi^4}{168}\left(\frac{T^c}{T}\right)^4 \cdots\right] \quad (4)$$

Second virial coefficient data from the compilation by Dymond[7] were then used with the critical data given in Table I[8] and eq 4 to generate equations in ϕ and κ. These equations were solved in all combinations for the two unknowns; the results are very consistent, bearing in mind the variation in reported second virial coefficient values (smoothed values were used). All the solutions are within 4% of the arithmetic mean values, which were used as the starting point for a variational calculation of virial coefficients from eq 3. This confirms the accuracy of prediction of the second virial coefficient data by the values found for ϕ and κ over the temperature range 250–450°K. Reasonable agreement is also found with the predictions of the McGlashan and Potter reduced equation of state, in which, for the noble gases, the parameter n is set as unity.

The parameters ρ and l for various spherocylindrical molecules were determined by the method given in the next section and used in the equation for the interactions of molecules with line cores whose interactions followed the Sutherland–Kihara potential which was derived in part I

$$B = \frac{\tilde{N}}{2}[V_{star} - 3V_{sph}\sum\alpha_n(x) - 2V_{cyl_{l+2}}\sum\beta_n(x) - V_{ex}\sum\gamma_n(x)] \quad (5)$$

where $x = \phi(T^c/T)$ to calculate second virial coefficient values corresponding to the values of ϕ and κ calculated for spherical molecules. This was done for oxygen, nitrogen, and ethane. All the values are too positive, and we concluded that this was due to the spherocylinders requiring a value of ϕ different from that for spheres.

It is impractical to formulate a simple equation from eq 5 from which ϕ may be deduced after substitution of experimental virial coefficient values. Therefore a variational calculation of virial coefficients from eq 5 for a wide range of ϕ in the temperature range 280–470°K was carried out. Critical data from Table I, and molecular parameters from Table II, were used and predicted virial coefficients were compared with data from Dymond.[7] The best value of ϕ corresponding to $\kappa = 1.17$ was found to be 2.65 ± 0.05.

We deal later with mixed virial coefficients (B_{12}) for interactions of spheres with spherocylinder. For this case ϕ was chosen arbitrarily as the geometric mean of the spherical and spherocylindrical values $2.49 = (2.65 \times 2.33)^{1/2}$, κ being kept at 1.17.

(5) M. L. McGlashan and D. J. B. Potter, *Proc. Roy. Soc., Ser. A*, **267**, 478 (1962).

(6) E. A. Guggenheim and M. L. McGlashan, *ibid.*, **206**, 448 (1951).

(7) J. H. Dymond and E. B. Smith, "The Virial Coefficients of Gases—A Critical Compilation," Clarendon Press, Oxford, 1969.

(8) Table I contains ionization potentials, McGlashan and Potter "n" values, and critical data. Most of these values appear in ref 22 and 32. Table III contains calculated and observed mixed second virial coefficients. These tables will appear immediately following this article in the microfilm edition of this volume of the journal. Single copies may be obtained from the Reprint Department, ACS Publications, 1155 Sixteenth Street, N.W., Washington, D. C. 20036. Remit check or money order for $3.00 for photocopy or $2.00 for microfiche.

Evaluation of the Size and Shape Parameters

It has been customary in the past to estimate the size parameter (r^*) for the Lennard-Jones potential from critical volumes using eq 2b, but with r^* replacing ρ. This has been done only for spherical molecules or for molecules which may conveniently be regarded as spherical.[9] Many authors have treated a wide range of grossly asymmetric molecules as being spherical in this context, and it is indicative of the insensitivity of the second virial coefficient over a narrow temperature range to the model and potential that satisfactory agreement with experimental data has been obtained. Alternative procedures for the estimation of the size parameter have been put forward by several workers.[10]

For spherical and quasi-spherical molecules we have used eq 2b to calculate $\rho\kappa^{1/3}$. For spherocylindrical molecules (which here we take to mean molecules with a line core), the equivalent excluded volume relationship which follows from eq 13 of part I is

$$V^c = \tilde{N}\left[\frac{4}{3}\pi(\rho\kappa^{1/3})^3 + 2\pi(\rho\kappa^{1/3})^2 l + \frac{\pi}{2}\rho\kappa^{1/3}l^2\right] \quad (6)$$

With the line-core model for the n-alkanes, assigning the same size parameter throughout, and setting the length of each core as $p/(n-1)$ (where n is the number of carbon atoms and p is the n-alkane unit core length), the values of p and $\rho\kappa^{1/3}$ should be obtained by a least-squares fitting of critical volume data to a quadratic in $(n-1)$. This procedure (using $3 \leqslant n \leqslant 8$) gives

$$10^6 V^c = 94.10 + 52.24(n-1) + 0.50(n-1)^2$$

Comparing coefficients with eq 6 we find

$$\tilde{N}\left[\frac{4}{3}\pi(\rho\kappa^{1/3})^3\right] = 94.10 \times 10^{-6} \quad (7a)$$

$$\tilde{N}[2\pi(\rho\kappa^{1/3})^2 p] = 52.24 \times 10^{-6} \quad (7b)$$

$$\tilde{N}\left[\frac{\pi}{2}(\rho\kappa^{1/3})p^2\right] = 0.50 \times 10^{-6} \quad (7c)$$

These equations may be solved in three pairs, when the two pairs of solutions involving eq 7c are found to have $p < 0.40$ Å. The remaining pair of solutions, from eq 7a and 7b, is

$$\rho\kappa^{1/3} = 3.341 \text{ Å} \quad (8a)$$

$$p = 1.236 \text{ Å} \quad (8b)$$

The values of p found by use of eq 7c are surprisingly small, while the value given as eq 8b is very close to the values 1.25–1.27 Å which have been deduced on a strictly stereochemical analysis of a n-alkane structure with the carbon atoms coplanar and arranged regularly as dictated by normal bond angles and lengths.[11] Further, the value for $\rho\kappa^{1/3}$ (eq 8a) associated with this value of p is close to that found for methane (see Table II) as would be expected.

Clearly then the solution given as eq 8a and 8b is the most reasonable, and if these values are accepted, eq 7c and the l^2 term in eq 6 which gives rise to it must be questioned. It may be seen from part I that this term in eq 6 results from cylinder–cylinder interactions, and it would seem that for our model to fit n-alkane critical volume data we must postulate that there is a smaller contribution to the critical volume from this type of interaction than would have been expected from a straightforward calculation of excluded volume.[12]

The coefficient of the l^2 term has to be multiplied by 0.103 before agreement with experiment (using $\rho\kappa^{1/3}$ and p as given by eq 8a and b) is reached, so that eq 6 becomes

$$V^c = \tilde{N}\left[\frac{4}{3}\pi(\rho\kappa^{1/3})^3 + 2\pi(\rho\kappa^{1/3})^2 l + 0.103\frac{\pi}{2}\rho\kappa^{1/3}l^2\right] \quad (9)$$

In this calculation of size and length parameters and in the subsequent calculations for other homologous series, we have adhered to a rigid line-core model which with a Sutherland–Kihara potential generates an impenetrable spherocylindrical molecular model, but we have not sought to define the atomic configuration within this spherocylinder. Our model need not imply that the carbon atoms are along the line core of coplanar, but we suggest that in its rotation the molecule effectively occupies a spherocylindrical region of space. The line core upon which we based our part I discussion will lie at the center of this volume.

The size parameter for the alk-1-enes was taken to be identical with that derived for the n-alkanes and given in eq 8a. Then eq 9 was solved for the unit length parameter. The n-perfluoroalkanes were assumed to have the same unit length parameter as the n-alkanes (which were given as eq 8b) and this was used in eq 9 to derive $\rho\kappa^{1/3}$.

The results of these calculations are given in Table II together with experimental and calculated critical volumes.

The size parameters for diatomic molecules were evaluated using the known critical volumes given

(9) (a) A. E. Sherwood and J. M. Prausnitz, *J. Chem. Phys.*, **41**, 429 (1964); (b) L. W. Flynn and G. Thodos, *Progr. Int. Res. Therm. Trans. Props.*, 352 (1962); L. I. Stiel and G. Thodos, *J. Chem. Eng. Data*, **7**, 234 (1962).

(10) See, for example, T. Kihara, *Rev. Mod. Phys.*, **25**, 831 (1953).

(11) J. V. Champion and G. H. Meeten, *Trans. Faraday Soc.*, **64**, 238 (1968); S. A. Mumford, *J. Chem. Soc.*, 4897 (1952); N. G. Parsonage and R. C. Pemberton, *Trans. Faraday Soc.*, **63**, 311 (1967).

(12) The authors are grateful to one of the referees for reminding them that this postulate is consistent with analyses of other types of thermodynamic data where investigators have used surface contact point or surface energy distribution models. In such cases the ends of the molecules seem to be the most important contributors to the property. See, for example, A. J. B. Cruickshank, B. W. Gainey, C. P. Hicks, and T. M. Letcher, *ibid.*, **65**, 2356 (1969).

Table II: Size Parameters for Molecules

Substance	Shape[a]	$\rho\kappa^{1/3}$, Å	l, Å	Critical volume, m³/mol × 10⁶ Calcd	Critical volume, m³/mol × 10⁶ Exptl
Helium	s	2.840	...	57.8	57.8
Neon	s	2.548	...	41.75	41.74
Argon	s	3.101	...	75.26	75.27
Krypton	s	3.319	...	92.28	92.24
Xenon	s	3.611	...	118.8	118.8
Hydrogen	s/c	2.379	0.742[b]	50.0	50
Nitrogen	s/c	2.821	1.098[b]	90.1	90.1
Oxygen	s/c	2.610	1.207[b]	76.4	76.4
Carbon monoxide	s/c	2.847	1.128[b]	93.2	93.2
Carbon dioxide	s/c	2.487	2.310[b]	94.2	94.2
Nitrous oxide	s/c	2.519	2.320[b]	97.4	97.4
Methane	s	3.398	...	99.0	99.0
Ethane	s/c	3.245	1.536[b]	148.2	148.2
Propane	s/c	3.341	2.473	200.6	200.6
n-Butane	s/c	3.341	3.709	255.3	255.1
n-Pentane	s/c	3.341	4.946	311.1	311.5
n-Hexane	s/c	3.341	6.182	367.8	368.0
n-Heptane	s/c	3.341	7.418	425.5	426
n-Octane	s/c	3.341	8.655	484.3	484
Ethylene	s/c	3.099	1.330[b]	124.0	124
Propylene	s/c	3.341	1.978	179.0	180.5
But-1-ene	s/c	3.341	3.215	233.4	241.0[c]
Pent-1-ene	s/c	3.341	4.451	288.7	288.9[c]
Hex-1-ene	s/c	3.341	5.687	345.0	344.6[c]
Hept-1-ene	s/c	3.341	6.924	402.3	401.2[c]
Oct-1-ene	s/c	3.341	8.160	460.4	458.8[c]
n-C_4F_{10}	s/c	4.056	3.709	404.9	397
n-C_5F_{12}	s/c	4.056	4.946	486.1	490[d]
n-C_6F_{14}	s/c	4.056	6.182	568.6	575[d]

[a] s, sphere (point core); s/c, spherocylinder (line core). [b] "Tables of Interatomic Distances and Configurations in Molecules and Ions," The Chemical Society, London, 1958. [c] Estimated in ref 24. [d] Estimated by M. G. D. Garner and J. C. McCoubrey, *Trans. Faraday Soc.*, **55**, 1524 (1959).

in Table II and spectroscopically determined atomic separations with eq 9. Triatomic molecules were treated similarly, but using spectroscopic data on the separation of the extreme atoms. All the data and derived quantities are given in Table II.

Comparison with McGlashan and Potter's Reduced Equation

The relation between the present treatment and the reduced equation of state proposed by McGlashan and Potter is demonstrated as follows.

Expansion of eq 3 in powers of ϕ, followed by substitution of the sphere–sphere values of ϕ and κ derived above, gives us

$$\frac{B}{V^c} = 0.427 - 0.996\left(\frac{T^c}{T}\right) - 0.386\left(\frac{T^c}{T}\right)^2 - 0.180\left(\frac{T^c}{T}\right)^3 - 0.0750\left(\frac{T^c}{T}\right)^4 \quad (10)$$

which is of the same form as the reduced equation of state of McGlashan and Potter

$$\frac{B}{V^c} = 0.430 - 0.886\left(\frac{T^c}{T}\right) - 0.694\left(\frac{T^c}{T}\right)^2 \quad (11)$$

In view of the fact that eq 10 represents a truncated infinite series, we do not expect an exact correlation between coefficients of powers of reduced temperature. But nevertheless the agreement between corresponding coefficients is unexpectedly good.

The Prediction of Mixed Second Virial Coefficients

To apply the formulas of part I to the prediction of the second virial coefficient for an unlike interaction it is necessary to be able to predict the "mixed" pseudocritical temperature, T_{12}^c, together with the unlike interaction size parameter ρ_{12}. The McGlashan and Potter equation of state similarly requires T_{12}^c, but in the place of ρ_{12} an estimate of the mixed pseudocritical volume, V_{12}^c, is required.

Hudson and McCoubrey[13] have shown that T_{12}^c may be estimated in terms of properties of the pure

(13) G. M. Hudson and J. C. McCoubrey, *Trans. Faraday Soc.*, **56**, 761 (1960).

Table IV: Standard Deviations between the Experimental Value of B_{12} and the Calculated Value

System	Temp range, °K	Standard deviation, m³/mol × 10⁶ (i)[a]	(ii)[b]	(iii)[c]	(iv)[d]
Methane					
Ethane	273–323	1.4	4.5	1.9	1.4
Propane	310–510	2.8	11.5	10.5	11.2
n-Butane	344–510	8.7	10.9	8.6	10.4
n-Pentane	310–510	25.6	14.4	5.1	5.5
Carbon dioxide	310–510	4.8	4.8	1.2	9.1
Carbon dioxide					
Ethane	310–510	21.4	17.2	17.6	8.0
Propane	310–510	37.1	21.4	26.8	6.9
n-Butane	377–477	53.0	22.5	25.8	2.0
Nitrogen					
Ethane	277–510	7.5	5.9	4.5	4.0
n-Butane	427–477	26.5	11.5	9.4	6.9
Carbon dioxide	298–398	1.4	1.5	8.6	9.3
n-Octane					
Hydrogen	373–573	30.0	4.2	4.1	4.2
Carbon monoxide	373–573	42.3	15.5	5.5	12.4
Propane	353–413	121.0	31.5	59.2	60.1
Ethane					
Propylene	377–477	6.1	4.0	4.3	4.3
Propane					
n-Heptane	338–414	64.8	6.8	9.2	8.9
Propene					
Hept-1-ene	324–411	12.2	81.1	34.5	34.5
n-Butane					
n-Perfluorobutane	283–323	133.8	60.4	214.7	88.0
n-Pentane					
n-Perfluoropentane	307–383	261.6	162.8	186.6	147.0
n-Perfluorohexane	308–384	319.7	154.9	244.6	63.7

[a] (i), McGlashan and Potter equation with geometric mean rule for T_{12}^c. [b] (ii), McGlashan and Potter equation with Hudson and McCoubrey rule for T_{12}^c. [c] (iii), new equations with geometric mean rule for T_{12}^c. [d] (iv), new equations with Hudson and McCoubrey (Kihara) rule for T_{12}^c.

species by use of London's formulation[14] of molecular dispersion forces

$$T_{12}^c = (T_{11}^c T_{22}^c)^{1/2} \frac{2(I_1 I_2)^{1/2}}{(I_1 + I_2)} \frac{V_{11}^c V_{22}^c}{(V_{12}^c)^2} \qquad (12)$$

where I_1 and I_2 are the ionization potentials of molecules 1 and 2, respectively. With equal ionization potentials and critical volumes this combining rule reduces to the geometric mean.

Other combining rules based on the various theories of intermolecular attractive forces have been put forward by various workers.[15-18] A further rule which has not previously been published may be derived by elimination of polarizabilities from the Slater–Kirkwood theory,[19] giving eq 13, where N_1 and N_2 are the effective number of outer-shell electrons in molecules 1 and 2, respectively.

All these semitheoretical rules give similar results,

$$T_{12}^c = \frac{2(T_{11}^c T_{22}^c)^{2/3}(N_1 N_2)^{1/3}}{[(V_{11}^c N_2)^2 T_{11}^c]^{1/3} - [(V_{22}^c N_1)^2 T_{22}^c]^{1/3}} \times \frac{[V_{11}^c V_{22}^c]^{4/3}}{(V_{12}^c)^2} \qquad (13)$$

but ionization potentials are most readily available of the quantities required and so we shall use the Hudson and McCoubrey combining rule. We shall compare its predictions with those of the geometric mean rule so that the effect of energy and size differences on the final virial coefficients may be gauged.

(14) F. London, *Trans. Faraday Soc.*, **33**, 8 (1937).
(15) J. G. Kirkwood, *Phys. Z.*, **33**, 57 (1932).
(16) B. E. F. Fender and G. D. Halsey, Jr., *J. Chem. Phys.*, **36**, 1881 (1962).
(17) R. J. Munn, *Trans. Faraday Soc.*, **57**, 187 (1961).
(18) F. Kohler, *Monatsh.*, **88**, 857 (1957).
(19) J. C. Slater and J. G. Kirkwood, *Phys. Rev.*, **37**, 682 (1931).

As given in eq 12, the Hudson and McCoubrey rule is applicable solely to spherical molecules, as the London theory actually gives an equation in terms of the size and energy parameters.[13] It has been successfully used by Cruickshank, Windsor, and Young[20] together with the critical volume combining rule

$$V_{12}^{c} = {}^{1}/_{8}[(V_{11}^{c})^{1/3} + (V_{22}^{c})^{1/3}]^{3} \qquad (14)$$

which was derived assuming spherical symmetry and McGlashan and Potter's reduced equation of state to predict mixed second virial coefficients for hydrocarbons, permanent gases, and related substances. For use with our new equations we will revert to the form involving size parameters, as we are not here making any assumptions regarding spherical symmetry in general[21,22] and are attempting to avoid such a simplification. Thus we shall calculate our mixed pseudo-critical temperatures using the relationship

$$T_{12}^{c} = (T_{11}^{c}T_{22}^{c})^{1/2}\frac{2(I_1I_2)^{1/2}}{(I_1 + I_2)}\frac{\rho_{11}^{3}\rho_{22}^{3}}{\rho_{12}^{6}} \qquad (15)$$

and we shall assume that the unlike interaction size parameter is given by

$$\rho_{12} = {}^{1}/_{2}(\rho_{11} + \rho_{22}) \qquad (16)$$

Comparison with Experiment

We have calculated mixed second virial coefficients by four separate methods. In the first two of these we have reproduced work by Cruickshank, *et al.*,[20] using the empirical equation of McGlashan and Potter[5] together with (i) the geometric mean T_{12}^{c} combining rule, and (ii) the Hudson and McCoubrey T_{12}^{c} combining rule, and then using the same two T_{12}^{c} formulas we have calculated B_{12} values using eq 5 of this paper which was derived in part I. The critical and other data employed are given in Tables I[8] and II, and the calculated virial coefficients are in Table III.[8] For these unlike interactions we used the arithmetic mean of the n's for the pure components which are given in Table II.

Table IV gives a summary of the results of Table III expressed in the form of standard deviations according to the small sample formula

$$s = \sqrt{\frac{\sum \delta B_{12}^{2}}{n - 1}}$$

This work confirms the conclusion of Cruickshank, Windsor, and Young[20] that the Hudson and McCoubrey critical temperature combining rule predicts experimental results generally closer than the geometric mean combining rule when used in conjunction with McGlashan and Potter's equation. It should be noted that due to slight differences in data employed in the calculations, the standard deviations quoted here in Table IV differ slightly in some cases from those in Table II of the earlier paper.[20]

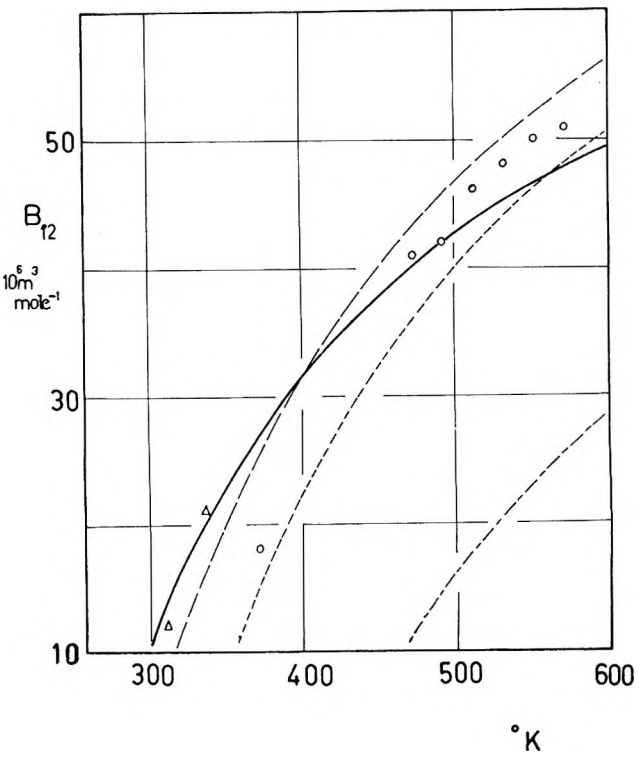

Figure 1. B_{12} values for the system hydrogen–n-octane: experimental values: Δ, Gainey, ref 25a; O, Connolly, ref 25b. Calculated lines: ——, McGlashan and Potter equation using Hudson and McCoubrey T_{12}^{c}; — — —, McGlashan and Potter equation using geometric mean T_{12}^{c}; — —, new equation using Hudson and McCoubrey T_{12}^{c}; – – –, new equation using geometric mean T_{12}^{c}.

In some cases, in particular for mixtures of hydrocarbons, the geometric mean rule provides closer predictions than does the Hudson and McCoubrey formula. The latter might well involve an exaggerated allowance for size differences as the use of eq 13 and 14 in eq 1 seeks to impose spherical symmetry on the molecules concerned. It appears that the size parameters for the hydrocarbons are more nearly equal than such a procedure would imply. Unfortunately the use of the more precise critical volume equation, eq 9, together with the pseudo-critical temperature given by eq 15, does not materially affect results as given by the McGlashan and Potter equation.

Cruickshank, Windsor, and Young favorably compared their predicted results with those of Huff and Reed,[23] who used the Pitzer and Curl reduced equation of state.[4]

All the systems analysed by Cruickshank, Windsor, and Young have been reevaluated, except those in-

(20) A. J. B. Cruickshank, M. L. Windsor, and C. L. Young, *Trans. Faraday Soc.*, 62, 2341 (1966).

(21) J. E. Lennard-Jones, *Proc. Roy. Soc., Ser. A*, 106, 463 (1924).

(22) A. L. Myers and J. M. Prausnitz, *Physica*, 28, 303 (1962).

(23) J. A. Huff and T. M. Reed, III, *J. Chem. Eng. Data*, 8, 306 (1963).

volving sulfur hexafluoride, benzene, and cyclohexane, and various side-chain hydrocarbons to which the new equations do not apply as they stand. We have included in addition the results of McGlashan and Wormald on the propene–hept-1-ene system,[24] and, in Table III only, some results for hydrocarbon–permanent gas and hydrocarbon–carbon dioxide systems measured by Gainey[25a] at 298.2 and 308.2°K.

The new equations and combining rule developed in these two papers reproduce the experimental results better than the McGlashan and Potter–Hudson and McCoubrey combination in 13 out of the 20 systems for which standard deviations of the predicted results from the experimental results are given in Table IV; for one of the remaining systems the standard deviations are equal. The additional results of Gainey listed in Table III are not, in general, reproduced as well by our new procedure as by that of Cruickshank, Windsor, and Young.

The B_{12} results of Connolly[25b] and Gainey[25a] for the hydrogen–*n*-octane system over the temperature range 313–573°K are compared in Figure 1 with the predictions of each of the approaches which we have used here.

When compared with the predictions of the McGlashan and Potter reduced equation of state, the experimental pure second virial coefficients, B_{11}, for nitrogen, oxygen, carbon monoxide, nitrous oxide, ethane, and ethylene are reproduced more closely by the new equations, in the temperature range above the critical temperature. The new equation predicts values for carbon dioxide which are too positive, and here the McGlashan and Potter equation proves slightly more successful, though both procedures give the wrong temperature variation. Predicted B_{11} values are very similar by both methods for spherical molecules, but for spherocylindrical molecules the new equations are better provided that the asymmetry ratio of the molecule (defined as the ratio of core length to size parameter ρ) is less than 1.2, and that the temperature is above the critical, as mentioned earlier.

Previous work has shown that the Sutherland potential when used with Keesom's equation[9a] gives results which are too negative below the critical temperature, and since our new equations reduce to that of Keesom for spherical molecules, it is hardly surprising that a similar trend is observed here. The McGlashan and Potter equation is far more successful in this region. Naturally this inadequacy below the critical temperature for pure substances is accompanied by a similar result for mixed virial coefficients below the pseudocritical temperature.

It is probable that our line-core model is inadequate for chain molecules above four atoms, though such a conclusion is obscured by the failure of the Sutherland potential which we have just discussed. Connolly and Kandalic[26] employed a similar model for the hydrocarbons with a Kihara 12:6 potential and attributed their poor prediction of experimental results to such a breakdown of the model.

Conclusion

In spite of the physical unreality of the molecular model which we have assumed, the new equations appear to be adequate for the prediction of second virial coefficients inside a limited range of substances and temperatures. The temperature restriction could be removed by making ϕ and κ functions of temperature or by the introduction of a Kihara 12:6 potential.[27,28] Fitting and prediction of experimental virial coefficients could be improved by assignment of suitable hard cores in the place of line cores, but it seems unlikely that a rigid core model could ever prove adequate for chain molecules of more than four atoms.

Acknowledgments. Both authors acknowledge financial support from the Science Research Council, England. This work would have been impossible without the facilities provided by the University of Bristol Computer Unit.

(24) M. L. McGlashan and C. J. Wormald, *Trans. Faraday Soc.*, **60**, 646 (1964).

(25) (a) B. W. Gainey, Ph.D. Thesis, University of Bristol, 1967; (b) J. F. Connolly, *Phys. Fluids*, **4**, 1494 (1961).

(26) J. F. Connolly and G. A. Kandalic, *ibid.*, **3**, 463 (1960).

(27) J. M. Prausnitz and A. L. Myers, *AIChE J.*, **9**, 5 (1963).

(28) J. M. Prausnitz and R. N. Keeler, *ibid.*, **7**, 399 (1961).

Two-State Thermodynamics and Transport Properties for Water as Zeroth-Order Results of a "Bond Lattice" Model

by C. Austen Angell

Department of Chemistry, Purdue University, Lafayette, Indiana 47907 *(Received November 12, 1970)*

Publication costs assisted by the Department of the Interior, Office of Saline Water

A simple model for the anomalous excess thermodynamic properties of water is described which, without postulation of molecular species, leads to a "two-state" thermodynamic description as zeroth-order approximation. The model, which is consistent with the common notion that water is best regarded as a disrupted tetrahedral network, involves the concept of elementary configurational excitations of an initially totally connected random network ground-state quasi-lattice. The zeroth-order equations allow a better description of the configuration heat capacity of water and its temperature dependence than those achieved by "mixture model" two-state equations. The model also appears consistent with proton magnetic resonance chemical shift data and with the broad-band aspects of infrared and Raman spectral findings. With an additional postulate concerning the cooperative nature of the flow process, but without additional parameters, the non-Arrhenius temperature dependence of viscosity and other relaxation processes is correctly described and the negative "volume of activation" is accounted for. A glass transition near 159°K is predicted. It is suggested that first-order corrections to the model, which would take into account the cooperative aspects of hydrogen bonding in water suggested by recent quantum-mechanical calculations on static groups, effect mainly the low temperature properties. Their inclusion may lead to an account of the accelerating negative thermal expansion coefficient observed for highly supercooled water.

It has been very common to discuss thermodynamic, dynamic, and structural properties of liquid water in terms of contributions from two[1-8] (sometimes more)[9] "structural species" which are taken to coexist in a temperature- and pressure-dependent thermodynamic equilibrium. If one divides the equilibrium thermodynamic properties of water into contributions from vibrational and configurational degrees of freedom according to the argument of Eisenberg and Kauzmann,[10] then such "mixture" models interpret the configurational contributions simply in terms of the energy or volume changes accompanying the change in concentration of the different species promoted by change of temperature (specific heat, expansitivity) or pressure (compressibility). Mixture models, although fairly successful in accounting for the thermodynamic properties of water, raise conceptual problems, and the writer, for one, finds the idea that the isotropic ice lattice should melt to yield an ideal solution of two distinct molecular species contrary to intuition. Less restrictive cluster models[11,12] are not supported by low angle X-ray scattering studies,[13] and Frank[14] recently concluded that of the mixture class of theory, only some form of interstitial model[15-17] now seems acceptable. So far, however, statistical treatments of such models[17] have failed to yield the correct configurational heat capacity, perhaps because they always have too much order built into them.

In this paper we present a simple method for analyzing the Bernal and Fowler[18] disrupted tetrahedral network model which, in zeroth-order approximation, allows one to recover thermodynamic relations for the anomalous aspects of water which are of mixture model-like form and simplicity. Qualitative consideration of the next order of approximation suggests that grosser

(1) The models described in the following references may not represent the current views of the authors concerned (G. E. Walrafen, T. A. Litovitz, private communications).

(2) K. Grjotheim and J. Krogh-Moe, *Acta Chem. Scand.*, **8**, 1193 (1954). In introducing their treatment, these authors seem to have in mind a model similar to the present one, though their ensuing analysis utilizes the language (liquids A and B mixing ideally) of other mixture models.

(3) G. Wada, *Bull. Chem. Soc. Jap.*, **34**, 955 (1961).

(4) A. Smith and A. Lawson, *J. Chem. Phys.*, **22**, 351 (1954).

(5) C. M. Davis, Jr., and T. A. Litovitz, *ibid.*, **42**, 2563 (1965).

(6) C. M. Davis, Jr., and J. Jarzinski, *Advan. Molec. Relaxation Processes*, **1**, 155 (1968).

(7) G. E. Walrafen, *J. Chem. Phys.*, **40**, 3249 (1964); *ibid.*, **44**, 1546 (1966); *ibid.*, **47**, 114 (1967); *ibid.*, **48**, 244 (1968).

(8) J. D. Worley and I. M. Klotz, *ibid.*, **45**, 2868 (1966).

(9) M. S. Jhon, J. Grosh, T. Ree, and H. Eyring, *ibid.*, **44**, 1465 (1966).

(10) E. Eisenberg and W. Kauzmann, "The Structure and Properties of Water," Oxford University Press, New York, N. Y., 1969.

(11) H. S. Frank and W. Y. Wen, *Discuss. Faraday Soc.*, **24**, 113 (1957).

(12) G. Nèmethy and H. Scheraga, *J. Chem. Phys.*, **36**, 3382 (1962).

(13) A. A. Narten and H. A. Levy, *Science*, **165**, 447 (1969). This article includes a discussion of relevant unpublished results by Hendricks.

(14) H. S. Frank, *ibid.*, **169**, 635 (1970).

(15) O. Ya. Samoilov, *Zh. Fiz. Khim.*, **20**, 12 (1946).

(16) L. Pauling in "Hydrogen Bonding," D. Hadzi, Ed., Pergamon Press, Elmsford, N. Y., 1969.

(17) H. S. Frank and A. S. Quist, *J. Chem. Phys.*, **34**, 604 (1961).

(18) S. D. Bernal and R. H. Fowler, *ibid.*, **1**, 515 (1933).

anomalies, for which there is already some evidence, await the investigators of strongly supercooled water.

The Bond Lattice and Statistical Thermodynamic Relations

The treatment commences with the postulate that water, if it could be cooled indefinitely below its equilibrium freezing point without crystallization occurring, would, like the analogous liquid SiO_2, tend to settle into a totally connected random tetrahedral network structure. We adopt such a network as the configurational ground state of our model. That such a structure can be achieved with only mild bond strains has been demonstrated by model building for the related cases SiO_2[19] and Ge.[20] Such models have led to radial distribution functions and densities close to those of the experimental substances. These structures are readily generated using standard molecular model tetrahedral cores and flexible connecting rods (tubes), by constructing a pentagon and randomly adding tetrahedra to it. Surprisingly, there is little if any choice about the bond orientation for each added tetrahedron, implying, as pointed out by Bell and Dean,[21] that the configurational entropy of the structure may be very small. Due to the bond strains, however, the internal energy of such structures is always considerably in excess of that of the crystalline modifications.

To obtain a lattice on which to make the desired calculations we now abstract from the quasi-lattice of water molecules a new lattice, which we call the "bond lattice," by regarding each point of interaction between a water molecule and its near neighbors as a point in the new lattice (Figure 1a). In water there are four such points (hence the tetrahedral lattice), two proton donating and two proton accepting. We regard the whole region of space between neighboring oxygens along the lone pair-to-proton axis as the bond-lattice point. This construction amounts to a coordinate transformation in which a set of strongly interacting matter points is replaced by a new set (twice the number for a tetrahedral lattice) of weakly interacting energy points. This is appropriate, since our concern is with the thermodynamic consequences of the thermal disruption of hydrogen bonds, which is equivalent to "turning off" the interaction between adjacent molecules. At this point, therefore, we adopt the common, but contentious,[10] position that hydrogen bonds can be broken or at least abruptly weakened (see below). We regard this "turning-off" of much of the interaction as the essential energetic part of an *elementary configurational excitation* of the quasi-lattice. This excitation, which is the basis of our treatment, is visualized by us as follows. A group of molecules in a particular, already strained arrangement becomes unstable to the increasing amplitudes of vibration of its members and relieves the instability by a cooperative act in which a near-neighbor pair of oxygens "snaps" out of line along the O-H···O axis, and the various neighbors make small readjustments of position (centers of molecular vibration) to reduce average local strain to a minimum. Figure 1b shows how this process may lead to a substantial negative volume increment.

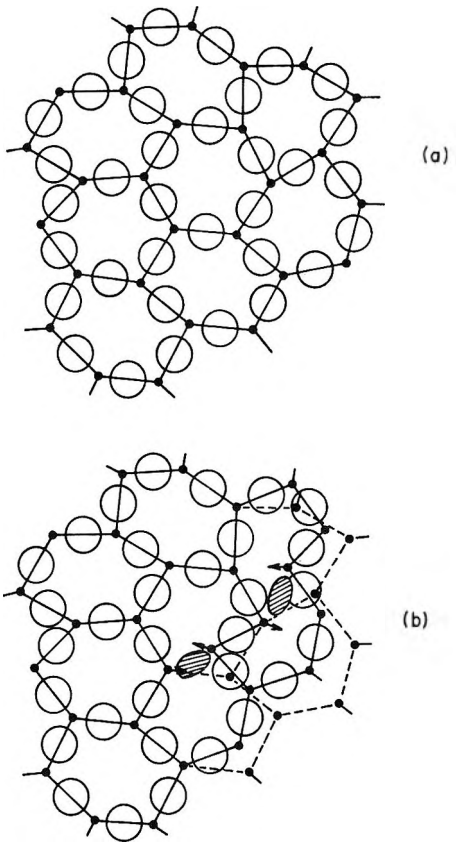

Figure 1. (a) Two-dimensional representation of relation between bond lattice and point lattice for disordered three-coordinate system serving as two-dimensional analog of tetrahedral vitreous water lattice. Point lattice is computer-generated random network conforming to specified average bond angle taken from the work of P. F. Aubourg and A. R. Cooper (to be published). (b) Same lattice after two excitations, showing collapse to smaller "volumes" in accord with negative ΔV of excitation.

If we ignore, for the moment, the distribution of initial bond energies consequent on the strain inherent in the random network, we can then consider each bond-lattice element as capable of existing in two states, "on" (intact bond) or "off" (broken bond).[22,23] Assigning an

(19) R. J. Bell, N. F. Bird, and P. Dean, *J. Phys. C., Ser.* **2**, 1, 299 (1968).

(20) D. E. Polk, *J. Noncryst. Solids*, **5**, 365 (1971).

(21) J. Bell and P. Dean, *Phys. Chem. Glasses*, **9**, 125 (1968).

(22) Evidence for distinct "on" and "off" states for covalent bond interactions in the partially covalent zinc chloride glass quasi-lattice has recently been provided by probe anion (CN^-) spectroscopy (see ref 23) and it seems entirely possible that the directional covalent part of the H-bond interaction in the condensed phase (R. A. Coulson in "Hydrogen Bonding," D. Hadzi, Ed., Pergamon Press, Elmsford, N. Y., 1959, p 339) may provide the basis for similar "on"–"off" behavior in the water quasi-lattice. In this case our "turning off" process replaces strong H bonds by weaker ones.

(23) C. A. Angell and J. Wong, *J. Chem. Phys.*, **53**, 2053 (1970).

energy, ϵ, to the "turning-off" process and recognizing that the entropy is increased by distributing "off" elements across the bond lattice, we can immediately calculate the equilibrium number of "off" elements (broken bonds) at temperature T by a standard lattice statistics argument, treating the case where the total number of lattice points is temperature invariant.[23] This yields

$$n_x = 2N\left(1 + \exp\frac{\epsilon}{kT}\right)^{-1} \quad (1)$$

where n_x is the number of "off" elements, and N is the number of water molecules (for convenience considered to be Avogadro's number throughout this paper). In arriving at this expression the zeroth-order assumption that interactions between lattice elements can be neglected has been made, *i.e.*, a given element is assumed unconscious of whether or not its neighbors are "on" or "off." This assumption is the equivalent of the mixture model assumption of ideal mixing of different species, and amounts to disregarding evidence for cooperative effects in hydrogen bonding of water molecules.[11,24] Thus in zeroth-order approximation the present model perpetuates a weakness common to mixture models although it does so within what seems to us a more appealing conceptual framework. Order–disorder theory suggests possible ways of proceeding to higher order approximations, but as one of our aims is to show how mixture model thermodynamic relations can be obtained without postulating molecular species, we will proceed on the zeroth-order basis, and defer until later discussion of how cooperative effects may affect our conclusions.

The configurational heat capacity for a system with the above distribution law is that of the well-known Schottky anomaly,[25] *viz.*

C_v (for N particles, electrons, lattice elements, etc.) =

$$Nk\left(\frac{\epsilon}{kT}\right)^2 \frac{\exp(\epsilon/kT)}{[1 + \exp(\epsilon/kT)]^2} \quad (2)$$

$$= Nk\left(\frac{\epsilon}{kT}\right)^2 (N_x)(1 - N_x) \quad (3)$$

where $N_x = n_x/2N$ is the mole fraction of "off" elements at temperature T. This heat capacity is however restricted to a maximum value of 0.9 cal/(mol deg). reached at $T = 0.42\epsilon/k$, a contribution too small to be of interest in accounting for the changes of 3–4.5 cal/(deg mol) of elements or 0.5 mol of water encountered in practice. This difficulty is, however, readily overcome when it is recognized that the breaking of bridge bonds must affect the vibrational frequency spectrum characterizing the vibrational degrees of freedom of the lattice, increasing the density of low frequency states at the expense of the high frequency density (see, *e.g.*, ref 19). Since this implies an increase in vibrational entropy on excitation of lattice elements, such excitations become more probable, and the work of excitation ϵ should be modified to represent a net work term $\epsilon_x - Ts_x$ where ϵ_x now contains a small vibrational enthalpy contribution and s_x is the net increase in lattice entropy per excitation. Since the entropy of distribution of "off" elements through the lattice is not affected by this modification, the distribution law, eq 1, is modified only by replacement of ϵ by $\epsilon_x - Ts_x$ in the exponential term.

Finally, if we consider a constant pressure system, and use "per mole of elements" quantities for the excitation parameters, eq 1 can be rewritten

$$\frac{n_x}{2N} = N_x = \left(1 + \exp\frac{\Delta E + P\Delta V - T\Delta S}{RT}\right)^{-1} \quad (4)$$

Apart from the factor 2, this is the same as the expression for the population of "species 2" (the "close-packed species") in more familiar two-state models.[1-6] Our treatment thus provides a statistical justification for the idea evident in other authors' thinking[26] that "species 2" is best interpreted as the broken hydrogen bond rather than as a molecular species.

The configurational heat capacity expression corresponding to the eq 4 distribution law is

$C_{v(conf)}$(per mole of H_2O) =

$$2R\left(\frac{\Delta E}{RT}\right)^2 \frac{\exp(\Delta E - T\Delta S)/RT}{[1 + \exp(\Delta E - T\Delta S)/RT]^2} \quad (5)$$

$$= 2R\left(\frac{\Delta E}{RT}\right)^2 N_x(1 - N_x)$$

according to which C_v can now reach very large values, dependent only on the value assigned to ΔS. The factor 2, which distinguishes eq 5 from previous two-state heat capacity equations, is important since it shows that if the breaking of H bonds in random fashion is the important energetic event then the appropriate ΔH and ΔS parameters should reproduce the heat capacity of 0.5 mol of water. This permits the use of a smaller ΔS parameter which in turn (see below) makes it possible to correctly describe the temperature dependence as well as the magnitude of the experimental data. The origin of this improvement is clearly the fact that, in contrast with earlier published treatments, the present model places no restrictions on the bonds which can be broken. In the related expressions for expansivity and compressibility (see, *e.g.*, ref 5 and 6), the presence of the molar volume in the equations removes the distinction between expressions of the present and previous treatments.

In seeking to test these expressions and to obtain values for the model parameters, problems are encountered. In contrast to the case of viscous liquids, experiments

(24) J. Del Bene and J. A. Pople, *J. Chem. Phys.*, 52, 4858 (1970).
(25) W. Schottky, *Phys. Z.*, 22, 1 (1921); *ibid.*, 23, 9 (1922).
(26) See, *e.g.*, G. E. Walrafen in "Water, a Comprehensive Treatise," F. Franks, Ed., Plenum Press, New York, N. Y., 1971, Chapter 6.

to separate the configurational from the vibrational contribution to the thermodynamic properties cannot yet be performed (except for the case of dielectric constant[27]). However, since the vibration frequencies of water are known, the configurational heat capacity can be assessed with some confidence by subtraction of the calculated vibrational contribution (which is essentially the heat capacity of ice) from the measured value. We consider this quantity, $C_{v(conf)}$, provides the best basis for fixing the parameters ΔE and ΔS of eq 5. The configurational heat capacity of 0.5 mol of water, as determined by Eisenberg and Kauzmann,[10] is shown as $\Delta C_{v(exptl)}$ in Figure 2. Also shown, as $\Delta C_{v(calcd)}$, is the theoretical (eq 5) plot obtained using the parameters ΔE = 1900 cal/mol of bonds and ΔS = 4.8 cal/(mol deg). The agreement is fairly good (~5%) at all temperatures. Previous two-parameter models have always overestimated the temperature dependence. Complete coincidence can, of course, be achieved by use of additional parameters as in effect was demonstrated recently by Walrafen[26] using water molecules as species with mole fractions assigned on the basis of the number of neighbors to which they were bonded. Figure 2 also shows, as $\Delta C_{v(F)}$, the measured increase in heat capacity on fusion. (Actually, $\Delta C_{p(F)}$ is measured, but for water near 4° $C_p \approx C_v$.) A better fit to the Eisenberg–Kauzmann estimate could be made by more refined choices of parameters, but both the estimate and the model are in our opinion too crude to warrant fitting beyond two significant figures.

Substitution of the above parameters into eq 4 yields the percentage of the possible hydrogen bonds which are broken as a function of temperature. Representative figures are 25% at T = 0° and 42% at 75°.

Using the above ΔH and ΔS values and the Litovitz estimate[28] for the configurational compressibility, we obtain from the two-state compressibility equation[5,6] $\Delta V = \pm 4.2$ cm³/mol of bonds, ΔV being the average decrease in lattice volume for each mole of bonds which are broken. Substitution of this into the two-state equation for expansivity[5,6] yields $\alpha_{conf} = -11.2 \times 10^{-4}$ deg^{-1} at 0°, the negative value offsetting the positive vibrational contribution at low temperatures to yield the familiar density maximum at 4°. Although the above value of $\alpha_{(conf)}$ is comparable with results from other two-state models,[5,6,11] we consider it excessively large and probably a consequence of the requirement implicit in a two-state treatment that the system explore the same degrees of freedom under changing pressure as under changing temperature. This difficulty need not arise in a more realistic treatment of the random network problem in which a distribution of energies, hence volumes (not necessarily correlated with energies), is made available to the lattice element,[29] but we will not dwell on this aspect of the treatment here.

The model, like previous theoretical treatments of water, leads to reasonable agreement with certain other

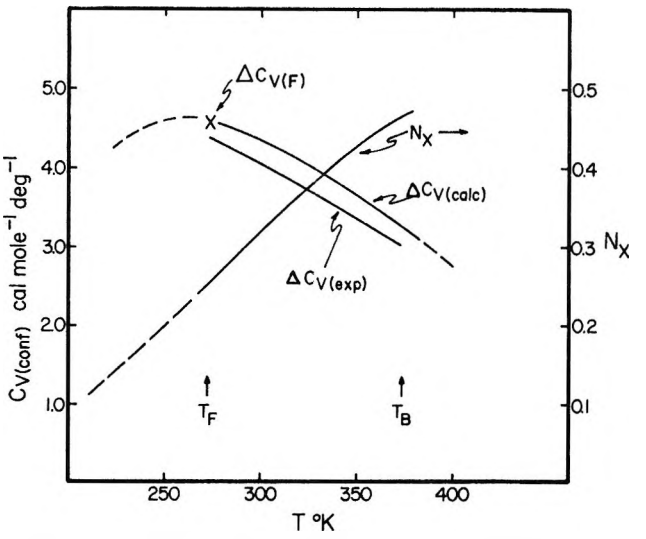

Figure 2. Excess (configurational) heat capacity ($\Delta C_{v(calcd)}$) and broken bond fraction, N_x, as function of temperature for water according to "bond-lattice" model, for molecular parameters ΔE = 1900 cal/mol and ΔS = 4.8 eu. Comparison is made with (a) the Eisenberg–Kauzmann estimate ($\Delta C_{v(exptl)}$) based on experimental heat capacity and vibrational frequencies, and (b) the change in heat capacity of H_2O on fusion ($\Delta C_{v(F)}$).

measured properties such as the temperature dependence of proton chemical shift[30,31] ($\delta_{"on"} - \delta_{"off"}$ = 4.3 ppm (calcd) compared with ≈5 ppm (theor)), and the more contentious[10] "two-species equilibrium" Raman[7,25] and infrared[8,32] spectra (which yield ΔH = 2.5 ±0.6,[7] 2.4,[8] 2.3 ± 0.4[32] kcal/mol). Particularly the broad band aspects of these spectra are expected from the distribution of bond energies characteristic of the random network, but even here there are possible alternative explanations of the spectral findings. It is therefore perhaps more interesting to consider the relevance of the present model in areas to which previous models have not been, or could not be, applied. The rest of the paper is therefore devoted to discussion of nonequilibrium (transport) and low temperature properties.

Nonequilibrium Properties

All the foregoing leaves quite unanswered the question of why water is a liquid; the thermodynamic argument does not require the lattice elements (or rather

(27) (a) C. H. Collie, J. B. Hasted, and D. M. Riston, *Proc. Roy. Soc., Ser. A*, **60**, 145 (1948); (b) N. V. Chekalin and M. I. Shakhparonev, *Zh. Struk. Khim.*, **9**, 896 (1968).

(28) W. Slie, A. Donfor, and T. Litovitz, *J. Chem. Phys.*, **44**, 3712 (1966).

(29) C. A. Angell and K. J. Rao, Proceedings of the Third International Conference on Physics of Non-Crystalline Solids, Sheffield, Sept 1970, papers to be published in "Amorphous Solids," R. W. Douglas and B. Ellis, Ed., Wiley, New York, N. Y., 1971, and *J. Chem. Phys.*, to be published.

(30) N. Muller, *ibid.*, **43**, 2555 (1965).

(31) J. C. Hindman, *ibid.*, **44**, 4582 (1966).

(32) W. A. Senior and R. E. Verrall, *J. Phys. Chem.*, **73**, 4242 (1969).

the molecules they link) to rearrange with respect to one another at any stage since the excitation on which the thermodynamics depends involves only small reversible displacements. Hence, as stated so far, we have only a theory for an excited amorphous solid. The same may be said of previous mixture models for water when the statistical basis of the mixing entropy in an ideal solution is remembered.

Since translational molecular motion in the fully bonded ground-state structure would seem to be proscribed, we consider the possibility that mass transport arises as a natural consequence of statistical fluctuations in the local concentrations of "off" elements as N_x increases with increasing temperature. If, in the vicinity of some minimum local concentration of broken bonds, groups of now-unrestrained molecules cooperatively redistribute themselves, then a sequence of such rearrangements may serve to release perturbing shear or electrical stresses and thus permit irreversible viscous flow or dielectric relaxation. Mass transport and the process of maintaining equilibrium between vibrational and configurational degrees of freedom in this case are inseparable.

We have been led to test the notion[33] that the probability of such cooperative rearrangements occurring, $p(R)$, is an exponential function of the broken bond fraction, N_x

$$p(R) = Z \exp(-\gamma/N_x) \tag{6}$$

where N_x is given by eq 4, γ is a constant taken for the present case to have value unity, and Z is a probability normalization factor of order unity. In examining this function we have had in mind (a) Miller's[34] fit of the water viscosity data to the empirical Vogel–Tammann–Fulcher (VTF) equation (which is commonly used to describe non-Arrhenius relaxation behavior in liquids) *viz.*

$$\eta = A \exp[B/(T - T_0)] \equiv A \exp\left[\frac{1}{C(T - T_0)}\right] \tag{7}$$

where A, B, and T_0 are constants, T_0 being 150°K for water, and (b) the observation from Figure 2 that N_x in the range of normal measurement is an almost linear function of temperature with an extrapolated value of zero at ~160°, *i.e.*, $N_x \approx C(T - 160)$.

Using eq 6, the relaxation time for water, τ, can be written

$$\tau = \frac{\tau_0}{p(R)} = \tau_0 Z^{-1} \exp(1/N_x) \tag{8}$$

where τ_0 would be of the order of the period required for a group of water molecules to rearrange, each moving roughly a molecular diameter, 2.8 Å, at a velocity intermediate between the gas kinetic velocity, 3.55×10^4 cm/sec at 0°, and the speed of sound in water, 1.58×10^5 cm/sec at 0°.

On this basis, we expect τ at 0° in the range $7.8 \times 10^{-13} Z^{-1} \exp(0.25)^{-1}$ ($= 5.0 \times 10^{-11}$ sec) to $1.94 \times 10^{-13} Z^{-1} \exp(0.25)^{-1}$ ($= 1.26 \times 10^{-11}$ sec), if we take Z as unity. These values span the experimental dielectric relaxation time of 1.78×10^{-11} sec at 0° measured by Collie, *et al.*[27] At 75° the calculated values are in the range 7.6 to 2.0×10^{-12} sec compared with the experimental value 3.22×10^{-12} sec.

We may apply this idea to the prediction of the temperature dependence of viscosity, which is very accurately known, by noting the relation between viscosity and relaxation time given by Herzfeld and Litovitz.[35]

$$\eta = G_\infty \tau$$

where G_∞ is the infinite frequency shear modulus. With eq 8 this then yields

$$\eta = G_\infty \tau_0 Z^{-1} \exp(1/N_x) = \eta_0 \exp(1/N_x) \tag{9}$$

where τ_0 of eq 9 is not necessarily the same as that of eq 8. By fixing the preexponential term using the measured viscosity at 0°, we can use eq 9 with the parameters from Figure 1 to calculate the course of the viscosity with changing temperature between −9 and 100°. A comparison of the calculated curve with the experimental plot using data from the "Handbook of Physics and Chemistry" is given in the form of an Arrhenius plot in Figure 3. The temperature dependences of τ_0 and G_∞ will individually be weak in comparison with the exponential term, and since they will also have opposite signs, and thus tend to cancel, only the exponential term has been considered in calculating the Figure 3 curve.

Remarkably enough, not only are the average slopes of the calculated and experimental plots the same, but the systematic departures from Arrhenius behavior observed for water[36] are quite closely reproduced. Dielectric relaxation times[27] show the same temperature dependence as viscosity within experimental error of the former. Equation 9 predicts a rapidly increasing viscosity at subzero temperatures, the calculated viscosity for supercooled water being shown by the inset to Figure 3. Water would evidently become a glass at ~159°K ($\eta = 10^{13}$ P) if crystallization did not intervene. This temperature is to be compared with that of the value 162°K suggested by Miller[37] from an application of the VTF equation referred to above. A glassy form of water obtained by deposition from the vapor onto a cold plate has been found to exhibit the glass transition at 139°K,[38] though it has been pointed out

(33) C. A. Angell, *J. Chem. Educ.*, **47**, 583 (1970).

(34) A. A. Miller, *J. Chem. Phys.*, **38**, 1568 (1963).

(35) K. Herzfeld and T. A. Litovitz, "Absorption and Dispersion of Ultrasonic Waves," Academic Press, New York, N. Y., 1959.

(36) L. Korson, W. Drost-Hansen, and F. J. Miller, *J. Phys. Chem.*, **73**, 351 (1969).

(37) A. A. Miller, *Science*, **163**, 1325 (1969).

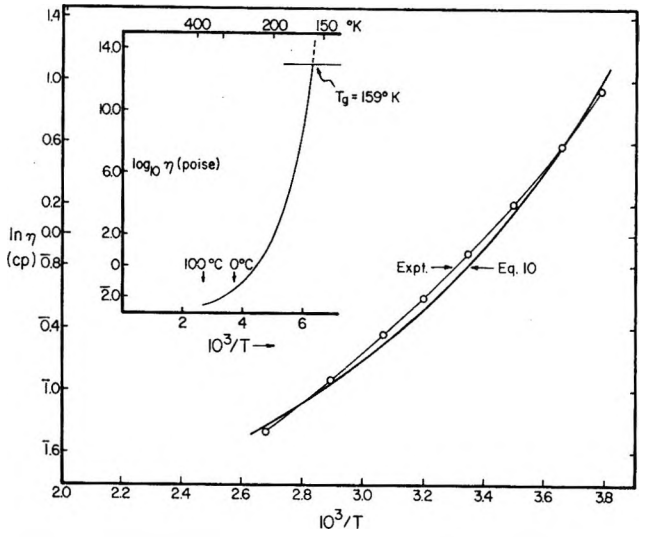

Figure 3. Viscosity dependence on temperature according to bond lattice critical cluster model, compared to experimental plot. Inset: predicted low temperature viscosity and glass transition temperature, T_g (occurs when $\eta \approx 10^{13}$ P), for supercooled water from bond-lattice model.

elsewhere[39] that this temperature is somewhat lower than expected from thermodynamic data taken at normal temperatures (see also below) and some mystery attaches to the exact relation of this glass to ordinary water.

On the other hand, eq 8, like the VTF equation, does not corectly predict the relaxation times at higher temperatures[40] where η is found in many liquids to return to Arrhenius behavior. Certainly it seems that any predictions based on a quasi-lattice representation of the liquid should not be expected to hold at the very high degrees of lattice disruption and vibrational excitation encountered above 100°. Indeed one should probably be wary of their apparent success at the more moderate temperatures.

Equation 8 has, in common with the Cohen and Turnbull "free volume" model derivation of the VTF equation,[41] the absence of any "activation energy" in the normal sense of the term. We have attempted, in analogy to Cohen and Turnbull's "critical void" postulate, to utilize the concept of a "critical cluster" or "critical concentration" of broken bonds to derive eq 7 from statistical considerations, so far with unconvincing results. Thus we will regard eq 8 and 9 as intuitively appealing but nevertheless empirical relations. At the same time we must stress the advantages that (1) no "zero excitation temperature," T_0, need be assumed, since this is taken care of by the form of eq 4 for N_x, and (2) the non-Arrhenius relaxational behavior is accounted for irrespective of the direction of volume change with temperature.

We will also note another significant feature of eq 9. If we use eq 4 to substitute for N_x, and then ask what quantity the conventional "activation volume" for viscous flow, $\Delta V_{(\eta)}^{\dagger}$ represents, we find

$$\Delta V_{(\eta)}^{\dagger} = RT\frac{\mathrm{d}\ln\eta}{\mathrm{d}P} = RT\frac{\mathrm{d}\ln(G_\infty\tau_0)}{\mathrm{d}P} + RT\frac{\mathrm{d}}{\mathrm{d}P}\left[1 + \exp\left(\frac{\Delta E + P\Delta V - T\Delta S}{RT}\right)\right] = RT\frac{\mathrm{d}\ln(G_\infty\tau_0)}{\mathrm{d}P} + \Delta V\exp(\Delta E/RT) \quad (10)$$

thus immediately explaining the negative activation volume for water[10] observed at low temperatures where the second term in eq 10 will be dominant (we earlier identified the value of ΔV as -4.2 ml/mol). $\Delta V_{(\eta)}^{\dagger}$ would evidently become very large at subzero temperatures. Since ΔG itself is pressure dependent, increasing with increasing pressure (eq 4), the second term in eq 1 decreases with increasing pressure, and thus the observed minimum in the pressure–viscosity relation is also predicted by eq 10. This line of thought suggests that the pressure dependence of the dielectric relaxation time may serve as an alternative source of information on the value of ΔV.

Cooperative Aspects and Low Temperature Behavior

It was noted earlier that the simple two-state thermodynamic relations were obtained at the cost of excluding from the model the evidence that hydrogen bonds form and break cooperatively.[11,24] The quantum-mechanical calculations of Pople[24] show this to be a strong enough effect in static groups that some influence should be felt even in dynamical situations where vibrational amplitudes for all quasi-lattice modes are substantial. Moreover, strong effects should be found under the more ordered and vibrationally less extreme conditions near the melting point and below.

It is readily seen from the following one-dimensional representation of the interactions characteristic of our problem that the inclusion of cooperative effects is the natural first-order refinement of the model. Comparison with a similar representation of the much-studied Ising problem (theory of the λ-type transition) will then suggest to us how the cooperative nature of hydrogen bonding should modify the thermodynamic properties of water obtained from our zeroth-order treatment given above.

Chain Representation of System with Cooperative Bond Excitations

ground state

O α_1 O α_1 O α_1 O α_1 O α_1 O α_1 O α_1 O α_1 O

1st excited state

O α_1 O α_1 O α_1 O α_3 O α_2 O α_3 O α_1 O α_1 O

(38) (a) J. A. McMillan and S. C. Los, *Nature*, **206**, 806 (1956); (b) M. Sugisaki, H. Suga, and S. Seki, *Bull. Chem. Soc. Jap.*, **41**, 2586, 2591 (1968).

(39) C. A. Angell and E. J. Sare, *J. Chem. Phys.*, **52**, 1058 (1970); *Science*, **168**, 280 (1970).

(40) J. C. Hindman, private communication, and *J. Chem. Phys.*, **74**, 1267 (1970).

(41) M. H. Cohen and D. Turnbull, *ibid.*, **31**, 1164 (1959).

Here the α's represent the interaction energies between nearest neighbor molecules, and the broken bond is represented by displacement arrows. The primary bond-breaking energy is $(\alpha_1 - \alpha_2)$ and is the only term considered in the zeroth-order treatment (where it was given the symbol ϵ_x). The contribution due to the weakening effect of the primary bond break on the neighboring bonds is given by $2(\alpha_1 - \alpha_3)$. Thus the total energy of the excitation may be represented as the sum of cooperative and noncooperative terms. In the bond lattice representation of the same interactions we have

ground state O ϵ_1 O ϵ_1 O ϵ_1 O ϵ_1 O ϵ_1 O

1st excited state O ϵ_1 O ϵ_1 O ϵ_2 ● ϵ_2 O ϵ_1 O

$\epsilon_1 \ll \alpha_1$

and O ⟶ ●, $\Delta E = \epsilon_x$

"on" ⟶ "off"

excitation energy $\Delta E = \epsilon_x + 2(\epsilon_1 - \epsilon_2)$

(zeroth-order case, $\epsilon_1 = \epsilon_2$)

The latter representation closely resembles the Ising chain from which it differs only by the presence of the noncooperative term O ⟶ ●, $\Delta E = \epsilon_x$.

Ising Chain (Using Familiar Spin-up ⟶ Spin-down Symbolism)

ground state ⊕ ϵ_1 ⊕ ϵ_1 ⊕ ϵ_1 ⊕ ϵ_1 ⊕ ϵ_1 ⊕

1st excited state ⊕ ϵ_1 ⊕ ϵ_1 ⊕ ϵ_2 ⊕ ϵ_2 ⊕ ϵ_1 ⊕

excitation energy, $\Delta E = 2(\epsilon_1 - \epsilon_2)$

While the thermodynamic properties of the Ising chain are readily evaluated, the solutions for the more interesting higher-dimensional cases are extremely complicated. Various approximate solutions, however, are available and are described in standard texts (*e.g.*, ref 42). One of the early orders of approximation is found to be equivalent to the Bragg–Williams approximation of the cooperative transition in which the observed Λ form of the heat capacity was shown to result qualitatively if the energy required for each disordering step decreases as the disorder increases, *i.e.*, if the energy, ΔE, is temperature-dependent and vanishes at T_c, the transition temperature. Without solving the cooperative bond lattice problem in detail we can therefore hope to obtain its main thermodynamic properties by representing the excitation energy as the sum of a temperature-independent (noncooperative) term and a temperature-dependent (cooperative) term; *i.e.*, $\Delta E = \Delta E_0 + \Delta E_1(T)$, with ΔE_1 vanishing at some temperature determined by the magnitude of the cooperative term. The consequences of this form of excitation energy for the heat capacity of the bond lattice were examined recently by Rao and Angell[29] in a consideration of the glass transition phenomenon. They showed the inclusion of $\Delta E_1(T)$ leads to a sharpened heat capacity maximum at lower temperatures but, because of the vanishing of the contribution due to $\Delta E_1(T)$, does not change the high temperature values. Applying this result to the case of water, where the cooperative character may be unusually pronounced, we expect that the heat capacity of water should remain accountable by zeroth-order expressions at normal temperatures, but instead of going through the slow maximum around 260°K seen in Figure 1 would continue to increase in an accelerating fashion with decreasing temperature before coming suddenly down again as $N_x \to 0$.

Although the heat capacity data below 0° needed to test this expectation are not available, low temperature expansivities (which are correlated to the heat capacity through terms in the "broken bond" fraction) may be obtained from the recent +4 to −34° density study of Zheleznyi.[43] According to these data the expansivities become increasingly negative, indeed at a quite hair-raising rate, as the temperature is lowered below −10°. The data suggest that heat capacities approaching 50 cal/(deg mol) which would certainly demand a cooperative mechanism for their explanation, may be measurable using some suitable capillary or droplet technique.

Beside being consistent with the above discussion, such high heat capacities would also be of interest in that they imply that the entropy of fusion is being lost from the supercooling liquid water even more rapidly than previously suggested.[39] This suggests that a completely bonded state would be approached at temperatures above 200°K, making the nature of the vapor-deposited glassy water phase, which exhibits a glass transition at 139°K,[38] appear even more puzzling than at present. It is worth noting that a rather similar problem is encountered in trying to relate the nature and properties of the metallic high coordination number liquid phase of germanium to the four-coordinated glassy phase formed by vapor deposition or liquid–liquid phase separation techniques.[44]

Concluding Remarks

We have presented a model for water which, while in fair accord with intuition, provides a clear basis for statistical-mechanical assessment of the equilibrium thermodynamic properties. With a detailed solution of the cooperative problem along lines indicated in the preceding section, this could become an adequately sophisticated theory for the substance. The most serious approximation, or departure from reality, may lie in the assumption that hydrogen bonds can be broken. Although widely espoused, this idea requires the existence of a saddle point in the energy *vs.* distance-orientation

(42) T. L. Hill, "Statistical Mechanics," McGraw-Hill, New York, N. Y., 1956.

(43) B. V. Zheleznyi, *Zh. Fiz. Khim.*, **43**, 2343 (1969). The low temperatures were reached by making the measurements in ~10-μ capillaries to reduce the chances of ice nucleation.

(44) J. de Neufville and D. Turnbull, *Discuss. Faraday Soc.*, in press.

coordinate for neighboring water molecules, and there are some reasons for believing this may not correspond well with true situation.[10,45] Even so, the success of lattice gas theories for description of the gas–liquid critical phenomenon shows that complicated cooperative problems can be adequately described by models whose departure from physical reality may be considerably grosser than any apparent in the present model. Thus further development of the model seems well worthwhile, with a proper working out of the theory for the cooperative bond chain and lattice being the first requirement.

It seems probable to the writer that the ability to describe the behavior of strongly supercooled water will provide the most severe tests of theories of water which concern themselves with properties near the melting point where water exhibits its greatest anomalies. At the moment it seems there is a need for more experimental data in this very interesting region.

Acknowledgments. Support of this work by a grant from the U. S. Department of Interior, Office of Saline Water, is gratefully acknowledged. The author is also indebted to Dr. K. J. Rao of this laboratory and Dr. R. E. Hester (University of York) for discussion of the ideas contained in this paper. The helpful comments of Dr. J. C. Hindman and Professor H. S. Frank on the manuscript have also been appreciated.

(45) F. H. Stillinger, private communication.

The Kinetics of Nickel Murexide Formation in Several Solvent Systems

by C. T. Lin and John L. Bear*

Department of Chemistry, University of Houston, Houston, Texas 77004 *(Received March 1, 1971)*

Publication costs assisted by the Robert A. Welch Foundation

The stability constants and rate constants for the formation of the one-to-one complex of nickel(II) with singly charged murexide in H_2O, 25% DMSO–H_2O, 50% DMSO–H_2O, and 50% ethanol–H_2O have been determined at different temperatures. The stability constants were calculated from spectrophotometric data, and the kinetic studies were made on a temperature-jump apparatus. The thermodynamic and kinetic parameters obtained from these measurements for the nickel(II) system are interpreted in terms of the dielectric constant of the mixed solvent and intermolecular interactions in the solvents. The rate constants, enthalpy of activation, and enthalpy of reaction at 25° and 0.1 M ionic strength for the reaction $Ni^{2+} + H_2L^- \underset{k_r}{\overset{k_f}{\rightleftharpoons}} NiH_2L^+$ are $k_f = 1.8 \times 10^3\ M^{-1}\ sec^{-1}$, $k_r = 1.15\ sec^{-1}$, $\Delta H_f^* = 11.9$ kcal mol^{-1}, and $\Delta H^\circ = -1.6$ kcal mol^{-1} in H_2O; $k_f = 4.2 \times 10^3\ M^{-1}\ sec^{-1}$, $k_r = 0.43\ sec^{-1}$, $\Delta H_f^* = 11.8$ kcal mol^{-1}, and $\Delta H^\circ = -5.6$ kcal mol^{-1} in 50% DMSO–H_2O; and $k_f = 9.0 \times 10^3\ M^{-1}\ sec^{-1}$, $k_r = 0.83\ sec^{-1}$ in 50% ethanol–H_2O, respectively. The slowness of nickel(II) murexide complexation reactions compared to other similar nickel(II) systems reported in the literature is explained on the basis that the rates of stepwise dissociation of metal–ligand bonds are comparable to the rates of stepwise formation.

Introduction

For the divalent ions of the first transition series, the rates of the metal–ligand substitution reactions in aqueous solution can be explained by three mechanisms. The rate-determining step of complex formation is either strongly dependent on the nature of the metal ion[1] or sterically controlled by the entering ligand,[2] or accelerated through the formation of hydrogen bonds between the coordinated water and the attacking ligand.[3] It has been found that steric hindrance affects the cobalt(II) system more than the nickel(II) system in a sterically controlled mechanism.[2,4] Recently an abnormal reaction rate between nickel(II) and ligands having peptide linkages has been reported.[5] The rates for the reaction between cobalt(II) and these ligands are normal, while for nickel(II), they are slower than the normal values.

In light of these observations, the detailed kinetics

(1) M. Eigen and K. Tamm, *Z. Elektrochem.*, **60**, 93 (1962).

(2) K. Kustin, R. F. Pasternack, and E. Weinstock, *J. Amer. Chem. Soc.*, **88**, 4610 (1966).

(3) D. B. Rorabacher, *Inorg. Chem.*, **5**, 1891 (1966).

(4) A. Kowalak, K. Kustin, R. F. Pasternack, and S. Petrucii, *J. Amer. Chem. Soc.*, **89**, 3126 (1967).

(5) K. Kustin and R. F. Pasternack, *J. Phys. Chem.*, **73**, 1 (1969), and the earlier references cited therein.

and thermodynamics of the nickel(II) murexide complexation reaction in H_2O, ethanol–H_2O, and DMSO–H_2O solutions have been studied. This system was chosen because the forward rate constant reported for cobalt(II) murexide is in the above normal range while that for nickel(II) is smaller than expected.[6]

The solvent effects on the stability constants and rate constants in the various mixed solvents are derived from the results determined independently from the spectrophotometric and temperature-jump measurement.

Experimental Section

The stock solution of nickel ion was standardized by an ion-exchange technique and then diluted to the desired values. Absolute ethanol, DMSO, and murexide powder were used without further purification. Sodium perchlorate was used to regulate the ionic strength of the solutions to 0.1 *M*. The murexide solution was freshly prepared for each determination. The pH was adjusted by dropwise addition of a solution of NaOH and/or $HClO_4$.

The temperature-jump apparatus constructed in this laboratory is similar to that described by Hammes and Fasella.[7] The T-jump cell was thermostated by a constant temperature water–ethylene glycol mixture circulating directly through the ground electrode of the cell. Blank experiments with solutions containing only the metal ion or the ligand did not show any relaxation effects. A log plot gave the relaxation time of the reaction which was characterized by a single relaxation step. Each relaxation time represents an average of several photographic determinations. The standard deviation for the determinations is ±10%.

The Klotz and Ming method[8] for the determination of stability constants by spectrophotometry was employed. Absorption spectra and optical densities were determined at several temperatures with a Hitachi uv spectrophotometer.

1. Thermodynamic Section. It is well known that murexide may be used as an end-point indicator for metal titrations. The monovalent anion of this dye is protonated at about pH 2. Although the second acid association of the murexide ion in H_2O occurs at pH 9, the deprotonation[9] of nickel murexide (monovalent species) begins to be observed at pH 5.6. This is evident from the fact that the spectrum of nickel murexide above this pH value starts to show the departure from that at lower values. Therefore, the deprotonation reaction contributes neither to the equilibration nor to the kinetics of the nickel murexide reaction as long as the pH of the aqueous solution is kept below 5.6. The pK value for the deprotonation should be much higher than 5.6, and there is no need to determine this value for the present study. Similarly, the pH limits could be established for the singly charged murexide ion and its reaction with nickel in the mixed solvents. Even though the pH values in the mixed solvents may not represent the exact H^+ ion concentrations, they do provide the safe working range. The pH values were measured on a Beckman research model pH meter. A typical set of the stability constant studies is presented in Table I.

Table I: Stability Constants (K_1) for the One-to-One Nickel(II) Murexide Complex Formation, $Ni^{2+} + H_2L^- \rightleftarrows NiH_2L^+$, in 50% DMSO Aqueous Solution at Ionic Strength = 0.1 *M* $NaClO_4$, pH 5.3, and Temperature 20°

Ni^{2+}, *M*	H_2L^-, *M*	Transmittance,[a] %	$K_1 \times 10^{-4}$, M^{-1}
2×10^{-4}	1×10^{-5}	71.5	1.06
		70.3	1.29
1×10^{-4}	1×10^{-5}	75.5	1.18
		75.6	1.15
5×10^{-5}	1×10^{-5}	80.6	1.21
		80.0	1.30

K_1 (av value) = $1.20 \times 10^4 \pm 9\%$

[a] Transmittance was measured at 460-nm wavelength.

Stability constant measurements were made at one temperature for nickel(II) murexide in 25% aqueous DMSO and 50% aqueous ethanol and at three temperatures in water and 50% aqueous DMSO. The results are summarized in Table II.

Table II: Stability Constants (K_1) for the One-to-One Nickel(II) Murexide Complex Formation, $Ni^{2+} + H_2L^- \rightleftarrows NiH_2L^+$, in the Various Solvent Systems (Ionic Strength = 0.1 *M* $NaClO_4$)

Solvent system	Temp, °C	pH	K_1,[a] M^{-1}
H_2O	12	5.0	1.75×10^3
	20	5.0	1.65×10^3
	32	5.0	1.44×10^3
50% DMSO–H_2O	12	5.3	1.44×10^4
	20	5.3	1.20×10^4
	32	5.3	0.78×10^4
25% DMSO–H_2O	25	5.0	2.60×10^3
50% ethanol–H_2O	25	5.0	1.10×10^4

[a] The standard deviation varies from ±8 to ±15%.

The decrease in the stability constants with increasing temperature is less for the water system than that for the 50% aqueous DMSO system. The en-

(6) G. Geier, *Ber. Bunsenges. Phys. Chem.*, 69, 617 (1965).

(7) G. G. Hammes and P. Fasella, *J. Amer. Chem. Soc.*, 84, 4644 (1962).

(8) M. Klotz and W. C. Loh. Ming, *ibid.*, 75, 4159 (1953).

(9) A. E. Martell and M. Calvin, "Chemistry of the Metal Chelate Compounds," Prentice-Hall, Englewood Cliffs, N. J., 1952.

Table III: The Rate Constants and the Experimental Conditions for the Reaction $Ni^{2+} + H_2L^- \underset{k_r}{\overset{k_f}{\rightleftharpoons}} NiH_2L^+$, Studied at pH 5 and Ionic Strength = 0.1 M $NaClO_4$[a]

$C_{Ni^{2+}}$, M	$C_{H_2L^-}$, M	Temp, °C	τ, msec	k_f, M^{-1} sec^{-1}	Solvent
0.9×10^{-3}	1×10^{-4}	18.0	547	1.2×10^3	Water
1.5×10^{-3}	1×10^{-4}	21.0	386	1.3×10^3	Water
1.0×10^{-3}	1×10^{-4}	21.0	400	1.7×10^3	Water
0.6×10^{-3}	1×10^{-4}	21.0	503	1.6×10^3	Water
2.0×10^{-3}	1×10^{-4}	31.5	110	3.5×10^3	Water
1.0×10^{-3}	1×10^{-4}	31.5	171	3.5×10^3	Water
0.6×10^{-3}	1×10^{-4}	31.5	249	3.1×10^3	Water
3.3×10^{-4}	1×10^{-4}	31.5	307	3.2×10^3	Water
1.0×10^{-3}	1×10^{-4}	40.0	125	3.4×10^3	Water
0.6×10^{-3}	1×10^{-4}	40.0	140	3.9×10^3	Water
2×10^{-3}	1×10^{-4}	31.5	108	3.8×10^3	25% DMSO–H_2O
1×10^{-3}	1×10^{-4}	31.5	184	3.8×10^3	25% DMSO–H_2O
8×10^{-4}	1×10^{-4}	31.5	223	3.6×10^3	25% DMSO–H_2O
6×10^{-4}	1×10^{-4}	31.5	259	3.7×10^3	25% DMSO–H_2O
3.3×10^{-4}	1×10^{-4}	31.5	339	3.6×10^3	25% DMSO–H_2O
4×10^{-4}	5×10^{-5}	25.0	258	8.4×10^3	50% ethanol–H_2O
3×10^{-4}	5×10^{-5}	25.0	278	9.8×10^3	50% ethanol–H_2O
2×10^{-4}	5×10^{-5}	25.0	397	9.0×10^3	50% ethanol–H_2O
6.5×10^{-4}	6×10^{-5}	23.0	378	3.8×10^3	50% DMSO–H_2O
5.0×10^{-4}	5×10^{-5}	23.0	413	4.2×10^3	50% DMSO–H_2O
1×10^{-3}	10^{-4}	31.5	164	5.9×10^3	50% DMSO–H_2O
8×10^{-4}	7×10^{-5}	31.5	181	6.3×10^3	50% DMSO–H_2O
6.5×10^{-4}	6×10^{-5}	31.5	262	5.2×10^3	50% DMSO–H_2O
5×10^{-4}	5×10^{-5}	31.5	320	5.3×10^3	50% DMSO–H_2O
4×10^{-4}	4.5×10^{-5}	31.5	343	5.8×10^3	50% DMSO–H_2O
6.5×10^{-4}	6×10^{-5}	37.0	172	8.1×10^3	50% DMSO–H_2O
5×10^{-4}	5×10^{-5}	37.0	178	9.5×10^3	50% DMSO–H_2O
6.5×10^{-4}	6×10^{-5}	40.0	106	12.5×10^3	50% DMSO–H_2O
5×10^{-4}	5×10^{-5}	40.0	134	11.9×10^3	50% DMSO–H_2O

[a] $C_{Ni^{2+}}$ and $C_{H_2L^-}$ are the initial concentrations.

thalpy and entropy changes for the complex formation reaction were calculated from the temperature-dependent stability constants. For water solution, $\Delta H°$ is -1.6 ± 0.3 kcal/mol and $\Delta S°$ is 9.4 ± 1 eu. For 50% aqueous DMSO solution, $\Delta H°$ is -5.6 ± 0.5 kcal/mol and $\Delta S°$ is -0.3 ± 1.5 eu.

The sign and magnitude of the $\Delta S°$ value in aqueous solution is consistent with the so-called "chelate effect."[8] A similar result is not observed in the 50% aqueous DMSO solution which has a small and negative value of $\Delta S°$. The larger stability constant for nickel(II) murexide in 50% aqueous DMSO solution is mainly caused by a more negative enthalpy change for the complexation reaction.

Although the coordinating ability of DMSO has been studied for the Al(III),[10] Cr(II),[11a] and Fe(III)[11b] systems, the preferential solvation of nickel(II) ion in a DMSO–H_2O mixture has not been reported. Nevertheless, from the kinetic evidence, the larger stability constant in the DMSO–H_2O system can best be explained in terms of a larger k_f and a smaller k_r with respect to these values in H_2O.

2. Kinetic Section. By measuring the relaxation times for different concentrations at various temperatures, the forward rate constants (k_f) were calculated and are given in Table III. The k_f values were estimated according to

$$Ni^{2+} + H_2L^- \underset{k_r}{\overset{k_f}{\rightleftharpoons}} NiH_2L^+ \qquad (1a)$$

$$\frac{1}{\tau} = k_f(C_{Ni^{2-}} + C_{H_2L^-}) + \frac{k_f}{K_1} \qquad (1b)$$

where K_1 is the stability constant.

The k_f value (1.8×10^3 M^{-1} sec^{-1} at 25° and 0.1 M) is similar to that reported by Geier[6] (1.2×10^3 M^{-1} sec^{-1} at 12° and 0.1 M). A recent study carried out by the stopped-flow technique gave a value of 5.6×10^3 M^{-1} sec^{-1} at 25° and 0.006 M ionic strength.[12] A careful calculation shows the outer sphere ion-pair

(10) D. P. Olander, R. S. Marianelli, and R. C. Larson, *Anal. Chem.*, **41**, 1097 (1969).

(11) (a) K. R. Ashley, R. E. Hamm, and R. H. Magnuson, *Inorg. Chem.*, **6**, 413 (1967); (b) R. S. Drago, D. M. Hart, and R. L. Carlson, *J. Amer. Chem. Soc.*, **87**, 1900 (1965).

(12) C. H. Langford and H. G. Tsiang, *Inorg. Chem.*, **9**, 2346 (1970).

formation constant (K_0) is 2 M^{-1} at 25° and 0.1 M ionic strength and it is 3.9 M^{-1} at 25° and 0.006 M ionic strength. Therefore, these three results all indicate that the value of k_f/K_0 is at least 20 times below the solvent exchange rate constant reported in the literature. The plots of the concentrations against the reciprocal of the relaxation times also gave the forward and the reverse rate constants. They are in good agreement with those determined for eq 1b.

Since all of the solutions exhibited one relaxation time and the values of k_f evaluated from eq 1b are practically the same at a given temperature, it is possible to propose a combined single step relaxation process for the nickel(II) murexide system.

The mechanism for the complex formation between the metal ion and murexide may be expressed by the following scheme

$$M(H_2O)_6 + (A\text{–}B\text{–}C)_{aq}$$

$$\underset{k_{-1}}{\overset{k_1}{\rightleftharpoons}} \quad (H_2O)_5M(H_2O)(A\text{–}B\text{–}C)_{aq} \qquad K_0 = \frac{k_1}{k_{-1}}$$

$$\underset{k_{-2}}{\overset{k_2}{\rightleftharpoons}} \quad (H_2O)_5\text{–}M\text{–}A\text{–}B\text{–}C \qquad K_2 = \frac{k_2}{k_{-2}}$$

$$\underset{k_{-3}}{\overset{k_3}{\rightleftharpoons}} \quad (H_2O)_4\text{–}M\begin{matrix} A \\ | \\ B\text{—}C \end{matrix} \qquad K_3 = \frac{k_3}{k_{-3}}$$

$$\underset{k_{-4}}{\overset{k_4}{\rightleftharpoons}} \quad (H_2O)_3\text{–}M\begin{matrix} A \\ \diagup\ \diagdown \\ B \quad C \end{matrix} \qquad K_4 = \frac{k_4}{k_{-4}} \qquad (2)$$

where M represents the nickel(II) ion and A–B–C represents three binding sites of the attacking ligand. Charges on the ions are neglected for convenience. The first step is the formation of an ion pair. The next three steps involve the loss of a water molecule in each step from the inner hydration sphere of the metal ion and the formation of the metal–ligand bond.

With the assumption of a steady state for the intermediates $(H_2O)_5MABC$ and $(H_2O)_4M\begin{matrix} A \\ | \\ B\text{—}C \end{matrix}$, and a fast equilibrium for the ion-pair formation, the rates for the formation and dissociation of a tridentate complex may be represented by the following equations, respectively

$$k_f = \frac{K_0k_2k_3k_4}{k_{-2}k_{-3} + k_3k_4 + k_{-2}k_4} \qquad (3)$$

$$k_r = \frac{k_{-2}k_{-3}k_{-4}}{k_{-2}k_{-3} + k_3k_4 + k_{-2}k_4} \qquad (4)$$

In these equations the value of K_0k_2 is reduced to k_f by a factor of

$$\gamma = \frac{k_{-2}k_{-3} + k_3k_4 + k_{-2}k_4}{k_3k_4}$$

From the rate constants obtained in this study, it seems highly unlikely that the nickel(II) murexide substitution reaction is controlled by a "pure" steric effect,[13] because no such effect was found for the reaction between the more labile cobalt(II) ion and the monovalent anion (Table IV).

In a sterically controlled mechanism,[2] it has been suggested that the forward rate constant [$k_f = K_0k_2k_3/(k_{-2} + k_3)$] is $(k_{-2} + k_3)/k_3$ times slower than K_0k_2. Since the difficulty in ring closure is a function of the ligand, the contributions of the ring strain and entropy loss[2] to the activation process for ring closure should be the same regardless of whether the cation is nickel or cobalt. In accordance with the equation $k = (RT/Nh) \cdot e^{-\Delta G^*/RT}$, the value of k_3 should be reduced by the same order of magnitude as that of k_2 if both metal ions are reacting with the same ligand. Therefore a steric effect is more likely to be observed in the cobalt system. This is because the nickel complex is thermodynamically more stable than the cobalt complex; namely $K_2 = (k_2/k_{-2})(Ni^{2+}) > (k_2/k_{-2})(Co^{2+})$, we then have the relationships $(k_3/k_{-2})(Ni^{2+}) > (k_3/k_{-2})(Co^{2+})$, or $(k_3/(k_{-2} + k_3))(Ni^{2+}) > (k_3/(k_{-2} + k_3))(Co^{2+})$.

In this discussion we are assuming that the bonding and structure of nickel murexide and cobalt murexide are the same. Both systems have the same peak for the maximum absorption band at 460 nm. The chelate formation involves binding of the electron pair on the nitrogen atom between the rings of the monovalent murexide ion. This binding is believed to be the reason for shifting the peak of the absorption band of the free monovalent ion toward the ultraviolet when it is chelated with a metal ion.[9] Furthermore the variation of the forward rates in different solvents (Table III) is roughly proportional to that of ion-pair formation constants in the respective solutions. The ion-pair formation constants increase with decreasing bulk dielectric constants of the solutions. This means that the murexide ion is coordinated to nickel(II) as a monovalent ion rather than a neutral molecule.

An analysis of the rate data collected in Table IV may shed some light on the slowness of the nickel murexide complexation reaction. The value of K_0 calculated from Fuoss' equation[14] is accurate within a factor of 2 or 4. Uncertainty is also involved in a statistical factor (f).[15,16] This factor is the probability that the ligand

(13) A pure steric effect is defined as, in a sterically controlled mechanism, the release of the second or the subsequent water molecules is not affected by the formation of the first or the subsequent metal–ligand bonds.

(14) R. M. Fuoss, *J. Amer. Chem. Soc.*, **80**, 5059 (1958).

(15) R. Pearson and P. Ellgen, *Inorg. Chem.*, **6**, 1379 (1967).

Table IV: Rate Constants and Rate Ratios for Various Cobalt and Nickel Systems

Ligand	Charge	$k_f(Co^{2+})$, M^{-1} sec^{-1}	$k_f(Ni^{2+})$, M^{-1} sec^{-1}	$\frac{k_f(Co^{2+})}{k_f(Ni^{2+})}$	Reference
Malonic acid	−2	9×10^5	7×10^4	129	*d–c*
Cysteine	−2	6×10^6	2×10^5	30	*a*
Sulfuric acid	−2	3×10^6	2×10^5	15	*a*
Malonic acid	−1	7×10^5	3.1×10^3	225	*b, c*
Bicysteine	−1	6×10^5	2×10^4	30	*a*
Glycine	−1	5×10^5	2×10^4	25	*d*
α-Alanine	−1	6×10^5	2×10^4	30	*e*
α-Aminobutyric acid	−1	2.5×10^5	1×10^4	25	*f*
Murexide	−1	1.4×10^5 (at 12°)	1.0×10^3 (at 12°)	140	*g, h*
Glycylsarcosine	−1	4.6×10^5	2×10^3	230	*d*
Glycylglycine	−1	2×10^5	3.2×10^3	63	*d*
Triglycine	−1	3.1×10^5	1.7×10^3	183	*d*
Tetraglycine	−1	2.6×10^5	1.8×10^3	145	*d*
β-Alanine	−1	7.5×10^4	1×10^4	7.5	*e*
β-Aminobutyric acid	−1	2×10^4	4×10^3	5	*f*
Imidazole	0	1.3×10^5	5×10^3	26	*d*
1,10-Phenanthroline	0	1.4×10^5	3.9×10^3	36	*d*
Ammonia	0	9.5×10^4	3.3×10^3	29	*d*
		$Co(Phen)_2^{2+}$	$Ni(Phen)_2^{2+}$		
1,10-Phenanthroline	0	4×10^5	3.2×10^3, 3.2×10^2	125, 1250	*i*
		$Co(\alpha\text{-Abu})^+$	$Ni(\alpha\text{-Abu})^+$		
α-Aminobutyric acid	−1	1.9×10^6	1.5×10^4	127	*f*

[a] G. Davies, K. Kustin, and R. F. Pasternack, *Trans. Faraday Soc.*, **64**, 1006 (1968). [b] F. P. Cavasino, *Ric. Sci.*, **35** (II-A), 1120 (1965). [c] F. P. Cavasino, *J. Phys. Chem.*, **69**, 4380 (1965). [d] Reference 5. [e] Reference 2. [f] Reference 4. [g] Reference 6. [h] The forward rate constant for nickel murexide is an average value taken from ref 6 and this work. [i] Reference 23.

molecule will enter the primary solvation shell of the metal ion at a particular site when a coordinated water molecule leaves. The factor $(1 - f)$ represents the probability of water exchange, as the coordinated water molecule leaves the site remote from the ligand. Hence the solvent substitution rate should be a fraction of f below the solvent exchange rate. A direct comparison of the ratio of $k_f(Co^{2+})/k_f(Ni^{2+})$ with that of $k_{ex}(Co^{2+})/k_{ex}(Ni^{2+})$ will certainly eliminate some of the uncertainties inherent in the ion-pair formation constant and the statistical factor. As indicated in Table IV, the ratio of $k_{ex}(Co^{2+})/k_{ex}(Ni^{2+}) = 34$ for the solvent exchange reactions[17,25] agrees very well with that of $k_f(Co^{2+})/k_f(Ni^{2+})$ for a number of normal substitution reactions. The ratio for the ligands β-alanine and β-aminobutyric acid is less than 10. This is expected since the cobalt system is subject to a greater steric effect than is the nickel system. For the oligoglycines, the difference in the bonding model between these two systems may account for the observation of a larger ratio. Complexes formed with malonate and murexide ligands also have a larger ratio. For the nickel malonate complex formation reaction, the values of k_{-2} and k_3 have recently been evaluated.[18] They are 3.5×10^3 and 4.5×10^3 sec^{-1}, respectively. Thus the value of k_f becomes 1/1.8 times as large as that of k_0k_2. Similarly, k_{-2} can be estimated for the cobalt malonate system.[19–21] It is found to be 0.12×10^6 sec^{-1}. Since the rate of cobalt malonate formation is within the normal range, it requires that k_3 be much larger than k_{-2} or 0.12×10^6 sec^{-1}. Apparently, the formation of the first metal–ligand bond in the cobalt malonate system accelerates the release of the second water molecule as compared to the rate of release of the second water molecule (k_3) in the formation of nickel malonate. Recently Zeltmann and Morgan[22] reported that the exchange rate of H_2O in $Co(CNS)(H_2O)_5^+$ was four times larger than that in $Co(H_2O)_6^+$. As shown in Table IV, this acceleration effect is also observed in the studies of some bis or tris complex substitution reactions[4,23] (Co-

(16) H. P. Bennetto and E. F. Caldin, *Chem. Commun.*, 599 (1969).

(17) T. J. Swift and R. E. Connick, *J. Chem. Phys.*, **37**, 307 (1962).

(18) H. Hoffmann, *Ber. Bunsenges. Phys. Chem.*, **73**, 432 (1969).

(19) The value of k_{-2} was estimated from $K_1 = k_1/k_{-2}$. Here K_1 (12 M^{-1}) and k_f are the stability constant[20] and rate constant extrapolated to 0.1 M ionic strength for the formation of cobalt monoacetate. Since the cobalt malonate reaction is normal, the value of k_f (1.4×10^5 M^{-1} sec^{-1}) can be corrected from the cobalt malonate forward rate constant (9×10^6 M^{-1} sec^{-1}) by changing the ion-pairing formation constant. Compared to the published value for k_f (1×10^5 M^{-1} sec^{-1}) in nickel acetate,[21] the estimated value of 1.4×10^6 is reasonable.

(20) S. K. Siddhanta and S. N. Banerjel, *J. Ind. Chem. Soc.*, **35**, 323 (1958).

(21) R. G. Wilkins, *Accounts Chem. Res.*, in press.

(22) A. H. Zeltmann and L. O. Morgan, *Inorg. Chem.*, **9**, 2522 (1970).

Table V: Rate Constants and Activation Parameters for the Nickel(II) Murexide Formation, $N^{2+} + H_2L^- \underset{k_r}{\overset{k_f}{\rightleftharpoons}} NiH_2L^+$, in Various Solvent Systems at 25° and 0.1 M $NaClO_4$

Solvent system	k_f, M^{-1} sec^{-1}	k_r, sec^{-1}	$\Delta H_f^* + RT$, kcal/mol	ΔS_f^*, eu	$\Delta H_r^* + RT$, kcal/mol	ΔS_r^*, eu
H_2O	1.8×10^3	1.15	12.5	−3.6	14.1	−13
25% DMSO–H_2O	3.7×10^3[a]	1.43[a]	...	...	...	...
50% DMSO–H_2O	4.2×10^3	0.43	12.4	−2.4	18	−2.1
50% ethanol–H_2O	9.0×10^3	0.83	...	...	...	...

[a] The rates are at 31.5°.

$(Phen)_2^{2+}$ and Co(α-Abu)$^+$). Although the effect of the coordinated ligands on the rates of water substitution and exchange reactions for the nickel system has been examined extensively by Margerum[24] and Hunt,[25] respectively, there is little known about the cobalt system. However, the crystal field stabilization energy of d^8 configuration may offset some of the acceleration effect found in the cobalt systems.[4] Hence in the present studies, it is concluded that the inequality $k_3k_4 > k_{-2} \cdot k_{-3} + k_{-2}k_4$ makes the cobalt murexide reaction normal while the relationship $k_3k_4 \leq k_{-2}k_{-3} + k_{-2}k_4$ makes the nickel murexide reaction slower. The reason for the relatively large reverse rate constants (k_{-2} and/or k_{-3}) is probably the loss of resonance stability in the ligand upon the formation of metal–ligand bonds.

The rate constants extrapolated to 25° and the activation parameters obtained for the nickel murexide system in various mixed solvents are summarized in Table V. The values of ΔH_r^* and ΔS_r^* for the dissociation of nickel murexide were calculated from $\Delta H^\circ = \Delta H_f^* - \Delta H_r^*$ and $\Delta S = \Delta S_f^* - \Delta S_r^*$, respectively. Among the four mixed solvents, the value of k_f in 50% ethanol is the highest. This may be due to a larger K_0 value. The value of k_r in 50% DMSO is the lowest. On the basis of the less negative ΔS_r^* obtained in the DMSO–H_2O solvent, we suggest that a strong interaction between the nonaqueous solvent (*i.e.*, DMSO) and H_2O molecules may slow down the dissociation process of the complexation reaction.[26]

Acknowledgments. This work was supported by Grant E-196 from the Robert A. Welch Foundation.

(23) M. Eigen and R. G. Wilkins, *Advan Chem. Ser.*, No. 49 (1966).

(24) J. P. Jones, E. J. Billo, and D. W. Margerum, *J. Amer. Chem. Soc.*, 92, 1875 (1970).

(25) M. Grant, H. W. Dodgen, and J. P. Hunt, *ibid.*, 92, 798 (1970).

(26) A. A. Frost and R. G. Pearson, "Kinetics and Mechanism," Wiley, New York, N. Y., 1953.

Association Equilibria of Silver and Chloride Ions in Liquid Ammonium Nitrate–Water Mixtures. II. The Anhydrous Melt

by Mordechai Peleg

Department of Inorganic and Analytical Chemistry, The Hebrew University of Jerusalem, Jerusalem, Israel
(Received January 5, 1971)

Publication costs borne completely by The Journal of Physical Chemistry

The electromotive force of the cells

$$\text{Ag} \;\Big|\; \begin{matrix}\text{NH}_4\text{NO}_3\\ \text{MNO}_3\\ \text{AgNO}_3\end{matrix} \;\Big\|\; \begin{matrix}\text{NH}_4\text{NO}_3\\ \text{MNO}_3\\ \text{NH}_4\text{Cl}\\ \text{AgNO}_3\end{matrix} \;\Big|\; \text{Ag}$$

(M = Na or K) as a function of silver nitrate and ammonium chloride has been measured at 150° for the ammonium nitrate–sodium nitrate (80–20 g, 81 mol % NH_4NO_3) mixture and at 160° for the ammonium nitrate–potassium nitrate (86–14 g, 89 mol % NH_4NO_3) mixture. By applying the quasi-lattice model for molten salts the cation–ligand interaction energy for the Ag^+–Cl^- pair was evaluated as -5.01 ± 0.05 kcal/mol for the ammonium nitrate–sodium nitrate mixture and -5.10 ± 0.2 kcal/mol for the ammonium nitrate–potassium nitrate mixture. The value obtained by extrapolation from concentrated aqueous ammonium nitrate solution (-4.9 ± 0.1 kcal/mol) is in fair agreement.

Introduction

In a previous paper,[1] we reported measurements for the association constants of the silver ion with the chloride ion in liquid ammonium nitrate–water mixtures (mole ratio range, $H_2O:NH_4NO_3 = 0.4$–1.4) at a temperature of 110°. The results were discussed in terms of a quasi-lattice model based on that of molten salts as proposed by Braunstein[2,3] to explain hydration and association equilibria in these highly concentrated aqueous solutions. By applying the equation developed by Braunstein[3] and extrapolating to zero water content it is possible to obtain a value for the cation–ligand interaction energy. From the above mentioned results a value of 4.9 ± 0.5 kcal/mol was obtained for the Ag^+–Cl^- complex in anhydrous ammonium nitrate. It was thus of interest to attempt to measure the association constant for the Ag^+–Cl^- pair directly in anhydrous ammonium nitrate and to compare this value with that obtained by applying the quasi-lattice model of Braunstein to the results obtained from the concentrated aqueous ammonium nitrate solutions.

While results have been reported for Ag^+–Cl^- complex formation for most of the alkali metal nitrates and their mixtures,[4] to the best of the author's knowledge no results have been published for molten ammonium nitrate or its mixtures. Due to practical difficulties it was not possible to measure Ag^+–Cl^- complex formation in the pure ammonium nitrate system due to corrosion of the silver electrode. However, measurements were possible in mixtures of ammonium nitrate–sodium nitrate and ammonium nitrate–potassium nitrate.

Experimental Section

Electromotic force measurements were made on the concentration cell

$$\text{Ag} \;\Big|\; \begin{matrix}\text{NH}_4\text{NO}_3\\ \text{MNO}_3\\ \text{AgNO}_3\end{matrix} \;\Big\|\; \begin{matrix}\text{NH}_4\text{NO}_3\\ \text{MNO}_3\\ \text{AgNO}_3\\ \text{NH}_4\text{Cl}\end{matrix} \;\Big|\; \text{Ag}$$

(M = Na or K)

The apparatus and techniques employed in the present experiments were identical with those mentioned in a previous paper,[1] with the following amendment. The reference compartment was separated from the main solution by means of a coarse glass frit, since the highly viscous nature of the melt gave rise to a very high electrical resistance when a fine or medium glass frit was used in the reference compartment. A stream of dry nitrogen was used to blanket the melt at all times and this helped to produce stable readings.

The materials used were all Analar quality chemicals and the only treatment they received was drying. Addition of the chloride ion was made in the form of solid pellets. The cell itself was suspended in a well stirred molten salt bath (KNO_3–$NaNO_3$–$NaNO_2$ =

(1) M. Peleg, *J. Phys. Chem.*, **75**, 2060 (1971).

(2) J. Braunstein in "Ionic Interactions: Dilute Solutions to Molten Salts," S. Petrucci, Ed., Academic Press, New York, N. Y., 1971, Chapter 4.

(3) J. Braunstein, *J. Phys. Chem.*, **71**, 3402 (1967).

(4) Y. T. Hsu, R. B. Escue, and T. H. Tidwell, Jr., *J. Electroanal. Chem.*, **15**, 245 (1967).

44.2:6.9:48.9 mol %, mp 142°[5]) controlled to within ±0.1°. A Keithley 660A differential voltmeter was used to measure the emf of the cell.

Preliminary experiments using pure ammonium nitrate at a temperature just above that of its melting point (mp 169.2°) gave unstable readings and a continuous drift. This was due to the corrosive effect of the ammonium nitrate melt. Barclay and Crewe[6] have studied the thermal decomposition of ammonium nitrate and, while the mechanism of decomposition is complex, it appears that one of the products formed is HNO_3. Chloride ions also have been shown to catalyze the thermal decomposition of ammonium nitrate.[7]

A trial experiment carried out on an ammonium nitrate–sodium nitrate (80–20 g) mixture at 150° showed that a weighed piece of silver placed in this melt under exactly the same experimental conditions as were employed for the emf measurements remained uncorroded after 3 days. Similar experiments using an ammonium nitrate–potassium nitrate (86–14 g) mixture at 160° gave evidence of slight corrosion over a prolonged period of time.

Measurements were therefore made using the ammonium nitrate–sodium nitrate mixture as the solvent although a few runs were performed on the ammonium nitrate–potassium nitrate melt.

Owing to the low values of the solubility product for silver chloride (~10^{-8} mole ratio) in the solvents studied,[8] low concentrations of the silver ion and the chloride ion had to be employed. The silver ion concentration was thus limited to a range between about 1×10^{-4} and 3×10^{-4} (mol/mol of solvent melt), while the chloride concentration was varied between 1×10^{-5} and 6×10^{-5} (mol/mol of solvent melt). Preliminary experiments showed that the Nernst equation was obeyed with respect to the stoichiometric concentration of silver in the range under examination (Figure 1).

The concentration units are given as mole ratios, R

$$R_{Ag^+} = R_{AgNO_3} = \frac{n_{AgNO_3}}{n_{NH_4NO_3} + n_{MNO_3}}$$

$$R_{Cl^-} = R_{NH_4Cl} = \frac{n_{NH_4Cl}}{n_{NH_4NO_3} + n_{MNO_3}}$$

where M represents either Na or K and n is the number of moles of $AgNO_3$, NH_4NO_3, MNO_3, and NH_4Cl.

Procedure. A weighed amount of ammonium nitrate–sodium (or potassium) nitrate was added to the cell together with a known amount of silver nitrate. The cell was stoppered and suspended in the molten salt bath and a stream of dry nitrogen was allowed to pass over the melt. After attainment of thermal equilibrium, the empty reference compartment was placed in position and filled by applying a vacuum to the tube. The indicating silver wire and reference electrode wire were then introduced into their respective compartments. After about 1 hr the potential between the two compartments steadied and showed only a very slight drift of less than 1 mV/hr. This drift was probably due to the very slight evaporation of ammonium nitrate from the solution. This drift was compensated for in the calculations, the magnitude of the correction approaching about 10–15%, depending on the time between additions of chloride ions.

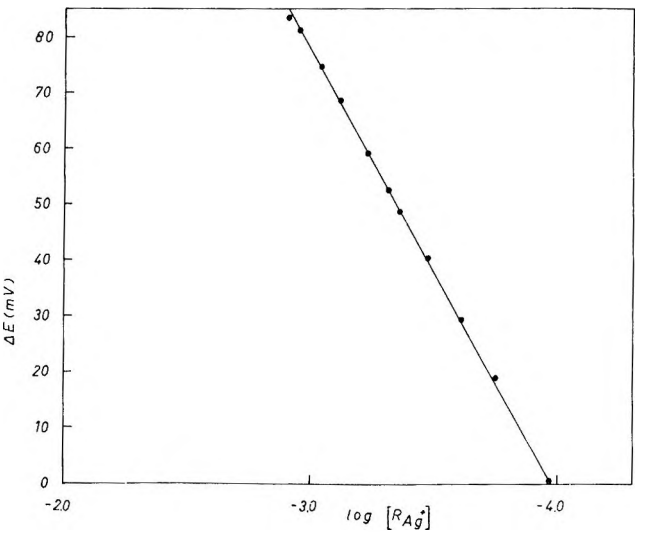

Figure 1. Typical Nernst plot for silver–silver ion electrode in ammonium nitrate–sodium nitrate solvent (81 mol % ammonium nitrate) at 150°.

Results

The emf's of the concentration cell were measured as a function of changing silver ion concentration at a temperature of 150° for the ammonium nitrate–sodium nitrate mixture and at 160° for the ammonium nitrate–potassium nitrate mixture. Owing to the low concentration of silver ions in solution, the change of cell emf on addition of chloride ions to the indicating compartment is related to the stoichiometric activity coefficient of silver nitrate by the formula

$$-\ln \gamma_{AgNO_3} = \frac{F}{RT} \Delta E$$

where ΔE is the difference between the emf of the cell in the presence and absence of chloride ions.[9] Thermodynamic equilibrium constants for association reaction $Ag^+ + Cl^- = Ag^+\text{–}Cl^-$ were calculated by the graphical analysis of the activity coefficients as described by Braunstein, *et al.*[10]

(5) T. Alexander, Jr., and S. G. Hindin. *Ind. Eng. Chem.*, **39**, 1044 (1967).

(6) K. S. Barclay and J. M. Crewe, *J. Appl. Chem.*, **17**, 21 (1967).

(7) A. G. Keenan and B. Dimitriades, *J. Chem. Phys.*, **37**, 1583 (1962).

(8) M. Peleg, to be published.

(9) J. M. C. Hess, J. Braunstein, and H. Braunstein, *J. Inorg. Nucl. Chem.*, **26**, 811 (1964).

(10) J. Braunstein, M. Blander, and R. M. Lindgren, *J. Amer. Chem. Soc.*, **84**, 1529 (1962).

$$K_1 = K_{AgCl} = -\lim_{\substack{R_{NH_4Cl}\to 0 \\ R_{AgNO_3}\to 0}} \left(\frac{\partial \ln \gamma_{AgNO_3}}{\partial R_{NH_4Cl}}\right)_{R_{AgNO_3}}$$

or

$$K_1 = -\lim_{R_{AgNO_3}\to 0} S_0$$

where

$$S_0 = \lim_{R_{NH_4Cl}\to 0} \left(\frac{\partial \ln \gamma_{AgNO_3}}{\partial R_{NH_4Cl}}\right)_{R_{AgNO_3}}$$

Typical plots of $-\log \gamma_{AgNO_3}$ against R_{Cl^-} for the ammonium nitrate–sodium nitrate solvent are shown in Figure 2. The potentiometric data appear as supplementary material in the microfilm edition.[11]

The slopes of the plots are different from those typically obtained (*cf.* the shape of a typical plot in Figure 3 of ref 1). The sudden change in slope is probably due to precipitation of silver chloride as the chloride concentration increases. Although the solubility product "constants" (K_{SP}) are not constant and increase with increasing silver ion content, their variation is not large and may be accounted for, as suggested by Braunstein,[12a] by the heat sink at the electrode–solution interface and/or by the possibility that the solid phase is not pure AgCl but a solid solution. At higher chloride ion concentration corrosion might also start to occur as suggested by Inman, *et al.*,[12b] since the chloride ion concentration may reduce the silver ion concentration below a level where corrosion is so significant as to affect the validity of the Nernst equation. However, the initial portions of the curves are valid and could be analyzed using the graphical method (Figure 3) described earlier and this produced a value of $K_1 = 2120 \pm 100$ (mol/mol of solvent)$^{-1}$ for the ammonium nitrate–sodium nitrate mixture (80–20 g) at a temperature of 150°. The equation developed by Blander, *et al.*,[13] based on the asymmetric quasi-lattice model for molten salts was utilized to evaluate the Ag–Cl interaction energy

$$K_1 = Z(\alpha - 1) \qquad (1)$$

where $\alpha = \exp(-\epsilon_c/kT)$,[1] ϵ_c being the cation–ligand interaction energy and Z the coordination number, generally chosen as 6. For the mixed nitrate solvent ϵ_c was -4.93 ± 0.05 kcal/mol.

It has been concluded (ref 13, p 230) from an examination of the data available for Ag–Cl complex formation in mixed molten alkali nitrates that ϵ_c is linearly proportional to the composition of the binary mixture melts; *i.e.*, the equation

$$\epsilon_c(\text{mix}) = N'\epsilon_c'(\text{solvent 1}) + N''\epsilon_c''(\text{solvent 2}) \qquad (2)$$

will probably hold in every case. Using eq 2 for the present solvent mixture and taking ϵ_c for Ag–Cl in pure molten $NaNO_3$ to be -4.59 kcal/mol,[14] a value of 5.01 $\pm$ 0.05 kcal/mol was obtained for the Ag–Cl interaction energy.

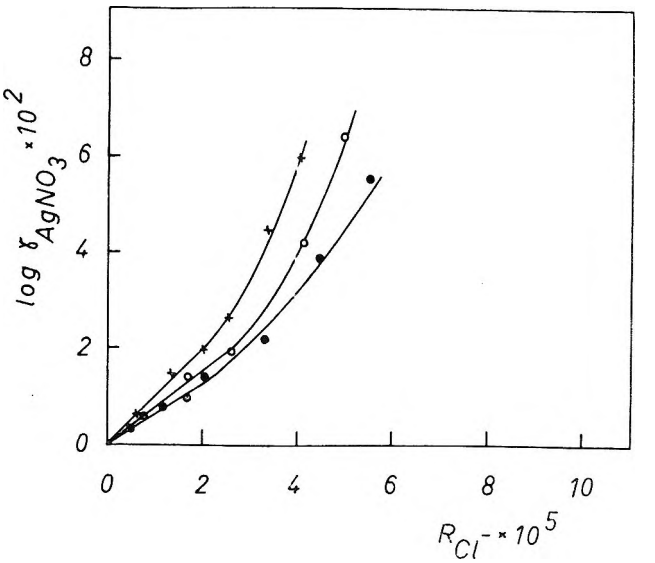

Figure 2. Plot of $-\log \gamma_{AgNO_3}$ *vs.* R_{Cl^-} in NH_4NO_3–$NaNO_3$ solvent (81 mol % NH_4NO_3) at 150°: +, $R_{Ag^+} = 1.06 \times 10^{-4}$; ○, $R_{Ag^+} = 2.2 \times 10^{-4}$; ●, $R_{Ag^+} = 3.08 \times 10^{-4}$.

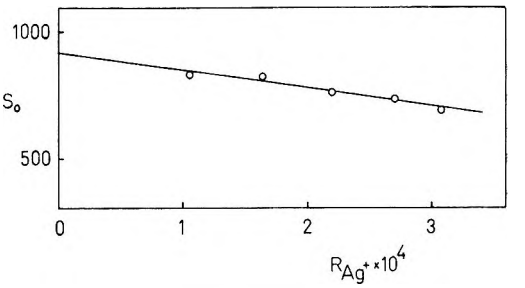

Figure 3. Limiting slope S_0 *vs.* R_{Ag^+} in NH_4NO_3–$NaNO_3$ solvent (81 mol % NH_4NO_3) at 150°.

Similarly, from the ammonium nitrate–potassium nitrate solvent at 160°, ϵ_c for the Ag–Cl complex in pure ammonium nitrate was calculated to be -5.10 ± 0.2 kcal/mol ($K_1 = 2400 \pm 400$ (mol/mol of solvent)$^{-1}$), $\epsilon_c = 5.16 \pm 0.1$ kcal/mol for the mixed solvent, while ϵ_c in pure potassium nitrate was taken to be -5.62 kcal/mol.[15] The larger value of the uncertainty range was due to the greater instability and drift in the experimental measurements; however, the ϵ_c value over-

(11) The potentiometric data appear immediately following this article in the microfilm edition of this volume of the journal. Single copies may be obtained from the Reprint Department, ACS Publications, 1155 Sixteenth St., N.W., Washington, D. C. 20036. Remit check or money order for $3.00 for photocopy or $2.00 for microfiche.

(12) (a) J. Braunstein, private communication; (b) D. Inman, B. Jones, and S. H. White, *J. Inorg. Nucl. Chem.*, **32**, 927 (1970).

(13) M. Blander in "Molten Salt Chemistry," M. Blander, Ed., Interscience, New York, N. Y., 1964.

(14) D. G. Hill, J. Braunstein, and M. Blander, *J. Phys. Chem.*, **64**, 1038 (1960).

(15) D. L. Manning, J. Braunstein, and M. Blander, *ibid.*, **66**, 2069 (1962).

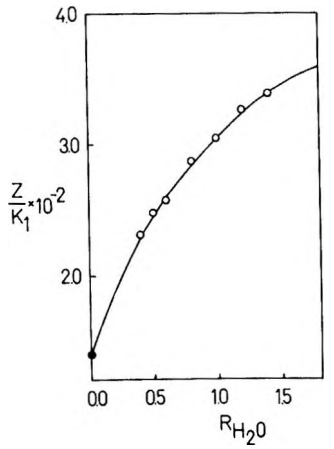

Figure 4. Plot of Z/K_1 *vs.* R_{H_2O} for NH_4NO_3–H_2O mixtures at T = 110°.

laps the value estimated from the NH_4NO_3–$NaNO_3$ data.

Assuming a value of $\epsilon_c = -5.01 \pm 0.1$ kcal/mol for the cation–ligand interaction energy to be more correct, a slight difference exists between this value and that obtained by extrapolation from concentrated aqueous ammonium nitrate solution ($\epsilon_c = -4.9 \pm 0.5$ kcal/mol)[1] but the estimates do overlap. Braunstein[3] developed the following equation to explain complex formation in concentrated aqueous solution

$$Z/K_1 = 1/\alpha + (\beta/\alpha)R_H \qquad (3)$$

where $\alpha = e^{-\epsilon_c/kT}$, $\beta = e^{-\epsilon_H/kT}$, ϵ_H is the cation–water interaction energy, and R_H is the mole ratio of water. If eq 3 is now replotted using the value for ϵ_c obtained from the anhydrous melt, together with the results obtained previously[1] from aqueous solutions, a graph as shown in Figure 4 is obtained. A straight line as was suggested earlier[1] for the region between $R_H = 0$ and $R_H = 1$ is not realized although in quite good correlation with the aqueous data. This suggests that the equilibrium constants reported earlier[1] had not yet reached the limiting behavior predicted by eq 3, which is only a limiting equation for low water contents—although it applies occasionally, empirically, to higher water contents.[2] Braunstein's assumption[2,3] in developing eq 3 from the quasi-lattice model of molten salts was that the water dipoles sit on the anion sublattice; *i.e.*, only the cations are hydrated. Presumably in the present case the nitrate anion competes with the ammonium cation for the water molecule and thus eq 3 does not hold. Other factors which might cause deviations from eq 3 include the possibility of change of coordination number and nonadditivity of pairwise interaction.[2,3] A measure of the limiting slope of the Z/K *vs.* R_{H_2O} plot leads to the value $\epsilon_H = -0.5$ kcal/mol as compared to the previous estimated value of $\epsilon_H = +0.5$ kcal/mol.[1] A value for $K_{12}(Ag_2Cl^+)$ of around 870 can be estimated from the slope plot in Figure 3.

The ionic radii of Na, K, and NH_4^+ are usually taken to be 0.98, 1.33, and 1.45 Å, respectively, based on X-ray crystallographic studies. Thus it might be expected in the light of the reciprocal Coulomb effect[16] that the stability of the Ag–Cl complex in molten ammonium nitrate would be about the same as, or slightly larger than, the value in molten potassium nitrate. The results indicate that the value of ϵ_c in ammonium nitrate (−5.01) falls in between those for sodium nitrate (−4.59) and potassium nitrate (−5.62). Thus it appears that the effective radius of the ammonium ion in the molten nitrate is less than that of the potassium ion. This is substantiated by the conclusion drawn by Braunstein, *et al.*,[17] that although K^+ and NH_4^+ have the same effective radius in dilute aqueous solution at 25°, the activity of water at high temperatures and high salt concentrations in ammonium nitrate[18] is closer to that in sodium nitrate than to that in potassium nitrate.[19]

Acknowledgment. The author wishes to thank Professor J. Braunstein for helpful suggestions.

(16) D. L. Manning, R. C. Bansal, J. Braunstein, and M. Blander, *J. Amer. Chem. Soc.*, **84**, 2028 (1962).

(17) J. Braunstein and H. Braunstein, *Inorg. Chem.*, **8**, 1558 (1969).

(18) A. N. Campbell, J. B. Fishman, G. Rutherford, T. P. Schaefer, and L. Ross, *Can. J. Chem.*, **34**, 151 (1956).

(19) L. P. Shpigel and K. P. Mischenko, *J. Appl. Chem. USSR*, **40**, 659 (1967).

The Effect of Adsorption Potential on the Hydrogen–Deuterium Exchange of Benzene at a Fuel Cell Electrode

by H. J. Barger, Jr.,* and A. J. Coleman

Electrochemical Division, U. S. Army Mobility Equipment Research and Development Center, Fort Belvoir, Virginia 22060 *(Received May 10, 1971)*

Publication costs assisted by the Technical Library, U. S. Army Mobility Equipment Research and Development Center

The effect of adsorption potential on the hydrogen–deuterium exchange of benzene at a fuel cell electrode was studied using 85% D_3PO_4 as the electrolyte. The exchange was monitored by continuously passing the effluent from an electrochemical cell into the ionization chamber of a mass spectrometer. The amount of exchange that occurred varied markedly with potential, increasing as the potential was lowered from 0.45 to 0.20 V *vs.* the dynamic hydrogen electrode. The isotopic distribution of the deuteriobenzenes differed with changing potential in such a way that two types of reactions were suggested, one involving stepwise exchange and the other multiple exchange.

Introduction

The hydrogen–deuterium exchange of benzene at a fuel cell electrode has been examined previously under a variety of conditions at 0.30 V *vs.* the dynamic hydrogen electrode.[1] It was observed that exchange occurred very rapidly, giving a distribution where C_6H_5D and C_6D_6 predominated. The overall exchange process appeared to be diffusion controlled and was thought to consist of at least two types of reactions. One reaction was suggested to involve stepwise exchange and the other multiple exchange. In this paper, the effect of the adsorption potential on the hydrogen–deuterium exchange of benzene was examined with the hope of gaining further insight into the nature of these reactions.

Experimental Section

Apparatus and Materials. The electrochemical cell used in this work was slightly modified from the one described earlier.[2] The thermocouple well was placed 1 cm from the working electrode to allow a more accurate temperature measurement in the reaction region. The cell temperature, usually 100°, was monitored with a calibrated chromel–alumel thermocouple and controlled to ±0.1°. To reduce the reactant mean residence time in the cell cavity and thereby minimize the probability of readsorption of benzene molecules, the volume of the gas cavity in front of the working electrode was decreased (2.68 to 1.98 cm^3).

The flow system was similar to that used previously[1] except that hand-operated valves were replaced by electric valves to allow a more rapid introduction of helium or a helium–benzene mixture into the gas cavity. The helium carrier gas, 99.99% minimum purity, was further purified by passing it through a heated tube (400°) filled with copper turnings to remove traces of oxygen. The portion of helium used for electrolyte stirring was passed through a D_2O saturator maintained at an appropriate temperature so that the D_3PO_4 concentration remained 85% regardless of the cell temperature. In these experiments, a benzene flow of 1.0 ml/sec and a saturator temperature of 0 ± 0.1° were used. This resulted in a benzene concentration of 3.5×10^{-7} mol/ml of helium that was passed over the working electrode.

The electronic control and recording apparatus used to conduct these experiments was the same as used earlier;[1] in addition, the same type working electrode and reactants, 85% D_3PO_4 in D_2O and benzene, were used. Potentials were measured against the dynamic hydrogen electrode (dhe) in the same medium.[3]

The effluent emerging from the cell passed through a series of stream splitters into the ionization chamber of a CEC 21-130 mass spectrometer. The spectra produced from the repetitive 2-sec scans were recorded on a CEC 5-124 oscillograph or collected *via* an automatic data acquisition system consisting of an XDS MD-41 multiplexer/digitizer and an XDS Sigma II computer. The computer was programmed to search for peaks in a preselected mass range, to make base line corrections if required, and to output the data on paper tape for later processing. In all cases, the mass spectra were determined at a low ionization potential to minimize fragmentation of the parent compound. Prior to each set of experiments, the ionizing voltage, field plate voltage, injector voltage, and repeller voltage were adjusted to the settings that gave the highest sensitivity consistent with no observable cracked fragments. Depending on the condition of the mass spectrometer, the ionizing voltage varied from about 9.5 to 14.6 V.

(1) H. J. Barger, Jr., and A. J. Coleman, *J. Phys. Chem.*, **74**, 880 (1970).

(2) H. J. Barger, Jr., and M. L. Savitz, *J. Electrochem. Soc.*, **115**, 686 (1968).

(3) J. Giner, *ibid.*, **111**, 376 (1964).

Experimental Procedure. The electrode pretreatment has been described previously[1,4] and in general consisted of a series of potential steps followed by a cathodic galvanostatic pulse. This procedure was used to obtain a reproducible catalyst surface and to determine the surface area of the working electrode. An experiment was begun by setting the working electrode at the potential of interest and starting the benzene–helium flow. The mass spectometer could be programmed to scan on starting the reactant flow or after a specified time delay. In those experiments where the adsorption potential was held constant, a delay of 30 sec was used. In other experiments, while benzene passed through the system, the working electrode potential was varied in steps of 20 or 50 mV; these steps were always in a cathodic direction so as not to mask subsequent data points with large quantities of C_6D_6 and C_6HD_5. A time delay of 100 sec was found to be optimum for this latter type of experiment.

On completion of the scanning, helium was used to sweep benzene from the lines and gas space. The electrode was cathodically pulsed to remove any adsorbed hydrocarbons, after which the pretreatment could be started again.

Results and Discussion

The percentages of the various deuterio isomers were obtained from the amplitudes of the mass peaks after correction for the contribution of naturally occurring C^{13}. No correction was made for differences in mass spectrometric sensitivities of the various deuteriobenzenes.[5] The total amount of exchange at any one time is reflected in the size of ϕ.[6] For 100 molecules of benzene, ϕ is defined as $\Sigma_{i=1}^{6} i\%C_6H_{6-i}D_i$. Thus the highest value ϕ could attain is 600. Plots of ϕ *vs.* time (initial time occurring when the electric valves were opened to let benzene enter the cell) were made in order to follow the course of exchange during the experiment. Figure 1 shows ϕ–time plots obtained with the earlier cell and with the present cell for the same adsorption potential, reaction temperature, and He flow rate. The time at which mass peaks are first observed and the time to reach the maximum value of ϕ are different, and the decline in ϕ after its maximum is much less with the present cell. In fact, because the decline in ϕ was so gradual under certain conditions, it appeared that a quasi-steady state existed shortly after ϕ maximum. The fact that steady state had not actually occurred was demonstrated by the continuous increase during an experiment in the sum of the intensities of all the compounds emerging from the cell. The differences in the two plots of Figure 1 are attributed to the decreased gas space in front of the electrode, the difference in the volume of the lines, and the replenishment of the deuterium concentration near the electrode by the addition of D_2O to the electrolyte.

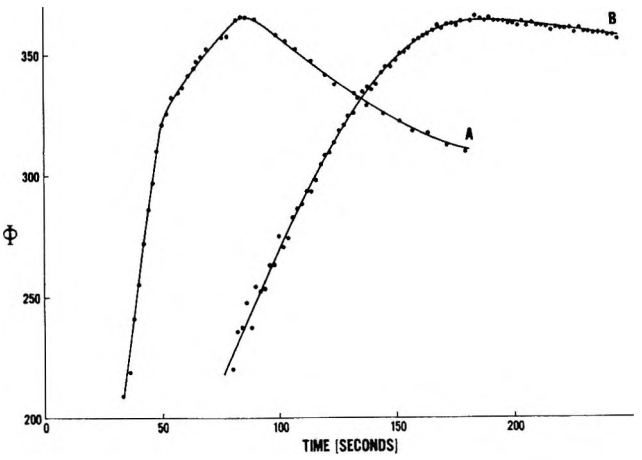

Figure 1. Plot of ϕ *vs.* time at 0.30 V, 1.00 ml/sec, and 100° for old cell (A) and present cell (B).

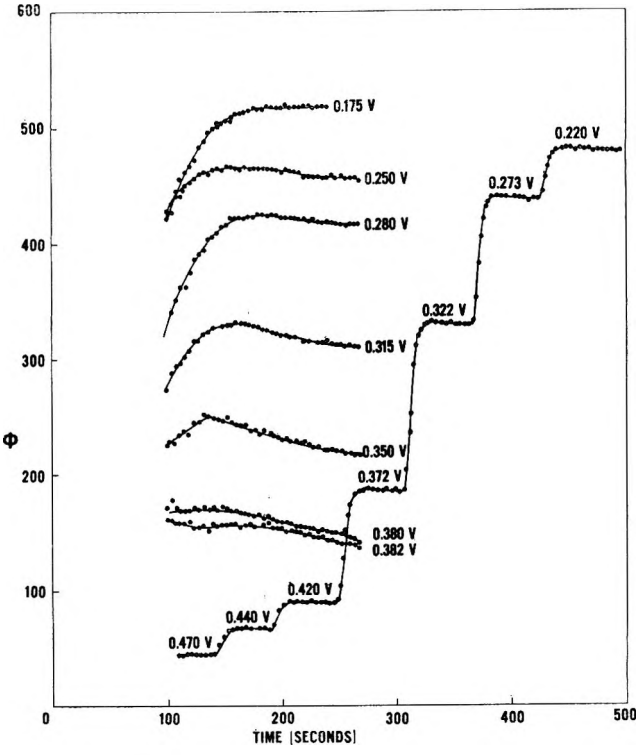

Figure 2. Variation of ϕ with time at various potentials at 1.00 ml/sec and 100°.

The effect of the electrode potential on the exchange benzene undergoes is shown in Figure 2. The family of curves on the left part of the graph represents separate experiments which differ only in the adsorption potential. The initial points (30–100 sec) are not in-

(4) (a) S. Gilman, *J. Phys. Chem.*, 67, 78 (1963); (b) S. B. Brummer, J. I. Ford, and M. J. Turner, *ibid.*, 69, 3424 (1965).

(5) S. Meyerson, H. M. Grubb, and R. W. Vander Haar, *J. Chem. Phys.*, 39, 1445 (1963).

(6) J. R. Anderson and C. Kemball, *Advan. Catal.*, 9, 51 (1957).

cluded for the sake of clarity. The experiments run at low potentials, 0.30 to 0.20 V, generally gave ϕ–time plots which rose quickly with time until a maximum was reached and then slowly declined. On the other hand, ϕ–time plots at relatively high potentials (0.38 V and above) usually started at or near the maximum value of ϕ achieved during that run and then declined. The observation that the decrease in ϕ after its maximum was gradual led to an attempt to study several potentials in succession without intervening pretreatment. If this proved feasible, the time required for a set of experiments would be tremendously shortened, increasing the likelihood that the experimental conditions, *i.e.*, state of the electrode, reaction temperature, and reactant concentration, remained constant for the set. The right portion of Figure 2 shows a typical experiment; the reaction temperature and flow rate are the same as used to obtain the family of curves in the same figure. The working electrode was exposed to benzene for 110 sec at 0.47 V before collecting data. This delay allowed time for the electrode to reach its quasi-steady state thus conserving core memory for later data. Data were collected at 0.47 V for 30 sec after which time the potential of the working electrode was lowered in 20–50-mV increments. Approximately 60 sec was allowed at each potential before switching to a lower one. The transition time between potentials was usually between 1 and 3 sec as measured on a time based X–Y recorder. In Figure 3A, the maximum value of ϕ for both types of experiments in Figure 2 is plotted against the corresponding electrode potential. It is apparent both types of experiments show the same relationship between ϕ and adsorption potential. If the exchange reactions depend on the nature of the electrocatalyst surface including adsorbed intermediates, one may infer that intermediates on the electrode depend on the electrode potential of the moment and not on previous, more anodic potentials. These intermediates presumably change to accommodate the different electrode potential or desorb during the voltage transition.

Based on the distribution of deuterio isomers at the maximum value of ϕ, we previously suggested that two types of exchange reactions were occurring, one involving multiple exchange, *i.e.*, 5 or 6 D atoms per benzene intermediate during one residence on the surface and the other involving stepwise, single exchange.[1] The C_6D_6, C_6HD_5, and half the $C_6H_2D_4$ were thought to come from the former process, and stepwise exchange produced the remainder of the deuterio isomers. These exhange processes were named ϕ_1 and ϕ_2 where $\phi_1 = \%C_6H_5D + 2 \times \%C_6H_4D_2 + 3 \times \%C_6H_3D_3 + {}^4/_2 \times \%C_6H_2D_4$ and $\phi_2 = {}^4/_2 \times \%C_6H_2D_4 + 5 \times \%C_6HD_5 + 6 \times \%C_6D_6$. Thus $\phi = \phi_1 + \phi_2$. Figure 3B is a plot of ϕ_1 and ϕ_2 *vs.* potential using the data of Figure 3A. The left ordinate is for ϕ_2 and the right ordinate ϕ_1. The ϕ_2 curve closely resembles the ϕ plot in Figure 3A because of the relatively small contribution

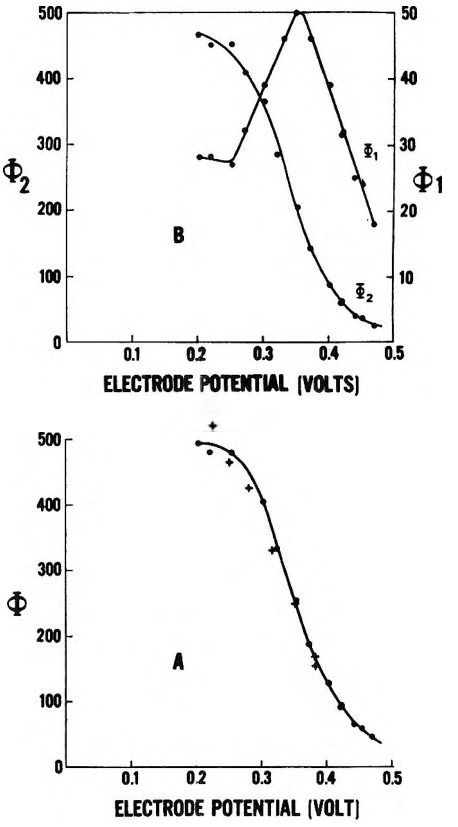

Figure 3. (A) The maximum value of ϕ from Figure 2 *vs.* adsorption potential for variable potential experiments (●) and constant potential experiments (+). (B) Plot of ϕ_1 and ϕ_2 at the maximum value of ϕ *vs.* adsorption potential.

of ϕ_1 at the lower potentials. The effect of adsorption potential on ϕ_1 was unexpected. At about 0.35 V, there appears to be a change in the exchange process which causes the value of ϕ_1 to decline. This effect was reproducible, occurring always within 15 mV of 0.35 V for the reaction conditions of Figure 3. The decline in ϕ_1 may be explained by the readsorption of partially exchanged benzene at potentials below 0.35 V. Thus, a portion of the benzene reacting by the ϕ_1 process is counted in the ϕ_2 total. Alternatively, the results might be explained by assuming ϕ_1 and ϕ_2 reflect the relative number of the two types of reaction sites at any given potential and that the ratio of ϕ_1 to ϕ_2 sites varies from potential to potential. Based on preliminary data in which the flow rate (and thus the mean time of the reactant in the cell cavity) was varied, the peak value of ϕ_1 occurred at potentials higher than 0.35 V with a slower flow rate. This suggests the former explanation is correct since the longer the time the reaction products are exposed to the catalyst the greater the opportunity for readsorption.

Using the data of Figure 2 and summing the percentage of the deuterio isomers for the ϕ_1 and ϕ_2 processes, *i.e.*, $\Sigma\phi_1 = \%C_6H_5D + \%C_6H_4D_2 + \%C_6H_3D_3 + {}^1/_2\%C_6H_2D_4$, as a function of potential gave the curves shown in Figure 4. These curves are similar in shape to the

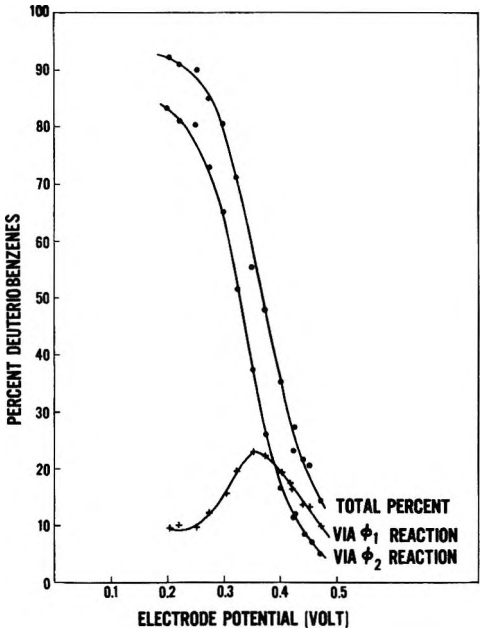

Figure 4. Plot of percentage of benzene exchanged *vs.* adsorption potential.

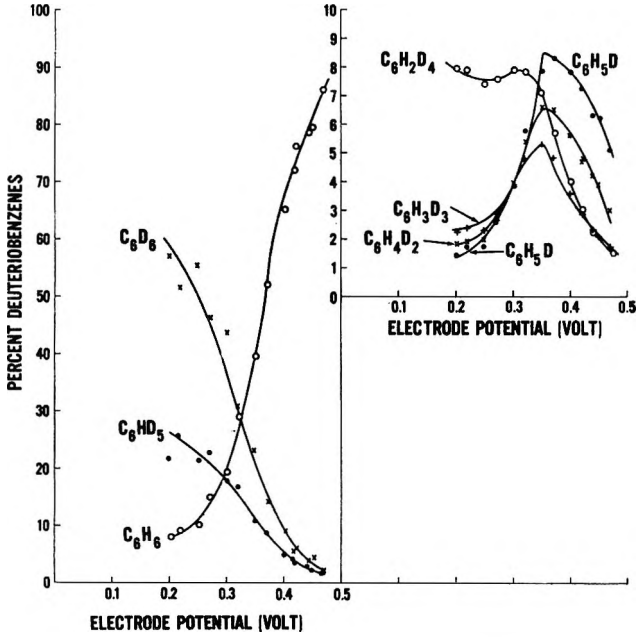

Figure 5. The effect of adsorption potential on the relative concentrations of the deuterio isomers for the same experiments represented in Figure 2.

ϕ_1 and ϕ_2 plots in Figure 3B. When Figure 4 is broken down to the percentage of each deuterio isomer, the curves of Figure 5 are obtained. The adsorption potential is seen to have an inverse effect on the C_6H_6 percentage compared to that of C_6D_6. Due to its relatively large weighting factor, the shape of the C_6D_6 curve resembles the shape of the ϕ and ϕ_2 plots in Figure 3B. The dependence of C_6H_5D, $C_6H_4D_2$, and $C_6H_3D_3$ on potential are remarkably similar but differ from $C_6H_2D_4$ as would be expected if this compound were partially pro-

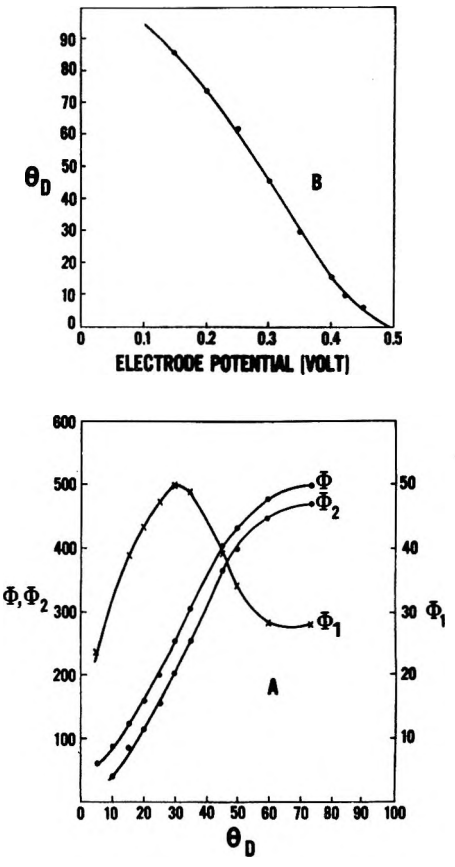

Figure 6. (A) Plot of ϕ, ϕ_1, and ϕ_2 *vs.* deuterium coverage, θ_D. (B) Plot of θ_D *vs.* electrode potential.

duced by another type of reaction (multiple exchange) as well as by successive ϕ_1 type reactions. The C_6HD_5 concentration followed C_6D_6 but began a slight decline about 0.20 V. This was somewhat surprising since we had expected an increase in the concentration of C_6HD_5 at the low potentials as a result of the depletion of the D concentration on the electrocatalyst and in the electrolyte adjacent to the electrode due to the relatively large amount of exchange occurring at these potentials. Apparently the electrolyte stirring was sufficient to maintain a high concentration of available D on the electrocatalyst.

Thus far, we have observed a considerable effect of adsorption potential on the hydrogen–deuterium exchange which benzene undergoes at a fuel cell electrode. However we have not discussed the underlying cause of the effect. A possible explanation is that the potential of the working electrode determines how much deuterium is on the catalyst surface which might in turn be related to the amount of exchange that occurs. Following the procedure of Bold and Breiter,[7] the deuterium coverage as a function of potential was measured for the fuel cell electrode. Figure 6B is a plot of the percentage of the surface area covered by deuterium,

(7) W. Bold and M. W. Breiter, *Z. Elektrochem.*, **64**, 897 (1960); M. W. Breiter, *Trans. Faraday Soc.*, **60**, 1445 (1964).

θ, as a function of potential. When the values of ϕ, ϕ_1, and ϕ_2 obtained at a given potential were plotted against the deuterium coverage, θ, at that same potential, the curves of Figure 6A were obtained. The ϕ curve has a reasonably linear region stretching from a coverage of 10 to 50% or a potential range of 0.42 to 0.28 V. The substantial deviation from linearity at the low potentials (high deuterium coverages) can be explained by a high concentration of hydrogen on the surface as a result of the facile exchange at the low potentials, by formation of cyclohexane, and/or by diffusion limitations of the cell and electrode. Although the first suggestion may contribute some to the decreased value of ϕ, it is not expected to be a major factor based on the comparison of C_6D_6 and C_6HD_5 percentages as discussed above. Deuteration of C_6D_6 or C_6HD_5 to give deuteriocyclohexanes would decrease their respective concentrations and thus ϕ. However we have detected no cyclohexanes at potentials above 0.20 V. The last explanation seems to be most likely. On passing the reactant through the cell at any flow rate, there is always a certain fraction that does not contact the electrode. This fraction becomes significant at the low potentials where, due to the large concentrations of deuterium on the surface, the probability of exchange is high each time the reactant contacts the catalyst. The unreacted benzene results in an achievable upper limit of ϕ below the absolute maximum of 600 and causes the deviation from linearity of the dependence of exchange on deuterium coverage.

As the deuterium coverage on the catalyst surface depends on the electrode potential, the concentration of the exchange sites, defined as an atom or group of atoms where benzene can adsorb adjacent to atoms on which deuterium is adsorbed, is also dependent on the electrode potential. If the exchange process is comprised of stepwise (ϕ_1) or multiple exchange (ϕ_2) reactions for each benzene residence on the electrode, two types of reaction sites are required. The question arises as to whether these sites differ only in the number of adjacent deuterium atoms or whether the structure of the site differs so that the adsorbed intermediates are different. Based on the effect of potential on the isomeric distribution (Figure 5), especially the close similarity of C_6H_5D, $C_6H_4D_2$, and $C_6H_3D_3$, we favor the latter explanation. The intermediate giving rise to the ϕ_1 products is suggested to be σ bonded to the surface, and the one giving the ϕ_2 products may be π bonded to the catalyst. These types of intermediates in exchange reactions on platinum have been discussed in detail previously.[6,8,9] This picture of the exchange process at a fuel cell electrode is clouded by second site adsorptions which become critical as the deuterium surface coverage increases. To obtain a more precise understanding of these processes, we shall attempt to selectively poison one type of site.

Acknowledgments. The support of Dr. J. R. Huff, the help of Mr. G. W. Walker in determining the deuterium coverage as a function of potential, and the assistance of Mr. D. H. Bomkamp in programming the computer are gratefully acknowledged.

(8) J. L. Garnett, R. J. Hodges, and W. A. Sollich-Baumgartner, *Proc. 4th Int. Congr. Catal.*, 1 (1968), and references cited therein.

(9) J. J. Rooney, *Chem. Brit.*, 2, 242 (1966).

Application of the Polanyi Adsorption Potential Theory to Adsorption from Solution on Activated Carbon. III. Adsorption of Miscible Organic Liquids from Water Solution[1]

by David A. Wohleber and Milton Manes*

Chemistry Department, Kent State University, Kent, Ohio 44240 *(Received February 16, 1971)*

Publication costs assisted by the Pittsburgh Activated Carbon Division, Calgon Corporation

Adsorption isotherms, from water solution onto activated carbon, have been determined over a wide concentration range for the following miscible organic liquids: acetic acid, acetone, acetonitrile, dimethylformamide, isopropyl alcohol, *n*-propyl alcohol, *p*-dioxane, and pyridine. The data agree with predicted isotherms calculated by the Hansen–Fackler modification of the Polanyi adsorption potential theory, using only the solute refractive index and molar volume, together with the characteristic curve for the carbon as determined from gas phase adsorption data.

Introduction

Earlier work in this series has dealt with the application of the Polanyi adsorption potential theory[2] to the adsorption onto activated carbon of (a) solids from solution in various solvents,[3] and (b) partially miscible organic liquids from water.[4] The work described here is an extension of earlier work to the adsorption onto activated carbon of miscible organic liquids from water solution, in particular, the adsorption of acetic acid, acetone, acetonitrile, dimethylformamide, isopropyl alcohol, *n*-propyl alcohol, *p*-dioxane, and pyridine, with special emphasis on adsorption in the low and trace concentration ranges.

The present study was aimed at extending the scope of available adsorption data on a single carbon for the purpose of finding relations between gas and liquid phase adsorption. We were in particular interested in determining the extent to which solution adsorption isotherms could be predicted from the polarizability per unit volume of the solutes and solvent as estimated from their refractive indices, without direct determination of the gas phase adsorption isotherms. This is particularly important because of interest in the removal of trace quantities from water, where the low capacities observed cannot be conveniently attained in vapor phase investigations.

Theoretical Considerations

The underlying theory is essentially the Hansen–Fackler[5] modification of the Polanyi adsorption potential theory; it gives the composition of the adsorbate liquid in any given region of the adsorption space in terms of the composition of bulk liquid and the adsorption potential per unit volume ($\alpha = \epsilon/V$) of each solution component. Since the adsorption potential varies over the adsorption space, the adsorbate composition varies similarly over the adsorption space and the total amount adsorbed is calculated by an integration over the entire adsorption space. The Hansen–Fackler treatment was used here with the following adaptations. (1) The "characteristic curve" for the carbon (*i.e.*, ϵ/V *vs.* the volume adsorbed) was taken from earlier gas phase adsorption data.[3] (2) The scale factor, γ, relating ϵ/V at any adsorption volume (ϕ) to the corresponding characteristic curve was estimated (following Manes and Hofer, Hofer and Manes,[6] and Wohleber and Manes) from the refractive index (n) using the formula

$$V_s \equiv \frac{\alpha_s}{\alpha_h} \cong \frac{p_s}{p_7} \tag{1}$$

where

$$p_i = \frac{n_i^2 - 1}{n_i^2 + 2} \tag{2}$$

and the subscripts s and 7 refer to the solute and to heptane, the latter being taken as a typical hydrocarbon. (3) The scale factor γ for water was estimated from earlier liquid phase adsorption data;[4] however, the estimate did not differ appreciably from the estimate based on the vapor phase adsorption of water.

(1) Based on a thesis submitted by David A. Wohleber to Kent State University in partial fulfillment of the requirements for the Ph.D. degree.

(2) M. Polanyi, *Verh. Deut. Phys. Ges.*, **16**, 1012 (1914); **18**, 55 (1916); *Z. Elektrochem.*, **26**, 370 (1920); *Z. Phys.*, **2**, 111 (1920).

(3) M. Manes and L. J. E. Hofer, *J. Phys. Chem.*, **73**, 584 (1969).

(4) D. A. Wohleber and M. Manes, *ibid.*, **75**, 61 (1971).

(5) R. S. Hansen and W. V. Fackler, Jr., *ibid.*, **57**, 634 (1953).

(6) L. J. E. Hofer and M. Manes, *Chem. Eng. Progr. Symp. Ser.*, **65** (96), 84 (1969).

The important equations, all taken from Hansen and Fackler, are

$$-\alpha_{s1} + \frac{RT}{\bar{V}} \ln\left(\frac{x_{1\phi}}{x_{1B}}\right) = -\alpha_{s2} + \frac{RT}{\bar{V}} \ln\left(\frac{x_{2\phi}}{x_{2B}}\right) \quad (3)$$

$$\frac{V\Delta c_1}{m} = \int_0^{\infty} \left[\frac{x_{1\phi}}{\bar{V}_{1\phi}} - \frac{x_{1B}}{\bar{V}_{1B}}\right] d\phi \quad (4)$$

where $\bar{V}_1$ and $\bar{V}_2$ are the molar volumes at temperature T, x is the mole fraction, the subscripts ϕ and B refer to the adsorbed and bulk phases, V is the volume of the bulk solution, and Δc_1 is the difference between the initial and final concentrations in the solution.

Experimental Section

Isotherms for the adsorption of water–organic mixtures containing less than 10 mol % organic solute were determined at 25° for aqueous solutions of acetic acid, acetone, acetonitrile, dimethylformamide, isopropyl alcohol, *n*-propyl alcohol, *p*-dioxane, and pyridine.

The adsorbent (Pittsburgh Activated Carbon Co., grade CAL activated carbon), apparatus, and experimental techniques were the same as described in the preceding article,[4] except that pyridine was analyzed by ultraviolet spectrophotometry. Solute concentrations as low as 20 ppm were determined.

The molar volume of each adsorbate in the adsorbed phase was assumed to be equal to the molar volume of bulk liquid at 25°.

Data and Results

The γ_s for each organic adsorbate, calculated by eq 1, is given in Table I along with γ_s for water (γ_1 of Wohleber and Manes). These values were used in eq 4 to calculate the adsorption from water for each organic solute, shown as the curves in Figures 1, 2, and 3. [This integration was done using a Fortran IV program and a Burroughs 5500 computer.] Except for acetic acid and *p*-dioxane, the calculated curves agree with the experimental data (points) over a wide range of capacities and bulk phase concentrations. The deviations, although slight, are systematic rather than random and are due to a small error in the estimated value of γ.

Anomalously high adsorption of organic acids on activated carbon has been reported by Boehm[7] and by Coughlin and Ezra,[8] who attribute it to chemical interaction between the acid and surface groups on the carbon. The anomalously low adsorption of *p*-dioxane may be attributed to steric hindrance to closest approach of the adsorbate to the carbon surface, an effect that was postulated by Manes and Hofer to explain the anomalous behavior of cyclohexane, an isomorph of *p*-dioxane.

Table I

Adsorbate	γ_s
Acetic acid	0.96
Acetone	0.93
Acetonitrile	0.90
Dimethylformamide	1.09
Isopropyl alcohol	0.98
n-Propyl alcohol	0.99
p-Dioxane	1.08
Pyridine	1.27
Water	0.28

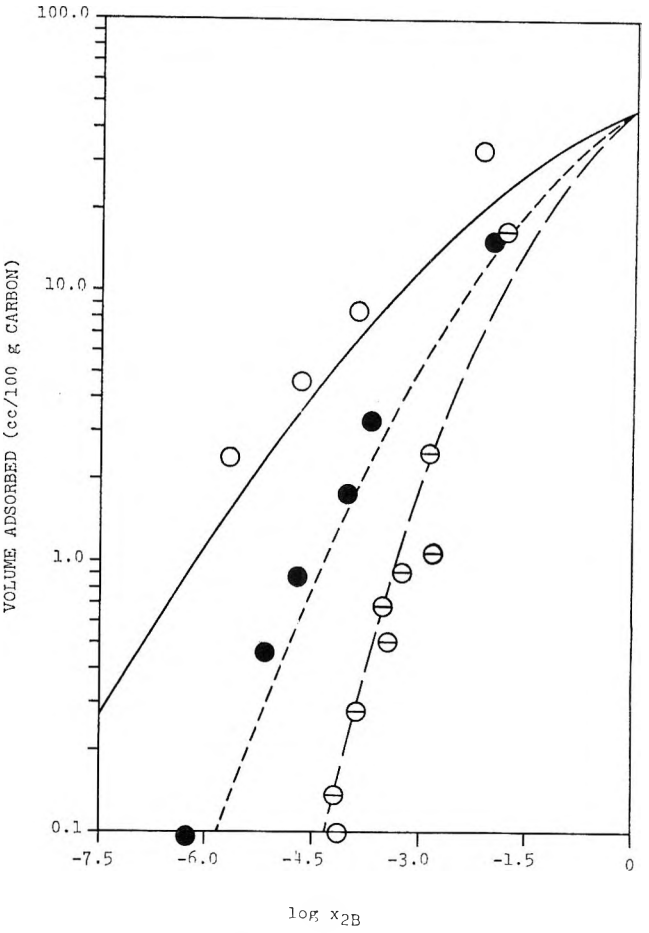

Figure 1. Adsorption isotherms for acetone, ●, acetonitrile, ⊖, and pyridine, ○; plotted as volume adsorbed *vs.* mole fraction in the bulk phase; temperature 25°. (Curves are calculated from theory.)

Discussion

The agreement of the data with theory over a wide range of concentrations and capacities (as wide a range as was investigated in earlier work on gas phase adsorption[9]) demonstrates the applicability of the Hansen–Fackler modification of the Polanyi adsorption potential theory, as well as the refractive index approximation of Manes and Hofer. Moreover, the Hansen–

(7) H. P. Boehm, *Advan. Catal.*, 16, 179 (1966).

(8) R. W. Coughlin and F. S. Ezra, *Environ. Sci. Technol.*, 2 (4), 291 (1968).

(9) R. J. Grant, M. Manes, and S. B. Smith, *AIChE J.*, 8, 403 (1962).

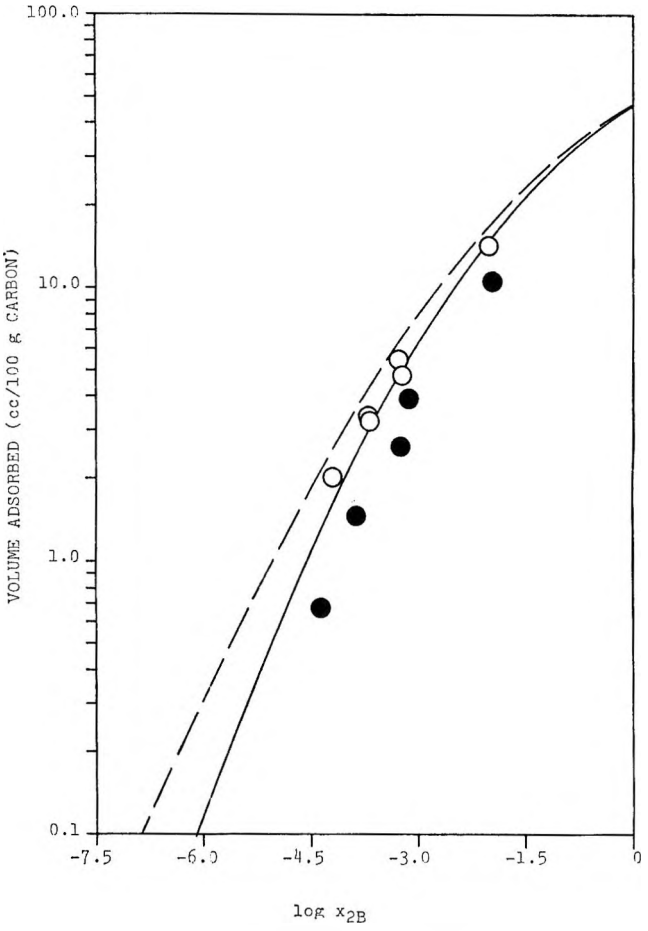

Figure 2. Adsorption isotherms for isopropyl alcohol, ●, and dimethylformamide, ○; plotted as volume adsorbed *vs.* mole fraction in the bulk phase; temperature 25°. (Curves are calculated from theory: isopropyl alcohol, —, and dimethylformamide, — —.)

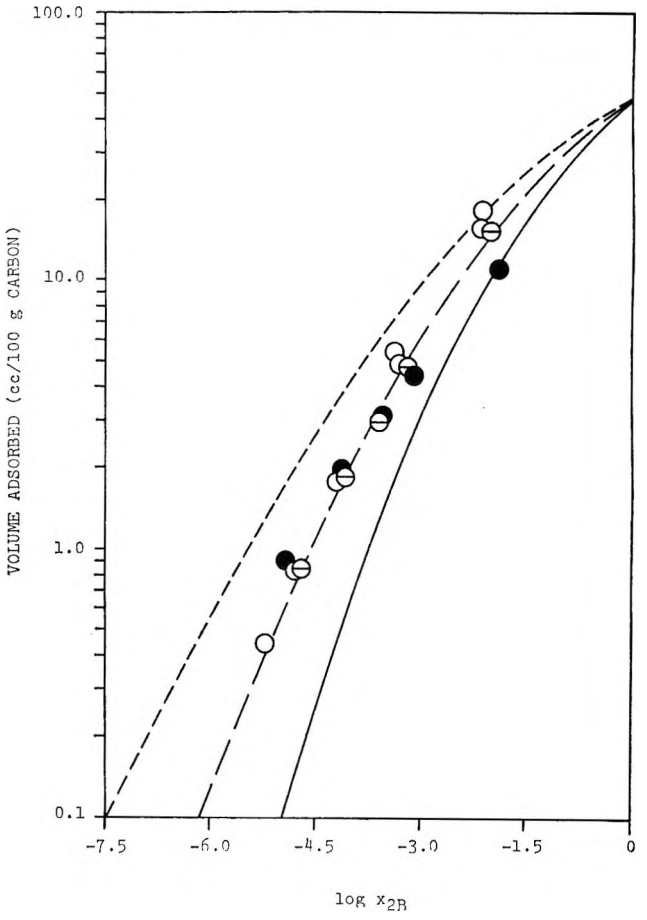

Figure 3. Adsorption isotherms for *n*-propyl alcohol, ⊖, acetic acid, ●, and *p*-dioxane, ○; plotted as volume adsorbed *vs.* mole fraction in the bulk phase; temperature 25°. (Curves are calculated from theory: *n*-propyl alcohol, — —, acetic acid, ——, *p*-dioxane, — — —.)

Fackler treatment is confirmed over concentration ranges several orders of magnitude below their experimentally accessible limit. The Hansen–Fackler treatment is probably more accurate than our data indicate, since these data contain the combined errors of all of the approximations. However, the overall estimation method, even with the combined errors, suffices to estimate adsorption isotherms well into the trace concentration range.

In this work, we have made no attempt to account for adsorption over the entire concentration range, partly because of the increased analytical difficulties and partly because we would expect anomalies from specific chemical interactions with surface groups to be magnified at the lowest adsorption potentials. Nevertheless, the work covers about five orders of magnitude of concentration and covers the region of most interest to adsorption applications.

Since the number of liquids miscible with water is rather limited, one could determine empirical values of γ for each such liquid, in which case one would be able, with minimal data, to predict the adsorption isotherm of any such liquid, not only over a wide range of capacities but, in all likelihood, for a wide variety of activated carbons.

Finally, although the determination of the characteristic curve of a new carbon from liquid phase adsorption is simpler for partially miscible solutes,[4] one should be able to determine it from adsorption of miscible liquids by inverting the Hansen–Fackler calculation, if one is not interested in the high capacity range.

Conclusions

The Hansen–Fackler modification of the Polanyi adsorption potential theory, together with the Manes–Hofer approximation for predicting relative adsorption potentials from refractive index, can be used to estimate the adsorption of a wide variety of miscible organic liquids, from water, onto activated carbon over a wide capacity range, and in particular, down to the trace concentration region. Deviations from theory are ascribable to specific chemical interactions or steric effects (neither of which is included in the Polanyi theory).

Acknowledgment. This work was supported in part by a grant from the Pittsburgh Activated Carbon Division, Calgon Corporation. In addition, D. A. Wohlleber received support from an N.D.E.A. Title IV fellowship and from the Goodyear Tire and Rubber Fellowship Fund.

Osmotic Coefficients of One Molal Alkali Metal Chloride Solutions over a 300° Temperature Range[1]

by W. T. Lindsay, Jr.,* and Chia-tsun Liu

Westinghouse Research Laboratories, Pittsburgh, Pennsylvania *(Received April 5, 1971)*

Publication costs assisted by the Westinghouse Research Laboratories

Osmotic coefficients are reported for approximately 1 *m* solutions of LiCl and CsCl at 25° intervals from 125 to 275 and 300°. These results are summarized with previously determined osmotic coefficients for 1 *m* solutions of HCl, LiCl, NaCl, KCl, RbCl, and CsCl to give an overall view of individual ionic character in these solutions from the freezing points to high temperatures. Excess enthalpies and entropies are calculated for the water in 1 *m* HCl, LiCl, NaCl, and CsCl. Individual ionic character decreases considerably in high temperature 1 *m* solutions of these salts.

Introduction

The individual ionic character of alkali metal halides in moderately concentrated aqueous solutions has been of long-term interest in the development of the physical chemistry of electrolytes. This subject has had various interpretations, with most recent discussions focusing on the differing effects of the ions on water structure.

A principal manifestation of individual ionic character is the wide variation of activity and osmotic coefficients for alkali metal halide salt solutions at or near room temperature, yet little attention has been given to the temperature dependence of this phenomenon. In this paper we report determinations of osmotic coefficients for approximately 1 *m* solutions of lithium chloride and cesium chloride from 125 to 275 and 300°. By many criteria, these two salts have very different effects on water structure at room temperature, LiCl being regarded as a "structure maker" and CsCl as a "structure breaker." Summarizing the experimental results of this work with other data for these and other salts gives a clear picture of the temperature dependence of 1 *m* osmotic coefficients for alkali metal chloride and hydrochloric acid solutions from their freezing points to temperatures as high as 300°. The comparison shows that individuality of ionic character in these solutions decreases markedly at high temperatures.

Experimental Section

The experimental method used in this work determined the difference between the vapor pressures of solution and pure water, each contained in separate but identical pressure vessels held at the same temperature. The apparatus and techniques developed for this measurement at temperatures to 300° have been described elsewhere in some detail.[2-4] Stating the essential features in brief, the important criterion of negligible difference between the temperatures of the two vessels was achieved by a "double thermostating" method, with the two vapor pressure cells symmetrically installed in a massive aluminum block, the block being immersed in a vigorously stirred thermostat bath regulated to a constancy of ±0.002° or better. A bellows arrangement confined water vapor to the isothermal environment of the cells. A differential transformer system was used to sense the position of each bellows, allowing balancing of cell internal steam pressures with externally applied helium gas pressure

(1) Presented in part at the 153rd National Meeting of the American Chemical Society, Miami Beach, Fla., April 1967.

(2) W. T. Lindsay, Jr., and C Liu, OSW Research and Development Progress Report 347. Available from Superintendent of Documents, U. S. Government Printing Office, Washington, D. C. 20402.

(3) W. T. Lindsay, Jr., and T. S. Bulischeck, *Rev. Sci. Instrum.*, **41**, 149 (1970).

(4) C. Liu and W. T. Lindsay, Jr., *J. Phys. Chem.*, **74**, 341 (1970).

with a precision usually about ±0.2 Torr or better. (A greater degree of variability was encountered in a few cases at some of the higher temperatures; however, the pressure differences were still measurable with acceptably small standard deviations of 0.1 to 0.4%.) The difference between balancing gas pressures was then determined by a high pressure differential manometer or by a Texas Instruments quartz spiral Bourdon gauge in a pressure capsule. This arrangement has been used successfully to measure the vapor pressure lowering of high temperature NaCl solutions as dilute as 0.1 *m*.[4]

The measurements were carried out on analytical grade salts with a reported purity of 99.885% for LiCl (Fisher "Certified") and 99.9% for CsCl (Kawecki "High Purity"). Impurity levels many times those reported would have negligible effect on the results. The salts were dried in a vacuum oven at 100° for several days and used without further purification. For the lithium chloride runs, a degassed solution at a concentration of 0.9911 *m* at room temperature was prepared on a weight basis from the dried salt and triply distilled water following the previously described techniques. Measurements of vapor pressure differences between this solution and pure water followed the previously established procedures at temperatures 125, 150, 175, 200, 225, 250, and 275°. At 300°, a leak developed in the solution cell, causing a slow increase in concentration of the solution; hence, no valid data were obtained at this temperature. All other information (magnitude of absolute pressures at 125°, constancy of differential pressure measurements at each temperature, absence of gas in reference cell, etc.) indicates that the results at 275° and below are acceptable.

For the cesium chloride runs, the solution after preparation and degassing was at a slightly higher concentration of salt, 1.0075 *m* at room temperature. Satisfactory measurements were obtained with this solution at all temperatures 125 to 300°.

Results

The results are given in Table I. The concentrations reported in the table were calculated from the original concentrations of the solutions with correction for the evaporation of water needed to raise the steam density in the vapor volume of the cell, taking expansion of the liquid into account. Vapor pressures given for pure water were calculated at each temperature from the correlation of Smith, Keyes, and Gerry.[5]

Osmotic coefficients were calculated from the relation

$$\phi = \frac{1000}{\nu m M_1 RT}\left[RT \ln \frac{p_0}{p} - \int_p^{p_0}\left(\frac{RT}{p} - V_1^\circ(\mathrm{g})\right)dp - V_1^\circ(\mathrm{l})\Delta p\right] \quad (1)$$

where ϕ is the osmotic coefficient, ν is 2, m is molality,

Table I: Experimental Results for Nominally 1 *m* Solutions of LiCl and CsCl

Temp, °C	Molality at temperature, mol/1000 g H_2O	Vapor pressure lowering $\Delta p = p_0 - p$, Torr	Osmotic coefficient ϕ at $p = p_0$
	Lithium Chloride Solutions		
125	0.9934	60.46	0.960
150	0.9946	123.97	0.941
175	0.9989	233.46	0.918
200	1.0042	412.13	0.894
225	1.0121	686.48	0.861
250	1.0233	1101.45	0.825
275	1.0395	1709.89	0.778
300	...	...	...
	Cesium Chloride Solutions		
125	1.0096	55.24	0.862
150	1.0116	113.88	0.849
175	1.0148	215.98	0.835
200	1.0196	385.56	0.823
225	1.0267	646.33	0.798
250	1.0369	1044.12	0.771
275	1.0514	1648.22	0.740
300	1.0720	2543.39	0.695

M_1 is the molecular weight of water, R is the gas constant, T is absolute temperature, p_0 is the vapor pressure of pure water, p is the vapor pressure of the solution, Δp is $p_0 - p$, $V_1^\circ(\mathrm{g})$ is the analytical function of pressure and temperature for the molar volume of pure water vapor given by Smith, Keyes, and Gerry,[5] and $V_1^\circ(\mathrm{l})$ is the corresponding function for the molar volume of pure liquid water, used here as a valid approximation for the partial molal volume of water in the solution. The second term in the brackets is the correction for deviation of water vapor from perfect gas behavior, and the third term is a small correction for the purpose of reporting the osmotic coefficients at a pressure equal to the vapor pressure of pure water at each temperature.

Figure 1 shows the osmotic coefficients from this work designated by the solid circles and the solid line portions of the curves for LiCl and CsCl. Also shown by solid circles and a solid line are high temperature osmotic coefficients for NaCl. These NaCl data are calculated for a concentration of 1.0 *m* at 125 to 300° from a correlation equation that we developed earlier[2] to represent our own[4] and other[6-8] results on sodium chloride solutions at concentrations from 0.1 to 3 *m* at these temperatures.

The LiCl and CsCl points are those for the concen-

(5) L. B. Smith, F. G. Keyes, and H. T. Gerry, *Proc. Amer. Acad. Arts Sci.*, **69**, 137 (1934). See also J. H. Keenan and F. G. Keyes, "Thermodynamic Properties of Steam," Wiley, New York, N. Y., 1936.

(6) E. R. Gardner, P. J. Jones, and H. J. de Nordwall, *Trans. Faraday Soc.*, **59**, 1994 (1963).

(7) E. R. Gardner, *ibid.*, **65**, 91 (1969).

(8) B. M. Fabuss and A. Korosi, *Desalination*, **1**, 139 (1966).

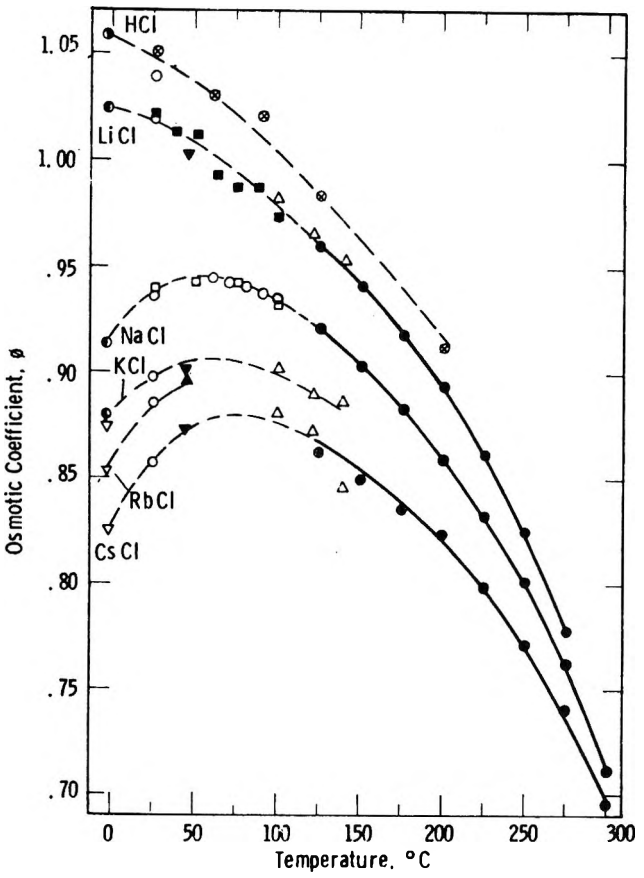

Figure 1. Temperature dependence of osmotic coefficients of 1 *m* alkali metal chlorides and HCl. This work and ref 2 (●), ref 18, 24, and 25 (○), ref 20 (■), ref 19 (□), ref 17 (▲), ref 13, 14, and 15 (△), ref 16 (▼), ref 12 (▽), ref 10 (◐), ref 11 (◑), ref 21 (⊗).

trations of Table I. We have no way of correcting these to exactly 1.0 *m* without additional data on concentration dependence of the osmotic coefficients. However, the high temperature osmotic coefficients for NaCl are only slightly dependent on concentration in the vicinity of 1 *m* because of the minima in the curves of osmotic coefficient *vs.* concentration. Considering (1) the effects of temperature on the shapes of these curves for NaCl and on the positions of their minima[4] and (2) the relative positions of the minima for the curves for LiCl, NaCl, and CsCl at room temperature,[9] it appears probable that osmotic coefficients for LiCl and CsCl at high temperatures are also only slightly dependent on concentration in the neighborhood of 1 *m*.

Discussion

On Figure 1 we have also shown points summarizing 1 *m* osmotic coefficient data for HCl, LiCl, NaCl, KCl, RbCl, and CsCl at room temperature and at as many other temperatures as possible. Some of these data were obtained from freezing point depressions,[10-12] some by isopiestic comparison,[13-17] some from boiling point elevations,[18] some by measurement of vapor pressure lowering,[2,4,19,20] and some were calculated from activity coefficients determined by emf methods.[21] Although the data are of varying degrees of reliability, they fall into an overall pattern that is consistent with the high temperature results we report. The complete set of curves shows a regular and systematic variation from HCl to CsCl, with no exceptions or anomalies. We believe Figure 1 to give a much clearer picture of the temperature dependence of 1 *m* osmotic coefficients for the alkali metal chlorides (and, by inference, of the effects of temperature on individual ionic character) than has heretofore existed.

Some observations may be noted from the information of Figure 1. First, the relative order of 1 *m* osmotic coefficients, HCl > LiCl > KCl > RbCl > CsCl, does not change from the freezing points to the highest temperatures for which there are data. Second, the spread between the osmotic coefficients decreases very greatly as the temperature increases. Third, above 100°, the temperature coefficients are all of the same sign and the curves are quite similar, in contrast to the situation at room temperature. Fourth, the temperatures of the maxima in the curves progress regularly from about 80° for CsCl to 60° for NaCl, with the maximum for LiCl about at the freezing point and the apparent maximum for HCl below the freezing point.

All of these observations are consistent with the notion that individual ionic character at room temperature is due primarily to structure in the solvent, which gives possibilities for both structure-making and structure-breaking effects of the ions according to the two-zone co-sphere model elaborated by Frank,[22] Gurney,[23] and

(9) G. Scatchard in "The Structure of Electrolytic Solutions," W. J. Hamer, Ed., Wiley, New York, N. Y., 1959, Chapter 2.

(10) G. Scatchard and S. S. Prentiss, *J. Amer. Chem. Soc.*, **55**, 4355 (1933).

(11) H. M. Chadwell, *ibid.*, **49**, 2795 (1927). Interpolated for 1.0 *m*.

(12) G. Karagunis, A. Hawkinson, and G. Damköhler, *Z. Phys. Chem. (Leipzig)*, **151**, 433 (1930). Interpolated for 1.0 *m* as required.

(13) C. S. Patterson, L. O. Gilpatrick, and B. A. Soldano, *J. Chem. Soc.*, 2730 (1960), using ϕ_{NaCl} = 0.935 at 99.6°.

(14) B. A. Soldano and C. S. Patterson, *J. Chem. Soc.*, 937 (1962), using ϕ_{NaCl} = 0.924 at 121.1°.

(15) B. A. Soldano and M. Meek, *ibid.*, 4424 (1963), using ϕ_{NaCl} = 0.911 at 140.3°.

(16) K. L. Hellams, C. S. Patterson, B. H. Prentice, III, and M. J. Taylor, *J. Chem. Eng. Data*, **10**, 323 (1965), using ϕ_{NaCl} = 0.942 at 45°.

(17) L. L. Makarov, Y. G. Vlasov, and V. I. Isotov, *Russ. J. Phys. Chem.*, **38**, 1297 (1964). Isopiestic ratio at 1.3 *m* NaCl used with ϕ_{NaCl} = 0.942 at 45° and 1.0 *m*.

(18) R. P. Smith, *J. Amer. Chem. Soc.*, **61**, 500 (1939).

(19) H. F. Gibbard, Jr., Ph D. Thesis, Department of Chemistry, Massachusetts Institute of Technology, 1966. Data are for concentrations 1.046 to 1.049 *m*.

(20) H. F. Gibbard, Jr., personal communication, July 7, 1970. Data are for concentrations 1.0208 to 1.0238 *m*.

(21) R. S. Greeley, W. T. Smith, Jr., M. H. Lietzke, and R. W. Stoughton, *J. Phys. Chem.*, **64**, 1445 (1960).

(22) H. S. Frank and M. W. Evans, *J. Chem. Phys.*, **13**, 507 (1945).

(23) R. W. Gurney, "Ionic Processes in Solution," Dover Publications, New York, N. Y., 1953.

others. The net effect of these opposing influences can be widely variable in sign and magnitude for ions of various sizes. On the other hand, only structure enhancement is possible in the thermally disrupted solvent at high temperatures, where the similarities of the curves of Figure 1 are more striking than the differences. Particularly, the similar slopes at high temperatures suggest that CsCl, RbCl, KCl, and NaCl become more like LiCl, which is regarded as a structure maker even at room temperature.

The similarities and differences in the data for these solutions can be examined in another way by displaying correlations between excess enthalpy and excess entropy for the solvent. For this purpose, the data for HCl, LiCl, NaCl, and CsCl were fitted by a least-squares procedure to a cubic polynomial of the form

$$\phi = a_0 + a_1T + a_2T^2 + a_2T^3 \qquad (2)$$

where T is temperature in degrees Kelvin and a_0, a_1, a_2, and a_3 are constants. Double weight was given to the identical 25° values tabulated by Robinson and Stokes[24] and by Wu and Hamer,[25] because of the large number of high quality measurements that these authors have correlated. All others, including our own, were given single weight. The excess partial specific enthalpy H_1^{ex} was calculated by differentiating the resulting expressions[26] according to the relation

$$H_1^{ex} = \nu mRT^2\partial\phi/\partial T \qquad (3)$$

and the excess partial specific entropy S_1^{ex} was calculated from the relations

$$F_1^{ex} = \nu mRT(1 - \phi) \qquad (4)$$

and

$$S_1^{ex} = (H_1^{ex} - F_1^{ex})/T \qquad (5)$$

where F_1^{ex} is the excess partial specific Gibbs free energy (per kilogram of H_2O).[27] The results are shown by Figure 2, where H_1^{ex} is plotted against TS_1^{ex}. The magnitude of F_1^{ex} can be determined for any point on this plot by the vertical or horizontal distances from the line marked $F_1^{ex} = 0$, for which $H_1^{ex} = TS_1^{ex}$.

It should be recognized that the exact magnitudes of the values calculated for S_1^{ex} and H_1^{ex} at each temperature depend to some extent on the analytical form of the equations assumed to represent the data. On the other hand, the correlation of S_1^{ex} with H_1^{ex} for each salt is relatively insensitive to the choice of equation; *i.e.*, qualitatively equivalent results are obtained whether quadratic, cubic, or quartic polynomials are used. The cubic equations fit the data with an accuracy sufficient to illustrate the points discussed below. Table II gives the values of the parameters of eq 2 for HCl, LiCl, NaCl, and CsCl.

The solid lines of Figure 2 may be viewed as a correlation between solvent excess enthalpy and solvent excess entropy for solutions of a single salt in a series of solvents with progressively varying dielectric constant and extent of structure. These lines are quite accurately linear for both HCl and LiCl over the complete temperature range of the data. The lines for NaCl and CsCl are both curved at the lower temperatures, but they approach linearity at the higher temperatures. These observations indicate no major qualitative change in the nature of the interactions in solution for HCl and LiCl as the temperature increases. They indicate also that the interactions in solution for NaCl and CsCl at the lower temperatures are qualitatively different from those of these same salts at higher temperatures, and from HCl and LiCl at any temperature, conclusions that are consistent with those that can be inferred from Figure 1.

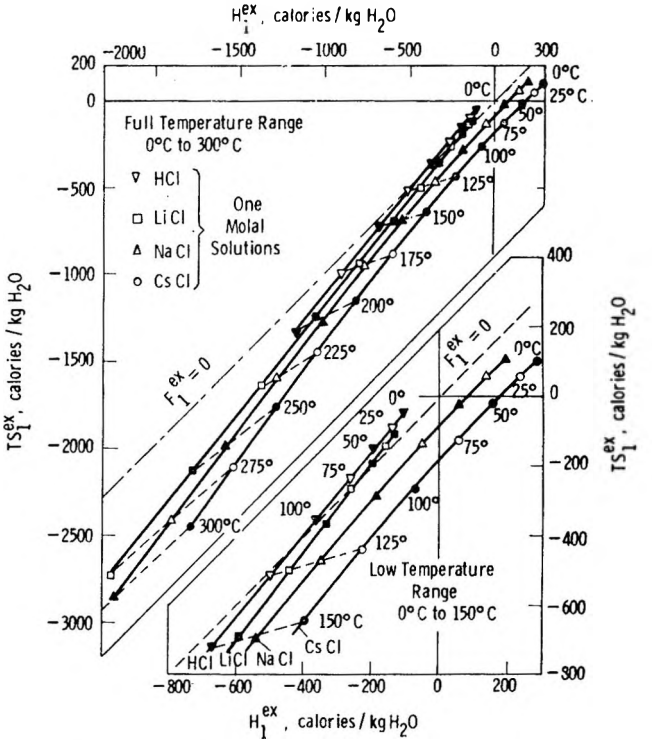

Figure 2. Correlations of excess enthalpy with excess entropy for the water in 1 *m* CsCl, NaCl, LiCl, and HCl at temperatures 0 to 300°. Points are shown at 25° intervals beginning at 0° for each solution.

(24) R. A. Robinson and R. H. Stokes, "Electrolyte Solutions," Academic Press, New York, N. Y., 1959.

(25) Y.-C. Wu and W. J. Hamer, U. S. National Bureau of Standards Report 9908, "Electrochemical Data. Part XI. Osmotic Coefficients and Mean Activity Coefficients of Aqueous Solutions of HCl, HBr, HI and the Chlorides, Bromides and Iodides of the Alkali Metals at 25°C," Sept 6, 1968.

(26) Direct differentiation of the data with respect to temperature is not strictly at constant pressure, since the high temperature osmotic coefficients are reported at pressures equal to the vapor pressure of water at each temperature. We have estimated the correction for NaCl solutions that is required to compensate for this procedure, by using partial molal volumes derived from the density correlation of J. L. Haas, Jr., *Amer. J. Sci.*, **269**, 490 (1970). The corrections are negligible for 1 *m* solutions of NaCl. They are assumed negligible also for 1 *m* solutions of LiCl and CsCl.

(27) See H. L. Friedman, "Ionic Solution Theory," Interscience, New York, N. Y., 1962, for a discussion of these excess partial functions.

Table II: Parameters for Representation of 1 *m* Osmotic Coefficient Data as a Function of Temperature

	HCl	LiCl	NaCl	CsCl
Temp range, °C	−3.93 to 200	−3.80 to 275	−3.39 to 300	−2.14 to 300
Number of data points	7	20	19	14
Parameters for eq 2				
a_0	1.22202	1.31819	0.279727	0.00625499
10^2a_1	−0.130086	−0.220256	0.431668	0.551187
10^6a_2	0.408428	0.608859	−0.809664	−1.05079
10^9a_3	−5.75394	−7.04722	3.31285	5.25157
Standard error of estimate for osmotic coefficient	0.006793	0.003585	0.003640	0.007537

Significant new information from Figure 2 is shown by the dashed lines. These indicate linear correlations, at each temperature from 300° down to about 125°, between solvent excess enthalpy and solvent excess entropy for the different solutes. Both excess enthalpy and excess entropy for the water are more negative in solutions of the chlorides with the smaller cations. We believe these correlations and their progressively varying slopes are as one would expect for the effect of ion size on degree of solvation in a series of unstructured polar solvents with differing dielectric constants. It would be very desirable to make a quantitative test of this contention by comparison of the data with theoretical calculations based on a suitable model. This task may be more readily achievable for unstructured aqueous solutions at high temperatures than accomplishment of the more complex theoretical development needed at lower temperatures.

The above-mentioned linear correlations break down completely at temperatures below 100°, as shown in clearer detail in the lower part of Figure 2. We believe this is evidence strongly suggestive of a new factor coming into play at the lower temperatures, namely, the effect of water structure in amplifying the influence of ion size on the thermodynamic properties of electrolyte solutions.

Osmotic coefficients are only one of the many kinds of solution properties that show the influence of solute individuality despite similarity of ionic charge and electronic structure. The variation of 1 *m* osmotic coefficients for the alkali metal chlorides and hydrochloric acid over a very wide temperature range is consistent with the following hypotheses concerning the more general phenomenon of individual ionic character. (1) Individual ionic character for these solutions diminishes greatly at high temperatures. (2) Individual ionic character for these solutions at room temperature is due primarily to the presence of hydrogen-bonded structures in the solvent. (3) Residual individual ionic character at high temperatures is due mostly or entirely to differences in extent of hydration.

The comparisons presented in this paper illustrate the value that measurements over a very wide temperature range have for interpretation of phenomena in aqueous solutions.

Acknowledgment. This work was performed under contract from the Office of Saline Water. We wish also to acknowledge Mr. T. S. Bulischeck for his valuable assistance with the experimental work.

Excess Gibbs Energy of Mixing of 1,2,4-Trimethylbenzene and 1,3,5-Trimethylbenzene with Several Nitroparaffins by Total Intensity Rayleigh Light Scattering at 30°[1a]

by M. Elizabeth Derrick[1b] and H. Lawrence Clever*

Department of Chemistry, Emory University, Atlanta, Georgia 30322 *(Received December 14, 1970)*

Publication costs assisted by The National Science Foundation

The excess Gibbs energy of mixing and activity coefficients for the binary solutions of nitromethane, nitroethane, and 2-nitropropane with 1,3,5-trimethylbenzene and of nitromethane and nitroethane with 1,2,4-trimethylbenzene were measured by a total intensity Rayleigh light scattering technique at 30°. All five solutions show positive excess free energy of mixing with a maximum of 0.29, 0.20, 0.13, 0.26, and 0.17 kcal mol^{-1}, respectively.[2]

Binary solutions composed of a polar and a nonpolar component may have many interactions that contribute to the nonideality of the solution. In the case of nitroparaffin–hydrocarbon solutions, there are reports of nitro compound–aromatic hydrocarbon associations[3,4] and there are reports of nitroparaffin self-association[5] either into dimers or into chain-like aggregates in nonpolar solvents. Additional evidence of self-association of the nitroparaffin in the solutions is the report of upper critical solution temperatures in toluene–nitroethane[6] and in 1,2,4-trimethylbenzene and 1,3,5-trimethylbenzene solutions with nitromethane.[7]

The excess Gibbs energy from vapor pressure measurements at 45° has been reported for benzene–nitromethane[8] and toluene–nitroethane[6] solutions. The present work reports activity coefficients and excess Gibbs energy of mixing for the five binary aromatic hydrocarbon–nitroparaffin solutions: 1,3,5-trimethylbenzene with nitromethane, nitroethane, and 2-nitropropane, and 1,2,4-trimethylbenzene with nitromethane and nitroethane. The thermodynamic properties were determined from the total intensity Rayleigh light scattering at a wavelength of 546 nm and at a temperature of 30°.

The total intensity Rayleigh scattering technique for the determination of activity coefficients and excess Gibbs energy of mixing has been developed over the past several years.[9-13] In favorable cases where the binary solution pure components differ in refractive index by at least 0.1 unit and the excess Gibbs energy is $\geq$75 cal mol^{-1} and positive, the maximum error in excess free energy by the method may be as high as 15–20%. In the less favorable cases of either small positive or negative excess free energy, the maximum errors may be much larger. In the systems studied in the present work the favorable conditions are met and we believe the light scattering method does give the correct order of the excess free energy.

The total Rayleigh scattering, R_{90}, can be separated into an isotropic contribution, R_{is}, and an anisotropic contribution, R_{an}, by the Cabannes relation. In pure liquids the isotropic scattering is due to density fluctuations, R_d. In solutions two further terms contribute to the isotropic scattering, a concentration fluctuation term, R_c, and a density–concentration fluctuation cross term, $R^{\#}$. The total isotropic Rayleigh scattering from

(1) (a) This work was supported by National Science Foundation Grant GP-8364 and presented in part at the Southeastern Regional Meeting of the American Chemical Society, Richmond, Va., Nov 1969. (b) Holder of an NDEA Fellowship 1967–1970.

(2) Experimental values of mole fraction, depolarization, total intensity Rayleigh scattering at 546 nm and 30°, density, smoothed values of $\Delta n/\Delta X_2$, and calculated solution refractive indices at 546 nm for the five solutions will appear immediately following this article in the microfilm edition of the journal. Single copies may be obtained from the Reprint Department, ACS Publications, 1155 Sixteenth St., N.W., Washington, D. C. 20036. Remit check or money order for $3.00 for photocopy or $2.00 for microfiche.

(3) R. F. Weimer and J. M. Prausnitz, *Spectrochim. Acta*, **22**, 77 (1966).

(4) N. B. Jurenski and P. A. D. deMaine, *J. Amer. Chem. Soc.*, **86**, 3217 (1964).

(5) M. S. Smith, Jr., and P. A. D. deMaine, *J. Miss. Acad. Sci.*, **12**, 97 (1966).

(6) R. V. Orye and J. M. Prausnitz, *Trans. Faraday Soc.*, **61**, 1338 (1965).

(7) H. L. Clever, Q. R. Pirkle, Jr., B. J. Allen, Jr., M. E. Derrick, *J. Chem. Eng. Data*, in press.

(8) I. Brown and F. Smith, *Aust. J. Chem.*, **8**, 501 (1955).

(9) D. J. Coumou and E. L. Mackor, *Trans. Faraday Soc.*, **60**, 1726 (1964).

(10) G. D. Parfitt and J. A. Wood, *ibid.*, **64**, 2081 (1968).

(11) R. L. Schmidt and H. L. Clever, *J. Phys. Chem.*, **72**, 1529 (1968).

(12) H. H. Lewis, R. L. Schmidt, and H. L. Clever, *ibid.*, **74**, 4377 (1970).

(13) M. Kerker, "The Scattering of Light," Academic Press, New York, N. Y., 1969, Chapter 9.

a solution is the sum $R_{is} = R_d + R_c + R^{\#}$. Definitions and an outline of the calculation of activity coefficients and excess Gibbs energy are in an earlier paper.[12]

To apply the light scattering technique we measure the total Rayleigh scattering, R_{90}, and the depolarization, ρ_u. We also measure, when literature results are not available, the refractive index of the pure components and the $\Delta n/\Delta X_2$ and $\Delta n/\Delta c_2$ values for the solutions at the wavelength used in the scattering measurement.

Notes on the Calculations. The isotropic scattering is calculated from the total scattering by the Cabannes relation

$$R_{is} = R_{90}\left(\frac{6 - 7\rho_u}{6 + 6\rho_u}\right) \quad (1)$$

In order to evaluate R_d, $R^{\#}$, and R_{id}, several factors must be either experimentally measured or approximated from theory or empirical equations.[9,11]

In earlier work we used the Clausius–Mosotti equation with a dense media correction evaluated by Schmidt[11,12] to calculate values of $N(\partial\epsilon/\partial N)_T$ as

$$N(\partial\epsilon/\partial N)_T = (n^2 - 1)(n^2 + 2)(1 - 0.07345)/3 \quad (2)$$

Two empirical equations, one due to Eykman,[14] eq 3, and the other to Meeten,[15] eq 4, have been suggested.

$$N(\partial\epsilon/\partial N)_T = (2n^2 + 0.8n)(n^2 - 1)(n^2 + 0.8n + 1) \quad (3)$$

$$N(\partial\epsilon/\partial N)_T = (n^2 - 1)(23 + 7n^2)/30 \quad (4)$$

Equation 2 rearranges to the same form as Meeten's equation but with different numerical constants

$$N(\partial\epsilon/\partial N)_T = (n^2 - 1)(18.5 + 9.3n^2)/30 \quad (5)$$

The three equations are compared for a series of pure liquids in Figure 1. The Meeten equation appears to be the more generally applicable equation and has been used in all of the calculations reported here.

The pure component isothermal compressibility can be estimated[16] from R_d for the pure liquid, if a literature value is not available. Values of the pure component isothermal compressibilities estimated from R_d are given in Table I. These values were used in the calculations except for nitromethane where the value of 73×10^{-12} cm²/dyn interpolated from experimental values reported in the literature[17] was used. An estimated value of 66×10^{-12} at 25° is also reported.[18] The solution isothermal compressibilities are calculated from the pure liquid values assuming them to be additive in volume fraction which was corrected for the excess volume of mixing.

Experimental Section

Chemicals. Benzene (Phillips, 99 mol %) shaken with concentrated sulfuric acid, washed with water until neutral to litmus, dried over $CaSO_4$, and distilled from calcium hydride was used as a standard in the light scattering measurement.

1,2,4-Trimethylbenzene (Phillips research grade, samples of 99.57 and 99.89 mol % purity) was used without further purification. If the samples were not used soon after receipt, they developed peroxides as evidenced by the formation of a black precipitate when the hydrocarbon contacted mercury. 1,3,5-Trimethylbenzene (Eastman, practical grade) was dried over $CaSO_4$, distilled under reduced pressure from over cal-

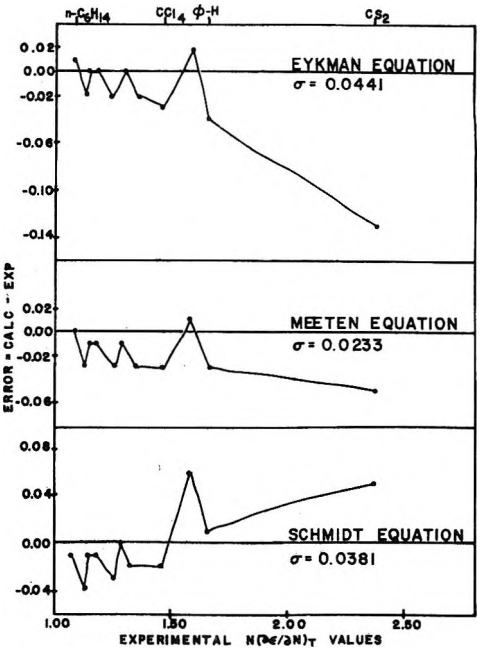

Figure 1. Comparison of $N(\partial\epsilon/\partial N)_T$ values for pure liquids at 23° calculated from the empirical equations of Eykman, of Meeten, and of Schmidt. From left to right the liquids are *n*-hexane, methyl ethyl ketone, isooctane, *n*-octane, *n*-decane, cyclohexane, *n*-hexadecane, carbon tetrachloride, toluene, benzene, and carbon disulfide.

Table I: Isothermal Compressibilities Estimated from the Rayleigh Scattering of the Pure Liquids, 30°

Compound	$K_T \times 10^{12}$, cm² dyn⁻¹
Benzene	102.8 ± 0.1
1,2,4-Trimethylbenzene	80 ± 3
1,3,5-Trimethylbenzene	89 ± 1
Nitromethane	68 ± 11
Nitroethane	63 ± 1.5
1-Nitropropane	65
2-Nitropropane	70 ± 1.5

(14) J. F. Eykman, *Recl. Trav. Chim. Pays-Bas*, **14**, 185 (1895).

(15) G. H. Meeten, *Nature*, **218**, 761 (1968).

(16) R. L. Schmidt, *J. Colloid Interface Sci.*, **27**, 516 (1968).

(17) "International Critical Tables," Vol. III, McGraw-Hill, New York, N. Y., 1926, p 35.

(18) M. S. Malmburg and E. R. Lippincott, *J. Colloid Interface Sci.*, **27**, 591 (1968).

cium hydride, and distilled a second time from over metallic sodium, bp 79° at 42 Torr. Nitrogen was bubbled through the distillate if it was to be stored several days before using.

The nitroparaffins were purified by drying over $CaSO_4$ and distilling under reduced pressure: nitromethane, Fisher Reagent grade, bp 60° at 183 Torr; nitroethane, Matheson Coleman and Bell, practical grade, bp 57° at 97 Torr; 1-nitropropane, Eastman, practical grade, bp 74° at 97 Torr; 2-nitropropane, Eastman practical grade, bp 61° at 100 Torr. Nitromethane-d_3 (Diaprep, Inc., 99% minimum isotropic purity) was used as received. Refractive indices only are reported in this paper for 1-nitropropane and nitromethane-d_3.

Sample Preparation. Solutions were prepared by weight. Solutions for the density and the differential refractometer measurements were prepared in a special weighing bottle[19] which allowed solution compositions to be corrected for vapor losses. Just prior to making either the light scattering or depolarization measurements, the solutions were filtered through a Flotronics membrane silver filter (FM-25 0.2 μ) directly into the sample cell.

Light Scattering. All light scattering measurements were made with a Brice-Phoenix Series 2000 universal light scattering photometer. Details of the measurement and instrument calibration procedures were given in earlier papers.[11,16] Measurement of depolarization using the angular dependence of scattering employed in previous work[11,12] was found to be unsatisfactory for these solutions. In the present work the depolarization values were measured by determination of the intensity of the horizontally and vertically polarized scattered light at 90° to the incident beam. Benzene was used as the calibration standard for the instrument and all depolarization values were corrected additively by an amount necessary to correct the depolarization of benzene to 0.41 and 0.42 at 546 and 436 nm, respectively. Measurements were carried out at the 436-nm wavelength only for the 1,3,5-trimethylbenzene–nitroethane solutions because of a slight fluorescence of nitromethane and 2-nitropropane at that wavelength. The total Rayleigh scattering, R_{90}, and the depolarization, ρ_μ, are given in Table IV.[2]

Refractive Index and Its Change with Composition. The refractive indices of nitroethane, 1-nitropropane, and 2-nitropropane were measured at the sodium D (589 nm) and the mercury e (546 nm) and g (435 nm) wavelengths at 30° by the method of minimum deviation.[20] Measurements were made at several temperatures near 30° and the 30° refractive index given in Table II was obtained by a linear extrapolation in temperature. Refractive indexes of the pure hydrocarbons[21] and nitromethane[22,23] were taken from the literature.

The gradient of the concentration dependence of refractive index is an important term in R_{id} and R^f. Direct determination of values of $\Delta n/\Delta C_2$ and $\Delta n/\Delta X_2$ were made with a Brice-Phoenix Model BP-2000-V differential refractometer. The experimental values of $\Delta n/\Delta X_2$ are shown in Figure 2. Smoothed values of $\Delta n/\Delta X_2$ and values of the solution refractive indices calculated from $\Delta n/\Delta X_2$ values assuming the literature value of the hydrocarbon refractive index is valid are given in Table V.[2]

Table II: The Refractive Index of Some Nitroparaffins[a]

Compound	Temp, °C	Refractive index: Na D 589.3 nm	Hg_e 546.1 nm	Hg_g 435.8 nm
Nitromethane	30	1.37730[b]	1.37948[b]	1.38874[b]
Nitromethane-d_3	30	1.3757[c]	1.3777[c]	1.3869[c]
Nitroethane	30	1.38750 (1.38754)[d]	1.38960	1.39804
1-Nitropropane	30	1.39755 (1.39755)[d]	1.39932	1.40781
2-Nitropropane	30	1.39031 (1.39028)[d]	1.39280	1.40099

[a] Values not footnoted measured by the method of minimum deviation. [b] From ref 22. [c] From differential refractometer measurement between CH_3NO_2 and CD_3NO_2. [d] From ref 23.

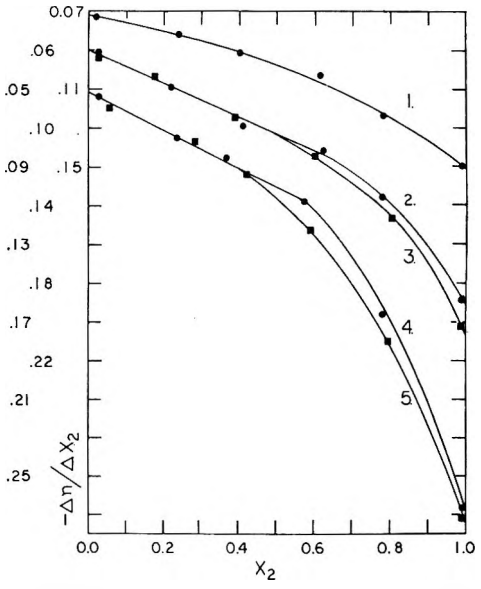

Figure 2. Plots of $-\Delta n/\Delta X_2$ *vs.* X_2, at 30° and 546 nm: 1, 1,3,5-trimethylbenzene (1)–2-nitropropane (2); 2, 1,3,5-trimethylbenzene (1)–nitroethane (2); 3, 1,2,4-trimethylbenzene (1)–nitroethane (2); 4, 1,3,5-trimethylbenzene (1)–nitromethane (2); 5, 1,2,4-trimethylbenzene (1)–nitromethane (2).

(19) R. Battino, *J. Phys. Chem.*, **70**, 3408 (1966).
(20) H. L. Clever and M. L. Taylor, Jr., *J. Chem. Eng. Data*, **16**, 91 (1971).
(21) A. F. Forziati, *J. Res. Nat. Bur. Stand.*, **44**, 373 (1950).
(22) C. J. Thompson, H. J. Coleman, and R. V. Helm, *J. Amer. Chem. Soc.*, **76**, 3445 (1954).
(23) E. E. Toops, Jr., *J. Phys. Chem.*, **60**, 304 (1956).

Table III: Activity Coefficients and Excess Gibbs Free Energy of Mixing at 30° (Free Energy Units, kcal mol^{-1})

	1,2,4-Trimethylbenzene (1) with						1,3,5-Trimethylbenzene (1) with								
	Nitromethane (2)			Nitroethane (2)			Nitromethane (2)			Nitroethane (2)			2-Nitropropane (2)		
X_2	f_1	f_2	ΔG^E	f_1	f_2	ΔG^E	f_1	f_2	ΔG^E	f_1	f_2	ΔG^E	f_1	f_2	ΔG^E
0.0	1.00	(6.41)	0.0	1.00	(6.65)	0.0	1.00	(10.9)	0.0	1.00	(7.62)	0.0	1.00	(4.68)	0.0
0.1	1.02	3.88	0.095	1.04	2.87	0.085	1.04	4.84	0.115	1.04	3.42	0.095	1.03	2.35	0.07
0.2	1.08	2.88	0.165	1.11	1.94	0.13	1.12	3.15	0.19	1.11	2.26	0.15	1.10	1.67	0.105
0.3	1.16	2.31	0.215	1.19	1.58	0.155	1.22	2.43	0.245	1.20	1.79	0.185	1.16	1.40	0.125
0.4	1.28	1.92	0.245	1.28	1.38	0.165	1.36	1.99	0.275	1.31	1.52	0.20	1.22	1.26	0.13
0.5	1.47	1.63	0.26	1.40	1.23	0.165	1.56	1.67	0.29	1.46	1.34	0.20	1.30	1.18	0.125
0.6	1.74	1.42	0.26	1.57	1.12	0.15	1.89	1.44	0.285	1.65	1.21	0.19	1.38	1.12	0.12
0.7	2.16	1.26	0.235	1.78	1.05	0.125	2.40	1.26	0.255	1.90	1.12	0.165	1.48	1.08	0.10
0.8	2.93	1.14	0.195	1.97	1.01	0.09	3.32	1.13	0.205	2.24	1.06	0.125	1.62	1.04	0.08
0.9	4.87	1.05	0.12	2.11	1.00	0.045	5.41	1.04	0.125	2.84	1.02	0.075	1.91	1.02	0.05
1.0	(12.4)	1.00	0.0	(2.19)	1.00	0.0	(12.4)	1.00	0.0	(4.28)	1.00	0.0	(2.70)	1.00	0.0

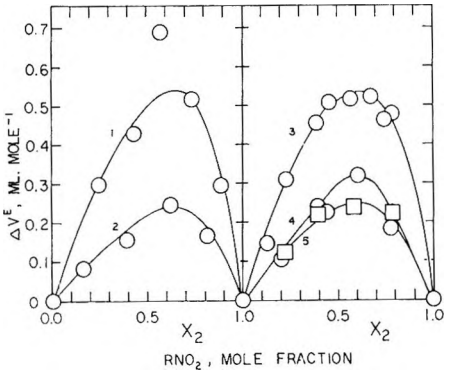

Figure 3. Excess volume *vs.* mole fraction nitroparaffin, 30°: 1, 1,2,4-trimethylbenzene (1)–nitromethane (2); 2, 1,2,4-trimethylbenzene (1)-nitroethane (2); 3, 1,3,5-trimethylbenzene (1)–nitromethane (2); 4, 1,3,5-trimethylbenzene (1)–nitroethane (2); 5, 1,3,5-trimethylbenzene (1)–2-nitropropane (2).

Density and Excess Volume. Solution densities were determined in 15-ml pycnometers with graduated 1.00-mm diameter necks. The temperature for the density measurements was controlled to ±0.02°. The densities are given in Table IV[2] and the excess volumes calculated from the densities are shown in Figure 3.

Results and Discussion

The total intensity Rayleigh scattering, depolarization, and densities of the solutions are given in Table IV.[2] Figure 4 shows the values of R_c, R_d, $R^{\#}$, and R_{id} for the 1,3,5-trimethylbenzene solutions at 546 nm. The 436-nm values from nitroethane–1,3,5-trimethylbenzene are included in the figure. Both the 436- and and 546-nm values were used in the calculation of the thermodynamic properties of the nitroethane solution. Table III gives the solution activity coefficients and excess Gibbs free energy of mixing at 0.1 mole fraction intervals.

All five solutions show positive deviation from ideality in both the excess free energy (Table III) and the excess volume (Figure 3). In the two hydrocarbons

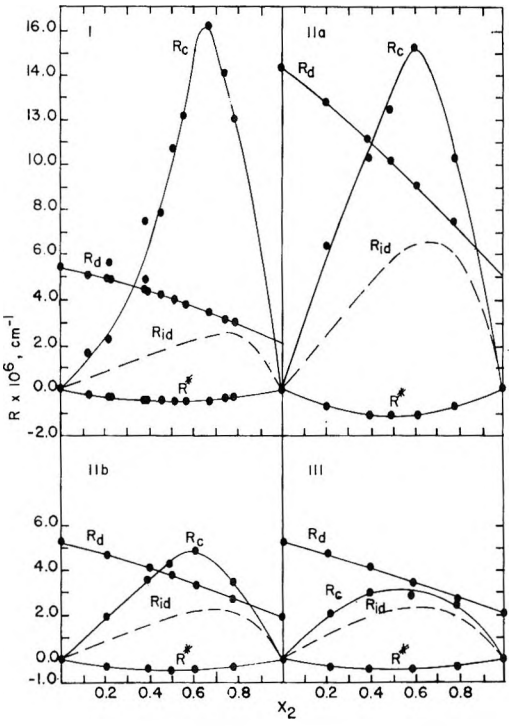

Figure 4. Plots of R_c, R_d, $R^{\#}$, and R_{id} *vs.* X_2, 30°: I, 1,3,5-trimethylbenzene (1)–nitromethane (2), 546 nm; IIa, 1,3,5-trimethylbenzene (1)–nitroethane (2), 436 nm; IIb, 1,3,5-trimethylbenzene (1)–nitroethane (2), 546 nm; III, 1,3,5-trimethylbenzene (1)-2-nitropropane (2), 546 nm.

the order of positive deviation decreases in the order nitromethane > nitroethane > 2-nitropropane. The positive excess free energy appears to increase with increasing basicity of the hydrocarbon for both nitromethane and nitroethane, although the trend is within the experimental accuracy of the method. The excess Gibbs energy from vapor pressure measurements at 45° for nitromethane–benzene[8] and nitroethane–toluene[6] solutions support the suggested trend.

Upper consolute solution temperatures of −16° for nitromethane–1,3,5-trimethylbenzene and −31° for nitromethane–1,2,4-trimethylbenzene were found. No

liquid–liquid immiscibility was observed in the nitroethane or 2-nitropropane solutions down to Dry Ice temperatures.[7]

The solution components have properties that must contribute to the observed excess Gibbs energies of mixing. The aromatic hydrocarbons are basic. The basicity of aromatic compounds increases with the number of methyl groups on the ring,[24] and there are indications that 1,3,5-trimethylbenzene is more basic than 1,2,4-trimethylbenzene.[25] There are uv spectroscopic studies that have been interpreted as nitroparaffin–aromatic hydrocarbon[2,26] and nitroaromatic–aromatic hydrocarbon[3,27] associations which increase in magnitude as the basicity of the hydrocarbon increases. Contrary to what is observed here, such associations would lead to an increasing negative excess Gibbs energy as the hydrocarbon basicity increases.

The nitroparaffins are polar compounds having gas-phase dipole moments[28] of 3.44–3.57 D for nitromethane, 3.61–3.70 D for nitroethane, 3.60–3.75 D for 1-nitropropane, and 3.76 D for 2-nitropropane, and liquid-phase dipole moments[29] of 3.17 and 3.19 D for nitromethane and nitroethane, respectively. Such polar compounds are likely associated through dipole–dipole interactions into dimers and possibly higher order aggregates. In addition it has been suggested that nitromethane may be associated in the pure liquid through hydrogen bonding.[30] The nitroparaffins may occur as nitro and aci forms in equilibrium.[31] It is through the enolic hydrogen in the aci form that hydrogen bonding is proposed in nitromethane forming dimers or possibly higher order aggregates with other aci or nitro forms.

We have attempted several calculations assuming simple models[32] of a competition between the self-association of nitroparaffin for nitroparaffin and the association of nitroparaffin with hydrocarbon. Neither the assumption of the formation of a nitroparaffin dimer and a 1:1 nitroparaffin–hydrocarbon complex or a simple nitroparaffin chain association and a 1:1 nitroparaffin–hydrocarbon complex gave a satisfying fit to the observed free energy.

Another possible explanation of the observed excess Gibbs energy is to attribute it completely to the nature of the self-association of the nitroparaffin. Self-association as a dimer results in a positive excess Gibbs energy while a long-chain-like association in which the size of the "complex" is much greater than the "solvent" can lead to a negative excess Gibbs energy.[33] A combination of dimer and long-chain associations can give a positive excess Gibbs energy of smaller magnitude than dimer formation. Such differences in self-association may appear between nitromethane and either nitroethane or 2-nitropropane in the hydrocarbon solutions.

There have been efforts to interpret depolarization and various functions of depolarization in terms of changes in the liquid-state structure.[16,34] Inspection of the depolarization values in Table IV[2] shows the nitromethane solutions have a pronounced minimum in depolarization about 0.6 mole fraction nitromethane which is not as evident in the nitroethane and 2-nitropropane solutions. It may be that there is a predominant dipole moment effect in nitromethane which is not so pronounced in the other nitroparaffins in solutions of the aromatic hydrocarbons. Small concentrations of aromatic hydrocarbon may be causing sufficient changes in the local field that a change in the local order of the nitromethane results.

The nitroparaffin–aromatic hydrocarbon solutions appear to be quite complex. A more complete thermodynamic description of these solutions would be helpful in making a choice among the various possibilities that lead to the nonideality of these solutions. We plan to measure the heats of mixing of these solutions in the near future.

Acknowledgment. We thank Dr. R. L. Schmidt for his interest and suggestions, and the Emory University Computer center for use of the computer.

(24) E. L. Mackor, A. Hofstra, and J. H. van der Waals, *Trans. Faraday Soc.*, **34**, 2681 (1962).

(25) S. Ehrenson, *J. Amer. Chem. Soc.*, **83**, 4493 (1961); **84**, 2681 (1962).

(26) R. Anderson, R. Cambio, and J. M. Prausnitz, *A.I.Ch.E. J.*, **8**, 66 (1962).

(27) C. C. Thompson, Jr., and P. A. D. deMaine, *J. Phys. Chem.*, **69**, 2766 (1965).

(28) A. L. McClellan, "Tables of Experimental Dipole Moments," W. H. Freeman and Co., San Francisco, Calif., 1963.

(29) E. S. Proskauer, J. A. Riddick, and E. E. Toops, Jr., "Organic Solvents," "Techniques of Organic Chemistry," A. Weissberger, Ed., Vol. VII, Interscience, New York, N. Y., 1955.

(30) R. C. Paul, R. Kaushal, and S. S. Pahil, *J. Indian Chem. Soc.*, **42**, 483 (1965).

(31) D. Turnbull and S. H. Maron, *J. Amer. Chem. Soc.*, **65**, 212 (1943).

(32) J. M. Prausnitz, "Molecular Thermodynamics of Fluid-Phase Equilibria," Chapter 7, Prentice-Hall, Englewood Cliffs, N. J., 1969.

(33) I. Prigogine and R. Defay, "Chemical Thermodynamics," longmans Green and Co., New York, N. Y., 1954, p 419.

(34) Y. Sicotte and M. Rinfret, *Trans. Faraday Soc.*, **58**, 1090 (1962).

Thermodynamics of Aqueous Solutions of Tetrabutylammonium Carboxylates. Model Systems for the Hydrophobic Interaction in Proteins[1]

by Siegfried Lindenbaum[2]

Oak Ridge National Laboratory, Oak Ridge, Tennessee 37830 *(Received May 3, 1971)*

Publication costs assisted by Oak Ridge National Laboratory

Apparent molal heat contents, ϕ_L, and osmotic and activity coefficients at 25° are reported for aqueous solutions of tetrabutylammonium butyrate, valerate, heptylate, pelargonate, and caprate. These data have been used to calculate excess enthalpies, H^{EX}, free energies, G^{EX}, and entropies, TS^{EX}, for these systems. The values for ϕ_L are the largest yet observed for 1–1 electrolytes. These large exothermic heats of dilution are attributed to the increased hydrogen bonding induced in the solvent under the influence of both cationic and anionic hydrophobic groups. The thermodynamics of the dilution of concentrated aqueous solutions of tetrabutylammonium carboxylates is compared to the disorder–order transition in protein denaturation.

Introduction

Thermodynamic studies and other properties of aqueous solutions of tetraalkylammonium salts[3-6] and salts of carboxylic acids[7-9] have suggested that these electrolytes, possessing hydrophobic moieties in their structure, cause increased hydrogen bonding of the solvent. This apparent increased solvent structure in aqueous solutions has been most pronounced for solutions of salts which also form crystalline clathrate hydrates. Tetra-*n*-butylammonium fluoride, for example, forms a clathrate hydrate with composition $Bu_4NF \cdot 32.8H_2O$.[10] Thermodynamic studies of aqueous solutions of Bu_4NF[5,11] have strongly supported the suggestion[6] that tetrabutylammonium ions increase hydrogen bonding in the solvent. Further evidence that this interpretation is correct comes from recent X-ray scattering measurements on aqueous solutions of Bu_4NF.[12] The radial distribution function determined in this study was accurately fitted by a model in which it was assumed that the fluoride ion was indistinguishable from an oxygen atom. The fluoride ion apparently does not interfere, or interferes only minimally, in the formation of the hydrogen-bonded water cage around the hydrophobic tetrabutylammonium ion. The larger halide ions interfere in this hydrophobic structure formation to an increasing extent.[13] This structure formation as measured by apparent molal heat content[4] is greatest for tetrabutylammonium fluoride and diminishes as the size of the halide ion increases and becomes less compatible with the water structure.

The purpose of this study was to determine how the hydrophobic nature of tetraalkylammonium ions would manifest itself in the thermodynamic properties of aqueous solutions if the negatively charged counterion also possessed hydrophobic properties.

Exothermic heats of dilution increasing with hydrocarbon chain length[8,9] were measured for sodium salts of carboxylic acids. Straight-chain carboxylate ions are also apparently effective in increasing the hydrogen bonding of water. It was therefore of great interest to determine the effect on aqueous solvent thermodynamic properties of solutions of tetraalkylammonium carboxylates, salts in which both cationic and anionic moieties have hydrophobic water structure enhancing properties. Some of these salts, for example tetra-*n*-butylammonium butyrate and tetra-*n*-butylammonium valerate, also form crystalline clathrate hydrates,[14] suggesting that in aqueous solution these salts will also increase the hydrogen bonding of the solvent. Since both the cation and anion contribute to the hydrophobic solvent hydrogen bonding or "hydration of the second kind,"[15] it might be speculated that the

(1) Research sponsored by the U. S. Atomic Energy Commission under contract with the Union Carbide Corporation. Presented in part before the Division of Physical Chemistry, H. S. Harned Memorial Symposium, 160th National Meeting of the American Chemical Society, Chicago, Ill., Sept 1970.

(2) Pharmaceutical Chemistry Department, School of Pharmacy, The University of Kansas, Lawrence, Kans. 66044.

(3) S. Lindenbaum and G. E. Boyd, *J. Phys. Chem.*, **68**, 911 (1964).

(4) S. Lindenbaum, *ibid.*, **70**, 814 (1966).

(5) S. Lindenbaum, *ibid.*, **73**, 4334 (1969).

(6) H. S. Frank, *Z. Phys. Chem. (Leipzig)*, **228**, 367 (1965).

(7) H. Snell and J. Greyson, *J. Phys. Chem.*, **74**, 2148 (1970).

(8) S. Lindenbaum, *ibid.*, **74**, 3027 (1970).

(9) S. Lindenbaum, *J. Chem. Thermodyn.*, in press.

(10) R. K. McMullan, M. Bonamico, and G. A. Jeffrey, *J. Chem. Phys.*, **39**, 3295 (1963).

(11) W-Y. Wen, S. Saito, and C. Lee, *J. Phys. Chem.*, **70**, 1244 (1966).

(12) A. H. Narten and S. Lindenbaum, *J. Chem. Phys.*, **51**, 1108 (1969).

(13) (a) J. E. Desnoyers, M. Arel, G. Perron, and C. Jolicoeur, *J. Phys. Chem.*, **73**, 3346 (1969); (b) A. H. Narten, *ibid.*, **74**, 765 (1970).

(14) G. Beurskens, G. A. Jeffrey, and R. K. McMullan, *J. Chem. Phys.*, **39**, 3311 (1963).

heats of dilution of these solutions would be more negative than those of tetrabutylammonium fluoride.

However, it has also been suggested that a special "water structure enforced ion pairing"[16] occurs when both cation and anion are large and hydrophobic. If this interaction persisted in dilute solutions of these salts, the net interaction with the solvent would be diminished, and the enthalpy of dilution would be smaller than that observed for tetrabutylammonium fluoride.

Experimental Section

Solutions of tetra-*n*-butylammonium hydroxide were prepared by treating a solution of pure recrystallized[3] tetra-*n*-butylammonium bromide with freshly precipitated silver hydroxide. The concentration of Bu_4NOH in the filtrate was determined by titrating an aliquot with standard HCl solution. Weighed aliquots of the tetrabutylammonium hydroxide solution were neutralized with stoichiometric amounts of carboxylic acid (Fluka, Puriss).[9] Stock solutions of tetra-*n*-butylammonium butyrate (C_4), valerate (C_5), heptylate (C_7), pelargonate (C_9), and caprate (C_{10}) were prepared in this manner and diluted by weight. All solutions were deliberately prepared to be on the alkaline side of the equivalence point.

Heats of dilution were measured as previously described.[4,5] The slightly alkaline tetrabutylammonium carboxylate solutions were always diluted with 0.001 *m* sodium hydroxide solution in the calorimeter dewar so as to avoid measuring the heat accompanying a hydrolysis or neutralization reaction.

Osmotic coefficients were measured using the gravimetric isopiestic vapor pressure comparison technique.[3,17] Solutions of sodium chloride were used as comparison standards. Difficulty was experienced in achieving equilibrium for dilute solutions of tetrabutylammonium pelargonate and caprate. These salts may have a tendency to decompose or hydrolyze in dilute solution.

Results and Calculations

Apparent molal heat contents, ϕ_L, for Bu_4NBut, Bu_4NVal, and Bu_4NHept are given in Figure 1 as a function of molality. Data for Bu_4NF,[5] NaVal,[9] NaBut,[9] and NaAc[18] are included for comparison.[19]

The data from the isopiestic equilibration studies are summarized in Table I. Solutions whose molalities are listed on the same horizontal line are in isopiestic equilibrium with each other. Osmotic coefficients, ϕ (Figure 2), were calculated using the equation

$$\nu_r m_r \phi_r = \nu m \phi \qquad (1)$$

which is valid for solutions in isopiestic equilibrium.[17] The subscripts, r, refer to the reference electrolyte, sodium chloride; ν is the number of ions into which the electrolyte dissociates; m is the molality (mol/1000 g of water). Mean molal activity coefficients, γ, were calculated from these data with eq 2, where γ_r is the

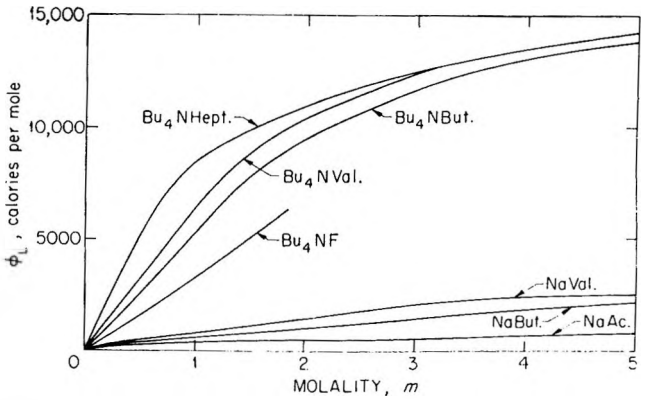

Figure 1. Apparent molal heat contents of aqueous solutions of tetrabutylammonium carboxylates *vs.* molality at 25°. Data for Bu_4NF, NaAc, NaBut, and NaVal are included for comparison.

$$\ln \gamma = \ln \gamma_r + \log R + \int_0^{m_r\gamma_r} \frac{R-1}{m_r\gamma_r}\, dm_r\gamma_r \qquad (2)$$

mean molal activity coefficient of sodium chloride and R is the isopiestic ratio defined by

$$R = \frac{\nu_r m_r}{\nu m} \qquad (3)$$

Osmotic and activity coefficients of sodium chloride were interpolated using the equations of Lietzke and Stoughton[20]

$$\phi = 1 - \frac{S}{A^3 I}\left[(1 + AI^{1/2}) - 2\ln(1 + AI^{1/2}) - \frac{1}{1 + AI^{1/2}}\right] + BI + CI^2 + DI^3 \qquad (4)$$

$$\ln \gamma = -\frac{S}{1 + AI^{1/2}} + (2B)I + (^3/_2C)I^2 + (^4/_3D)I^3 \qquad (5)$$

where $S = 1.17202$ at 25° and for NaCl A, B, C, and D have the values 1.45397, 0.0223565, 0.00930838, and

(15) H. G. Hertz and M. D. Zeidler, *Ber. Bunsenges. Phys. Chem.*, 68, 82 (1964).

(16) R. M. Diamond, *J. Phys. Chem.*, 67, 2513 (1963).

(17) R. A. Robinson and R. H. Stokes, "Electrolyte Solutions," Academic Press, Inc., New York, N. Y., 1959.

(18) V. B. Parker, "Thermal Properties of Aqueous Uni-univalent Electrolytes," NSRDS-NBS2, National Bureau of Standards, Washington, D. C., 1965.

(19) The calorimetric data will appear immediately following this article in the microfilm edition of this volume of the journal. Single copies may be obtained from the Reprint Department, ACS Publications, 1155 Sixteenth St., N.W., Washington, D. C. 20036. Remit check or money order for $3.00 for photocopy or $2.00 for microfiche.

(20) M. H. Lietzke and R. W. Stoughton, *J. Phys. Chem.*, 66, 508 (1962).

Table I: Osmotic and Activity Coefficients of Aqueous Solutions of Tetrabutylammonium Carboxylates at 25°

NaCl[a]			Bu_4NBut			Bu_4NVal		
m	ϕ	γ	m	ϕ	γ	m	ϕ	γ
0.0985	0.933	0.780	0.0956	0.961	0.828	0.0920	0.998	0.924
0.3778	0.920	0.697	0.3412	1.019	0.855	0.3428	1.014	0.969
0.5268	0.921	0.679	0.4622	1.049	0.891	0.4571	1.061	1.033
0.7167	0.926	0.666	0.6066	1.094	0.953	0.6293	1.055	1.045
1.074	0.938	0.656	0.8752	1.152	1.057	0.9647	1.045	1.057
1.165	0.942	0.655	0.9490	1.156	1.072	1.059	1.036	1.050
1.546	0.959	0.658	1.233	1.203	1.181	1.427	1.039	1.062
2.100	0.989	0.672	1.731	1.200	1.254	2.045	1.016	1.045
3.101	1.052	0.720	2.784	1.172	1.325	3.078	1.060	1.104
4.163	1.128	0.798	3.948	1.189	1.439	4.058	1.157	1.250
6.149	1.282	0.994	6.002	1.313	1.780	5.679	1.388	1.750

NaCl[a]			Bu_4NHept			Bu_4NPel			Bu_4NCap		
m	ϕ	γ	m	ϕ	γ	m	ϕ	γ	m	ϕ	γ
0.1175	0.931	0.769	0.1096	0.997	0.90	0.2050	0.534	0.30	0.3547	0.308	0.15
0.2442	0.922	0.722	0.2385	0.944	0.83	0.6152	0.366	0.14	0.7088	0.318	0.10
0.4317	0.921	0.689	0.5463	0.727	0.59	1.012	0.393	0.11	1.085	0.366	0.08
0.4524	0.921	0.687	0.5896	0.706	0.57	1.051	0.396	0.11	1.122	0.371	0.08
0.8873	0.931	0.660	1.367	0.604	0.37	1.693	0.488	0.09	1.747	0.473	0.07
1.318	0.949	0.655	1.924	0.650	0.34	2.205	0.567	0.08	2.245	0.557	0.06
2.345	1.003	0.681	2.983	0.789	0.35	3.250	0.724	0.09	3.289	0.715	0.06
2.556	1.016	0.691	3.196	0.813	0.35	3.466	0.749	0.09	3.491	0.744	0.06

[a] See ref 17.

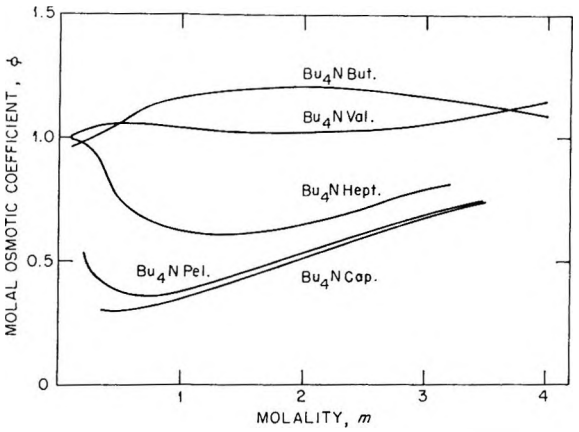

Figure 2. Osmotic coefficients of aqueous solutions of tetrabutylammonium carboxylates at 25°.

-0.00053621, respectively, and I is the ionic strength, equal to the molality for a 1:1 electrolyte.

The calculation of activity coefficients by use of eq 2 requires the evaluation of the integral from infinite dilution to the desired concentration. The isopiestic technique rarely provides accurate data for concentrations below 0.1 m, and for tetrabutylammonium pelargonate and tetrabutylammonium caprate reproducible data could not be obtained below 0.2 and 0.35 m, respectively. The integral term thus requires a guess at the variation of $(R - 1)/m_r\gamma_r$ with $m_r\gamma_r$ from the lowest concentration for which a measured value of R is obtained to infinite dilution. The activity coefficients given in Table I are therefore subject to correction when data in more dilute solutions become available. The values reported for Bu_4NBut and Bu_4NVal are probably accurate within ± 0.005. The activity coefficients of Bu_4NHept, Bu_4NPel, and Bu_4NCap differ much more from those of NaCl, and the integral term of eq 2 is consequently a larger fraction of log γ. These values are therefore subject to a much larger error and should be regarded as approximate estimates. For this reason activity coefficients for these three salts are given to only two significant figures.

Excess molal thermodynamic functions were calculated according to the equations[21]

$$H^{EX} = \phi_L \quad (6)$$

$$G^{EX} = 2RT(1 - \phi + \ln \gamma) \quad (7)$$

$$TS^{EX} = H^{EX} - G^{EX} \quad (8)$$

where H^{EX}, G^{EX}, and S^{EX} are the excess molal enthalpy, free energy, and entropy, respectively. These quantities are plotted in Figure 3 for five tetrabutylammonium carboxylates and also for tetrabutylammonium fluoride to serve as a basis for comparison. The osmotic and activity coefficients required for the calculation of G^{EX} for Bu_4NF were taken from the paper of Wen, Saito, and Lee.[11] The apparent molal heat contents of aqueous solutions of Bu_4NF have also been reported.[5]

(21) H. L. Friedman, "Ionic Solution Theory," Interscience, New York, N. Y., 1962.

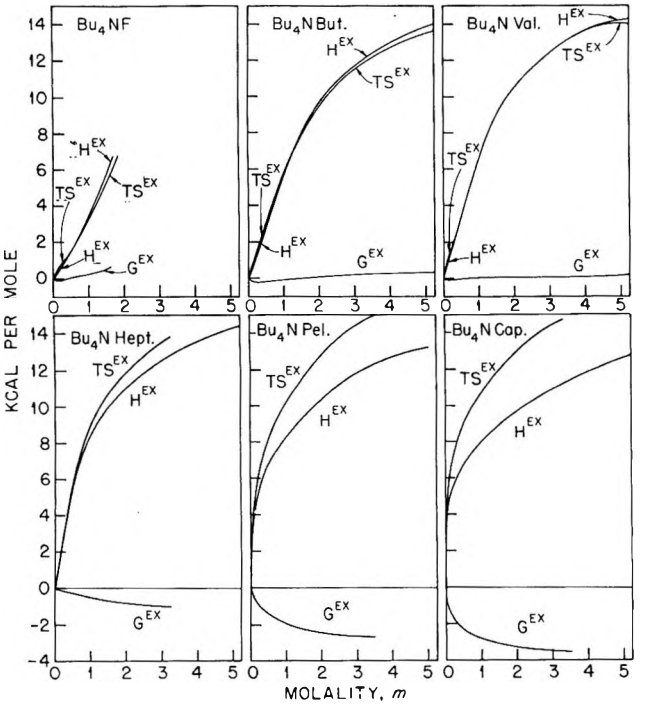

Figure 3. Excess thermodynamic functions *vs.* molality for aqueous solutions of tetrabutylammonium carboxylates at 25°.

Discussion

The apparent molal heat contents of aqueous solutions of tetrabutylammonium carboxylates are larger than those of any other 1–1 electrolyte reported in the literature. These exothermic heats of dilution are attributed to the formation of more complete hydrogen-bonded water cages as water is added in the dilution process. The increase of ϕ_L with concentration for tetraalkylammonium halides has been attributed to[22a,b] an increase in the overlap of the hydration cages with concentration. This overlap is even greater for tetrabutylammonium carboxylates since both cations and anions compete for the available water molecules to form hydration spheres. For this reason, ϕ_L for Bu_4NBut at a given molality is far greater than the sum of ϕ_L for Bu_4NF[5] and ϕ_L for NaBut[9] at the same molality.[8]

These large values of ϕ_L or H^{EX} (Figure 3) are also paralleled by large values of TS^{EX}. This change in entropy on dilution is a measure of the increased structure or order in the solution per mole of solute for the transition from the overlap (disorder) condition in concentrated solution to the completed hydrophobic hydration sphere (ordered) condition at infinite dilution.

The magnitude of TS^{EX} increases with the carboxylate chain length over the entire concentration range. H^{EX} is almost identical with TS^{EX} for Bu_4NBut and Bu_4NVal over the concentration range studied. In concentrated solution H^{EX} decreases with increasing carboxylate chain length and G^{EX} becomes more negative. These lower values for G^{EX} at higher concentrations also suggest increased association or overlap as the size of the anion increases. The osmotic coefficients (Figure 2) appear to be too large to allow for ion association or ion pairing, especially for Bu_4NBut and Bu_4NVal. However, it has been pointed out by Friedman and Rasaiah[23] that large osmotic coefficients may be expected on the basis of the excluded volume of ions having such large ionic radii. The large values of ϕ given in Figure 2 for Bu_4NBut and Bu_4NVal do not therefore necessarily provide evidence that ion association does not occur.

Hydrophobic Bonding

The interaction between hydrophobic species in aqueous solutions may be compared to the interaction between neighboring nonpolar groups in the native conformation of proteins. It has been suggested by Kauzmann[24] that the hydrophobic moieties are attracted and stabilized in the native conformation because of the unfavorable negative entropy change accompanying the interaction of these unfolded hydrophobic groups with the solvent. This solvent induced stabilization has been referred to as "hydrophobic bonding" or, more correctly, the "hydrophobic interaction." Theoretical calculations[24-26] and thermodynamic studies[27] have tended to support this mechanism.

Our interpretation of the thermodynamics of dilution of aqueous solutions of tetrabutylammonium carboxylates is similar to the "hydrophobic interaction" interpretation of protein denaturation. Concentrated solutions of Bu_4NBut, for example, with extensive overlap of hydration spheres or possibly ion association, may be compared to a protein in its native configuration. The dilution process for Bu_4NBut solutions is accompanied by a loss in entropy due to the formation or completion of hydration spheres; this process is analogous to the denaturation process in which nonpolar groups on a protein are exposed to the solvent, leading to the formation of hydrogen-bonded water cages. The thermodynamics of dilution of Bu_4N carboxylate solutions and the denaturation of proteins suggest a disorder–order transition. Aqueous solutions of tetrabutylammonium carboxylates may therefore serve as model systems for proteins stabilized in their native configuration by the "hydrophobic interaction."

(22) (a) R. H. Wood, H. L. Anderson, J. D. Beck, J. R. France, W. E. deVry, and J. L. Soltzberg, *J. Phys. Chem.*, **71**, 2149 (1967); (b) R. H. Wood and H. L. Anderson, *ibid.*, **71**, 1871 (1967).

(23) H. L. Friedman and J. C. Rasaiah, private communication; see also J. C. Rasaiah, *J. Chem. Phys.*, **52**, 704 (1970).

(24) W. Kauzmann, *Advan. Protein Chem.*, **14**, 1 (1959).

(25) G. Nemethy and H. A. Scheraga, *J. Phys. Chem.*, **66**, 1773 (1962).

(26) G. Nemethy, *Angew. Chem., Int. Ed. Engl.*, **6**, 195 (1967).

(27) J. F. Brandts and L. Hunt, *J. Amer. Chem. Soc.*, **89**, 4826 (1967).

An important difference between the model for protein denaturation proposed by Kauzmann and the model suggested in this paper should be pointed out. The Kauzmann model consists of the transfer of an organic molecule from an organic solvent to a dilute aqueous solution, whereas the model proposed here consists of the transfer of a tetraalkylammonium salt from a concentrated aqueous solution to a dilute aqueous solution. Whereas the heat and entropy behave similarly for these two reactions the volume changes may be different. For the Kauzmann model the volume change is *negative*, whereas for the dilution of tetraalkylammonium halides[28] the volume change is *positive*.[29] Apparent molal volumes of sodium carboxylates in aqueous solution however *decrease* on dilution.[30] Volumes of tetrabutylammonium carboxylates have not been reported and would be of great interest. Further investigations will be required to determine which of these model systems more closely resembles the hydrophobic interaction–denaturation process in proteins.

(28) W. Y. Wen and S. Saito, *J. Phys. Chem.*, **68**, 2639 (1964).

(29) The author is indebted to Dr. J. F. Brandts for pointing out this important difference between the two models.

(30) G. M. Watson and W. A. Felsing, *J. Amer. Chem. Soc.*, **63**, 410 (1941).

Levitation Calorimetry. IV. The Thermodynamic Properties of Liquid Cobalt and Palladium

by J. A. Treverton and J. L. Margrave*

Department of Chemistry, Rice University, Houston, Texas 77001 *(Received December 2, 1970)*

Publication costs assisted by the U. S. Atomic Energy Commission

Levitation calorimetry has been used to study the thermodynamic properties of liquid cobalt and palladium. Heats of fusion and specific heats for the liquid metals are summarized below. The emissivities of the liquid metal surfaces were also determined.

	ΔH_m, cal/g-atom	ΔS_m, cal/deg K g-atom	$C_p(l)$, cal/deg K g-atom	$\mathcal{E}_{\text{H500 Å}}^{\text{liquid}}$ (at mp)
Cobalt	3670 ± 70	2.08 ± 0.04	11.58 ± 0.19	0.358 ± 0.006
Palladium	3940 ± 70	2.16 ± 0.04	9.18 ± 0.23	0.374 ± 0.004

Introduction

This publication presents the results of an investigation of the thermodynamic properties of liquid cobalt and palladium by levitation calorimetry. These determinations were made as part of a general program to provide thermodynamic data for liquid metals with melting points above 1500°. Most of these elements have not been studied before although the data would have many important practical[1] and theoretical[2] applications.

Liquid cobalt has been studied previously,[3–6] and two recent determinations of the heat of fusion[5,6] agree well. However, there is only one recent determination of the specific heat,[6] and this was made over a relatively short temperature range (90°). It appeared worthwhile, therefore, to repeat the determination here and obtain C_p values over the larger temperature ranges possible in levitation calorimetry. No previous experimental thermodynamic data are available for liquid palladium.

New emissivity data were determined to correct the brightness temperatures of levitated samples to their true temperatures.

Experimental Section

Materials. Foils (0.001 and 0.005 in.; 99.5% purity)

(1) J. L. Margrave, "Thermodynamic Properties of Liquid Metals, High Temp.–High Press.," in press.

(2) J. A. Treverton and J. L. Margrave, *J. Chem. Thermodyn.*, in press.

(3) R. Wust, A. Meuthen, and R. Durrer, *Forsch. Gebiete Ingenieurw.*, 204 (1918).

(4) S. Umino, *Sci. Rept. Tohoku Univ., First Ser.*, **15**, 576 (1926).

(5) O. Vollmer, R. Z. Kohlhaas, and M. Braun, *Z. Naturforsch.*, **21**, 181 (1966).

(6) O. Kubaschewski, *Z. Elektrochem.*, **54**, 275 (1950).

for lining the calorimeter and rod (0.25 in. diameter; 99.95% purity) for the levitation samples were purchased from A. D. MacKay Inc. All materials were used without further purification.

Procedure. Essentially the calorimeter was a drop calorimeter in which the furnace was replaced by a glass chamber containing a radiofrequency heating and levitation coil. Temperatures of the levitated sample were measured by a Leeds and Northrup 8641 automatic recording optical pyrometer (serial No. 1720818). A Dymec quartz thermometer (Model 28 A) was used to monitor the temperature rise of the calorimeter. A full description of the apparatus appears in ref 7 and 8.

Results

Unless otherwise stated all uncertainty intervals quoted in this section are twice the standard deviation of the mean.

Temperature Measurement. The optical pyrometer was calibrated using the IPTS-1948 temperature scale,[9] and this scale was used in all the following calculations. Conversion of the data to the IPTS-1968 scale can be made using the data given in ref 10.

All pyrometer temperatures were corrected for window absorbance and emissivity. The equations used to make the corrections are given in ref 11.

The Determination of Emissivity. As has already been reported for most of the other elements studied by levitation calorimetry,[2,8] the melting points of both cobalt and palladium were clearly defined by plateaus in the temperature–time trace obtained from the pyrometer. Correction of the plateau temperature for window absorbance gave the brightness temperature of the liquid metal at its melting point. The relationship given in ref 11 between true and apparent temperatures was then used to determine the emissivities. The results of the determination are summarized in Table I.

Table I: Emissivity Determination

	Cobalt	Palladium
No. of determinations	6	5
Mean brightness melting point, K	1633.1 ± 2	1689.0 ± 2
True melting point, K	1766	1825
Reference for melting point	9	9
Emissivity	0.358 ± 0.006	0.374 ± 0.005
Emissivity reported in ref 13	0.36	0.37

Calorimetric Results. The calorimetric results are summarized in Tables II and III. Experiments no. 6 for cobalt and no. 8 and 10 for palladium were rejected because of poor temperature control of the samples, prior to dropping them into the calorimeter. Cobalt experiments no. 11, 12, and 13 were also rejected as the generator coil was inducing eddy currents in the calorimeter block during these experiments. A linear least-squares fit was made for each set of data, and the equations derived were used to calculate the enthalpy at each experimental temperature. The mean per cent deviation of the experimental and calculated enthalpies of 0.56% for cobalt and 0.54% for palladium lie close to the limits expected when optical pyrometry is used to determine temperatures.

Table II: Results of the Calorimetric Measurements on Liquid Cobalt

Experiment no.	Temperature, K	$H_T - H_{298}$,[a] cal/g-atom Exptl	Calcd from eq a	% deviation[b]
19	1774	16,770	16,630	−0.8
15	1807	16,900	17,010	0.7
14	1873	17,850	17,780	−0.3
2	1893	18,010	18,010	−0.1
1	1951	18,790	18,680	−0.6
3	1998	19,170	19,220	0.3
4	2081	20,050	20,190	0.7
5	2086	20,050	20,240	1.0
7	2193	21,570	21,480	−0.4
8	2306	22,620	22,790	0.8
9	2326	23,140	23,020	−0.5
10	2345	23,390	23,240	−0.6

[a] The linear least-squares fit to the above data is

$$H_T - H_{298} = 11.5822T - 3916.32 \text{ cal/g-atom} \quad (a)$$

The standard deviation of the experimental from calculated points = 120 cal/g-atom. [b] The average per cent deviation = 0.6%.

Determination of ΔH_m, ΔS_m, and C_p. Further analysis of the data in Tables II and III gave

$$H_T - H_{298} = 11.5822\ (\pm 0.1962)(T - T_m) + 16{,}538.0\ (\pm 67) \text{ cal/g-atom} \quad (1)$$

for cobalt and

$$H_T - H_{298} = 9.1766\ (\pm 0.2282)(T - T_m) + 15{,}023.0\ (\pm 74) \text{ cal/g-atom} \quad (2)$$

for palladium.

The error limits included in these equations are estimates of the standard deviations of the slopes and intercepts of all the equations that would be obtained if

(7) D. W. Bonnell, A. K. Chaudhuri, A. L. Ford, and J. L. Margrave, *High Temp. Sci.*, **2**, 203 (1970).

(8) J. A. Treverton and J. L. Margrave, Proceedings of 5th Symposium on Thermophysical Properties, Boston, Mass., Oct 2, 1970, pp 489–494.

(9) H. F. Stimson, *J. Res. Nat. Bur. Stand.*, **42**, 209, 217 (1949); *ibid.*, **65A**, 139 (1961).

(10) F. D. Rossini, *J. Chem. Thermodyn.*, **2**, 447 (1970).

(11) W. D. Kingery, "Property Measurement at High Temperatures," 1st ed, Wiley, New York, N. Y., 1959, p 12.

Table III: Results of the Calorimetric Measurements on Liquid Palladium

Experiment no.	Temperature, K	$H_T - H_{298}$,[a] cal/g-atom Exptl	Calcd from eq b	% deviation[b]
9	1846	15,170	15,220	0.3
1	1890	15,730	15,620	−0.7
3	1907	15,720	15,780	0.3
2	1932	16,020	16,010	−0.1
4	1957	16,320	16,230	−0.6
15	2023	16,700	16,850	0.9
11	2045	16,940	17,040	0.6
14	2082	17,260	17,380	0.7
12	2132	17,940	17,840	−0.6
13	2171	18,450	18,200	−1.4
7	2225	18,730	18,690	−0.2
5	2226	18,670	18,700	0.2
6	2334	19,590	19,700	0.5

[a] The linear least-squares fit to the above data is

$$H_T - H_{298} = 9.1766T - 1724.34 \text{ cal/g-atom} \quad \text{(b)}$$

The standard deviation of the experimental from calculated points = 110 cal/g-atom. [b] The average per cent deviation = 0.5%.

the series of experiments on each metal were to be repeated infinitely.

Using the solid data of ref 12 and melting points from ref 9 and eq 1 and 2, the heats and entropies of fusion were calculated. The slopes of (1) and (2) gave the liquid specific heats. Finally, enthalpy, entropy, and free energy functions were calculated and these are summarized in Tables IV and V.

Table IV: Thermodynamic Functions for Liquid Cobalt

Temperature, K	$H_T - H_{298}$, cal/g-atom	$S_T - S_{298}$, cal/(K g-atom)	$-\frac{G_T - H_{298}}{T}$, cal/(K g-atom)
1766	16,540	16.39	14.20
1800	16,930	16.61	14.38
1850	17,510	16.93	14.64
1900	18,090	17.24	14.90
1950	18,670	17.54	15.15
2000	19,250	17.83	15.38
2050	19,830	18.12	15.63
2100	20,410	18.40	15.86
2150	20,990	18.67	16.09
2200	21,560	18.94	16.32
2250	22,140	19.20	16.54
2300	22,720	19.45	16.75
2350	23,300	19.70	16.96
(2400)[a]	(23,880)	(19.94)	(17.17)
(2450)	(24,460)	(20.18)	(17.38)
(2500)	(25,040)	(20.42)	(17.58)
(2550)	(25,620)	(20.65)	(17.78)

[a] Values in parentheses were obtained by extrapolation beyond the limits of the experimental measurements.

Table V: Thermodynamic Functions for Liquid Palladium

Temperature, K	$H_T - H_{298}$, cal/g-atom	$S_T - S_{298}$, cal/(K g-atom)	$-\frac{G_T - H_{298}}{T}$, cal/(K g-atom)
1825	15,020	14.77	15.57
1850	15,250	14.89	15.69
1900	15,710	15.14	15.91
1950	16,170	15.38	16.12
2000	16,630	15.61	16.33
2050	17,090	15.84	16.54
2100	17,550	16.06	16.74
2150	18,010	16.27	16.93
2200	18,460	16.48	17.13
2250	18,920	16.69	17.32
2300	19,380	16.89	17.50
2350	19,840	17.09	17.68
(2400)[a]	(20,300)	(17.28)	(17.86)
(2450)	(20,760)	(17.47)	(18.04)
(2500)	(21,220)	(17.66)	(18.21)

[a] Values in parentheses are obtained by extrapolation beyond the limits of experimental measurements.

Discussion

Emissivity Data. It will be seen from Table I that the experimental emissivity values for both metals agree closely with the values reported in ref 13. In both cases the reported values lie within the uncertainty limits of the experimental results. The agreement provides further evidence for the validity of the experimental technique used.

Variation of Emissivity with Temperature. The results obtained for cobalt and palladium do not suggest any change in emissivity with increase in temperature. Significant changes would probably produce a systematic deviation of the experimental points from the least-squares straight line fit, and this is not observed for either element over the temperature ranges studied.

It might be argued that the effect of change in emissivity is being cancelled out by a superimposed curvature in the enthalpy *vs.* temperature plot. Until reliable emissivity data become available over wide temperature ranges or new methods of temperature measurement at high temperatures become available, this question will not be completely resolved. A wide range of metals has now been studied by levitation calorimetry[2,7,8] and in none of them has any curvature in the enthalpy–temperature plots been observed. It is hard to believe that the exact cancelling out of the two effects would occur in every case, unless both effects are insignificant.

Comparison with Previous Work. Cobalt and pal-

(12) R. Hultgren, R. L. Orr, and K. K. Kelley, "Supplement to Selected Values of Thermodynamic Properties of Metals and Alloys," Lawrence Radiation Laboratory, Berkeley, Calif. (Cobalt, 1966, and Palladium, 1968).

(13) W. F. Roeser and H. T. Wensel, "Handbook of Chemistry and Physics," 50th ed, The Chemical Rubber Co., Cleveland, Ohio, 1969, p E 273.

Table VI: Summary of Experimental Data and Comparison with Previously Reported Values

	Cobalt	Reference	Palladium	Reference
ΔH_m, cal/g-atom	3670 ± 70	This work	3940 ± 70	This work
	3870 ± 60	5	(4197)[a]	12
	3750 ± 300	6		
C_p, cal/(K g-atom)	11.58 ± 0.19	This work	9.18 ± 0.23	This work
	9.68	5	(8.30)	12
ΔS_m, cal/(K g-atom)	2.08 ± 0.04	This work	2.16 ± 0.04	This work

[a] Values in parentheses are estimates.

Table VII

Element	T_M, K	C_p^{liq} at T_M	$H_{T_M} - H_{298}$, cal/g-atom	ΔH_M, cal/g-atom	ΔS_M, cal/deg K g-atom
Co	1767	11.96 ± 0.27	16,494 ± 94	3600 ± 90	2.04 ± 0.05
Pd	1827	9.84 ± 0.33	15,076 ± 87	4000 ± 90	2.19 ± 0.05

ladium samples were dropped into the calorimeter with maximum temperatures of 2360 and 2339 K, respectively. Excessive vaporization of the liquid samples prevented calorimetric measurements at higher temperatures.

The levitation calorimetry results for cobalt do not agree well with the previously reported values (see Table VI) although the heat of fusion does lie within the uncertainty limits of the value reported by Kubaschewski.[6] The heat of fusion of Vollmer, Kohlhaas, and Braun[5] is 10% higher, and their specific heat is 20% lower than the values reported here. Because the C_p and ΔH_m measurements were determined from data obtained over a much larger temperature range (600 K as opposed to 90 K) and also because of the freedom from uncertainties due to container contamination, it is felt that the levitation calorimetry results are more reliable.

The agreement of the experimental and estimated data for palladium is relatively poor, but similar comparisons for other liquid metals have also shown large discrepancies.[2,8]

Note Added in Proof. Conversion of the data for Co and Pd to the new temperature scale, IPTS-1968, and with a small correction for radiation losses during the fall into the calorimeter leads to the improved values shown in Table VII.

Acknowledgments. Calorimetric research at Rice University is supported by the U. S. Atomic Energy Commission, the National Aeronautics and Space Administration, and the Robert A. Welch Foundation.

Thermal Negative Ion Emission from Binary Cesium Halide Mixtures on a Niobium Surface[1]

by Hiroyuki Kawano

Department of Chemistry, Faculty of Science, Ehime University, Bunkyo-Cho, Matsuyama, 790, Japan
(Received June 4, 1971)

Publication costs borne completely by The Journal of Physical Chemistry

Time variation of thermal negative ion emission was examined with unitary and binary systems of cesium halides on a niobium wire at 1450°. For unitary systems the emission patterns of F^-, Cl^-, Br^-, and I^- were essentially the same. In binary systems, however, a "suppression effect," similar to that in the case of thermal positive ion emission from binary alkali metal iodides, was observed. Namely, the emission pattern of the heavier halide ion (X_H^-) was quite different from the corresponding pattern in the unitary system, and also the integrated ion currents of Cl^-, Br^-, and I^- were reduced to 12, 41, and 52% by the presence of CsF, CsCl, and CsBr, respectively. These changes were not observed for the lighter halide ion (X_L^-). The present results can be explained by a "recombination model" proposed in the previous work. Namely, the observed effect results from the fact that the presence of CsX_L enhances the recombination of X_H^- with Cs^+ on the emitting surface and hence promotes the vaporization of X_H^- in the form of CsX_H. Ionization efficiencies of F^-, Cl^-, Br^-, and I^- emitted from the corresponding unitary systems of CsX are 0.074, 0.016, 0.0051, and 0.0020%, respectively.

Introduction

When a binary mixture of alkali metal iodides is heated on a metal surface, the positive ion current of the lighter alkali metal (M_L) is considerably reduced, although that of the heavier one (M_H) remains unchanged. This phenomenon was reported as a "suppression effect" in a previous paper,[2] and also a "recombination model" was proposed to explain this effect. Namely, the presence of the heavier alkali metal iodide (M_HI) enhances the recombination of M_L^+ with I^- on the filament surface.[2] This model suggests that an element with a lower ionization efficiency is suppressed in ion emission by the presence of another element with a higher ionization efficiency. One would expect a similar phenomenon to occur in thermal negative ion emission also.[3] When a binary cesium halide mixture, for example, is heated to a high temperature on a metal surface, it may be the heavier halogen that is suppressed in ion emission, because calculations similar to the Born–Haber cycle suggest that the heavier halogen is less readily emitted in the form of a negative ion and hence has a lower ionization efficiency. In order to verify these assumptions that the suppression effect may also occur in thermal negative ion emission and that the experimental results to be obtained may be explained reasonably by the recombination model, we have carried out our experiments using a mass spectrometer. The features of the present experiments may be summarized as follows.

(1) An aqueous solution of known concentration of a cesium halide or of a binary mixture of cesium halides was prepared, and a definite volume of the solution was transferred to a niobium filament.

(2) For unitary and binary systems of the halides, negative ion currents were measured according to the time (t) that had elapsed after the heating current of the filament was turned on. By comparing the results between the unitary and binary systems, the effect of a lighter cesium halide (CsX_L) on the emission of a heavier halide ion (X_H^-) from CsX_H was investigated for a variety of systems.

(3) The ionization efficiency ($\beta(X^-)$) of the ion X^- emitted from various sample systems was determined by measuring the ion yield ($Q(X^-)$) collected by a Faraday cage during the period when t = 0 to 60 min. Of the ions emitted for an infinite time, more than 99% were collected during the initial period of 60 min after the filament was heated to 1450°.

(4) To confirm our previous conclusion that the suppression effect does not originate from the change in the work function of the emitting surface,[4] thermal electron current (j) was measured simultaneously with negative ion currents for the various sample systems mentioned above. Contrary to thermal positive ion emission, thermal negative ion emission generally makes it possible to determine the change in work function directly. This is one of the reasons why the suppression effect has been examined in negative ion emission. This paper describes the results obtained in these experiments which verified the above assumptions.

(1) Supported in part by the Grant-in-Aid from the Ministry of Education of Japan.

(2) H. Kawano and H. Inouye, *J. Phys. Chem.*, 71, 712 (1967).

(3) H. Inouye and H. Kawano, *Oyo Buturi*, 38, 1145 (1969).

(4) H. Kawano and H. Inouye, *Mass Spectr.*, 16, 323 (1968).

Experimental Section

The 2.6-cm radius Dempster type single-focusing mass spectrometer employed in the previous work was used with some modifications in this work. The ion source consisted of a niobium wire 0.12 mm in diameter, the central part of which was coiled into a spiral to facilitate coating with the sample solution. The ion drawing-out voltage applied between the filament and the first plate (P_1) of the ion accelerating system was 50 V, the value of which was sufficient enough to arrest a space charge effect due to thermal electrons. The filament was heated to 1450° with a stabilized alternating current. Filament temperature was determined with an optical pyrometer.

Prior to a run, the filament was heated to about 2000° under a pressure of 5×10^{-7} Torr for about 30 hr to remove occluded halogen impurities. Then 1 μl of the sample solution was placed on the filament with a hypodermic microsyringe. The concentration of each cesium halide in every solution was 0.075 M. The halide ion current ($i(X^-)$) reaching the Faraday cage was measured with a vibrating reed electrometer, the maximum sensitivity of which was 1×10^{-16} A/scale division. In order to increase the transmission efficiency ($\tau(X^-)$) of the ion X^- to be studied, both of the defining slits were enlarged to about 1 mm in width, approximately ten times larger than in the previous work. The total negative emission current to P_1 was measured with a microammeter and taken as an approximation of the electron current (j) because the ion current included in the total current was negligible (less than 10^{-2}) compared with the electron current. Except where otherwise stated, the experimental conditions and procedures employed in this work were the same as in the previous work.

Results

A typical pattern of I^- emitted from the unitary system of CsI is shown in Figure 1, together with that of the thermal electron (e^-). Similar patterns were observed for other unitary systems of CsF, CsCl, and CsBr. Namely, the ion current $i(X^-)$ reaches a maximum at $t \simeq 2$ min, after which it decreases monotonically with time. The electron current j, on the other hand, always shows a monotonical decrease. All the ionic and electronic emission curves were similar within experimental errors of about ±15 and ±5%, respectively. They were used as comparison references for binary systems.

Figure 2 indicates the emission curves obtained for a binary system of CsBr–CsI (1:1 in mole ratio) by solid lines and also those for the CsI system by broken lines for comparison. For the electron emission, there exists little difference between the two systems (curves 5 and 6). In the I^- emission, however, there is a great difference between the two. Namely, in the binary system (curve 1), $i(I^-)$ does not show the maximum that appears at $t \simeq 2$ min in the CsI system (curve 2), but it does show a different maximum at a later time when $i(Br^-)$ has decreased to some extent after passing its own maximum at $t \simeq 2$ min. The value of $Q(I^-)$ is reduced to 0.52 ± 0.07 of that in the unitary system of CsI, although the amount of the CsI sample coated on the filament was the same in both of the systems (*i.e.*, 7.5×10^{-8} mol). The presence of CsBr produces a marked change in both the emission pattern and the current of I^-, as indicated by an arrow in Figure 2. On the other hand, the pattern of Br^- in the binary system (curve 3) was essentially the same as in the unitary system of CsBr (curve 4), and $Q(Br^-)$ was also much the same (*i.e.*, 0.99 ± 0.12 of that in the unitary system of CsBr). Thus the I^- emission from CsI is suppressed by the presence of CsBr on the same surface.

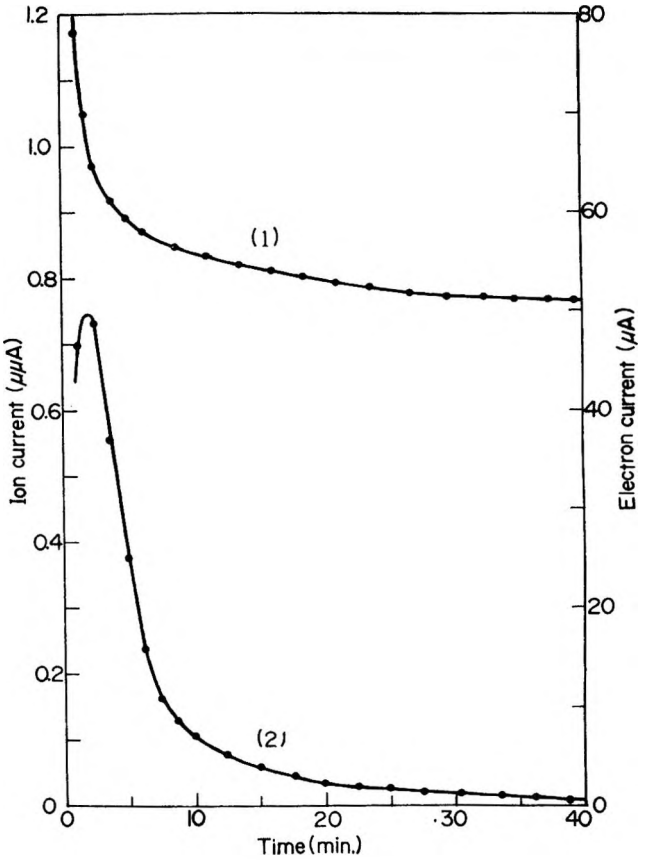

Figure 1. Time variation of both ionic and electronic emission from the unitary system of CsI (7.5×10^{-8} mol) on a niobium wire heated to 1450°: curve 1, e^-; curve 2, I^-.

Similar results were obtained for other binary systems (1:1 in mole ratio). Both the emission patterns and the currents of Cl^- and F^- obtained for CsBr–CsCl and CsCl–CsF systems, respectively, were virtually the same as those for the corresponding unitary systems. However, the Br^- and the Cl^- emission from the respective binary systems mentioned above changed in pattern in the same way as the I^- emission from the CsI–CsBr system changed, and also they reduced in current to 0.41 ± 0.07 and 0.12 ± 0.02, compared with

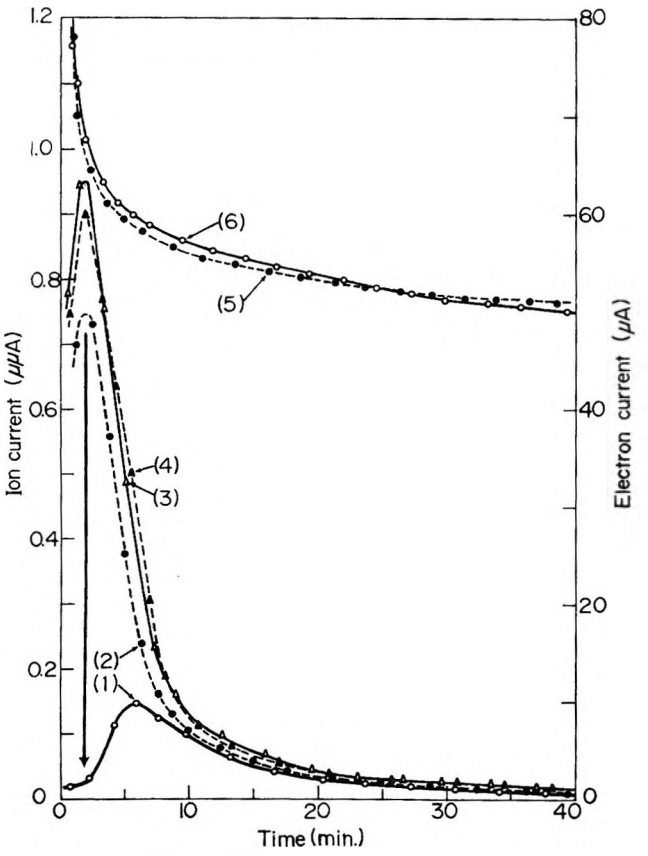

Figure 2. Emission curves obtained for the binary system (CsI–CsBr, 1:1 in mole ratio) and for the unitary systems (CsI and CsBr) on a niobium wire at 1450°: curve 1, I^- from CsI–CsBr; curve 2, I^- from CsI; curve 3, Br^- from CsI–CsBr; curve 4, Br^- from CsBr; curve 5, e^- from CsI; curve 6, e^- from CsI–CsBr.

$Q(Br^-)$ and $Q(Cl^-)$ in the unitary systems of the corresponding halides, respectively.

The ionization efficiency is given by

$$\beta(X^-) = Q(X^-)/\tau(X^-)M(CsX)Ne \qquad (1)$$

Here, $M(CsX)$ is the molar number of the CsX sample coated, N is Avogadro's number, and e is the elementary charge. The results obtained for each unitary cesium halide system of 7.5×10^{-8} mol on the niobium wire at 1450° are as follows: F^-, 0.074 ± 0.009%; Cl^-, 0.016 ± 0.002%; Br^-, 0.0051 ± 0.0008%; I^-, 0.0020 ± 0.0003%. The tendency that $\beta(X^-)$ decreases with the increasing atomic number of the halogen X is also found except for F^- by other workers[5,6] in spite of a large difference in the experimental conditions employed by the three groups of workers.

Discussion

The above results show that the X_H^- emission from CsX_H is changed in pattern and current by the presence of CsX_L. This phenomenon is essentially the same as that observed previously in the positive ion emission. Namely, only one of the two elements coexisting in the form of alkali metal halides with a common cation or anion changes in ion emission pattern and also decreases in ion current, while the other is virtually free from such variations. This result shows that the "suppression effect" occurs in negative ion emission also, as was assumed. The reason for this effect is discussed in detail from three viewpoints as follows.

1. Charge Transfer. A charge transfer reaction, $X_H^- + X_L \rightarrow X_H + X_L^-$, on the filament surface may be suggested as a possible reason for the effect. Namely, a part (ϵ) of the X_H^- ions which would be emitted in the form of gaseous X_H^- ions in the unitary system of CsX_H may leave the ionic state in the binary system of CsX_H–CsX_L because of the charge transfer and evaporate in the form of neutral molecules, $^1/_2(X_H)_2$. If the suppression effect were caused by the above reaction, $i(X_L^-)$ should increase by $\epsilon\tau(X_L^-)$ as $i(X_H^-)$ decreases by $\epsilon\tau(X_H^-)$. Such a result, however, has not been observed in this work; $i(X_L^-)$ is independent of $i(X_H^-)$.

2. Work Function Change. Thermal electron current (j) decreases according as the time t elapses, as may be seen in Figure 1. This result suggests that the work function (ϕ) changes with t. The time variation of the work function, $\phi(t) - \phi(t_0) \equiv \Delta\phi(t)$, can be calculated from eq 2.

$$\Delta\phi(t) = kT \ln j(t_0)/j(t) \qquad (2)$$

where t_0 is the reference time. The result obtained by inserting the data of Figure 1 into eq 2 is shown as curve (1) in Figure 3, where 40 min is taken as t_0. In a short period of t = 0 to 10 min during which the suppression effect occurs to a great extent, ϕ is found to change by about 0.1 eV. Suppose that ϕ also changes when the sample varies from the unitary system (1, CsX_H) to the binary system (2, CsX_H–CsX_L); the work function change, $\phi_1 - \phi_2 \equiv \Delta\phi_{12}$, is given by eq 3 or 4.

$$\Delta\phi_{12}(e^-) = kT \ln j_2/j_1 \qquad (3)$$

$$\Delta\phi_{12}(X_H^-) = kT \ln i_2(X_H^-)/i_1(X_H^-) \qquad (4)$$

where i_1 and i_2 (or, j_1 and j_2) are the emission currents detected at the same time (t) for the CsX_H and the CsX_H–CsX_L systems, respectively. If the suppression effect originates from the change in work function, $\Delta\phi_{12}(X_H^-)$ should be equal to $\Delta\phi_{12}(e^-)$ at any given t, because both X_H^- and e^- were emitted simultaneously from the same surface. In the initial period of 10 min, however, there exists a large discrepancy between the two, as may be seen in Figure 3, where curves (2) and (3) are obtained by inserting the data of Figure 2 into eq 3 and 4, respectively. In addition, $\Delta\phi_{12}(e^-)$ is always in the neighborhood of zero, showing that ϕ is virtually independent of the sample systems investigated. These results may give confirmation for our

(5) J. W. Trischka, D. T. F. Marple, and A. White, *Phys. Rev.*, **85**, 136 (1952).

(6) A. Persky, E. F. Greene, and A. Kuppermann, *J. Chem. Phys.*, **49**, 2347 (1968).

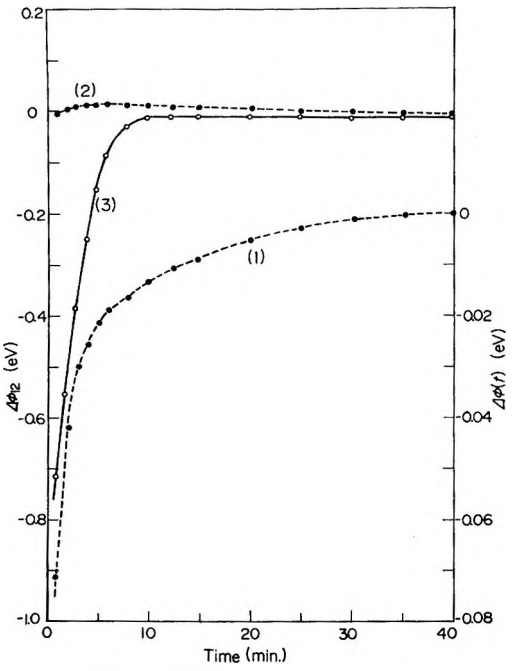

Figure 3. Change in work function calculated from the data of Figure 1 or 2: curve 1, $\Delta\phi(t)$ calculated for e^- emitted from the CsI system by using eq 2; 40 min is taken as the reference time, t_0; curve 2, $\Delta\phi_{12}(e^-)$ calculated for e^- emitted from both the CsI and the CsI–CsBr systems by using eq 3; curve 3, $\Delta\phi_{12}(I^-)$ calculated for I^- emitted from both the CsI and the CsI–CsBr systems by using eq 4.

previous conclusion that the suppression effect cannot be explained reasonably by the change in work function.

3. Recombination. The recombination model proposed in the previous work suggests that it is the element with a lower ionization efficiency that is suppressed in ion emission. For the negative ion emission in this work, $\beta(X^-)$ is found to decrease with the increasing atomic number of X. Therefore, application of this model to the present work leads to the conclusions that the emission of X_H^- is suppressed in the system of CsX_H–CsX_L and that X_H^- is enhanced to recombine with Cs^+ by the presence of CsX_L. Namely, a part (α) of the X_H^- ions which would be emitted as gaseous X_H^- ions in the unitary system of CsX_H recombines on the filament surface with the Cs^+ ions supplied from $Cs^+X_L^-$, and evaporates in the form of neutral molecules CsX_H. Consequently, $i(X_H^-)$ reduces to $1 - \alpha$, as shown schematically in Figure 4. Processes a, c, and d cause thermal ion emission from the cesium halides on the filament. Process b is assumed to explain the suppression effect, which causes additional evaporation in the form of neutral molecules. This model implies that the decrease in ion emission due to the suppression effect is accompanied by the increase in neutral evaporation. This correlation between the two was clarified directly in the previous work, by measuring simultaneously the time variation of both ionic and neutral evaporation from various sample systems.

The recombination fraction of X_H^- is given by

$$\alpha(X_H^-) = 1 - i_2(X_H^-)/i_1(X_H^-) \qquad (5)$$

Figure 5 shows an example of the time variation of $\alpha(I^-)$ and also that of the Br^- emission from the CsBr–CsI system. The patterns of both $\alpha(I^-)$ and $i_2(Br^-)$ are quite similar to each other within experimental error in this work, showing that $\alpha(I^-)$ varies according to $i_2(Br^-)$. Namely, $\alpha(I^-)$ is very large during the time when the Br^- emission is intense and hence when an abundance of spare cesium ions is produced from Cs^+Br^- on the filament surface. Similar results were obtained for the other binary systems investigated. The characteristic that $\alpha(X_H^-)$ alters according to $i_2(X_L^-)$ may give additional support to the recombination model.

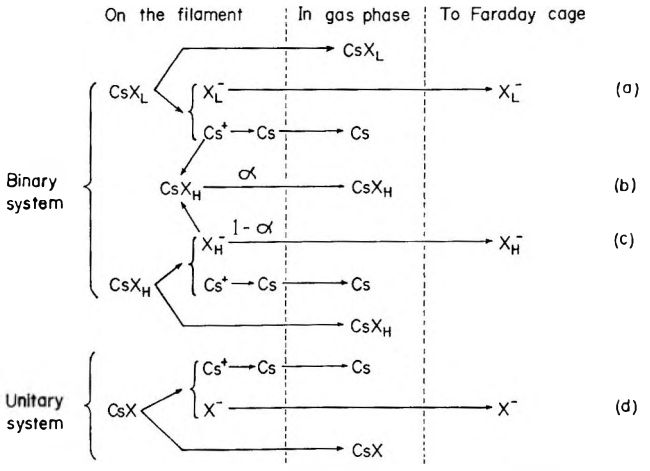

Figure 4. Scheme of the ion emission processes occurring in this experiment. Here, α is the recombination fraction of the X_H^- ions, and is given by eq 5.

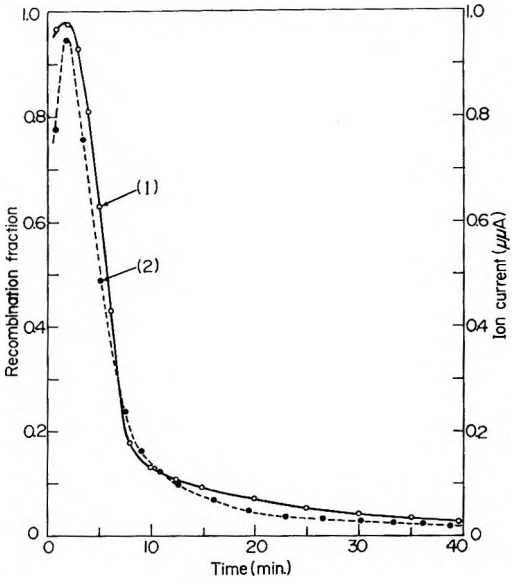

Figure 5. Time variation of the recombination fraction, $\alpha(I^-)$, and the dependence of $\alpha(I^-)$ on the Br^- emission: curve 1, $\alpha(I^-)$ due to the presence of CsBr; curve 2, $i_2(Br^-)$ in the CsI–CsBr system. Curve 1 is obtained from the data of curves 1 and 2 in Figure 2 by using eq 5.

When the two adsorption equilibria, $(Cs^+)_a + (X_H^-)_a \rightleftarrows (CsX_H)_a$ and $(Cs^+)_a + (X_L^-)_a \rightleftarrows (CsX_L)_a$, are coexistent on the filament surface, the following relation holds

$$\frac{K(CsX_H)}{K(CsX_L)} = \frac{[CsX_H]/[X_H^-]}{[CsX_L]/[X_L^-]} = \frac{f(CsX_H)/f(X_H^-)}{f(CsX_L)/f(X_L^-)} \exp\left\{\frac{E(CsX_H) - E(CsX_L)}{kT}\right\} \quad (6)$$

where K is the equilibrium constant, f is the partition function, and E is the energy liberated in the reaction $(Cs^+)_a + (X^-)_a \rightarrow (CsX)_a$. An estimation from thermochemical data by considering a suitable energy cycle indicates that $E(CsX_H) > E(CsX_L)$. Assuming that the preexponential factor in eq 6 is approximately equal to unity, then

$$\frac{d}{d[Cs^+]}\left\{\frac{[CsX_H]}{[X_H^-]}\right\} > \frac{d}{d[Cs^+]}\left\{\frac{[CsX_L]}{[X_L^-]}\right\} \quad (7)$$

Addition of CsX_L to CsX_H causes an increase in the cesium ion concentration and makes the equilibria shift to the right. The inequality in (7) shows that the magnitude of the shift, or the degree of an increase in the concentration ratio $[CsX]/[X]$, is much larger for CsX_H than for CsX_L. Therefore, X_H^- is enhanced to recombine with Cs^+ by the presence of CsX_L on the emitting surface and therefore decreases in ion emission. On the other hand, X_L^- is almost free from such a recombination, and hence the emission of X_L^- is virtually independent of the presence of CsX_H.

These considerations indicate that the suppression effect observed can be explained reasonably by the recombination model without conflict with the experimental results.

Conclusions

In this way our assumptions have been verified. This result leads to the following conclusions. (1) When a binary mixture of alkali metal halides with a common cation or anion is heated to a high temperature on a metal surface, there occurs, more or less, a suppression effect on thermal ion emission, irrespective of the polarity of the ions to be emitted. (2) It is the element (Z_l) with a lower ionization efficiency that is suppressed in ion emission. Namely, the effect occurs in the direction indicated by the series

$$Cs \longrightarrow Rb \longrightarrow K \longrightarrow Na \longrightarrow Li \quad \text{(in positive ion emission)}$$

$$F \longrightarrow Cl \longrightarrow Br \longrightarrow I \quad \text{(in negative ion emission)}$$

The reverse effect does not occur. Namely, the emission of the element (Z_h) with a higher ionization efficiency is independent of the presence of Z_l. (3) This suppression effect originates from the fact that the presence of Z_h enhances the recombination of Z_l with the common cation or anion on the emitting surface and hence promotes the vaporization of Z_l in the form of a neutral molecule of alkali metal halide.

Photoinduced Hole–Electron Recombination in a γ-Irradiated Single Crystal of L-Cystine Dihydrochloride[1]

by Kazuyuki Akasaka,* Shiro Kominami, and Hiroyuki Hatano

Department of Chemistry, Faculty of Science, Kyoto University, Kyoto 606, Japan *(Received March 1, 1971)*

Publication costs borne completely by The Journal of Physical Chemistry

Photoinduced recombination of electrons and holes produced by γ irradiation and subsequently trapped as disulfide ions at 77°K in a single crystal of L-cystine dihydrochloride has been studied by esr and optical absorption spectroscopy. Whereas the disulfide anion gives an absorption around 400 nm, the corresponding cation gives a broad absorption peaking at 550 nm. The wavelength dependence of the photoinduced decay of esr signals in the irradiated crystal has given evidence that the recombination is initiated by the photoexcitation of the cationic species. The first-order nature of the decay indicates that the recombination takes place between the ion pair separated by at least a few molecules as estimated from the line width of the esr signal. An electron tunneling is suggested for the mechanism.

Introduction

In a previous work,[2] we studied the radiation damage process in a single crystal of L-cystine dihydrochloride by esr spectroscopy, in which we reported the production of the disulfide anion by γ irradiation at 77°K. Box and Freund[3] succeeded in observing the esr spectrum for the disulfide cation as well as for the anion in the same system by X-irradiation at 4.2°K. We have reexamined esr spectra from the same crystal γ-irradiated *in the dark* at 77°K and have detected the cationic as well as the anionic radical, both of which are found to be fairly stable even at 77°K, provided that the sample is kept in the dark. These radical ions, however, turned out to be unstable against photoillumination in the visible range at the same temperature. The ions are nothing but electrons and positive holes trapped in appropriate molecular orbitals of the disulfide compound in the crystalline state, and, as will be shown, the photoinduced change is brought about as a result of charge recombination between trapped electrons and holes somehow freed by photoillumination.

The phenomenon of the photoinduced charge recombination in an organic crystal is of considerable interest in relation to the radiation damage process as well as to electronic processes in an assembly of organic molecules, particularly of biological interest.[4] Previous studies on the photoinduced charge recombination process in organic systems such as in organosulfur compounds have been performed mostly in the glassy state[5] and few in a single crystal.[6] By virtue of the anisotropy in the esr spectra in a single crystal, the present system has enabled us to follow the cationic as well as anionic species separately and quantitatively. Moreover, the two oppositely charged disulfide ions can also be distinguished in the optical absorption spectrum.[7] Thus in the present paper, the wavelength dependence of the photoinduced decay of the esr signal in the visible range has provided evidence that it is the excitation of the cationic species, rather than the anionic species, that initiates the charge neutralization process in an irradiated single crystal of L-cystine dihydrochloride. A possible mechanism for the recombination process will be discussed.

Experimental Section

Single crystals of L-cystine dihydrochloride were obtained as previously described.[2] γ irradiation was performed in the dark at 77°K with ^{60}Co γ rays at a dose rate of 2.5×10^4 R/hr to a total dose of about 10^6 R. Uv irradiation was done also at 77°K for about 2 hr with a 400-W low-pressure mercury lamp (Toshiba H400-P) placed at about 10 cm from a crystal in a quartz tube. Esr measurements were done, usually right after irradiation, with X-band esr spectrometers (JEOL P-10 and MEX), both with a resonance cavity of TE_{102} mode with a window for light illumination. A temperature-control accessory was used for the study of the effect of temperature on the stability of the radi-

(1) An earlier part of the work was reported in the 9th Japanese Symposium on Radiation Chemistry, Osaka, Oct 1966.

(2) K. Akasaka, S. Ohnishi, T. Suita, and I. Nitta, *J. Chem. Phys.*, **40**, 3110 (1964).

(3) H. C. Box and H. G. Freund, *ibid.*, **41**, 2571 (1964).

(4) D. D. Eley and D. I. Spivey, *Trans. Faraday Soc.*, **49**, 79 (1960); A. Szent-Györgyi, "Introduction to a Submolecular Biology," Academic Press, New York, N. Y., 1960, p 50.

(5) (a) W. H. Hamill in "Radical Ions," E. T. Kaiser and L. Kevan, Ed., Interscience Publishers, New York, N. Y., 1968, p 321; (b) F. K. Truby, *J. Chem. Phys.*, **40**, 2768 (1964); (c) F. K. Truby, D. C. Wallace, and J. E. Hesse, *ibid.*, **42**, 3845 (1965); (d) S. B. Milliken, K. Morgan, and R. H. Johnsen, *J. Phys. Chem.*, **71**, 3238 (1967); (e) A. Torikai, S. Sawada, K. Fueki, and Z. Kuri, *Bull. Chem. Soc. Jap.*, **43**, 1617 (1970).

(6) M. Iwasaki and B. Eda, *Chem. Phys. Lett.*, **2**, 210 (1968).

(7) (a) J. Wendenburg, H. Mockel, A. Granzow, and A. Henglein, *Z. Naturforsch. A*, **21**, 632 (1966); (b) T. Shida, *J. Phys. Chem.*, **72**, 2597 (1968).

cals. The optical absorption spectrum at 77°K was taken with a spectrophotometer (Hitachi EPS-3T), equipped with a dewar containing liquid nitrogen in which a crystal was directly immersed with the aid of a paper holder. The crystal was about 0.7 mm thick with the (001) plane perpendicular to the incident light. All the treatments were done in the dark unless otherwise indicated.

The action spectrum for the photoinduced decay of the ionic species was obtained by illuminating the sample in the esr cavity with light from a 1-kW xenon lamp (Toshiba XL-1000) after passing through a monochromator (Shimadzu-Bausche & Lomb 33-86-25) with the slit set to a resolution of 7 nm, and observing the decay rate of esr signals at every 50-nm wavelength. The decay rate was obtained as the fraction of the signal of the cationic radical which had disappeared during, usually, the first 3 min of illumination at each wavelength. A correction was made for the intensity distribution of light from the xenon lamp–monochromator system by using a precalibrated photomultiplier (HTV R136).

Results

A. Esr Spectrum of Irradiated L-*Cystine Dihydrochloride.* The esr spectrum of a single crystal of L-cystine dihydrochloride γ-irradiated at 77°K *in the dark* is shown in Figure 1a. β absorption has been found to diminish only gradually over a week or so at 77°K, if the sample is kept in the dark.

The principal values and directions of the g tensor for the β absorption are tabulated in Table I. The β absorption, like α,[8] has a single esr absorption for all orientations of the crystal despite the C_2 symmetry axis passing through the SS bond. Such a behavior can be expected only with a radical ionized at the disulfide group. β shows a nine-line hyperfine structure in some orientations of the crystal, again similarly to α. The nine-line structure can be explained by assuming the interaction of the unpaired electron with the two sets of equivalent protons in the methylene groups next to the disulfide group. As will be described later, β absorption diminishes with the corresponding decrease of α by photoillumination at 77°K. All these results are consistent with the assignment of β to a cationic radical $(RSSR)^+$, where the unpaired electron is localized equally on both sulfur atoms. The observed g tensor of the β absorption is quite analogous to that of the β reported by Box, *et al.*,[3,9] in the same material X-irradiated at 4.2°K and suggests that they are essentially the same radical.

In an effort to elucidate the radical structure for the γ[8] absorption, radicals produced by uv irradiation in a single crystal of L-cystine dihydrochloride were examined by esr spectroscopy. As is shown in Figure 2, the radical for the γ absorption is also produced by irradiation with a low-pressure mercury lamp at 77°K, in addition to a radical showing a triplet structure at $g \simeq 2.002$. This shows that the radical for γ is produced as a result

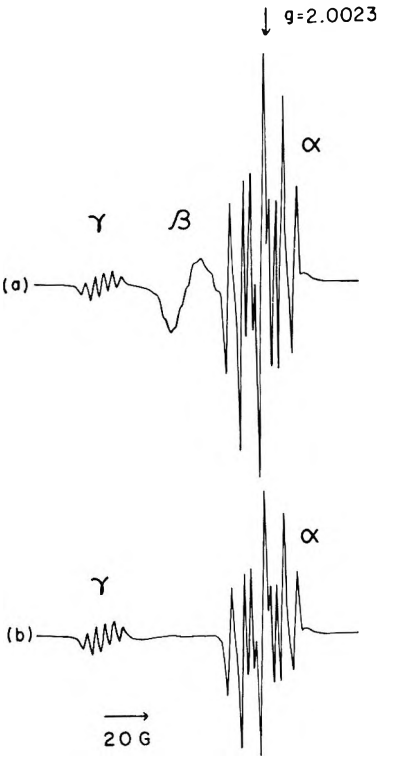

Figure 1. (a) Esr spectrum of a single crystal of L-cystine dihydrochloride γ-irradiated at 77°K in the dark. (b) The same as (a), but after photoillumination at 77°K in the visible range. These spectra are taken at 77°K at X-band with the static magnetic field parallel to the crystallographic c axis.

Table I: The Principal g Values and Direction Cosines for the Radical for β

Principal values	Direction cosines with respect to the a, b, and c' crystallographic axes[a]
2.033	(0.000, 1.000, 0.000)
2.029	(−0.251, 0.000, 0.970)
2.001[b]	(0.955, 0.000, 0.297)

[a] Reference 2. [b] This value is considerably uncertain because of the overlap of other absorptions around free-spin g value.

of a photoexcitation of the molecule, most probably through the absorption near 250 nm ascribed to the $n \rightarrow \sigma^*$ transition of the disulfide bond.[10] The resulting radical should then be a neutral radical, probably of a RS· type, which has been inferred from its principal g values.[2] It should be noted in this context that essentially no γ radical is produced from the thermal or the photoinduced decomposition of the ionic radicals, as will be described later. It appears plausible, therefore,

(8) α and γ are designated as α_I and β_1, respectively, in ref 2.

(9) H. C. Box, H. G. Freund, K. T. Lilga, and E. E. Budzinski, *J. Phys. Chem.*, **74**, 40 (1970).

(10) G. Bergson, G. Claeson, and L. Schotte, *Acta Chem. Scand.*, **16**, 1159 (1962).

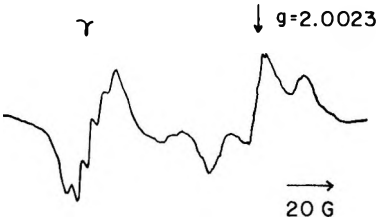

Figure 2. Esr spectrum of a single crystal of L-cystine dihydrochloride uv-irradiated at 77°K with a low-pressure mercury lamp. The spectrum is taken at 77°K at X-band with the static magnetic field parallel to the crystallographic c axis. The lower resolution in the γ absorption as compared to that in Figure 1 is partly due to a slightly inaccurate orientation of the crystal.

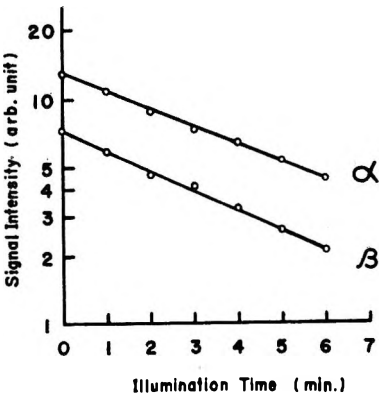

Figure 3. Decay patterns for the α and the β esr absorption under photoillumination with light around 550 nm at 77°K. For the α absorption, only the photobleachable part is plotted.

that the γ radical is also produced through a direct excitation of the molecule upon irradiation with γ rays at 77°K.

No positive indication, however, has been observed for the presence of a close radical pair, *i.e.*, R–S··S–R. One of the RS· radicals thus produced might have reacted with a surrounding molecule. The five-line structure for the γ signal must also involve interaction of the unpaired electron with nuclei probably of a neighboring molecule. It should also be noted that the R–S bond in the radical is directed away from its initial position, as judged from the direction of g_{max}. The definite identification of the radical structure for γ still awaits further study.

B. Photoinduced Change in the Esr Spectrum. When a freshly irradiated crystal showing an esr spectrum such as in Figure 1a is illuminated with light in the visible range for sufficiently a long time (a few minutes to some 30 min depending on the intensity of light), the β absorption disappears completely and α diminishes to about a half, as shown in Figure 1b. The γ absorption, on the other hand, remains practically unchanged, or increases slightly, if at all, during illumination. Essentially no further change in the spectrum takes place after the disappearance of the β absorption.

The intensity of β absorption and that of the bleachable part of α decreases exponentially with time during illumination as shown in Figure 3. These decay characteristics are independent of the wavelength of illumination chosen, except for the rate of decay which depends on the wavelength as will be shown later. From the double integration of the β and the α absorption, a comparable amount of decrease of the two oppositely charged radicals was roughly confirmed. It appears most reasonable to assume that the charge neutralization between the two oppositely charged radicals has somehow been brought about by photoillumination.

In contrast to the case of photobleaching, the thermal decay of the β absorption proceeds without the corresponding decrease of the α absorption. For example, at 125°K, β decreases in the dark almost completely within 30 min or so, leaving another weak signal, while α decreases only slightly. No more essential change in the spectrum occurs with subsequent photoillumination. If the weak signal remaining after the disappearance of β is subtracted, the decay follows a first-order reaction with respect to the β absorption with the exponential lifetime of 10 min at 125°K. The α and the γ absorption also decay, but only slightly, under the same condition. Thus, in contrast to the photoillumination, the thermal treatment causes primarily the self-decomposition of the primary cation radical into photounbleachable, and mostly nonparamagnetic, products instead of causing charge neutralization.

The fact that the radical for the γ absorption is independent of the photoinduced charge neutralization process is consistent with the assumption that this radical is electrically neutral.

C. Optical Absorption Spectrum and Action Spectrum for the Radical Decay. To have a further insight into the photoinduced charge recombination process, the absorption spectrum of the irradiated crystal and the action spectrum for the radical decay were measured, as described in Experimental Section. There are at least two absorption peaks at 77°K, one about 400 nm and the other around 550 nm as shown in Figure 4a. The optical density was such that at the absorption maximum of the 550-nm peak it is about 0.1. No absorptions are induced at the longer wavelength region. Whereas the former absorption does not disappear by photoillumination at 77°K, the latter disappears almost completely as seen in Figure 4b.

Disulfide anions have been reported to have absorption around 420 nm[7] by measurement in the glassy state, whereas disulfide cations absorb around 720 nm.[7b] The radical of the type RS· also has an absorption maximum around 400–420 nm.[5e,7a] It thus appears quite reasonable to attribute the absorption around 400 nm in Figure 4a to $(RSSR)^-$, the radical for α, as was suggested previously[2] and to a radical of RS· type, the radical for γ. The slight shoulder around 430 nm, which becomes appreciable in the spectrum after photoillumi-

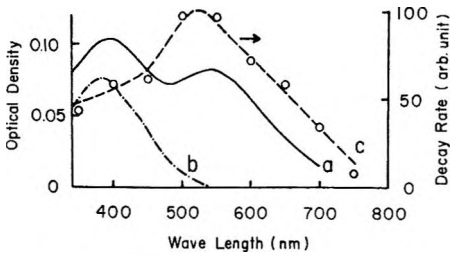

Figure 4. (a) The optical absorption spectrum of a single crystal of L-cystine dihydrochloride γ-irradiated at 77°K in the dark. (b) The same as (a), but after photoillumination at 77°K in the visible range. (c) The action spectrum for the decay of the esr signal (α and β) at 77°K, calibrated per number of incident photons. See text for the method of measurement.

nation, may correspond to either of these two species. The other absorption which diminishes with photoillumination, peaking around 550 nm, should then be attributed to the primary cation $(RSSR)^+$. Although there is a considerable shift in wavelength between the absorption of this species and the absorption around 710–780 nm reported as due to the cation of alkyl disulfides in the glassy state,[7b] the discrepancy may probably be ascribed firstly to the conformational difference of the molecule in the two cases, as the absorption involving the nonbonding orbitals of the disulfide group should depend considerably on the dihedral angle of the CSS'C' group,[10] and secondly to the difference in the degree of polarization of the surrounding medium.

If we take a simple view of the electronic structure of the CSS'C' group as in ref 2, the ground and the first excited configuration for the cationic radical will be

$$\psi_0 = \sigma_{c-s}^2\sigma_{c'-s'}^2\sigma_{s-s'}^2n_+^2n_-^1$$
$$\psi_1 = \sigma_{c-s}^2\sigma_{c'-s'}^2\sigma_{s-s'}^2n_+^1n_-^2 \quad (1)$$

Here, the molecular orbitals in each configuration are arranged in increasing order of energy with the same notations as in ref 2. Accordingly, the absorption at 550 nm or 18,000 cm^{-1}, the lowest energy transition observed for the cation, could reasonably be attributed to $n_+ \rightarrow n_-$, the transition between the nonbonding orbitals of the disulfide group.

The wavelength dependence of the decay rate, *i.e.*, the action spectrum for the photoinduced decay, is distributed over the whole visible range with a peak between 500 and 550 nm, as shown in Figure 4c. The reproducibility of the peak position was checked by several independent measurements to be within 25 nm. As is apparent in Figure 4, the action spectrum does not coincide with the absorption spectrum of the primary anion at all, but agrees fairly well with that assigned to the primary cation. This indicates that it is the excitation of the primary cation rather than the anion that initiates the charge neutralization process. The reason why, after the disappearance of β, the photoinduced decay of α is practically prohibited may now be obvious in this context.

Discussion

Since the γ-irradiated crystal is optically dilute, the rate of the photoexcitation of the cation will be proportional to the concentration of the cation itself. Therefore, the exponential time decay of the ionic species should indicate that the photoexcitation of the cation leads to charge recombination with a constant quantum yield. This would be expected if the primary ions are made somehow in pairs so that the excitation of a positive hole leads to a recombination with its partner electron trapped in a disulfide group of a nearby molecule. Otherwise, if the ions were made in a random fashion, the average distance between the opposite charges should increase and, therefore, the quantum yield would decrease, as the recombination reaction proceeds with time, leading to a nonexponential decay.

From the observed line width of the resonance for the anion radical, 2–3 G, which should be the maximum value for the magnetic dipolar contribution $(\sim\mu_e/r^3)$[11] from its partner cation radical, the lower limit for the distance between the radical pair is estimated to be some 20 Å (the length of two to four molecules depending on the direction in the crystal[12]), whereas the upper limit is placed at ~70 Å (the length of average ten molecules[12]) by assuming a uniform distribution of the ions with $G \simeq 3$.[9] Thus, it is clear that the charge neutralization process requires an intermolecular transfer of either an electron or a positive hole at least over a few molecular distances. Similar phenomena of intermolecular charge recombination initiated by the photoexcitation of a hole trapped in a sulfur orbital have also been found in single crystals of DL-methionine[13] and *N*-acetyl DL-methionine[14] γ-irradiated at 77°K.

In view of the local nature of the 550-nm excitation of the trapped hole and of the pairwise recombination between the opposite charges, it does not seem relevant for the present system to postulate a "valence band" structure through which a positive hole could migrate fairly freely to meet one of the trapped electrons.[15] Rather, these observations appear to be more consistent with a mechanism involving an electron tunneling between an electron–hole pair. It should be noted in this context that disulfide groups of two neighboring molecules are rather close with each other in a crystal of L-cystine dihydrochloride in the direction parallel to either the *b* or *c* axis, separated by a gap of about 1.9 Å[12] with the van der Waals radius of sulfur of 1.65 Å.[16] It

(11) A. Carrington and A. D. McLachlan, "Introduction to Magnetic Resonance with Applications to Chemistry and Chemical Physics," Harper and Row, New York, N. Y., 1967, p 186.

(12) L. K. Steinrauf, J. Peterson, and L. H. Jensen, *J. Amer. Chem. Soc.*, **80**, 3835 (1958).

(13) S. Kominami, K. Akasaka, and H. Hatano, to be published.

(14) S. Kominami, K. Akasaka, H. Umegaki, and H. Hatano, *Chem. Phys. Lett.*, **9**, 510 (1971).

(15) C. Kittel, "Introduction to Solid State Physics," 3rd ed, Wiley, New York, N. Y., 1967, p 299.

(16) B. M. Oughton and P. M. Harrison, *Acta Cryst.*, **12**, 396 (1959).

might be possible that the photoinduced intermolecular hole or electron tunneling occurs *via* the sulfur orbitals intervening between the hole–electron pair.

Electronic processes in organic crystals have so far been studied by such means as thermoluminescence[17] and conductivity measurements.[4] We expect that an experimental approach along the lines followed in the present work may throw a new light on electronic processes in organic crystals, particularly those of biological interest. Further experimental studies are in progress for more detailed understanding of the process.

Acknowledgments. We are indebted to Professor N. Itoh of Nagoya University for helpful discussions, and to Dr. T. Ban for his kind advice in measuring intensity distribution of the xenon lamp.

(17) L. G. Augenstine, J. G. Carter, D. R. Nelson, and H. P. Yockey, "Free Radicals in Biological Systems," Academic Press, New York, N. Y., 1961, p 149; S. Tahira, N. Shiomi, and T. Higashimura, *Bull. Inst. Chem. Res., Kyoto Univ.*, **41**, 48 (1963).

On the Mechanism of Ion Exchange in Crystalline Zirconium Phosphates. V. Thermodynamic Treatment of the Hydrogen Ion–Sodium Ion Exchange of α-Zirconium Phosphate[1a]

by A. Clearfield* and A. S. Medina[1b]

Chemistry Department, Ohio University, Athens, Ohio 45701 *(Received June 3, 1971)*

Publication costs assisted by the Petroleum Research Fund

It was previously shown that two separate reactions occur when sodium ion exchanges for hydrogen ion in α-zirconium phosphate. In the first reaction the crystals of composition $Zr(HPO_4)_2 \cdot H_2O$ are converted to $ZrNaH(PO_4)_2 \cdot 5H_2O$. In the second reaction the half-exchanged phase is converted to $Zr(NaPO_4)_2 \cdot 3H_2O$. The latter reaction is reversible but the first reaction appears to be irreversible. The end product of the replacement of sodium ions in $ZrNaH(PO_4)_2 \cdot 5H_2O$ by protons is $Zr(HPO_4)_2 \cdot 8H_2O$. It is shown that the first reaction is microscopically reversible and an explanation for the seeming irreversibility, based on structural concepts, is developed. Equilibrium constants, free energies, enthalpies, and entropies for the exchange reactions are given.

Introduction

The crystalline compound zirconium bis(monohydrogen orthophosphate) monohydrate, $Zr(HPO_4)_2 \cdot H_2O$, hereinafter called α-zirconium phosphate or α-ZrP, behaves as an ion exchanger.[2] Both monohydrogen phosphate groups can exchange their hydrogens for cations so that the exchange capacity of the crystals is 6.64 mequiv/g. In the case of sodium ion exchange one hydrogen is replaced at relatively low constant pH with the formation of the compound $Zr(NaPO_4)(HPO_4) \cdot 5H_2O$.[3] During this first state of exchange two solid phases, the unexchanged crystals and the half-exchanged phase, are in equilibrium with the exchanging solution. Following the replacement of the first hydrogen the pH rises (Figure 1) and the second hydrogen begins to exchange. In this second stage of exchange, the half-exchanged phase is converted to $Zr(NaPO_4)_2 \cdot 3H_2O$. Once again two solid phases are in equilibrium with the exchanging solution. The phases are the half-exchanged and the fully exchanged compounds which will hereafter be referred to as phase A ($Na^+ \cdot 5H_2O$) and phase D ($2Na^+ \cdot 3H_2O$), respectively.[3]

Only the second reaction is macroscopically reversible. When hydrogen ion replaces sodium ion in $Zr(NaPO_4)(HPO_4) \cdot 5H_2O$, the resultant unexchanged phase is not α-ZrP. Rather it is a more highly hydrated phase.[3,4] Thus, the titration curve exhibits a hyster-

(1) (a) Acknowledgment is made to the donors of the Petroleum Research Fund, administered by the American Chemical Society, for financial support of this work. (b) This paper is one of a series based upon the Ph.D. thesis of A. S. Medina presented to the Department of Chemistry, Ohio University, June 1971.

(2) A. Clearfield and J. S. Stynes, *J. Inorg. Nucl. Chem.*, **26**, 117 (1964).

(3) A. Clearfield, W. L. Duax, A. S. Media, G. D. Smith, and J. R. Thomas, *J. Phys. Chem.*, **73**, 3424 (1969).

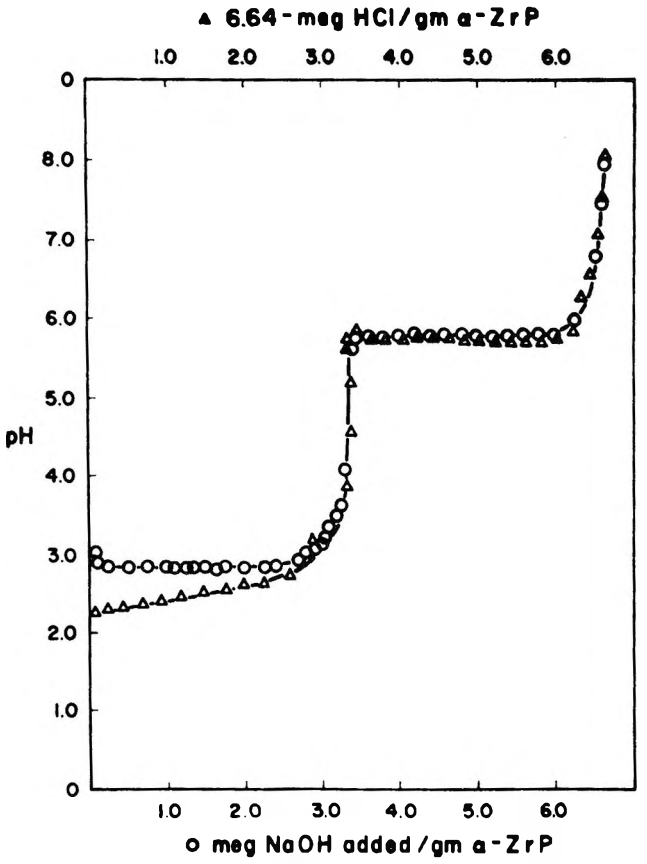

Figure 1. Potentiometric titration of α-ZrP by the batch equilibration method. Titrant: forward direction, 0.1 N NaOH + 0.1 N NaCl, ○; backward direction, 0.1 N HCl (NaCl concentration maintained constant at 0.1 N), △.

esis. Hysteresis phenomena are quite common with α-zirconium phosphate.[5]

In a recent study of the sodium ion–hydrogen ion exchange reactions of α-ZrP it was shown that the ionic strength remains constant during each stage of exchange.[6] The pH also remained constant from which it was concluded that changes in water content, electrolyte adsorption, and hydrolysis were negligible. However, since the *exchange system* did exhibit a hysteresis, the system was not treated by the methods of reversible thermodynamics. In this paper it will be shown that microscopic reversibility does indeed hold and the system can therefore be treated by familiar thermodynamic methods.

Experimental Section

Reagents and Analytical Work. Standard sodium chloride, sodium hydroxide, and hydrochloric acid solutions were prepared from reagent grade compounds. The base solution was standardized by titration against weighed amounts of primary standard (NBS potassium acid phthalate) and then used to standardize the acid solutions. The sodium chloride solution was standardized by gravimetric determination of chloride ion. Distilled, deionized water at pH 7 ± 0.1 was used throughout.

α-Zirconium phosphate crystals were prepared by the method of Clearfield and Stynes[2] from spectrographically pure zirconyl chloride and reagent grade phosphoric acid. *Anal.* Calcd for $Zr(HPO_4)_2 \cdot H_2O$ (corrected for the presence of ~2% Hf): ZrO_2, 41.11; P_2O_5, 46.97; H_2O, 11.82. Found: ZrO_2, 41.16; P_2O_5, 46.95; H_2O, 11.89 (loss on ignition). Spectrographic analysis showed the presence of less than 0.01% total metallic impurities and the X-ray diffraction pattern was that of the pure α-ZrP phase.

Equilibrations. Equilibrations were carried out in both the forward and reverse directions. In the former case precalculated amounts of standard sodium chloride solution and water were added from burets to polyethylene bottles containing weighed amounts of α-ZrP crystals. Then quantities of sodium hydroxide solution varying from 0 to 6.64 mequiv/g of crystals were added. During equilibration an amount of sodium ion equivalent to the added hydroxide is always exchanged.[3,6] Thus, the sodium chloride and water added was such as to yield final solutions with a constant (approximately 0.1 N) sodium ion concentration. The liquid volume to solid ratio was also kept constant at 100 ml/g of exchanger. The additions were made in a nitrogen atmosphere to nitrogen-filled containers. All samples were shaken for at least 48 hr in a constant-temperature bath maintained at 25 ± 0.05°. This length of time was sufficient to establish equilibrium as the results were identical with those obtained on samples which were shaken for 2 weeks. After equilibration a 10-ml sample of the solution phase was removed and centrifuged to separate solid particles from the liquid phase. Then a 5-ml aliquot of the clear solution was pipetted out and diluted to 500 ml. The sodium ion concentration of these solutions was determined by flame emission analysis on a Jarrell-Ash atomic absorption spectrometer, Model No. 82-536. The pH of the equilibrated samples was determined under nitrogen with a Heath pH recording electrometer, Model EUW-301, equipped with a Corning combination pH electrode with Ag–AgCl internal and glass electrode external. In some instances the sodium content of the solid was determined to ensure mass balance.

Equilibrations in the reverse direction were carried out as described above except that 3.32 or 6.64 mequiv of sodium hydroxide/g of α-ZrP was added along with the sodium chloride solution. These amounts of sodium hydroxide converted the α-ZrP to the half and fully sodium ion exchanged phases, respectively. After 48

(4) E. Torracca, G. Alberti, R. Platania, P. Scala, and P. Galli, "Ion Exchange in the Process Industries," Society of Chemical Industry, London, 1970, p 315.

(5) E. Torracca, *J. Inorg. Nucl. Chem.*, **31**, 1189 (1969).

(6) S. J. Harvie and G. H. Nancollas, *ibid.*, **32**, 3923 (1970).

hr of shaking, amounts of hydrochloric acid varying from 0 to 6.64 mequiv/g of original α-ZrP crystals were added. The solutions were then brought to a final volume of 100 ml/g of dry α-ZrP and a constant ($\sim$0.1 N) sodium chloride concentration. The amounts of reagents required were determined as follows. If v is the volume of sodium chloride solution required and c is its concentration in milliequivalents per milliliter, then $v = (10 - m)w/c$, where w is the weight of α-ZrP and m is the number of milliequivalents of HCl added per gram of α-ZrP. The number 10 arises from the fact that this is the total number of milliequivalents of NaCl present at equilibrium per gram of α-ZrP.

The water content of the solid phases at different relative humidities was determined by the isopiestic method or as described previously.[7]

Results

The sodium ion titration curve of α-ZrP crystals at $\mu = 0.1$ is given in Figure 1. Each of the end points in the titration curve represents a separate and distinct exchange reaction from a thermodynamic standpoint, and, therefore, each may be treated separately. The equation representing the ion-exchange reaction from 0 to 50% of exchange in the forward direction is

$$Zr(HPO_4)_2 \cdot H_2O + Na^+ + OH^- + 3H_2O \longrightarrow Zr(NaPO_4)(HPO_4) \cdot 5H_2O \quad (1)$$

If this reaction is reversible, then

$$K_1^{Na,H,OH} = \frac{\bar{a}_{Na_1}}{\bar{a}_{H_1}} \frac{1}{a_w^3} \frac{1}{a_{OH} a_{Na}} \quad (2)$$

where the quantities with bars represent activities of the indicated species in the solid phase, and those without the bars, activities in the solution phase. The subscript 1 refers to the exchange reaction from 0 to 50% of exchange but ions in solution are not subscripted by numerals. Reaction 1 does not appear to be reversible from the data in Figure 1. However, it will be shown below that the reaction exhibits microscopic reversibility so that eq 2 and other equations derived from it are valid.

Substituting the equivalent expression $K_w a_w / a_H$ for a_{OH} in eq 2 yields

$$K_1^{Na,H,OH} = \frac{\bar{a}_{Na_1}}{\bar{a}_{H_1}} \frac{1}{a_w^4} \frac{a_H}{a_{Na}} \frac{1}{K_w} \quad (3)$$

The activities of sodium and hydrogen ion in the solid are most easily represented in terms of equivalent fraction. The activities are then $\bar{a}_{Na_1} = [\bar{X}_{Na_1}] f_{Na}$ and $\bar{a}_{H_1} = [\bar{X}_{H_1}] f_H$, where the X's represent equivalent fractions and the f's the appropriate activity coefficients. At 50% of exchange the reaction as written in eq 1 is complete. Thus, $[\bar{X}_{Na_1}] = 1$ and $[\bar{X}_{H_1}]$ becomes very small. The above designation is equivalent to the statement that the entire solid is converted to the single phase $Zr(NaPO_4)(HPO_4) \cdot 5H_2O$ at half-exchange.

During each of the stages of the titration not only does the hydrogen ion activity remain constant over most of the titration as evidenced by the plateaus of Figure 1 but the sodium ion activity also is constant.[3,6] For the first stage of exchange a_{Na} was 0.0717 $\pm$ 0.0018. After addition of 0.05 mequiv of NaOH/g of α-ZrP it was determined that $\bar{X}_{Na_1} \cong 0.0075$ and $X_{Na} = 0.988$. Thus, the isotherm is almost rectangular (flat) indicating a very marked preference for hydrogen ion by the exchanger. Increasing the sodium ion concentration does not appreciably increase the sodium ion uptake and the exchange reaction must be driven to completion by neutralization of the exchanged hydrogen ion with sodium hydroxide.

The titration curve may be understood with the aid of the phase rule. The addition of successive amounts of sodium hydroxide does not change the concentration of sodium ion in solution but merely increases the ratio $\bar{X}_{Na_1}/\bar{X}_{H_1}$. The total number of phases in the system is 3, two solid phases and the solution. The number of components necessary to describe the system is also 3. One choice of components might be the sodium ion and hydrogen ion concentrations in solution and the mole fraction of one of the solids. Therefore, the number of degrees of freedom is zero since temperature and pressure are constant during the titration. The activity of sodium ion in the solid phase $Zr(NaPO_4)(HPO_4) \cdot 5H_2O$ and the activity of the first exchangeable hydrogen in α-ZrP crystals remain constant during the titration because their respective environments remain unchanged. If we choose as the standard reference state an activity of 1 for the pure solids, then $\bar{a}_{Na_1} = \bar{a}_{H_1} = 1$ during the titration. Thus, the phase rule requires that the activities of the ions in solution remain constant as is in fact observed along the plateau. As long as two solid phases are present, exchange occurs at constant pH. Actually, the pH begins to increase somewhat before the disappearance of the unexchanged crystals. This may be due to other factors such as strains set up within the crystals since the c axis increases markedly during exchange.[3]

For the standard states in the solution phase we choose the usual ones which make ion activities equal the corresponding molalities in infinitely dilute solutions. The reference state for the solvent is also the usual one in which $a_w = 1$ for the pure solvent. Equation 3 may now be solved for $K_1^{Na,H,OH}$. Microscopic reversibility would be shown to hold if at different values of the sodium ion activity in solution the pH was such as to keep $K_1^{Na,H,OH}$ constant. For this purpose it is better to eliminate the neutralization reaction and only consider the exchange reaction as given by

(7) A. Clearfield and A. S. Medina, *J. Inorg. Nucl. Chem.*, **32**, 2775 (1970).

$$Zr(HPO_4)\cdot H_2O + Na^+(aq) + 4H_2O(l) \rightleftharpoons Zr(NaPO_4)(HPO_4)\cdot 5H_2O + H^+(aq) \quad (4)$$

The equilibrium constant representing eq 4 is then

$$K_1^{Na,H,5H_2O} = \frac{\bar{a}_{Na_1} a_H}{\bar{a}_{H_1} a_w^4 a_{Na}} = K_1^{Na,H,OH} K_w \quad (5)$$

Taking negative logarithms and remembering that $\bar{a}_{Na_1} = \bar{a}_{H_1} = 1$ gives

$$pH = pK_1^{Na,H,5H_2O} + pNa' \quad (6)$$

where $pNa' = -\log a_{Na} a_w^4$. Thus, a plot of pH *vs.* pNa′ should be a straight line with slope of unity. This plot is shown in Figure 2. The slope of the straight line was found by least-squares methods to be 1.021 ± 0.029. pH and sodium ion concentration values were obtained from the flat portions of the titration curves at three different loadings. Mean molal activity coefficients for sodium chloride, taken from the compilation of Robinson and Stokes, were used in place of γ_{Na^+}.[8a] Water activities were obtained from the same source.[8b] Extrapolation of the straight line to pNa′ = 0 yields a value of $pK_1^{Na,H,5H_2O} = 1.689 \pm 0.045$ from which is derived $K_1^{Na,H,5H_2O} = 2.05\ (0.29) \times 10^{-2}$ and $\Delta G^\circ = 2.30 \pm 0.06$ kcal/mol.

Having demonstrated that eq 5 is valid, it is then possible to determine an approximate value of the equilibrium constant from a single point on the plateau of the titration curve. To demonstrate that this is so $K_1^{Na,H,5H_2O}$ was evaluated from 19 separate experimental points along the first plateau in Figure 1. These values of the equilibrium constant were averaged to yield $K_1^{Na,H,5H_2O} = 1.96\ (0.19) \times 10^{-2}$.

In the above determination of the equilibrium constant only the data along the plateau were utilized. An alternative treatment which utilizes all of the experimental data from 0 to 50% of exchange can be carried out by the method of Gaines and Thomas.[9] Equation 5 may be rewritten in the form

$$K_1^{Na.H.5H_2O} = K_{R_1}^{Na.H} \frac{\hat{f}_{Na_1}}{\hat{f}_{H_1} a_w^4} \quad (7)$$

where $K_{R_1}^{Na,H}$ is the corrected rational selectivity constant equal to

$$K_{R_1}^{Na,H} = \frac{[\bar{X}_{Na_1}] a_H}{[\bar{X}_{H_1}] a_{Na}} \quad (8)$$

Applying the thermodynamic treatment of Gaines and Thomas to these equations yields

$$\log K_1^{Na,H,5H_2O} = \int_0^1 \log K_{R_1}^{Na,H}\, d[\bar{X}_{Na_1}] - (n_2 - n_1) \log a_w \quad (9)$$

The integral may be evaluated by plotting $\log K_{R_1}^{Na,H}$ against $[\bar{X}_{Na_1}]$ and determining the area under the curve. This plot is shown in Figure 3 for the data at $\mu \cong 0.1$ from which a value of -1.80 ± 0.03 has been obtained for the integral. The contribution to $\log K_1^{Na,H,5H_2O}$ from the water activity term is +0.0052

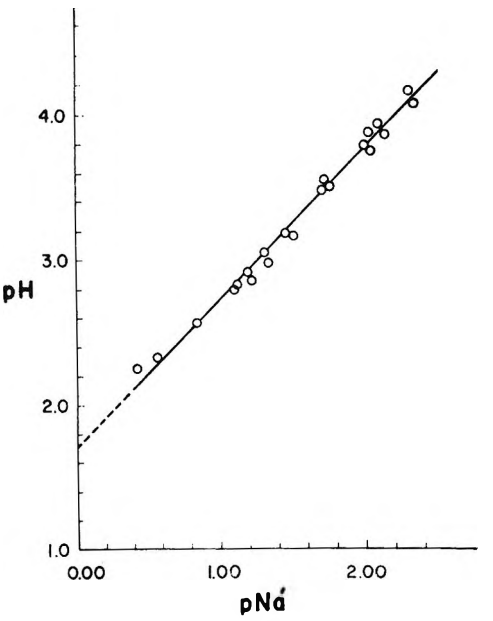

Figure 2. Plot of pH *vs.* pNa′ for the sodium ion exchange reaction whose equilibrium constant is $K_1^{Na,H,5H_2O}$.

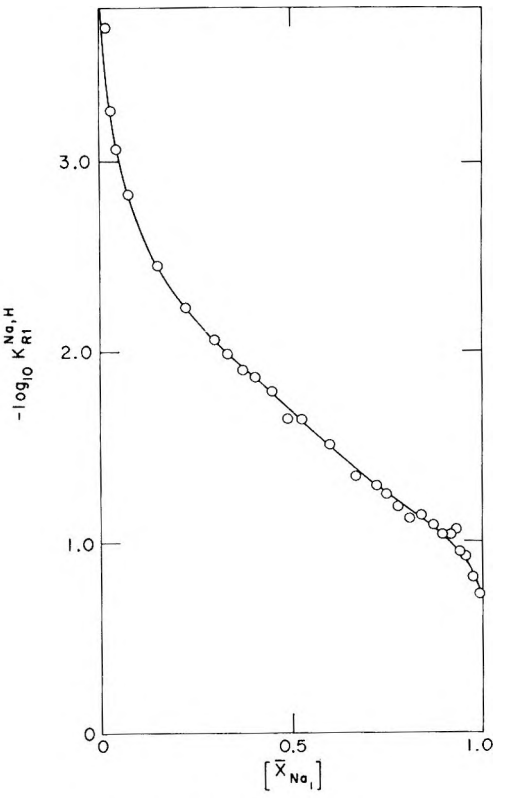

Figure 3. Plot of $-\log K_{R_1}^{Na,H}$ *vs.* $\bar{X}_{Na_1}$.

(8) R. A. Robinson and R. H. Stokes, "Electrolyte Solutions," Academic Press, New York, N. Y., 1959: (a) p 476; (b) p 477.

(9) G. L. Gaines and H. C. Thomas, *J. Chem. Phys.*, **21**, 714 (1953).

± 0.0017. Thus, $K_1^{Na,H,5H_2O}$ = (1.60 ± 0.12) × 10^{-2} and ΔG° = 2.45 ± 0.06 kcal/mol. This lower value of $K_1^{Na,H,5H_2O}$ was to be expected because of the higher pH values encountered at the beginning and near the end point of the titration curve.

The second stage of exchange may be treated in the same way as detailed above. However, in this case the reaction exhibits macroscopic reversibility as can be seen from Figure 1. The actual reaction is

$$Zr(NaPO_4)(HPO_4)\cdot 5H_2O + Na^+ + OH^- \rightleftharpoons Zr(NaPO_4)_2\cdot 3H_2O + 3H_2O \quad (10)$$

Eliminating the neutralization reaction from (10) gives the exchange reaction

$$Zr(NaPO_4)(HPO_4)\cdot 5H_2O + Na^+(aq) \rightleftharpoons Zr(NaPO_4)_2\cdot 3H_2O + H^+(aq) + 2H_2O(l) \quad (11)$$

The equlibrium constant for reaction 11 is

$$K_2^{Na,H,3H_2O} = \frac{\bar{a}_{Na_2} a_H a_w^2}{\bar{a}_{H_2} a_{Na}} \quad (12)$$

The subscript 2 in the above equations refers to the second replaceable proton or second cation. Once again since the exchanged phases are not solid solutions but are pure phases with unchanging composition $\bar{a}_{Na_2} = \bar{a}_{H_2} = 1$. Equation 12 may then be recast into logarithmic form as

$$pH = pK_2^{Na,H,3H_2O} + pNa'' \quad (13)$$

where $pNa'' = -\log (a_{Na}/a_w^2)$. A plot of pH *vs.* pNa'' at three different loadings is shown in Figure 4. The slope of the line is 0.891 and the value of pK obtained by extrapolation to pNa'' = 0 is 4.672 ± 0.046. This yields $K_2^{Na,H,3H_2O}$ = 2.13 (0.21) × 10^{-5} from which a free energy of 6.36 ± 0.06 kcal/mol is obtained.

Applying the method of Gaines and Thomas to the second stage of exchange yields

$$\log K_2^{Na,H,3H_2O} = \int_0^1 \log K_{R_2}^{Na,H}\, d[\bar{X}_{Na_2}] - (n_2 - n_1)\log a_w \quad (14)$$

where

$$K_{R_2}^{Na,H} = \frac{[\bar{X}_{Na_2}]}{[\bar{X}_{H_2}]}\frac{a_H}{a_{Na}}$$

The value of the integral determined by graphical integration of the forward titration data at $\mu \cong 0.1$ (Figure 5) was found to be −4.767 ± 0.0088. The contribution from the water activity term is −0.0026 ± 0.0021 so that $K_2^{Na,H,3H_2O}$ = (1.70 ± 0.05) × 10^{-5}. The value of the integral of eq 12 obtained from back-titration data was −4.733 ± 0.0088 from which is obtained, after addition of the water activity term, $K_2^{Na,H,3H_2O}$ = (1.85 ± 0.05) × 10^{-5}. This slight difference in the constants may be due to differing amounts of hydrolysis in the forward and reverse directions. However, the lower value of $K_2^{Na,H,3H_2O}$ obtained by integration relative to that obtained from extrapolation of eq 13 results from the upturn in pH at the second end point.

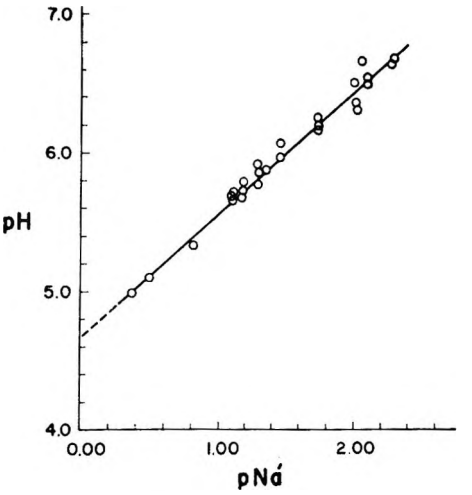

Figure 4. Plot of pH *vs.* pNa' for the sodium ion exchange reaction whose equilibrium constant is $K_2^{Na,H,3H_2O}$.

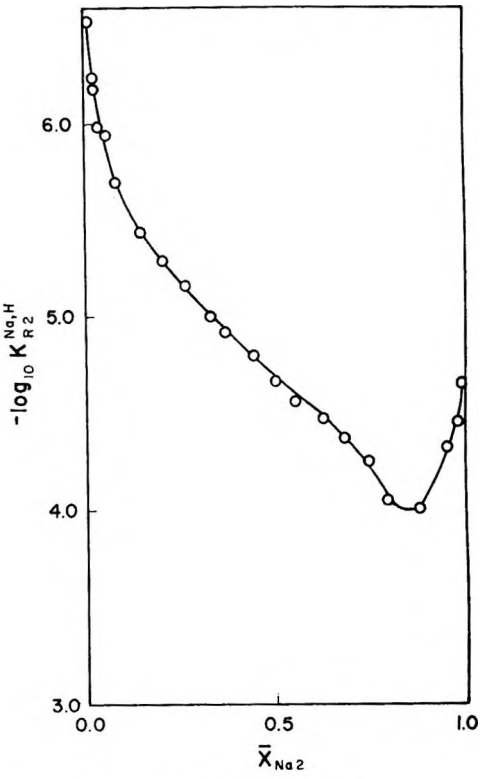

Figure 5. Plot of $-\log K_{R_2}^{Na,H}$ against $\bar{X}_{Na_2}$.

Titrations were also run at 35 and 55°. The titrant in each case was 0.1 M NaOH + 0.1 M NaCl. Actually the titrant was prepared by adding weighed amounts of sodium hydroxide and sodium chloride into a known weight of water so that the molality

Table I: Thermodynamic Data for Sodium Ion Exchange with α-ZrP

Temp, °C	$10^2K_1^{Na,H,5H_2O}$ [a]	$\Delta G°$, kcal mol^{-1}	$10^5K_2^{Na,H,3H_2O}$ [a]	$\Delta G°$, kcal mol^{-1}
25.0 ± 0.1	1.96 ± 0.19	2.33 ± 0.06	1.84 ± 0.10	6.45 ± 0.03
35.0 ± 0.1	1.19 ± 0.05	2.71 ± 0.01	2.59 ± 0.16	6.47 ± 0.02
55.0 ± 0.1	0.767 ± 0.033	3.17 ± 0.01	3.46 ± 0.17	6.70 ± 0.03
	$\Delta H°$ = −5.88 ± 0.81 kcal mol^{-1}		$\Delta H°$ = 3.95 ± 0.67 kcal mol^{-1}	
	$\Delta S°$ = −27.4 ± 3.0 eu		$\Delta S°$ = −8.1 ± 1.7 eu	

[a] Values obtained from titration data at $\mu \cong 0.1$.

could be calculated precisely. Mean molal activity coefficients at elevated temperatures were obtained from the compilation of Harned and Owen.[10] Hydrogen ion activities were determined from the pH values along the flat portions of the titration curves at several different loadings. The equilibrium constants so determined are collected in Table I together with the corresponding free energies. Plots of log K *vs.* $1/T$ from which $\Delta H°$ may be estimated are shown in Figures 6 and 7. These data may deviate somewhat from linearity. However, since only three points were available, the best straight line was drawn through them to obtain average $\Delta H°$ values for the temperature interval. This permitted the calculation of approximate $\Delta S°$ values also. The results are given in Table I.

The back-titration from 50 to 0% of sodium ion exchange is not treated here. During this reaction the interplanar spacings of the hydrogen ion containing phase decrease continuously with increasing acidity. The reasons for this change are not yet clear but may involve solid solution formation, changes in water content, or sorption of electrolyte from the solution phase. These points are under investigation and will be reported upon subsequently.

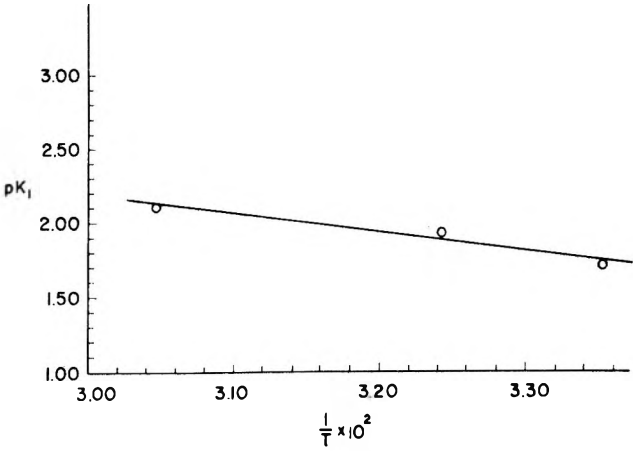

Figure 6. Dependence of $pK_1^{Na,H,5H_2O}$ upon temperature.

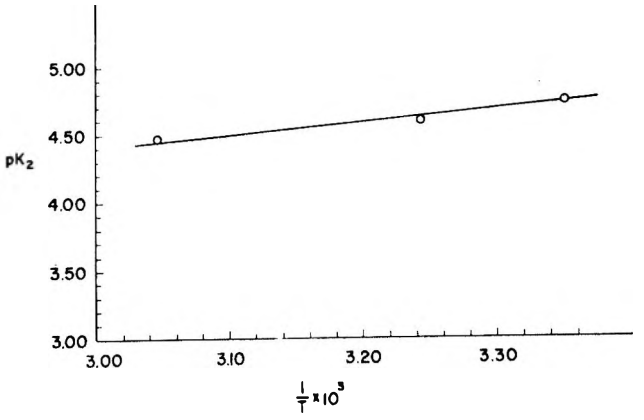

Figure 7. Dependence of $pK_2^{Na,H,3H_2O}$ upon temperature.

Discussion

Several aspects of the work reported here require comment. Most important are the reasons for the different paths the exchange reaction follows in the forward and reverse direction. It is possible to deduce an explanation from the structure of α-ZrP and its ion-exchange behavior. The structure is a layered one with an interlayer distance of 7.6 Å.[11] The layers are arranged in such a fashion that zeolitic type cavities are formed. The entranceways into the cavities are large enough to permit a spherical ion of 2.64-Å diameter to pass unobstructed.[3] The crystals do not swell when immersed in water. Thus, initially, unhydrated or partially hydrated ions must exchange in order to diffuse into the cavities. Large ions such as Rb^+ and Cs^+ do not exchange appreciably in acid solution.[2,12]

Sodium ion exchange must then occur in two stages. At the surface of the crystal the hydrated sodium ion gives up most of its water and diffuses into the cavity in either an unhydrated or at most a dihydrated species. The proton on the other hand probably forms a hydronium ion with the water molecule situated in the center of the cavity and diffuses out as such. Thus, the net change in water content of the crystals in this initial step is either zero or 1 mol of water. We propose that it is zero, *i.e.*, that the sodium ion brings in 1 mol of

(10) H. S. Harned and B. B. Owen, "The Physical Chemistry of Electrolytic Solutions," Reinhold, New York N. Y., 1958, p 726.
(11) A. Clearfield and G. D. Smith, *Inorg. Chem.*, **8**, 431 (1969).
(12) J. Albertsson, *Acta Chem. Scand.*, **20**, 1689 (1966).

water, because a half-exchanged monohydrate phase is known to exist.[3,7] With this assumption the initial exchange reaction becomes

$$Zr(HPO_4)_2 \cdot H_2O + Na^+(aq) \rightleftharpoons Zr(NaPO_4)(HPO_4) \cdot H_2O + H^+(aq) \quad (15)$$

However, water molecules can now diffuse into the cavities to rehydrate the sodium ions. In the process of rehydration the layers are spread apart to 11.8 Å. The amount of water taken in is then determined by the hydration energy and the energy required to spread the layers. Thus, the second step in the exchange reaction is

$$Zr(NaPO_4)(HPO_4) \cdot H_2O + 4H_2O \rightleftharpoons Zr(NaPO_4)(HPO_4) \cdot 5H_2O \quad (16)$$

The equilibrium constant $K_1^{Na,H,5H_2O}$ is then the combined constant for reactions 15 and 16. We may then write

$$K_1^{Na,H,5H_2O} = K_1^{Na,H,H_2O} K_1^{H_2O,5H_2O} \quad (17)$$

where

$$K_1^{Na,H,H_2O} = a_{H^+}/a_{Na^+} \quad (18)$$

is the equilibrium constant for reaction 15. Because the water activity term in eq 5 is small at low ionic strength, we have

$$K_1^{Na,H,H_2O} \cong K_1^{Na,H,5H_2O} \quad (19)$$

Isopiestic studies have shown that reaction 16 is reversible but takes place in two steps, there being a very unstable tetrahydrate intermediate.[7,13] The water activity (at 23 ± 2°) at which the pentahydrate and tetrahydrate are in equilibrium is 0.45 and 0.3 is the equilibrium water activity at which the monohydrate and tetrahydrate exist together. Thus, at the higher water activities of the exchange reactions a lower hydrate would be expected to convert to phase A ($Na^+ \cdot 5H_2O$).

Once the α-ZrP layers have been spread apart, further exchange reactions can occur with hydrated ions. Thus, when sodium ion replaces the second proton or when hydrogen ion replaces sodium ion, the ions do so in the hydrated condition. This makes no difference in the second stage of exchange because the interlayer spacings in phase A ($Na^+ \cdot 5H_2O$) and phase D ($2Na^+ \cdot 3H_2O$) are relatively large. However, since α-ZrP cannot accommodate hydrated cations, forward and reverse exchange reactions follow different paths. The reaction of phase A ($Na^+ \cdot 5H_2O$) with protons then results in the formation of an octahydrate. This phase readily loses water, when removed from solution, to re-form α-ZrP but so far it has not been possible to do the reverse.

Thus, the exchange reactions may be represented by Scheme I. Preliminary titration data show that the

Scheme I

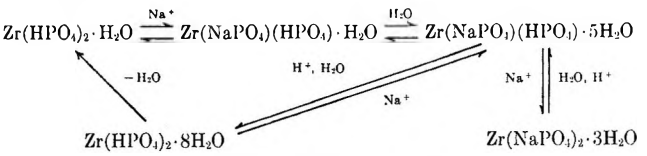

conversion of $Zr(HPO_4)_2 \cdot 8H_2O$ to phase A ($Na^+ \cdot 5H_2O$) is indeed reversible.[13]

The free energies of the sodium ion exchange reactions are both positive. However, in the first stage of exchange $\Delta H°$ is negative requiring a large negative $\Delta S°$ value. A qualitative rationale for these observations can be given. In the exchange reaction sodium initially gives up its water of hydration but then rehydrates inside the crystal. This behavior of the sodium ion results in only a minor contribution to $\Delta H°$ and $\Delta S°$. However, the hydrogen ion is originally unhydrated so that on passing into the solution it makes a large negative $\Delta H°$ contribution. At the same time the proton localizes several water molecules producing a large negative entropy. Most of the heat of hydration of the proton is consumed in breaking the PO–H bond and in expanding the layers from 7.6 to 11.8 Å. Thus, the net enthalpy change is small but the entropy effect is considerable. In the second stage of exchange the release of the second proton contributes about the same energy and entropy to the exchange reaction as before. However, the end product contains only three water molecules for two sodium ions. Thus, a large portion of the energy is now consumed in dehydrating the sodium atoms as well as breaking the PO–H bond. In addition energy is consumed in bringing the two sodium ions into close proximity. These effects in large measure account for the endothermic character of the second exchange reaction. Furthermore, the release of a number of water molecules by the sodium atoms results in the observed increase in entropy relative to the first exchange reaction.

Acknowledgment. We wish to thank Dr. Howard S. Sherry, Mobil Research and Development Corp., Princeton, N. J., for helpful discussions during the course of this study.

(13) A. S. Medina, Ph.D. Thesis, Department of Chemistry, Ohio University, June 1971.

Salt Effects in Alcohol–Water Solutions. An Application of Scaled Particle Theory to the Salting-Out of Polar Molecules[1,2]

by Floyd L. Wilcox and Eugene E. Schrier*

Department of Chemistry, State University of New York at Binghamton, Binghamton, New York 13901
(Received February 4, 1971)

Publication costs assisted by the National Institutes of Health

The variation of the activity coefficient of several alcohols with molality of added salt in aqueous solution has been obtained using the electrochemical method. The alcohols studied were methanol, ethanol, 1-propanol, and ethylene glycol while the salts used were sodium chloride, sodium bromide, and sodium iodide. The logarithm of the ratio of the activity coefficient of the alcohol in the salt solution to its activity coefficient in pure water could be expressed for each system in terms of the molalities of salt, m_1, and alcohol, m_2, as log $(\gamma_2/\gamma_2^\circ) = Am_1 + {}^2/_3Bm_1^{1.5} + {}^1/_2Cm_1^2 + Dm_1m_2$. Values of the four parameters for each system are given. It was shown that the limiting interaction parameter, A, for each system could be considered, to a good approximation, to be composed of additive contributions from the CH_3, CH_2, and OH groups comprising the molecule. The limiting interaction parameter was also calculated using equations obtained from the scaled particle theory by Masterton and Lee [*J. Phys. Chem.*, **74**, 1776 (1970)]. Good agreement was found between experimental and theoretical A values with the use of suitable values for the molecular parameters. This suggests that the scaled particle theory can be used in its present form to predict salt effects on polar nonelectrolytes in certain favorable cases.

Introduction

The study of salt effects on the activity coefficients of nonelectrolytes in aqueous solution has had a venerable place in the classical physical chemistry of solutions. Most experimental work done in the past, however, has concentrated on slightly soluble nonpolar nonelectrolytes. The recent interest in salt effects in biological systems, *e.g.*, in studies of conformational changes of macromolecules and in models for membrane structure and function, has pointed up the need for more data on the interactions of salts with small polar molecules. Information regarding such systems can serve to amplify the understanding of analogous interactions in the more complex biological cases.[3]

There has been an even more recent impetus to investigation of salt effects in aqueous systems. Shoor and Gubbins[4] and Masterton and Lee[5] have convincingly demonstrated the applicability of the scaled particle theory to the calculation of the limiting parameter characterizing the interaction between ions and a nonelectrolyte molecule in aqueous solution. Their treatments and comparisons between experimental results and theoretical calculations were based on systems involving nonpolar nonelectrolytes. A question of real interest is whether the theory can be used in its present form to account for effects on certain types of polar molecules.

In this work, the variation of the activity coefficients of alcohols with salt and alcohol molality in 12 alcohol–salt–water systems was investigated using the electrochemical method. A comparison of the limiting interaction parameters obtained from these data with those calculated from the scaled particle theory was the major objective.

Experimental Section

Materials. The salts, sodium chloride, sodium bromide, and sodium iodide, were ACS reagent grade and were used without further purification. They were dried at elevated temperature before use. Methanol and absolute ethanol were the best grade commercially available and were used without further purification. 1-Propanol was distilled using a Widmer column. The middle portion which distilled between 97.0 and 97.5° was retained. Ethylene glycol was vacuum distilled at 10 mm; the material retained was that which boiled at approximately 92°.

All the alcohols were subjected to gas chromatographic analyses and showed a purity of 99.9% or better. Analyses by Karl Fischer titration showed less than 0.01% water. The water content was maintained at a low level by storage over Linde 4A molecular sieves.

Electrode and Potential Measurements. Beckman general cationic and sodium ion glass electrodes and

(1) Taken in part from a thesis submitted by F. L. Wilcox to State University of New York at Binghamton in partial fulfillment of the requirements for the degree of Doctor of Philosophy, June 1971.

(2) This work was supported in part by Public Health Service Grant No. GM 11762 from the Institute of General Medical Sciences and by an N.D.E.A. Title IV Fellowship to F. L. Wilcox.

(3) E. E. Schrier and E. B. Schrier, *J. Phys. Chem.*, **71**, 1851 (1967).

(4) S. K. Shoor and K. E. Gubbins, *ibid.*, **73**, 498 (1969).

(5) W. L. Masterton and T. P. Lee, *ibid.*, **74**, 1776 (1970).

Corning sodium ion glass electrodes were used about equally for the measurements. Results obtained with the same solution using different electrodes were identical within experimental error. The silver–silver halide electrodes were prepared using procedures described in the literature.[6,7]

Potential measurements were made with two different instruments. One was a Keithley Model 630 potentiometric electrometer used in conjunction with a Model 6013 pH electrode adapter. This instrument was readable to ±0.01 mV and reproducible to ±0.03 mV. The other was a Beckman research pH meter which could be read to ±0.03 mV and was reproducible to ±0.05 mV. The voltage differences, ΔE (see below), obtained in the various systems investigated were in the range from 0 to 7 mV.

Temperature Control. An oil bath and a circulator controller were used to maintain a constant temperature of 25.0 ± 0.1°.

Method of Procedure. Since a detailed description of the electrochemical method has been given recently,[8] the discussion here will be brief and will consider mainly the modifications of the procedure previously described.

In the electrochemical method, the potential difference between two cells, A and B, of the type Na^+ sensitive electrode|NaX(m_1), alcohol(m_2), water|AgX, Ag is obtained. The cells are at the same molality of NaX but differ in the molality of alcohol. If the experimental procedure can account for the asymmetry potential differences between the glass electrode in the two cells, then it follows that[8]

$$\left(\frac{\Delta E}{\Delta m_2}\right)_{m_1} = \frac{2RT}{F}\left(\frac{\ln (\gamma_{1B}/\gamma_{1A})}{\Delta m_2}\right)_{m_1} = \frac{2RT}{F}\left(\frac{\Delta \ln \gamma_1}{\Delta m_2}\right)_{m_1} \quad (1)$$

where ΔE is the potential difference between cells A and B, Δm_2 is the difference in the molalities of alcohol in the two cells, and γ_{1B} and γ_{1A} are the respective activity coefficients of the electrolyte.

If the measured ratio on the left-hand side of eq 1 varies linearly with nonelectrolyte molality, the ratio of the finite differences given on the right-hand side of eq 1 may be replaced by a partial derivative. As will be discussed below, this condition was met in these experiments. Equation 1 may then be written

$$\left(\frac{\Delta E}{\Delta m_2}\right)_{m_1} = \left(\frac{2RT}{F}\right)\left(\frac{\partial \ln \gamma_1}{\partial m_2}\right)_{m_1} \quad (2)$$

and, using the cross differentiation relationship,[8] we finally obtain

$$\left(\frac{\Delta E}{\Delta m_2}\right)_{m_1}\left(\frac{F}{2.303RT}\right) = \left(\frac{\partial \log \gamma_2}{\partial m_1}\right)_{m_2} \quad (3)$$

The molality, m_2, which is held constant in the partial derivative on the right-hand side of eq 3 is the alcohol molality midway between the alcohol molalities, m_{2A} and m_{2B}, in the cells A and B, respectively, used to evaluate ΔE. In other words $\Delta m_2 = m_{2B} - m_{2A}$ and $m_2 = (m_{2A} + m_{2B})/2$. In eq 3, γ_2 is the activity coefficient of the nonelectrolyte.

The experimental procedure followed was similar to that of Spink and Schrier.[8] Slight modifications were made to obtain the data more rapidly. For instance, the first two solutions used were a stock sodium halide solution and the same solution containing a fixed molality of alcohol. Immediately after the measurements were completed on these solutions, the one containing alcohol became the first member of a new pair. Transfer of the glass electrode between the solutions to eliminate the effect of the asymmetry potential was also done much as before. To expedite the taking of data in this case, an arbitrary criterion for accepting a set of measurements was used, *i.e.*, that transfers be made until the potential difference between the two solutions was constant to within 0.10 mV for three consecutive transfers. Use of these modifications allowed a larger amount of data to be taken in a shorter time with only slightly lessened accuracy compared to the previous work.

Results

The primary data resulting from these measurements were sets of values of $(\Delta E/\Delta m_2)_{m_1}$ over a range of alcohol and salt molalities for the 12 systems made from the four alcohols, methanol, ethanol, 1-propanol, and ethylene glycol, and the three salts, sodium chloride, sodium bromide, and sodium iodide. Measurements were made on systems involving the chloride at five different salt molalities in the range from 0.01 to 3.0 m salt. At each of these salt molalities, five alcohol molalities were investigated, ranging from 0.5 to 3.0 m alcohol. A similar scheme was employed for the systems involving sodium bromide but the electrolyte range was somewhat narrower, 0.05–2.0 m, owing to electrode instability at the extremes of the molality range. Since it is known[9] that silver iodide forms complexes with iodide ion at sodium iodide molalities greater than 0.1 m, this necessarily provided the upper limit of the electrolyte range. Measurements were therefore done at five salt molalities between 0.0075 and 0.1 m. The effect of this reduced range on the calculated parameters of fit will be discussed later.

An important point to consider is the dependence of $(\Delta E/\Delta m_2)_{m_1}$ on alcohol molality. For any given alcohol–salt combination, a straight line resulted when this quantity was plotted against alcohol molality at fixed

(6) D. J. G. Ives and G. J. Janz, Ed., "Reference Electrodes," Academic Press, New York, N. Y., 1961, p 179.

(7) H. B. Hetzer, R. A. Robinson, and R. G. Bates, *J. Phys. Chem.*, **66**, 1423 (1962); **68**, 1929 (1964).

(8) M. Y. Spink and E. E. Schrier, *J. Chem. Thermodyn.*, **2**, 821 (1970).

(9) R. G. Bates, *J. Amer. Chem. Soc.*, **60**, 2983 (1938).

Table I: The Coefficients and Their Standard Deviations for the Representation by Eq 4 and 5 of the Variation of the Activity Coefficient of Alcohols with Solute Molality in Aqueous Salt Solutions

		Coefficients and standard deviations				Fit
Salt	Alcohol	A, kg mol^{-1}	B, kg$^{1.5}$ mol$^{-1.5}$	C, kg^2 mol^{-2}	D, kg^2 mol^{-2}	standard deviation
NaCl	Ethylene glycol	0.0393 ± 0.0003	−0.00369 ± 0.0005	−0.0012 ± 0.0003	−0.0038 ± 0.0001	0.0007
NaCl	Methanol	0.0658 ± 0.0003	−0.0043 ± 0.0005	−0.0023 ± 0.0002	−0.0035 ± 0.0001	0.0018
NaCl	Ethanol	0.1180 ± 0.0004	−0.0135 ± 0.0007	−0.0013 ± 0.0004	−0.0071 ± 0.0001	0.0014
NaCl	1-Propanol	0.1654 ± 0.0010	−0.0037 ± 0.0023	0.0070 ± 0.0012	−0.0206 ± 0.0003	0.0012
NaBr	Ethylene glycol	0.0252 ± 0.0008	0.0051 ± 0.0017	−0.0082 ± 0.0010	−0.0044 ± 0.0003	0.0021
NaBr	Methanol	0.0555 ± 0.0013	0.0014 ± 0.0032	−0.0054 ± 0.0019	−0.0045 ± 0.0003	0.0039
NaBr	Ethanol	0.1007 ± 0.0006	−0.0134 ± 0.0016	−0.0006 ± 0.0010	−0.0076 ± 0.0002	0.0019
NaBr	1-Propanol	0.1331 ± 0.0014	−0.0243 ± 0.0036	0.0012 ± 0.0022	−0.0184 ± 0.0004	0.0042
NaI	Ethylene glycol	0.0065 ± 0.0003	−0.0145 ± 0.0012	0.0120 ± 0.0011	−0.0024 ± 0.0001	0.0009
NaI	Methanol	0.0431 ± 0.0012	−0.0344 ± 0.0127	0.0843 ± 0.0324	−0.0036 ± 0.0003	0.0021
NaI	Ethanol	0.0793 ± 0.0014	−0.0286 ± 0.0164	0.0392 ± 0.0417	−0.0082 ± 0.0002	0.0026
NaI	1-Propanol	0.0943 ± 0.0015	0.0109 ± 0.0186	−0.0914 ± 0.0468	−0.0194 ± 0.0003	0.0031

salt molality. In addition, varying the magnitude of Δm_2 around the same average m_2 in several systems produced no change in the value of $(\Delta E/\Delta m_2)_{m_1}$. We conclude therefore that the dependence of $(\Delta E/\Delta m_2)_{m_1}$ on alcohol molality is linear. This allows us to replace the ratio of differences of eq 1 by a partial derivative, *i.e.*, replace the right-hand side of eq 1 by the right-hand side of eq 2, *et seq.* It should be reiterated that the derivatives are taken at the alcohol molality, m_2, midway between m_{2A} and m_{2B}, the alcohol molalities in the cells used to evaluate ΔE.

Values of $(\partial \ln \gamma_2/\partial m_1)_{m_2}$ were calculated from the measured values of $(\Delta E/\Delta m_2)_{m_1}$ using eq 3. The extensive nature of the tables of original and calculated results does not permit reproduction here.[10] However, the data could be correlated by the equation[8]

$$\left(\frac{\partial \log \gamma_2}{\partial m_1}\right)_{m_2} = A + Bm_1^{0.5} + Cm_1 + Dm_2 \quad (4)$$

using a least-squares routine with an IBM 360-40 computer. The values of the parameters, A, B, C, and D, may be found in Table I along with their standard deviations. The standard deviation of the fit is the standard deviation of the average value of $(\partial \log \gamma_2/\partial m_1)_{m_2}$ for a given alcohol–salt–water system. The logarithm of the ratio of the activity coefficient of the alcohol in the salt solution, γ_2, to the activity coefficient of the alcohol in water, γ_2°, may be calculated using the parameters in Table I and the integrated form of eq 4, *viz.*

$$\log (\gamma_2/\gamma_2^\circ) = Am_1 + {}^2/_3Bm_1^{1.5} + {}^1/_2Cm_1^2 + Dm_1m_2 \quad (5)$$

Activity coefficients of the alcohols in water may be obtained from the equations presented by Knight and Kozak.[11]

The concordance of the experimental data and the values calculated using eq 4 is demonstrated in Figures 1–4 where the values of $(\partial \log \gamma_2/\partial m_1)_{m_2}$ for some representative systems is plotted along with the least-squares lines calculated using the data in Table I. The question of whether the difference in the range of salt molalities for the systems containing sodium iodide *vs.* those with sodium chloride introduced a discrepancy into the parameters was investigated in the following way. A fit was made using eq 4 of those data in the salt molality range 0.01–0.5 m for the systems sodium chloride–methanol–water and sodium chloride–ethanol–water. The parameters resulting from these calculations were compared with those given in Table I for the same system and were shown to agree to within their standard deviations. This agreement of the full range parameters with those for the limited range suggests that the values of the parameters for sodium iodide are not affected by the magnitude of the electrolyte range in which they were obtained.

Discussion

Inspection of the data in Table I reveals that there are observable trends in the A and D parameters only. The D parameter appears to be about the same for systems involving the same alcohol and becomes more negative in the series ethylene glycol, methanol, ethanol, and 1-propanol. These facts may reflect the relation of this parameter to the difference in the strength of solvation of the ions by water and the various alcohols. If we propose that only the cations are solvated by the OH group of the alcohols,[12] then a constancy of the D

(10) The complete tables of original and derived data may be found in the Ph.D. Thesis of F. L. Wilcox, State University of New York at Binghamton, 1971.

(11) (a) W. S. Knight, Ph.D. Thesis, Princeton, 1962; (b) J. Kozak, Ph.D. Thesis, Princeton, 1966.

(12) R. H. Stokes and R. A. Robinson, *J. Amer. Chem. Soc.*, **70**, 1870 (1948).

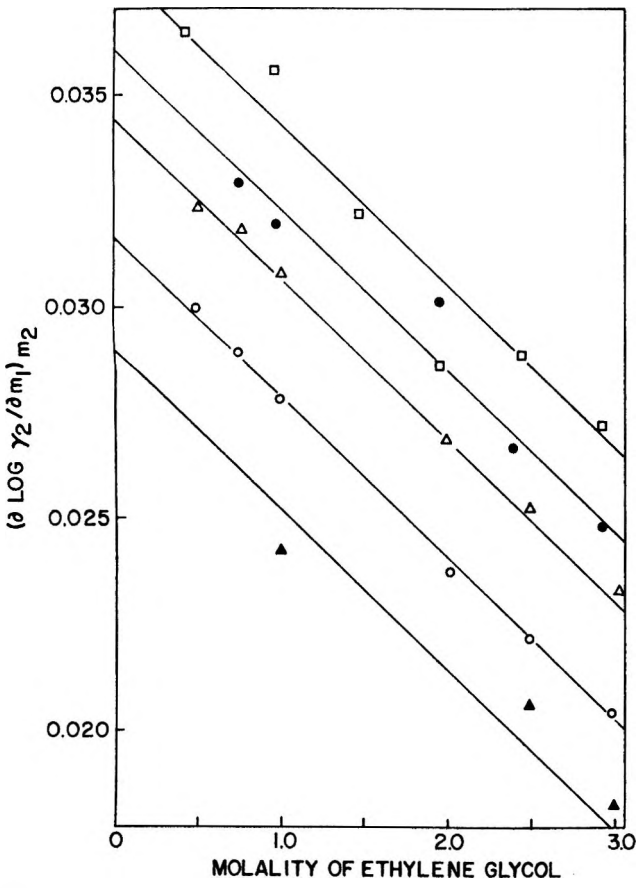

Figure 1. The derivative, $(\partial \log \gamma_2/\partial m_1)_{m_2}$, plotted as a function of the ethylene glycol molality, m_2, at the sodium chloride molalities: □, 0.1006; ●, 0.5101; △, 0.9980; ○, 2.0207; ▲, 3.1418.

value for a given alcohol in the presence of different sodium halides can be understood. A test of this idea could readily be made by substituting other ions for the sodium ion. The increasingly negative values of D encountered in going from ethylene glycol to 1-propanol may arise from the dielectric decrements of the alcohols increasing in that order. This would lead to strengthened ion–dipole interactions in line with the decrease in dielectric constants of the solutions.

We turn to a detailed consideration of the values of A, the limiting interaction parameter. The qualitative trends in the observable values are (1) the increase in the values, for a given salt, from the most polar compound, ethylene glycol, to the least polar, 1-propanol, and (2) the decrease of the effect produced by the salts, for a given alcohol, in the order sodium chloride, sodium bromide, sodium iodide. Both trends suggest a similarity between the behavior of the alcohols in sodium halide solutions and the behavior of nonpolar nonelectrolytes in like circumstances.[5]

This similarity may be examined more closely by using an empirical scheme to divide the A values into contributions from the various functional groups comprising the alcohol molecules. We assume[3] that

$$A = \sum_i a_i \tag{6}$$

where the a_i are the contributions to the limiting interaction parameter of each methyl, methylene, or hydroxyl group. An analogous statement is that the free energy of transfer of the alcohol from water to a salt solution (with the standard states for both solutions based on pure water) is the sum of additive contributions from the individual functional groups. The solutions are considered to be at infinite dilution with respect to the solutes.

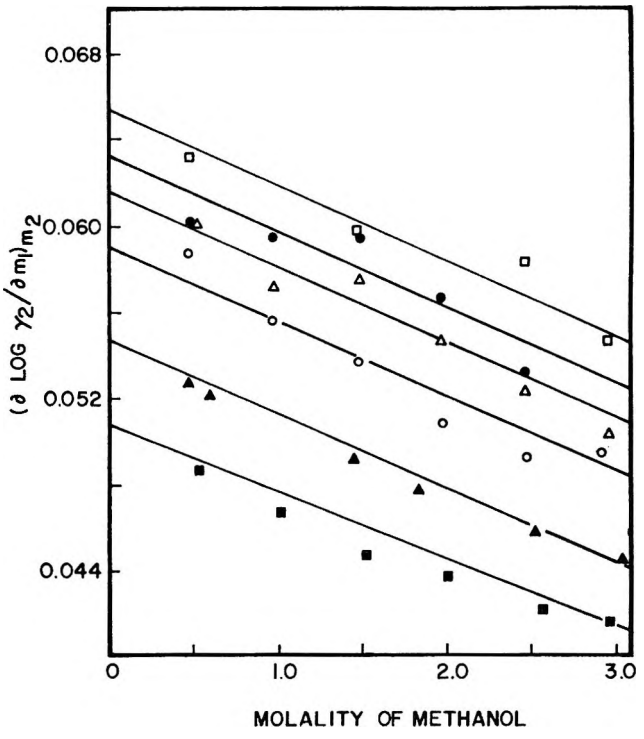

Figure 2. The derivative, $(\partial \log \gamma_2/\partial m_1)_{m_2}$, plotted as a function of the methanol molality, m_2, at the sodium chloride molalities: □, 0.01007; ●, 0.2494; △, 0.5057; ○, 1.0363; ●, 2.0920; ■, 3.1776. The lines from the top to the bottom of the figure are in order of increasing sodium chloride molality.

Consideration of the structural formulas of the alcohols studied here will show that it is necessary to have the value of the limiting interaction parameter, A, for only two alcohols and ethylene glycol to calculate the three group contributions for any particular salt. In other words, there are three different ways of calculating the group contributions, depending on which A value is not used. For example, let us use the A values for methanol, ethanol, and ethylene glycol to calculate the three group parameters. Now

$$A_{CH_3OH} = a_{CH_3} + a_{OH} \tag{7}$$

$$A_{CH_3CH_2OH} = a_{CH_3} + a_{CH_2} + a_{OH} \tag{8}$$

$$A_{HOCH_2CH_2CH_2OH} = 2a_{CH_2} + 2a_{OH} \tag{9}$$

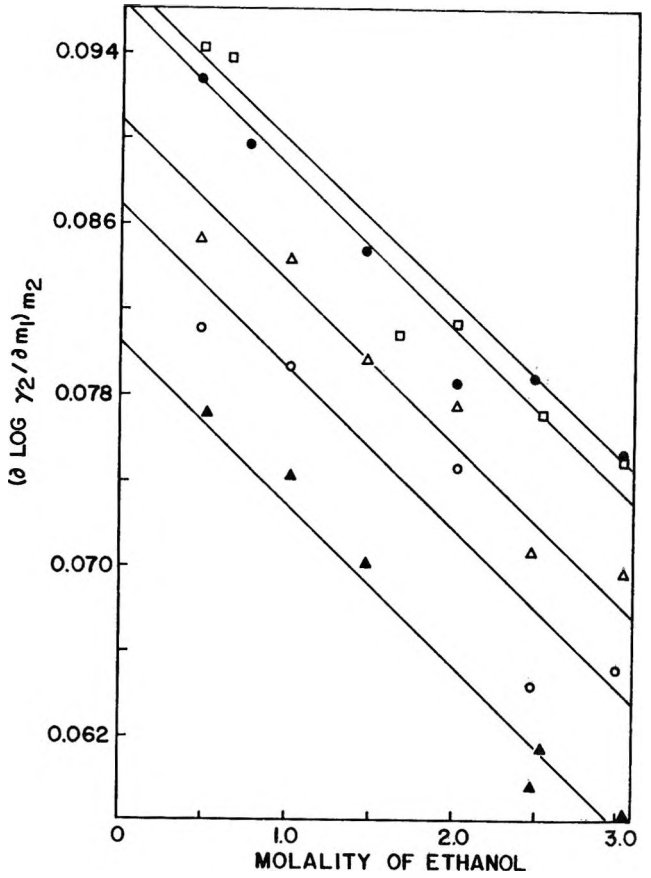

Figure 3. The derivative, $(\partial \log \gamma_2/\partial m_1)_{m_2}$, plotted as a function of the ethanol molality, m_2, at the sodium bromide molalities: □, 0.05003; ●, 0.1014; △, 0.5062; ○, 0.9670; ▲ 1.9953.

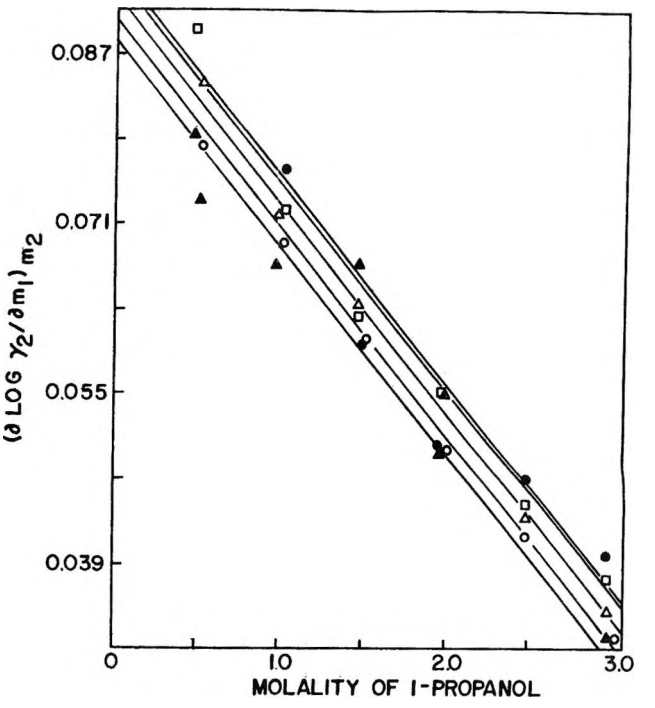

Figure 4. The derivative, $(\partial \log \gamma_2/\partial m_1)_{m_2}$, plotted as a function of the 1-propanol molality, m_2, at the sodium iodide molalities: □, 0.007975; ●, 0.01010; △, 0.04993; ○, 0.07466; ▲, 0.1001. The lines from the top to the bottom of the figure are in order of increasing sodium iodide molality.

therefore

$$a_{CH_2} = A_{CH_3CH_2OH} - 0.5A_{HOCH_2CH_2OH} \quad (10)$$

$$a_{OH} = A_{CH_3OH} - A_{CH_3CH_2OH} + 0.5A_{HOCH_2CH_2OH} \quad (11)$$

$$a_{CH_2} = A_{CH_3CH_2OH} - A_{CH_3OH} \quad (12)$$

in this calculation the parameter for 1-propanol is not used.

The results of doing this calculation using the four alcohol values for each salt are given in Table II. The column headed "alcohol not used" indicates which A value is not used in the calculation. The average group contributions obtained for each salt are also given in the table together with the standard deviations of these means. The standard deviations given with the individual group values are the resultant of propagating the standard deviations of the original A values.

Consideration of the values in Table II suggests that eq 6 is followed at least approximately in the systems investigated here. If the contributions were perfectly additive, the value calculated for each group contribution should be the same for a given salt regardless of which A values were used to obtain it. Another method of making the comparison is to calculate the A value for each alcohol–salt system using the average group contributions of Table II. The results of this calculation and the per cent deviation of the calculated values from the experimental values are given in Table III. The average of all the percentage deviations is 3.9%. This method of comparison also suggests that eq 6 is valid to a good approximation in these systems.

Comparison of these group parameters with those obtained from the data of other workers is interesting. In Table IV, we compare the group parameters of this work with those obtained from the data of Schrier and Schrier[3] on *N*-methylpropionamide and *N*-methylacetamide, and Morrison and Billet[13] on the C_1–C_4 alkanes. The previous data have been put on a molality basis. Although the CH_3-group parameters of Schrier and Schrier[3] compare favorably with those obtained here, we have not presented them in the table since they were not directly determined from experimental data.

Inspection of the data in this table reveals that there is a fairly consistent correlation of parameters obtained using the data of one class of compounds with those from another class. It is probably too soon to conjecture as to whether the constant difference observed between these results and those of Schrier and Schrier represents a real effect or is merely an artifact resulting from differences in the experimental methods.

Another trend worth noting is that a_{CH_2} calculated from $A_{CH_3CH_2OH} - A_{CH_3OH}$ and that calculated from $A_{CH_3CH_2CH_2OH} - A_{CH_3CH_2OH}$ are different, the difference

(13) T. J. Morrison and F. Billet, *J. Chem. Soc.*, 381 (1962).

Table II: Calculated Values of the Group Contributions

Salt	Alcohol not used	Group contributions a_{CH_3}	a_{CH_2}	a_{OH}
NaCl	Methanol	0.0984 ± 0.0016	0.0474 ± 0.0011	−0.0278 ± 0.0011
	Ethanol	0.0959 ± 0.0007	0.0498 ± 0.0005	−0.0301 ± 0.0005
	1-Propanol	0.0983 ± 0.0006	0.0522 ± 0.0005	−0.0325 ± 0.0005
Av contribution		0.0975 ± 0.0014	0.0498 ± 0.0024	−0.0301 ± 0.0024
NaBr	Methanol	0.0881 ± 0.0022	0.0324 ± 0.0015	−0.0198 ± 0.0016
	Ethanol	0.0817 ± 0.0020	0.0388 ± 0.0010	−0.0262 ± 0.0025
	1-Propanol	0.0881 ± 0.0020	0.0452 ± 0.0014	−0.0326 ± 0.0015
Av contribution		0.0860 ± 0.0037	0.0388 ± 0.0060	−0.0262 ± 0.0064
NaI	Methanol	0.0760 ± 0.0033	0.0150 ± 0.0021	−0.0117 ± 0.0021
	Ethanol	0.0654 ± 0.0023	0.0256 ± 0.0010	−0.0223 ± 0.0010
	1-Propanol	0.0760 ± 0.0022	0.0362 ± 0.0018	−0.0329 ± 0.0018
Av contribution		0.0725 ± 0.0061	0.0256 ± 0.0106	−0.0223 ± 0.0106

Table III: Comparison of Experimental A Values and Those Calculated Based on the Use of Eq 6 and the Average Group Contributions of Table II

Salt	Alcohol	A parameter Calcd	Exptl	Percentage deviation
NaCl	Methanol	0.0674	0.0658	+2.4
	Ethanol	0.1172	0.1180	−0.7
	1-Propanol	0.1670	0.1654	+1.0
	Ethylene glycol	0.0394	0.0393	+0.2
NaBr	Methanol	0.0598	0.0555	+7.8
	Ethanol	0.0986	0.1007	−2.0
	1-Propanol	0.1374	0.1331	+3.1
	Ethylene glycol	0.0252	0.0252	0
NaI	Methanol	0.0502	0.0431	+16.5
	Ethanol	0.0758	0.0793	−4.4
	1-Propanol	0.1014	0.0943	+7.5
	Ethylene glycol	0.0066	0.0065	+1.6

Table IV: Comparison of Group Contributions from Various Investigations

Salt	Group	This work	Schrier and Schrier[a]	Morrison and Billet[b]
NaCl	CH_3	0.098	...	0.084
NaCl	CH_2	0.050	0.063	0.032
NaBr	CH_2	0.039	0.051	...
NaI	CH_2	0.026	0.037	...

[a] From ref 3. [b] From ref 13.

between the values increasing in going from sodium chloride to sodium iodide. Although this could be the resultant of experimental error, this explanation appears unlikely. More probably, there may be a small difference between the values of a group parameter depending on whether it is directly attached to a polar group or a nonpolar group. The increase in the difference with increasing ion size may reflect the changing effect of the ions on water structure which may differ around the two types of CH_2 groups.

Even though it is obvious that more work is necessary to amplify the nature of these second-order effects, results have been obtained which are useful in a wide variety of application, *e.g.*, ref 3. Of more fundamental interest is the possibility of calculating the A parameters directly from molecular information, a problem to which we now turn.

The scaled particle theory has been applied to the calculation of A parameters by Shoor and Gubbins[4] and Masterton and Lee.[5] The equations they derived are strictly applicable only to spherical nonpolar nonelectrolytes. Even so, we felt that an attempt to calculate the A parameters for the alcohols could be made using the theory in its present form. We reasoned that the polar group was similar enough to the solvent so that specific ion–dipole interactions, *i.e.*, solvation of the ion by the polar group, would not be competitive with the more numerous interactions afforded by water. In this situation, any term which might be added to the theory to account for ion–dipole interaction could not accurately represent the orientation of the weak dipole of the alcohol in the ionic field. Including the dispersion interaction of the OH group with the ion and accounting for the volume of the OH group are still possible without modifying the theory.

We have therefore used eq 11, 19, and 32 of Masterton and Lee[5] to calculate the A parameters in the alcohol–salt–water systems. Molecular data found in the literature for the alcohols are given in Table V. The polarizabilities, with the exception of the value for methanol obtained from the literature, were calculated by adding bond refractions given by Hill, *et al.*[14] The literature value compares well with the calculated value in the case of methanol.

Turning to the Lennard-Jones parameters, we observe that there is a fair concordance among the different investigators with regard to the hard-sphere diame-

(14) N. E. Hill, W. E. Vaughn, A. H. Price, and M. Davies, "Dielectric Properties and Behavior," Van Nostrand-Reinhold, Princeton, N. J., 1969, p 238.

Table V: Molecular Parameters for the Alcohols

Molecule	Diameter, $\sigma \times 10^8$, cm	Force constant, ϵ/k, °K	Polarizability, $\alpha \times 10^{24}$, cm³	Reference
Methanol	3.666	452		*a*
	3.626	482		*b*
	3.69	234		*c*
			3.23	*d*
			3.27	*e*
Ethanol	4.370	415		*a*
	4.530	362		*b*
	4.34	324		*c*
			5.11	*e*
1-Propanol	4.71	495		*f*
	4.549	577		*b*
			6.96	*e*
Ethylene glycol			5.72	*c*

[a] J. O. Hirschfelder, C. F. Curtiss, and R. B. Bird, "Molecular Theory of Gases and Liquids," corrected ed with notes added, Wiley, New York, N. Y., 1954, p 1214. [b] R. C. Reid and T. K. Sherwood, "The Properties of Gases and Liquids," 2nd ed, McGraw-Hill, New York, N. Y., 1966, p 632. [c] From ref 15. [d] Landolt-Bornstein, "Zahlenwerte and Funktionen," Springer-Verlag, Berlin, 1951, Vol. I, part 3, p 510. [e] See text. [f] J. O. Hirschfelder, *et al.*, footnote *a*, p 1200; these values are derived for a Stockmayer potential function.

ter σ, but poor agreement for the force constants, ϵ/k. The first two sets of values for each alcohol have been obtained from data on the gaseous materials and may not be appropriate in calculations dealing with condensed phases. Wilhelm and Battino[15] derived their results by calculation from the properties of liquid alcohols. For this reason, we chose their values to use in the calculation of A parameters in the systems with methanol and ethanol. The results are shown in Table VI. There is fair agreement between the calculated and experimental values with the calculated quantities being higher than the experimental in the methanol systems and lower in those containing ethanol.[15a]

It is also interesting to derive the A parameters using force constants calculated for each alcohol using the equation of Mavroyannis and Stephen.[5,16] Actually the Mavroyannis–Stephen equation was substituted for ϵ_1/k in eq 19 of Masterton and Lee.[5] The value of the hard-sphere diameter for each alcohol was then used as a variable parameter so that the A values calculated for the sodium bromide systems were close to the experimental values. The diameter of the alcohol thus chosen was then used in the calculation of the A values for the other salt–alcohol systems. The results of these calculations are given in Table VII. It can be seen that there is good agreement between the calculated and experimental A values for all the systems investigated. The hard-sphere diameters derived in this way and given in Table VII compare favorably with those obtained from other properties of the alcohols (see Table V). The diameter derived for ethylene glycol lies intermediate between that for methanol and ethanol. There is no way to judge the reliability of this value.

Table VI: Comparison of Experimental A Parameters for the Alcohols with Those Calculated Using the Molecular Parameters of Wilhelm and Battino[a,b]

Alcohol	Salt	A(calcd)	A(exptl)
Methanol	NaCl	0.083	0.066
	NaBr	0.055	0.055
	NaI	0.046	0.042
Ethanol	NaCl	0.088	0.118
	NaBr	0.058	0.101
	NaI	0.037	0.079

[a] From ref 15. [b] See ref 15a.

Table VII: Comparison of Experimental A Parameters for the Alcohols with Those Calculated by Fitting to the Experimental Data for Alcohol–Sodium Bromide Systems[a]

Alcohol	Diameter, $\sigma \times 10^8$, cm	Force constant, ϵ/k, °K	Salt	A(calcd)	A(exptl)
Methanol			NaCl	0.062	0.066
	3.50	311	NaBr	0.036	0.055
			NaI	0.018	0.042
Ethanol			NaCl	0.112	0.118
	4.25	227	NaBr	0.084	0.101
			NaI	0.067	0.079
1-Propanol			NaCl	0.149	0.165
	4.80	198	NaBr	0.119	0.133
			NaI	0.103	0.095
Ethylene glycol			NaCl	0.040	0.039
	3.90	517	NaBr	0.005	0.025
			NaI	−0.016	0.007

[a] See ref 15a.

The value of the force constant calculated from the Mavroyannis–Stephen equation is given for each alcohol in the third column of Table VII. The values are in poor agreement with those derived from other alcohol properties given in Table V. The situation is analogous to that reported by Masterton and Lee[5] for benzene–salt–water mixtures and for the sodium chloride–cyclohexane–water system.[17] In these cases, the best fit to the experimental A values is given using the scaled par-

(15) E. Wilhelm and R. Battino, *J. Phys. Chem.*, in press.

(15a) NOTE ADDED IN PROOF. Equation 9 in the recent paper of Masterton, *et al.* [W. L. Masterton, D. Bolocofsky, and T. P. Lee, *ibid.*, 75, 2809 (1971)], has been used to bring the A(calcd) values onto the molality scale.

(16) C. Mavroyannis and M. J. Stephen, *Mol. Phys.*, 5, 629 (1962).

(17) Y. L. Chang and E. E. Schrier, unpublished data.

ticle theory with the literature value of the hard-sphere diameter and the force constant derived from the Mavroyannis–Stephen equation. The significance of this finding is not clear at the present time.

An attempt was also made to calculate the group parameters using scaled particle theory. Although there was fair agreement between the calculated and experimental values, the choice of parameters is arbitrary.[18] Qualitatively, it is possible to understand the additivity of group contributions to the A parameter based on additivity in the molecular properties such as polarizabilities, partial molal volumes, and molecular diameters which are used in the theoretical calculation. To the extent that the molecular properties are additive, it appears the A parameters can be considered to be comprised of additive contributions also.

The comparison in Table VI suggests that the scaled particle theory can be used in its present form to calculate data for polar molecules. The small contribution of the hydroxyl group (*cf.* Table II) to A makes alcohol–electrolyte–water mixtures particularly favorable systems to which to apply the theory. Seemingly, both continued empirical and theoretical study of the fine structure of these interactions will prove rewarding.

(18) For the details of this calculation, see ref 10.

NOTES

Calculation of Inter-Ring Proton Couplings

by George F. Adams

Propellants Laboratory, Picatinny Arsenal, Dover, New Jersey 07801
(Received May 27, 1971)

Publication costs assisted by the Propellants Laboratory, Picatinny Arsenal

Pople, *et al.*,[1] have adapted finite-field perturbation theory to the INDO approximate molecular orbital method[2] in order to calculate nmr spin-coupling constants. This note will discuss an application of this procedure.

Inter-ring proton couplings, especially those over more than four bonds, are of great interest in organic chemistry.[3] Much of the experimental work in this area has been done on substituted compounds. This limits the ability to correlate the information on inter-ring couplings with other molecular parameters. Jarvis and Moritz[4] have reported an attempt to determine experimentally the six inter-ring coupling constants in naphthalene. They were not able, however, to determine both the magnitude and sign of all these parameters.

Since previous INDO calculations of nmr spin-coupling constants have given good agreement with the experimentally determined values, we have used the INDO method to calculate the inter-ring proton couplings. The INDO and experimental results for naphthalene are given in Table I; the labeling of the protons is indicated in Figure 1.

Table I: Inter-Ring Proton Couplings in Naphthalene

Coupling	Calcd coupling constant	Obsd coupling constant
$J_{1,5}$	+1.80	+0.83
$J_{1,6}$	−0.44	−0.16
$J_{1,7}$	+0.54	+0.21
$J_{1,8}$	−0.58	...
$J_{2,6}$	+0.40	|0.28|
$J_{2,7}$	+0.02	...
$J_{1,3}$	+1.95	+1.25

In their paper, Jarvis and Moritz speculate that $J_{2,6}$ is negative, but the INDO calculations do not support this contention. This result is in agreement with Barfield's[5] suggestion that coupling should be positive between protons separated by an odd number of bonds and negative between protons separated by an even number of bonds. Of interest in this respect is the fact that the INDO calculation predicts $J_{1,3} = +1.95$. These protons are separated by an even number of bonds, and one would expect a negative coupling constant. The positive sign is an indication that there is a significant contribution to the coupling from the σ-electron framework. The calculated $J_{1,3}$ has the same sign as the experimentally determined $J_{1,3}$. The signs of the other proton–proton coupling constants are in agreement with the experimental signs, except for $J_{2,7}$. However, the magnitude of this calculated coupling infers that the suggestion of Jarvis and Moritz that $J_{2,7}$ is zero may be correct.

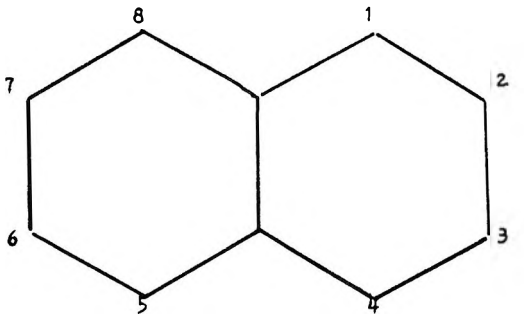

Figure 1. Labeling of the naphthalene protons. r_{C-C} = 1.40; r_{C-H} = 1.08; ∠CCC = ∠CCH = 120°.

There has been a question of the sensitivity of the calculated coupling constant to small changes in the molecular geometry. The naphthalene geometry in the calculation uses the bond lengths and angles suggested by Pople and Gordon.[6] Their suggested carbon–hydrogen bond length is 1.08 Å. Calculations were done for two other carbon–hydrogen distances, and the results are summarized in Table II. The variations in J are quite small, especially when one considers the semiempirical nature of the molecular orbital calculation. More significant is the fact that the calculated signs of the coupling constants are unaffected by these variations.

(1) J. A. Pople, J. W. McGiver, Jr., and N. S. Ostlund, *J. Chem. Phys.*, **49**, 2965 (1968).

(2) J. A. Pople, D. L. Beveridge, and P. A. Dobosh, *ibid.*, **46**, 2026 (1967).

(3) K. D. Bartle, D. W. Jones, and R. S. Mathews, *Rev. Pure Appl. Chem.*, **19**, 191 (1969).

(4) M. W. Jarvis and A. G. Moritz, *Aust. J. Chem.*, **24**, 89 (1971).

(5) M. Barfield, *J. Chem. Phys.*, **48**, 4463 (1968).

(6) J. A. Pople and M. S. Gordon, *J. Amer. Chem. Soc.*, **89**, 4253 (1967).

Table II: Variation in J with C–H Bond Length

Coupling	r_{C-H}, Å: 1.10	1.08	1.06
	Calculated coupling constant		
$J_{1,3}$	+2.19	+1.95	+1.74
$J_{1,5}$	+1.98	+1.80	+1.63
$J_{1,6}$	−0.47	−0.44	−0.40
$J_{1,7}$	+0.58	+0.54	+0.499
$J_{1,8}$	−0.62	−0.58	−0.54

Acknowledgment. This work was completed while the author was a National Research Council Resident Research Associate at Picatinny Arsenal. The author thanks the MUCOM DPSO for use of computer facilities. He also thanks Dr. Lee Pedersen of the University of North Carolina and Dr. Ted Vladimiroff of Picatinny Arsenal for encouragement and assistance.

Carbon-13 Nuclear Magnetic Resonance Spectrosopy. IV. Bromo-Substituted Ethanes and Ethylenes[1]

by Goh Miyajima*

Naka Works, Hitachi, Ltd., Ichige 882, Katsuta-shi, Ibaraki, Japan

and Kensuke Takahashi

Department of Synthetic Chemistry, Nagoya Institute of Technology, Gokiso-cho, Showa-ku, Nagoya, Japan *(Received January 11, 1971)*

Publication costs assisted by Sendenbu, Hitachi, Ltd.,

Carbon-13 nuclear magnetic resonance spectra have been investigated by many authors, but the data are not fully accumulated. In a previous report, chloro-substituted ethanes and ethylenes were studied.[2] As a comparison, other halogeno-substituted compounds with rather simple skeletons such as the above are interesting in many respects. This note presents the ^{13}C nmr data of bromo-substituted ethanes and ethylenes.

Most experimental procedures were similar to those described in the previous reports.[2,3] Chemical shifts of the samples were compared with a sample of 55% ^{13}C-enriched methyl iodide diluted with one-third volume of benzene, and then the values were recalculated to refer to CS_2. The signal of the methyl iodide was at 214.5 ppm from CS_2. Most compounds were measured in neat liquid. Ethyl bromide and dibromo- and tetrabromoethanes were obtained from commercial sources. Other samples were prepared by the usual methods of successive dehydrobromination, bromination, and debromination of dibromo- and tetrabromoethanes. CH_3CBr_3 could not be obtained in spite of much effort. Some of the compounds seem to be unstable under the measuring conditions, as the ^{13}C nmr signals sometimes changed with time. This feature was especially apparent in the ethylene derivatives; the reason is not clear at the present time. Some typical spectra are shown in Figure 1. The spectra with 800-Hz widths can be shown in full on an nmr chart, but further details of the signals must be observed on the expanded spectra taken with a sweep rate of 1–2.5 Hz/sec, as shown in Figures 1b and c.

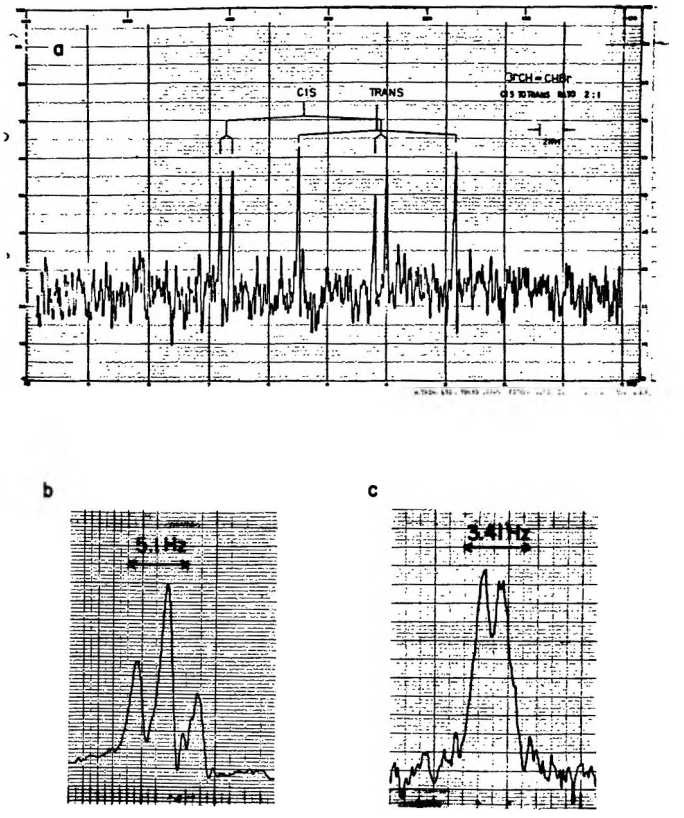

Figure 1. Typical carbon-13 nmr spectra: (a) a full spectrum of a mixture of *cis*- and *trans*-dibromoethylenes, with the signal averaged for 20 scans; (b) an expanded spectrum of CBr_3 in CH_2BrCBr_3 with 130 scans; (c) an expanded spectrum of half of $CHBr_2CHBr_2$ with 25 scans. Applied frequency increases from right to left at a constant magnetic field. The sweep rate for one scan was 50 ppm/64 sec, 51 Hz/128 sec, and 34 Hz/128 sec for (a), (b), and (c), respectively.

^{13}C nmr data for 14 bromo-substituted ethanes and ethylenes except CH_3CBr_3 are given in Table I. The data for vinyl bromide (no. 11) are only approximately given in Table I. It seems that the exact data for this compound must be obtained from the exact analysis. The case is the same for the corresponding data of vinyl

(1) Presented in brief at the 7th Symposium on Nuclear Magnetic Resonance Spectroscopy, Meijo University, Nagoya, Japan, Nov 1968, Abstract p 31.

(2) G. Miyajima and K. Takahashi, *J. Phys. Chem.*, **75**, 331 (1971).

(3) G. Miyajima, Y. Utsumi, and K. Takahashi, *ibid.*, **73**, 1379 (1969).

Table I: Carbon-13 Nmr Data of Bromo-Substituted Ethanes and Ethylenes

No.	Compound	Functional group	Shift, ppm: This study[a]	Shift, ppm: Others	$^1J_{CH}$, Hz: This study[b]	$^1J_{CH}$, Hz: Others	$^2J_{CH}$, Hz: This study[c]	$^2J_{CH}$, Hz: Others
1	CH_3CH_3			188.0[d]		124.9[e] 126[f] 127[d]		−4.5[e]
2	CH_3CH_2Br	CH_3		173.4[g] 173.5[d] 173.8[h]	129			2.1[g]
		CH_2Br		165.4[g] 165.5[d] 165.8[h]	152			4.0[g]
3	CH_3CHBr_2	CH_3	157.5	158.0[h]	131		<1.3	
		$CHBr_2$	152.4		180		5.0	
4	CH_2BrCH_2Br			161.3[g]	157			4.6[g]
5	$CH_2BrCHBr_2$	CH_2Br	152.4		156		1.2	
		$CHBr_2$	150.8		179		4.0	
6	CH_2BrCBr_3	CH_2Br	139.1		162			
		CBr_3	155.2				2.7	
7	$CHBr_2CHBr_2$		143.4		180		1.0	1.1[i]
8	$CHBr_2CBr_3$[j]	$CHBr_2$	135.1		179			
		CBr_3	149.0				<1.5	
9	CBr_3CBr_3[k]		140.3					
10	C_2H_4					156.4[e]		−2.4[e]
11	C_2H_3Br	CH_2	71.3	71.5[l] 71.8[n]	163	159.6[m] 163.8[m]	4.0	5.8[m]
		CHBr	79.0	78.3[n] 78.5[l]	201	196.1[m]	6.6 9.7	7.5[m] −8.5[m]
12	*trans*-$C_2H_2Br_2$		84.8	84.5[o]	204		<2.0	−0.4[p]
13	*cis*-$C_2H_2Br_2$		79.1	77.5[o]	200		15.0	14.7[p]
14	*gem*-$C_2H_2Br_2$	CH_2	66.5		167			
		CBr_2	96.7				1.3	
15	C_2HBr_3	CHBr	81.3		200			
		CBr_2	98.7				8.0	7.8[p]
16	C_2Br_4[q]		100.0					

[a] Referred to external CS_2; errors are estimated to be ±0.3 ppm. [b] Errors are estimated to be ±1.5 Hz. [c] Errors are estimated to be ±0.5 Hz. The sign of $^2J_{CH}$ was not determined except in the cases specifically given. [d] H. Spiesecke and W. G. Schneider, *J. Chem. Phys.*, **35**, 722 (1961). The shifts referred to C_6H_6 were converted into those referred to CS_2 by adding 65.2 ppm. [e] R. M. Lynden-Bell and N. Sheppard, *Proc. Roy. Soc., Ser. A*, **269**, 385 (1962). [f] N. Muller and D. E. Pritchard, *J. Chem. Phys.*, **31**, 1471 (1959). [g] Reference 3. [h] P. C. Lauterbur, *Ann. N. Y. Acad. Sci.*, **70**, 841 (1958). The shifts referred to $CH_3{}^{13}COOH$ were converted into those referred to CS_2 by adding 15.7 ppm. [i] R. Freeman and W. A. Anderson, *J. Chem. Phys.*, **39**, 806 (1963). [j] Measured for a 56 wt % solution in CCl_4. [k] Measured for a saturated solution in CS_2. [l] W. G. Schneider, private communication (1967). [m] R. M. Lynden-Bell, *Mol. Phys.*, **6**, 537 (1963). [n] G. E. Maciel, *J. Phys. Chem.*, **69**, 1947 (1965). [o] G. B. Savitsky and K. Namikawa, *ibid.*, **67**, 2754 (1963). [p] F. J. Weigert and J. D. Roberts, *ibid.*, **73**, 449 (1969). [q] Measured for a 39 wt % solution in CCl_4.

chloride reported earlier.[2] The $^1J_{CH}$ values for vinyl chloride reported in ref 2 were mistyped. They are correctly 198 and 162 Hz for the α and β carbons, respectively. The range of the shifts for bromoethanes (135.1–173.4 ppm) is narrower than that for chloroethanes (87.6–175.0 ppm)[2] but that for bromoethylenes (66.5–100.0 ppm) is broader than that for chloroethylenes (66.6–80.4 ppm).[2] The compounds are designated as $^{12}CH_{3-m}Br_mCH_{3-n}Br_n$ and $^{13}CH_{2-p}Br_pCH_{2-q}Br_q$. The chemical shifts are correlated to the numbers of the substituents, m, n, p, and q on the curves in Figures 2 and 3. In bromoethanes the shifts of the compounds with $m = 3$ are more shielded than those with $m = 2$ in the series of compounds with the same n. This higher shielding shift change in the compounds with larger m is a characteristic feature of bromoethanes as compared with chloroethanes. This tendency is opposite to the inductive effect of the substituent which causes the lower shielding shift. This tendency was previously noticed and discussed for substituted methane derivatives.[4] The cause of this higher shielding shift seems to be related to the steric factor because it is observed in the compound with larger m and with larger substituents. The shifts to higher shielding are also noticed for the ethylenes with larger p.

(4) W. M. Litchman and D. M. Grant, *J. Amer. Chem. Soc.*, **90**, 1400 (1968).

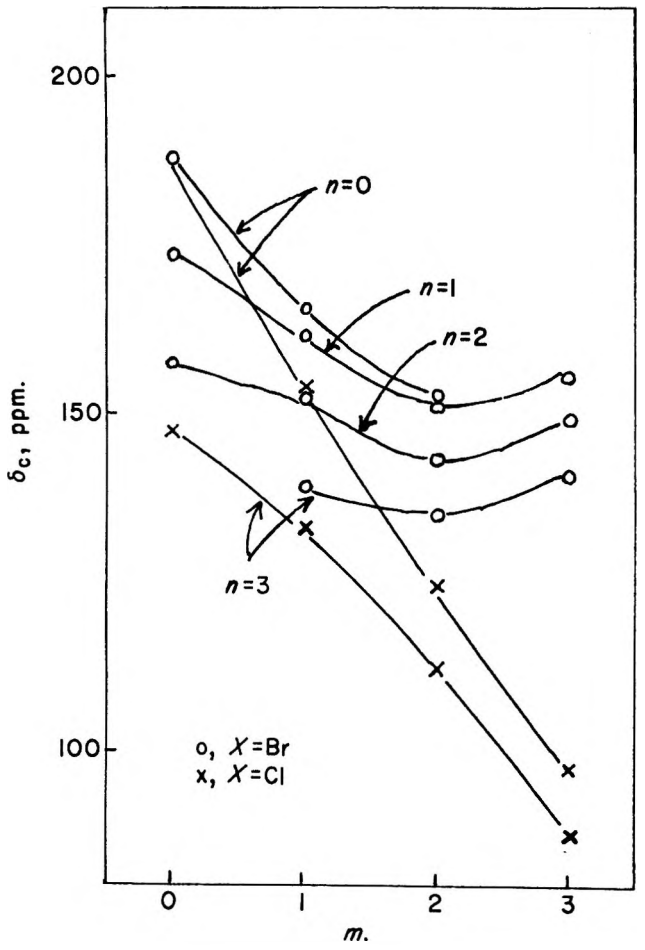

Figure 2. Carbon-13 chemical shifts in the series of $^{13}CH_{3-m}X_mCH_{3-n}X_n$.

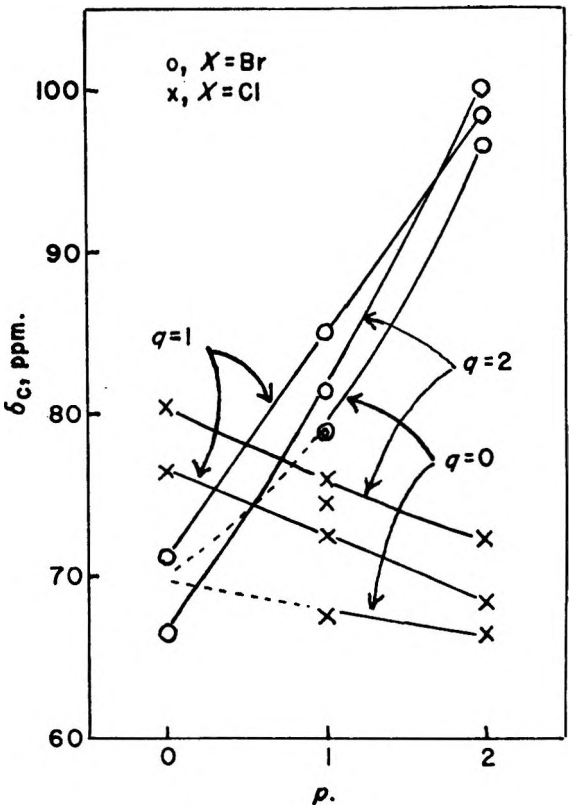

Figure 3. Carbon-13 chemical shifts in the series of $^{13}CH_{2-p}X_p{=}CH_{2-q}X_q$.

Acknowledgment. The authors wish to thank Professor Dr. F. Watari (Tohoku University) for supplying some of the compounds.

COMMUNICATIONS TO THE EDITOR

Apparent Triplet Yields of Pyrazine

Publication costs assisted by the Robert A. Welch Foundation

Sir: Pyrazine (1,4-diazine) has been shown to have very low quantum yields of fluorescence, of phosphorescence, and of decomposition in the vapor phase.[1,2] Thus it becomes important to know the triplet yield of pyrazine so as to determine whether or not the low fluorescent yield reflects an efficient internal conversion, or intersystem crossing process, or both.

We have attempted to determine the triplet yield of pyrazine by two of the more common methods, namely the photosensitized isomerization of *trans*-2-butene[3] and the photosensitized phosphorescence of biacetyl.[4] The two methods lead to significantly different results.

Figure 1 displays the photosensitized isomerization of *trans*-2-butene as a function of *trans*-2-butene pressure, for a fixed pyrazine pressure, at room temperature, with an exciting wavelength of 313.0 nm. Figure 2 is a plot of the reciprocal of these variables under the same experimental conditions. Figure 2 also shows a reciprocal plot of the results obtained with the cis isomer. The experimental quantum yields were calculated by standardizing the system using potassium ferrioxalate actinometry.[5] From Figure 1, the isomerization rate appears to level off at about 10 mm pressure of added olefin, indicating a quantum yield of isomerization of 0.28. The same quantum yield calculated from Figure 2 by an extrapolation to infinite olefin pressure is 0.34. (Likewise, from the extrapolated intercept for the cis data, a value of 0.53 is obtained.) To be consistent with accepted mechanisms of photoisomerization,[6,7] Φ_{isom} must be calculated at infinite olefin pressure. The estimate of the asymptote in Figure 1 gives a significantly lower yield.

In addition, the ratio of trans to cis isomers of 2-butene at the photostationary state has been determined as 0.9 ± 0.1. This was achieved by irradiating systems containing near-equilibrium mixtures of both isomers, so that the final photostationary state could be approached from both sides. This way, the need for long periods of irradiation of either pure isomer, with the attendant possibility of complicating side reactions, was obviated. Thus naively if a simple energy transfer mechanism is assumed,[6] the above results imply a triplet yield $\phi_T = 0.87$, calculated from the sum of ϕ_{CT} and ϕ_{TC}. However, since the branching ratio of unity found for a wide variety of compounds is not obtained here, the mechanism of the energy transfer process is complex in this case, and thus a simple addition of the two isomerization yields cannot be equated to the triplet yield.[8]

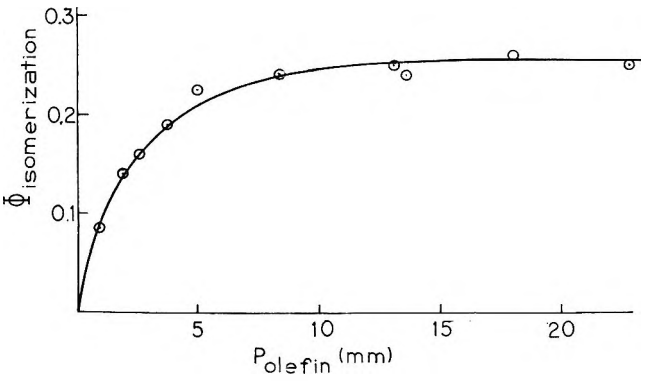

Figure 1. Quantum yield of isomerization of *trans*-2-butene in the pyrazine–butene system (irradiated at 313 mm and 25°) as a function of the butene pressure in millimeters.

The inverse of the sensitized biacetyl phosphorescent yield as a function of added biacetyl, at a fixed pyrazine pressure, at room temperature irradiated at 313.0 nm is plotted in Figure 3. From the accepted kinetics of the reactions,[4,9,10] it can be shown that the intercept in Figure 3 (*i.e.*, emission at infinite biacetyl pressure) is proportional to $1/\phi_P\phi_T$ where ϕ_P is the quantum yield of phosphorescence of biacetyl and ϕ_T is the triplet yield of pyrazine. Thus using benzene–biacetyl mixtures to standardize the system, and taking the benzene triplet yield to be 0.72,[9] the triplet yield of pyrazine is calculated to be 1.1 ± 0.1. In addition to these studies, the phosphorescent spectra of biacetyl, and biacetyl–pyrazine mixtures, irradiated at both 313.0 and 435.8 nm

(1) K. Nakamura, *J. Amer. Chem. Soc.*, **93**, 3138 (1971).

(2) M. Magat, N. Ivanhoff, F. Lahmani, and M. Pileni, *J. Chim. Phys.*, 212 (1970).

(3) R. B. Cundall and T. F. Palmer, *Trans. Faraday, Soc.*, **56**, 1211 (1960).

(4) H. Ishikawa and W. A. Noyes, Jr., *J. Chem. Phys.*, **37**, 583 (1962).

(5) C. G. Hatchard and C. A. Parker, *Proc. Roy. Soc., Ser. A.*, **235**, 518 (1956).

(6) E. K. C. Lee, H. O. Denschlag, and G. A. Haninger, Jr., *J. Chem. Phys.*, **48**, 4547 (1968).

(7) M. Tanaba, M. Kato, and S. Sato, *Bull. Chem. Soc. Jap.* **39**, 1423 (1966).

(8) F. Lahmani (private communication) has also found the branching ratio to be greater than unity, although her cis → trans figure is somewhat higher than ours. However, this slight discrepancy does not detract from the point made above; *i.e.*, the triplet yield based on the Cundall mechanism may well be invalid.

(9) W. A. Noyes, Jr., and I. Unger, *Advan. Photochem.*, **4**, 49 (1960).

(10) S. H. Jones and T. Brewer, submitted for publication in *J. Amer. Chem. Soc.*

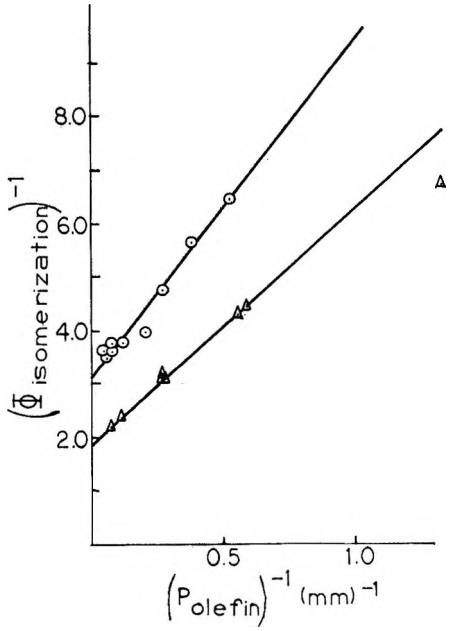

Figure 2. Inverse of isomerization quantum yield as a function of the inverse of *trans*-2-butene pressure, ⊙, and *cis*-2-butene pressure, △ (conditions same as Figure 1).

were recorded on an Aminco-Bowman spectrofluorometer. The fact that these emission profiles appear to be identical suggests that biacetyl is probably solely responsible for the luminescence in both cases.

At the present time, the discrepancy between the two methods and the two isomers is not fully understood, but it certainly indicates the caution that should be exercised in using these methods to determine triplet yields since it is clear that at least one and possibly both methods are unreliable. However, other workers[11] using certain benzenoid aromatic sensitizers have found the two methods to give results essentially in agreement.

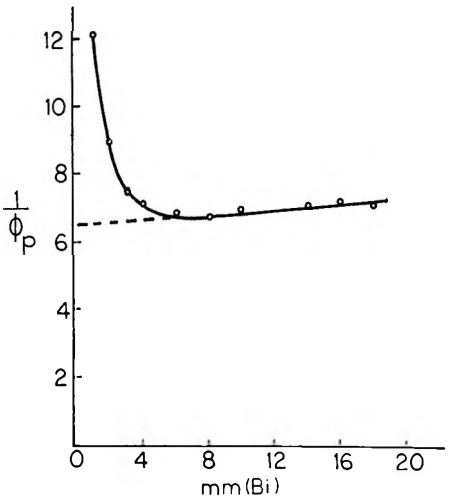

Figure 3. The inverse of sensitized emission of biacetyl in the pyrazine–biacetyl system (conditions as in Figure 1) as a function of biacetyl pressure in millimeters.

In order to shed more light on the general applicability of these methods, further work is in progress in this laboratory on various other compounds, including a more detailed study of pyrazine.

Acknowledgment. We wish to thank Dr. W. A. Noyes, Jr., for his advice and support during the course of this work. Also, financial assistance by the Robert A. Welch Foundation and the Camille and Henry Dreyfus Foundation is gratefully acknowledged.

(11) W. A. Noyes, Jr., and C. S. Burton, *Ber. Bunsenges. Phys. Chem.*, **72**, 146 (1968), and references cited therein.

DEPARTMENT OF CHEMISTRY
THE UNIVERSITY OF TEXAS AT AUSTIN
AUSTIN, TEXAS 78712

TERRY BREWER
S. H. JONES*

RECEIVED APRIL 30, 1971

Reprints from Chemical & Engineering News

On orders of $10 or less please remit check or money order

Keeping broadly informed challenges every person today. If you missed these features from recent issues of C&EN, you can still get copies by filling in the coupon below.

Population

A 2-part feature
David M. Kiefer, C&EN
Oct. 7 & 14, 1968 **75¢**

Mr. Kiefer finds that population is growing unchecked in much of the world, and that U.S. population will expand 50% in the next 30 years or so. Social as well as technological innovation is needed to thwart this advance. **10148**

Computers in Chemical Education

Dr. Frederick D. Tabbutt
Reed College
Portland, Oregon
January 19, 1970 **50¢**

A number of experiments with computers in education have been undertaken in the past few years. Some of the approaches to computer-assisted education now show promise as useful adjuncts as surrogate teachers. **11970**

Arthritis

A 3-part feature
Howard J. Sanders, C&EN
July 22, 29, & Aug. 12, 1968 **75¢**

Causes of arthritis are still a mystery, although more and more evidence points to infection as a possible trigger. Mr. Sanders discusses and examines the possible causes and the past, present, and future of treatment. **07228**

Industrial Research Careers

Howard Reiss
University of California
Los Angeles
June 29, 1970 **50¢**

A major concern of those beginning careers in science is, of course, where to carry out their careers—in a university, private industry, a foundation or wherever. An industrial research career can be a rewarding one, both professionally and financially. **62970**

Public Policy and the Environment

February 9, 1970 **50¢**

Speaking at the 158th ACS National Meeting, Lee DuBridge, Herbert Doan, and Barry Commoner urged cooperation among government, industry, and university in tackling environmental improvement. **02970**

Pollution Control Instrumentation

Michael Heylin, C&EN
February 15, 1971 **50¢**

Efforts to control air and water resources intelligently depends on the ability to detect and to monitor pollutants. The challenge to produce better instrumentation for this purpose is now receiving intense attention from industry and government researchers. **21571**

Allergy

Howard J. Sanders, C&EN
May 11, 1970 **50¢**

Although hay fever, bronchial asthma, and other allergies will not be conquered, they will be better understood and better treated. The expanding study of these diseases in fundamental scientific terms, using the latest research techniques, allergic disorders will yield more and more of their secrets that only a few years ago seemed almost unfathomable. **51170**

Food Additives

Howard J. Sanders, C&EN
October 10, 1966 **75¢**

Makers of food additives are keeping their eyes on the spectacular growth of new foods and the shifting moods of regulation-minded Washington. An array of chemicals enhances the wholesomeness, attractiveness, convenience, and nutritional value of American foods. **10176**

Technology Assessment

David M. Kiefer, C&EN
October 5, 1970 **50¢**

Technology assessment is an attempt—still halting and uncertain—to establish an early-warning system to control, direct, and, if necessary, restrain technological development so as to maximize the public good while minimizing the public risks. **10570**

Chemistry and the Atmosphere

Howard J. Sanders, C&EN
March 28, 1966 **75¢**

The earth's atmosphere is a vast, churning mixture of gases and trace quantities of liquids and solids. Held to the earth by the pull of gravity, it is the transparent envelope without which life on earth would cease to exist. **32866**

Career Opportunities The New Priorities

March 8, 1971 **50¢**

C&EN's annual career guide for chemists and chemical engineers. In the search for new priorities, new opportunities are emerging. Here C&EN looks at three such areas—food, shelter, and health. **03871**

Chaos in Science Teaching

Dr. Conrad E. Ronneberg
Professor Emeritus, Denison University
June 1, 1970 **50¢**

To many people familiar with the stiuation in teaching introductory science courses, both in high school and college, the situation is utter chaos. To place attempts to improve science teaching in proper perspective requires a brief review of the progress of science teaching since World II. **06170**

Artificial Organs

A 2-part feature
Howard J. Sanders, C&EN
April 5 and 12, 1971 **75¢**

The implanting of a total artificial heart in a human has been the most dramatic single advance to date in the field of artificial organs. In recent years, however, many other artificial organs have also been developed, and scientists foresee a vast increase in the number of body parts that, in the years ahead, will be replaceable by mechanical devices. **04571**

Scientific Societies and Public Affairs

K. M. Reese, C&EN
May 3, 1971 **50¢**

Scientific and engineering societies for many years have fostered research, published papers, and sponsored meetings without great regard for the world beyond their particular disciplines. Only in the past decade or so have the learned societies edged into the realm of public affairs. **05371**

1 to 49 copies—single copy price 50 to 299 copies—20% discount

Prices for larger quantities available on request

☐ 10148 ☐ 11970 ☐ 07228
☐ 62970 ☐ 02970 ☐ 51170
☐ 21571 ☐ 10176 ☐ 10570 ☐ 32866
☐ 03871 ☐ 06170 ☐ 04571 ☐ 05371

TO: REPRINT DEPARTMENT

ACS Publications
1155 Sixteenth St., N.W.
Washington, D.C. 20036

FROM:

Name _____

Street _____

City _____

State _____ Zip Code

Amount enclosed $ _____